NASA Contractor Report 3992

NASA-CR-3992 19880019510

Variable Sweep Transition Flight Experiment (VSTFE)-Parametric Pressure Distribution Boundary Layer Stability Study and Wing Glove Design Task

Rodger A. Rozendaal

NASA

NF01991

NASA Contractor Report 3992

Variable Sweep Transition Flight Experiment (VSTFE)-Parametric Pressure Distribution Boundary Layer Stability Study and Wing Glove Design Task

Rodger A. Rozendaal

Boeing Commercial Airplane Company
Seattle, Washington

N∧S∧

National Aeronautics
and Space Administration

Scientific and Technical
Information Branch

1986

FOREWORD

This report presents the results of the Variable Sweep Transition Flight Experiment Parametric Pressure Distribution Boundary Layer Stability Study and Glove Design Study conducted under NASA Contract NAS1-15325 from February 1983 through November 1984. This work was managed by the Laminar Flow Project office at the NASA Langley Research Center. D. B. Middleton and D. W. Bartlett are the technical monitors for the contract. Most of the work shown in this report was performed by R. A. Rozendaal of the Aerodynamics technical staff of the Boeing Commercial Airplane Company. He was given technical assistance by A. W. Chen, K. Kusunose, M. D. Murray, and T. C. VerSteegh of the Aerodynamics technical staff. Boeing managers participating in this work were G. W. Hanks, Program Manager; L. B. Gratzer, Project Manager, and A. L. Nagel, Aerodynamics Supervisor.

Special acknowledgment is given to Dr. L. M. Mack of the Jet Propulsion Laboratory for his help with the computer code used to calculate boundary layer stability.

CONTENTS

FIGURES

FIGURES (Continued)

FIGURES (Concluded)

1.0 SUMMARY

A 1980 NASA flight transition experiment with an F-111 airplane (ref. 1) indicated good prospects for obtaining significant amounts of laminar flow on the wings of medium-sized transport airplanes. However, the F-111 results also showed a need for more detailed measurements using improved instrumentation. To fill this need, NASA has initiated the Variable Sweep Transition Flight Experiment (VSTFE) to establish a boundary-layer transition data base for laminar-flow wing design. For this experiment, full-span upper surface gloves will be fitted to a variable sweep F-14 aircraft. The Boeing Company is under contract to NASA to provide design and analyses support for the program. This report documents the results of two initial tasks: a parametric pressure distribution/boundary-layer stability study and the design of an upper surface glove for Mach 0.8. Also included in this report are the analyses of the "cleanup" glove (smoothed basic wing) and the analyses of a glove designed by the NASA Langley Research Center for a Mach number of 0.7.

For the parametric pressure distribution/boundary-layer stability study, pressure distributions having midchord pressure gradients, $dc_p/d(s/c)$, of 0, -0.2, -0.4, -0.64, and -1.0 were studied. Cases were analyzed at chord Reynolds numbers of 15 and 30 million, wing sweep angles of 15, 20, and 25 deg, and Mach numbers of 0.78 and 0.70. Boundary layer stability analyses were conducted for each case and the calculated disturbance amplification factors were compared to the F-111 TACT NLF glove transition data to assess the potential research value of each pressure distribution. The results of the study provide a matrix of pressure distributions, sweep angles, and Reynolds numbers that generates a broad spectrum of different Tollmien-Schlichting (TS) and crossflow (CF) disturbance growth combinations.

Several general conclusions can be derived from the results of the study:

1. Of the two stability analysis methods used in this study, the compressible irrotational stationary (CIS) method was considered superior and was used in the glove design task.

2. Decreasing the pressure gradient in the midchord region of a swept wing tends to suppress TS disturbances but promote CF disturbances. Therefore a good wing design will probably require compromises to have good overall laminar flow, Mach, and lift capability.

3. This study showed that increasing Mach number tends to suppress TS disturbances and to promote CF disturbance growth if pressure distribution, Reynolds number, and sweep are held constant.

The results of the parametric pressure distribution/boundary-layer stability study were used in selecting the pressure distribution for the glove design that would generate a balanced growth of both TS and CF disturbances. A design point of 20 deg of sweep and 6100m (20,000 ft) altitude was selected for the Mach 0.8 glove, and the design pressure distribution has a midchord pressure gradient of about -0.6. Analysis of the final gloved configuration with a transonic analysis code indicates that the design pressure distribution was achieved over much of the F-14 variable sweep

1

outer wing panel. Analyses at off-design conditions indicate the midchord pressure gradient will be reduced to -0.45 at 10 700m (35,000 ft) altitude and Mach 0.8, and, as expected, the glove will tend to generate pressure distributions with leading-edge peaks at Mach 0.7. In addition, a ±5-deg increment in sweep should not significantly change the pressure distributions.

Analysis of the Mach 0.7 glove indicates that the midchord pressure gradient will vary from about -0.6 at 6100m altitude to essentially 0.0 at an altitude of 10 700m for Mach 0.7. At Mach 0.8, the pressure distributions will have steep favorable pressure gradients between 6100m and 10 700m altitude.

Since it is planned to fly both gloves concurrently (one on each wing panel), it was determined that the resulting asymmetry will be well within the rolling-moment control authority of the differentially actuated horizontal tail. The possibility of strong shocks causing excessive flow separation on the Mach 0.7 glove at Mach 0.8 is a concern that could not be addressed adequately within existing transonic analysis codes. However, the shock strength of the Mach 0.7 glove at Mach 0.8 and 20 deg of sweep is not greater than for the basic wing, which has some trailing-edge separation at this condition.

The possibility of attachment line contamination was assessed by calculating the attachment line momentum thickness Reynolds numbers at several flight conditions for each glove. Although there will probably not be a problem at 20 deg of sweep, the attachment line momentum thickness Reynolds numbers will exceed or approach the critical value of 100 at 25 deg of sweep for both gloves. Therefore, some form of protection against attachment line contamination (i.e., Gaster bump) should be considered.

Boundary-layer stability analyses were conducted on the three gloves to define the range of TS and CF disturbance growth. These analyses indicate that the three gloves should have substantial laminar flow for some flight conditions while providing good coverage of TS and CF disturbance growth combinations.

The fairing of the gloves back into the base wing, both on the lower surface and just ahead of the spoilers on the upper surface, must be done carefully to minimize possible boundary layer separation and excessively strong shocks. These areas need to be carefully monitored during the wind tunnel testing of the gloves.

2.0 INTRODUCTION

Recent investigations have led to increased optimism about the possibility of obtaining significant amounts of laminar flow on medium-sized commercial transports with only limited or no suction being required. In 1980, the NASA F-111 natural laminar flow glove flight-test program provided the first definitive results on the effects of wing sweep angle on boundary-layer transition (ref. 1). Relative to earlier assumptions (e.g., ref. 2), the F-111 results indicate shorter laminar runs for small sweep angles but longer laminar runs for larger sweep angles. However, the F-111 results are limited, and as a result, there is still an obvious need for additional flight-measured boundary-layer data for use in formulating more accurate transition criteria. Therefore NASA has initiated the Variable Sweep Transition Flight Experiment (VSTFE) to address this need. The VSTFE is an effort involving the NASA Langley Research Center and the NASA Ames/Dryden Flight Research facility with The Boeing Company providing design and analyses support under contract to Langley. Flight tests, starting toward the end of 1985, will be conducted at the Ames/Dryden Flight Research Facility. For this experiment, full-span upper surface gloves will be fitted to a variable sweep F-14 aircraft, and transition will be determined for a wide range of flight conditions and wing sweep angles. Three gloves have currently been defined for the program: A "cleanup" or minimum modification glove, a Mach 0.8 glove designed by Boeing and a Mach 0.7 glove designed by the NASA Langley Research Center (ref. 3). Boundary-layer stability calculations, together with the measured transition locations from the various gloves, will provide a transition prediction method that can be used for the design of future laminar flow aircraft.

2.1 OBJECTIVE AND SCOPE

The objective of this report is to document the results of two initial tasks: a parametric pressure distribution/boundary-layer stability study and the design of a Mach 0.8 glove. The first task was conducted to provide a data base from which wing-glove pressure distributions could be selected for glove designs. Boundary-layer stability analyses were conducted on a set of pressure distributions for various wing sweep angles, Mach numbers, and Reynolds numbers in the range of those anticipated for the flight test program, and these results are presented. The design procedure for the Mach 0.8 glove is described and boundary-layer stability calculations and pressure distributions are presented both at design and off-design conditions.

Also included in this report is the analysis of the "cleanup" glove that will be flight-tested initially and the analysis of the Mach 0.7 glove designed at NASA Langley.

2.2 APPROACH

The selection of VSTFE glove pressure distributions that would produce the most valuable transition data required that a family of candidate pressure distributions be systematically analyzed in terms of predicted transition locations. The best methods currently available for correlating transition data are based on linear boundary-layer stability theory (ref. 4). The theory is used to calculate the growth of disturbances in the boundary layer, and comparisons of the

calculated boundary-layer disturbance growth with experimental transition data can provide a useful transition criteria. This is illustrated in Figure 1, in which the F-111 NLF glove transition data (ref. 1) were analyzed in this manner. The shaded band corresponds to the calculated amplification factors (N) for both the Tollmien-Schlichting (N_{TS}) and crossflow disturbances (N_{CF}) at the point of transition as measured in flight. If transition locations for other pressure distributions are to be predicted from boundary-layer stability analyses and compared with the F-111 criterion, then the stability analysis method should be the same as that used to establish the criterion.

For the parametric pressure distribution boundary-layer stability study, a set of pressure distributions was defined and boundary-layer stability calculations were made for each pressure distribution at several wing sweep angles, Reynolds numbers, and Mach numbers. For each condition analyzed, the amplification factors (N_{TS} and N_{CF}) were compared with the transition criteria derived from the F-111 NLF glove data analysis (fig. 1 and ref. 1). The boundary-layer stability calculations were made with the same Boeing computer code that was used for the HLFC (ref. 2) and F-111 NLF glove data analysis (ref. 1). As discussed in Section 4.1, however, the code was applied differently in the HLFC study than in the later F-111 data analyses and consequently produced different results, particularly for the values of the crossflow amplification factors (N_{CF}). Since it was important to understand the differences in the two approaches for the current study, a discussion and comparison of results from both approaches are presented herein.

Before design of the Mach 0.8 glove could be initiated, it was necessary to verify that Boeing aerodynamic analysis codes could accurately predict the F-14 wing pressure distributions at transonic speeds. The Boeing A488 system (refs. 5 and 6) was available for modeling wing-fuselage combinations at transonic speeds, and the PANAIR panel code (ref. 7) was available for subcritical calculations. By comparing its predictions with flight-measured wing pressure data on the basic F-14, it was determined that the A488 system could accurately predict the flowfield of the F-14 outer (pivoting) wing panel over the flight range of interest. With the accuracy of the A488 system established, it was possible to proceed confidently with the glove design.

Once the design pressure distribution was chosen for the Mach 0.8 glove, a design procedure was used that generated the corresponding two-dimensional airfoil sections near the wing midspan. Since the glove would be formed by adding material to the existing wing, it was necessary that the new sections be outside the existing wing sections. These new sections formed a new wing which was analyzed three-dimensionally with the fuselage. If the 3D calculation indicated areas of the wing that required redesign to obtain the selected pressure distribution, then the process was repeated. Once the glove design was acceptable, boundary-layer stability calculations were performed to determine if the glove produced the disturbance growth combinations that had determined the design pressure distribution at the start. Also, off-design analyses were conducted on the glove to not only determine its flight performance as compared to the basic wing, but to determine how the pressure distributions and corresponding boundary-layer disturbance growths changed with varying flight conditions. This process, therefore, defined the Mach numbers and altitudes other than the design point where useful transition data could be obtained.

Analyses were also conducted on the two other gloves in the VSTFE: the "cleanup" glove which is a minimum modification smoothing of the basic F-14 wing and a Mach 0.7 glove designed by the NASA Langley Research Center. The "cleanup" glove, which will be the first glove to be flight-tested, was of interest because the basic F-14 wing pressure distributions have large favorable gradients, and analyses were conducted to determine the flight conditions at which this glove could produce useful transition data.

The Mach 0.7 glove has contours that differ significantly from both the Mach 0.8 glove and the basic F-14 wing. Since it is currently planned to fly the Mach 0.7 and Mach 0.8 gloves simultaneously, one on each wing panel, it was important to analyze each glove at the other glove's design point to determine if the asymmetry that will result can be controlled by the horizontal tail, which is differentially actuated for roll control.

This Page Intentionally Left Blank

3.0 SYMBOLS AND ABBREVIATIONS

3.1 ACRONYMS

CF   crossflow

CIS   compressible irrotational stationary

FICA   factored incompressible constant angle

FS   fuselage station

HLFC   hybrid laminar flow control

NLF   natural laminar flow

TS   Tollmien-Schlichting

VSTFE   Variable Sweep Transition Flight Experiment

WBL   wing butt line

3.2 MATHEMATICAL SYMBOLS

C_L airplane lift coefficient

c   chord

c_l section lift coefficient

c_p section pressure coefficient

h   altitude

M   Mach number

N   disturbance amplification factor, log of amplitude ratio

q   dynamic pressure

Re   Reynolds number

$Re_{\theta_{a.l.}}$ Reynolds number at the attachment line based on boundary layer momentum thickness

s   distance along the airfoil section surface

x   distance along airfoil chord

α angle of attack

α_i spatial amplification rate

α_r wave number

Λ sweep angle

ψ disturbance propagation angle

ω disturbance frequency

Note: A spatially varying disturbance in the boundary layer is assumed to take in the wave form:

$$e^{i[(\alpha_r + i\alpha_i)x - \omega t]}.$$

Here x is the wave vector direction and t is time. For the analyses in this report, temporal amplification does not occur, therefore ω is a real number. See Reference 4 for a more detailed definition and theoretical development.

3.3 SUBSCRIPTS

LE   leading edge

N   normal to sweep

s   parallel to the leading edge

t   at trip location

∞ conditions at infinity

3.4 SUPERSCRIPT

*   dimensional quantity

4.0 PARAMETRIC PRESSURE DISTRIBUTION/BOUNDARY LAYER STABILITY STUDY

4.1 SELECTION OF CONDITIONS

The purpose of the Parametric Pressure Distribution/Boundary-Layer Stability Study was to provide boundary-layer stability analyses for a systematic set of pressure distributions. These current results, when combined with those from the HLFC study (ref. 2), form a systematic set of data that could be used in selecting glove designs for the VSTFE. Early in the current study, however, it became clear that the boundary-layer stability analysis procedure used for analyzing the F-111 NLF glove data and the one used for the HLFC study, in some cases, gave considerably different disturbance amplification factors, particularly for crossflow. Although the analysis procedure used for the F-111 data is now preferred at Boeing, the HLFC results still represent systematic pressure distribution variations analyzed in a consistent manner.

Both boundary-layer stability analysis procedures use the same two computer codes: A552, a Boeing developed finite difference calculation of compressible turbulent or laminar boundary-layers on infinte (untapered) swept wings and the Mack code, a Boeing modification of a code that solves the boundary-layer stability equations for three-dimensional, linearized, parallel flow. The primary difference in how the Mack code was used for the HLFC study and the F-111 data analyses was in the calculation of the crossflow disturbance amplification factors. For the HLFC study, the crossflow disturbance amplification factor envelope was constructed from a series of disturbance frequences at a constant wave angle, ψ, while for the F-111 data analyses, the crossflow disturbance amplification factor envelope was constructed from a series of spanwise components of the wave number at zero frequency (an irrotational condition) as described by Mack in Reference 8. The analysis procedure as used in the HLFC study is referred to as the factored incompressible constant angle method while the procedure used for the F-111 data analyses is referred to as the compressible irrotational stationary method. The specific application of the Mack code for both analysis methods is given below:

The Factored Incompressible Constant Angle (FICA) Method (used in the HLFC study but now superseded)—Boundary layer parameters from the A552 code, run with compressibility accounted for, were used as input to the Mack boundary layer stability code. The Mack code was run incompressibly for several disturbance frequencies, and the resulting disturbance amplification envelope was factored to account for compressibility by an amount determined during the HLFC study (ref. 2). The compressibility factors were determined by a limited number of Mack runs done both with and without compressibility. Most of the Mack runs were done incompressibly because of the substantial cost savings over compressible runs. For crossflow (CF) disturbance growth calculations, a constant wave angle of 85.6 deg was used, and for Tollmien-Schlichting (TS) disturbances, 0 deg was used. The wave length, related to wave number by $\lambda = 2\pi/\alpha_r$, generally increases for both TS and CF cases as the solution proceeds further back on the wing and is a result of the eigenvalue solution at each station.

The Compressible Irrotational Stationary (CIS) Method (used in the F-111 study)—Boundary layer parameters identical to those used in the HLFC method were used for this method. The Mack code was run compressibly for all cases. The wave angle (ψ) chosen for TS disturbances was 40 deg. The amplification rate of TS disturbances is a weak function of wave angle, but 40 deg was found to be approximately the angle for maximum amplification when compressible calculations were performed. The CF disturbances were calculated for zero frequency using an "irrotational" condition as described by Mack in Reference 8. The irrotational condition is equivalent to requiring a constant spanwise (dimensional) wavelength. This method of CF calculation is considered more physically correct because flow visualization of transition on swept wings shows regularly spaced streamwise streaks, indicating standing waves in the crossflow direction. The disturbance amplification envelope was then constructed around a series of lines that each represent the amplification of a spanwise disturbance at a constant spanwise wavelength (or wave number). Coming from the solution to the eigenvalue problem, the resulting wave angle follows a constant spanwise wave number, α^*_{rs}. This angle tends to start out in the 80- to 85-deg range near the wing leading edge and rises rapidly toward an asymptotic value near 90 deg. The dissipation terms were neglected in these compressible analyses, reducing the system of equations from eighth to sixth order and saving considerable computer time. Earlier studies (ref. 8) showed that neglecting dissipation has a negligible effect on the resulting stability calculations at the Mach numbers used in this study.

For the present study, two new pressure distributions (P102 and P104) were analyzed by the FICA method, and these results, when combined with those from the HLFC study (P11, P12, and P13) provide a good definition of the trend of the boundary-layer disturbance amplification factors with systematic changes in pressure distribution and flight and sweep conditions. In addition, three of the pressure distributions (P102, P11, and P12) were analyzed with the CIS method, and the results are compared with those from the FICA method. Also included in the results are the effect of Mach number, Reynolds number, and sweep angle.

The five pressure distributions with their midchord slopes, d c_p/d (s/c), are shown in Figure 2. The pressure distributions are presented as functions of nondimensional surface distance (s/c) rather than the usual nondimensional chord distance (x/c) because the boundary layer equations are formulated using that parameter. The difference between (s/c) and (x/c) is small except near the leading edge. Figure 3 shows the details of the pressure distributions over the first 5% chord and the reflex in the distributions which results from using s/c rather than x/c. All pressure distributions in this study and the previous studies are considered to be those normal to the wing sweep, not streamwise. The conditions analyzed for each pressure distribution are given in the following tables.

10

Conditions Analyzed With FICA Method, $M_N = 0.78$

Pressure distribution	$Re_{c_N} \times 10^{-6}$	Λ, deg
P102	15	15
		20
		25
	30	15
		20
P104	15	15
		20
		25
	30	15
		20

Conditions Analyzed With CIS Method, $M_N = 0.78$

Pressure distribution	$Re_{c_N} \times 10^{-6}$	Λ, deg
P102	15	15
		20
		25
	30	15
		20
P11	15	15
		20
		25
	30	15
		20
P12	15	15
		20
		25
	30	15
		20

Conditions Analyzed With CIS Method, $M_N = 0.70$

Pressure distribution	$Re_{c_N} \times 10^{-6}$	Λ, deg
P102	15	25
P11	15	15
P11	15	25
P11	30	15
P12	15	25

For each of the 30 sets of conditions analyzed, disturbance amplification envelopes for both TS and CF disturbances were constructed using either the FICA or CIS calculation methods.

4.2 RESULTS

4.2.1 FICA Method

As outlined in the previous section, 10 cases were analyzed using the FICA method, five each for pressure distributions P102 and P104. The amplification envelopes constructed from the incompressible stability calculations were factored by amounts determined during the HLFC study (ref. 2) to account for compressibility. These factors are:

Factor	Where applied
0.90	To all crossflow (CF) envelopes
0.58	To P102 Tollmien-Schlichting (TS) envelopes
0.60	To P104 Tollmien-Schlichting (TS) envelopes

Figures 4 through 13 show disturbance amplification envelopes for the 10 cases analyzed for this part of the study. Incompressible and factored "compressible" envelopes are given, as well as the amplification for the individual disturbance frequencies, ω^*, used to generate the envelopes.

4.2.2 CIS Method

4.2.2.1 Mach 0.78 Cases

Fifteen cases with a normal Mach number of 0.78 were calculated using the CIS analysis method, five each for pressure distributions P11, P12, and P102. The sixth-order compressible equations were used for all these calculations. The disturbance wave angle for all the TS disturbances was 40 deg and the "irrotational" technique was applied for all the CF calculations. The disturbance frequency used for the CF calculations was zero.

During the CF calculations, the Mack code experienced problems in obtaining converged solutions at the higher wave numbers, α_r. Solutions at these wave numbers were needed to adequately define the crossflow disturbance amplitude envelopes. Two approaches to correct this problem were taken. An extrapolation method was used to sidestep the need for converged solutions at the higher wave angles. This is explained further in the Appendix. At the same time, modifications to the Mack code were initiated, funded by Boeing Independent Research and Development (IR&D). Because the modifications were not successful at first, Dr. L. M. Mack, the originator of the code, was contacted. He felt that his new version of the code that handled the solutions in a slightly different way should converge for the high wave number situations of this study. The code was obtained, converted to the Boeing CYBER computer, and several test cases sent with it were successfully run. It was difficult to get a case from the present study to run on the new version of the code, but that also was done. The results of this final test case and the discussions with Dr.

Mack, which were needed to make it work, pointed to some promising modifications that could be made to the Boeing version of the Mack code. These later changes were successful. The updated Boeing version can find converged solutions to as high a wave angle as is needed and also runs faster than previously. This code development was done with IR&D funding. By the time the code was improved, 14 crossflow envelopes had been constructed using the extrapolation technique as explained in the Appendix. Five of these were redone with the improved code, and the differences between envelopes that were done each way were not more than 2.5%. Because of the good agreement, the other nine extrapolation envelopes were not recalculated.

Figures 14 through 28 show the TS and CF envelopes for this part of the study. The different disturbance frequencies, ω^*, used to define the TS envelopes are noted, as well as the different spanwise components of the wave number $(\alpha_{r_s}^*)$ used to define the CF envelopes. CF envelopes done by the extrapolation technique are noted.

4.2.2.2 Mach 0.70 Cases

The five cases that were recalculated using a normal Mach number of 0.70 are noted in the table in Section 4.1. These calculations were done completely from the beginning with the boundary layer parameters recalculated using A552. The Mach number was changed for the boundary layer analyses, but the pressure distributions are identical except at the stagnation point, as noted in Figure 3. The stability calculations were done similarly to those for the higher Mach number cases, but the updated Mack code was used to construct all the CF envelopes. Figures 29 through 33 show the envelopes for the Mach number equal to 0.70 cases.

4.2.3 Comparisons

4.2.3.1 Effect of Pressure Distribution (FICA Method)

The two new pressure distributions for this study, P102 and P104, when combined with the pressure distributions from the HLFC study (P11, P12, and P13) give a set of distributions whose midchord slope (d c_p/d(s/c)) is consistently varied. However, by fixing the maximum local Mach number at an s/c of 0.6 (fig. 2), the c_p to which the flow expands at the leading edge is considerably different for each pressure distribution, and this has a significant effect on the crossflow disturbance growth in this region. Figure 34 presents the disturbance amplification factor envelopes for the five pressure distributions at a Reynolds number of 30×10^6 and 20 deg of sweep using the FICA method, and Figure 35 gives similar envelopes for the three pressure distributions analyzed with the CIS method. The pressure distributions with the lowest midchord slope have the most negative leading-edge c_P (i.e., P13 and P102). Although these pressure distributions produce lower crossflow disturbance growth (crossflow N-factors) aft of about 30% chord, they have higher crossflow N-factors in the leading-edge region. The same is not true for the Tollmein-Schlichting disturbances. The very steep initial flow accelerations produced by all the pressure distributions highly dampen the growth of TS disturbances in this region. In fact, there is no growth of TS disturbances in the first 5% chord. Aft of the leading-edge region, the pressure distributions with steeper slopes (i.e., P12 and P11) produce lower TS N-factors, which is exactly opposite the effect noted for crossflow disturbance growth. Therefore, in designing laminar flow wings when both TS

and CF disturbances are present, the pressure distribution selected will have to be a compromise in order to handle both types of disturbances. In addition, airfoils with favorable pressure gradients generally have degraded Mach/lift performance as compared to airfoils having slightly adverse or zero pressure gradients.

Figure 36 shows another way of presenting the TS and CF N-factors for the pressure distributions. TS and CF N-factors are plotted at one chordwise location (s/c = 0.4) for each Reynolds number, sweep and pressure distribution analyzed. TS amplification tends to rise with increasing sweep for constant Re, M_N, and pressure distribution because the effective velocity gradient in the disturbance propagation direction decreases roughly proportional to $\cos\Lambda$.

4.2.3.2 Comparison of Analysis Methods

Three pressure distributions were analyzed with the CIS stability method. Some comparisons of disturbance amplification envelopes for similar conditions done with each analysis method (CIS and FICA) are shown in Figures 37 through 39. The TS envelopes agree well, confirming the compressibility factoring method used in the HLFC study. The CF envelopes from the two methods are much different. This is due to the substantial difference between following a constant wave angle (ψ) with different frequencies (ω *) for the FICA method, and following constant spanwise wave numbers ($\alpha_{r_s}^*$) at zero frequency for the CIS method. Figure 40 shows an N_{TS}-N_{CF} diagram at 40% chord with results from both methods. It is clear that the stability calculations used to determine transition locations of possible wing designs must be compatible with the calculations used to develop the transition criterion that is applied.

4.2.3.3 Comparison of Mach Numbers

The five cases that were analyzed at a normal Mach number of 0.7, as well as at 0.78, showed that this magnitude of Mach number change did not have a large effect on disturbance growth, but it could have a large effect on the s/c at which a particular value of N_{TS} or N_{CF} occurred. Figure 41 compares envelopes at the two Mach numbers for one of the cases. The trends and magnitudes of the differences shown were consistent for all five cases: somewhat higher amplification at the lower Mach number for TS disturbances and less amplification for CF disturbances. These trends are reasonable if one considers N_{CF} to be proportional to crossflow velocity magnitude (which increases with increasing freestream Mach number) and N_{TS} to be inversely related to the streamwise velocity gradient (which also increases as freesteam Mach increases), with the c_p distribution held constant. The fact that the N_{CF} trend with Mach is opposite the trend shown for the FICA method (figs. 4-13) is due mostly to the difference in boundary layer calculations between the two methods. In the FICA method, the same boundary layer velocity parameters are used when calculating incompressible or compressible disturbance growth. The difference seen in that method for crossflow growth between compressible and incompressible cases is partially a result of the inclusion, or lack of it, of the compressible terms in the boundary layer stability equations used in the Mack code; these terms apparently act to lower the disturbance growth. In the CIS method, the boundary layer is recalculated for the Mach 0.7 and 0.78 cases so the crossflow velocity magnitude change due to different freestream velocities is included. Evidently, in the CIS method, the compressible terms in the stability equations are not sufficient to counteract the crossflow

14

velocity effect. Figure 42, an N_{TS}-N_{CF} diagram, shows the differences in the results at s/c = 0.4 for the five cases analyzed at both Mach numbers. Typical cruise Mach numbers of many subsonic transports are near or between M_N = 0.70 and 0.78 , so reasonable Mach number changes (approximately 0.05) in this range should not necessitate a recalculation of boundary layer stability if the Mach number is the only parameter changed. The F-111 transition criterion is derived from data taken near a normal Mach number of 0.8. It is not now known if this criterion itself is a function of Mach number. Therefore, similar transition data from other Mach numbers are badly needed.

4.2.4 Application to VSTFE Glove Designs

Figures 43 through 47 are N_{TS}-N_{CF} diagrams, including the F-111 transition criteria for chordwise locations of 20, 30, 40, 50, and 60%. These diagrams show that TS disturbances grow to relatively high levels early (10 to 20% chord), even with steep favorable pressure gradients. Once past this area, the TS amplification drops for the pressure distributions with steeper slopes, and the TS transition criteria become more favorable for CF amplification in the 6 to 9 range. These features show that an airfoil design whose midchord pressure gradient decreases as the minimum pressure point is approached might be the best compromise for maximum laminar run, lift, and Mach number.

When compared with the F-111 transition criterion, the results of this study are shown to suitably cover the range of flight and/or geometry conditions and pressure distributions that may be obtained during the VSTFE flight test. Charts similar to Figures 43 through 47 can be used to choose the flight conditions and pressure distribution designs that will provide the most useful flight transition data. These data and stability analyses will provide important additional points to supplement the F-111 transition criterion.

This Page Intentionally Left Blank

5.0 VSTFE GLOVE DESIGN

5.1 MODELING OF THE F-14 CONFIGURATION

In designing a glove for the VSTFE, it was necessary to develop an airfoil shape that will produce a certain predetermined pressure distribution that will generate boundary-layer disturbance growths in a range to both verify and expand on the F-111 NLF glove results reported in reference 1. This will require a wing that develops certain predetermined pressure distributions. To design a wing, or in the case of this task, a glove on an existing wing, the pressures on the wing at desired flight conditions must be available to the designer quickly and with reasonable accuracy. Fortunately, computer codes now exist that can perform this task on fairly complex wing-body-nacelle combinations at transonic speeds. This leaves the much more expensive and time consuming wind tunnel testing to be used only for verification of the final design.

The primary wing analysis tool that Boeing used during task 2 was the A488 system. This code consists of an improved version of Jameson's transonic full-potential finite volume FL028 program (ref. 5) coupled to a finite difference three-dimensional boundary layer analysis (ref. 6). The program cycles between potential flow and boundary layer calculations to obtain a converged result. Included in this system of codes is an advanced shock-boundary layer interaction model and a versatile grid generation method. The surface-fitted grid generation method developed by Yu (ref. 9) allowed a good representation of the critical portions of the F-14 geometry; nevertheless, the complexity of the geometry required validation of the A488 computational model.

The F-14 fuselage outer surface definition used during task 2 was supplied by NASA Langley Research Center as one-tenth scale cross sections traced on mylar. These sections included the engine nacelles and the inner, highly swept wing area that covers the wing pivot. This definition had been used for a wind tunnel model and contained some minor deviations from the production airplane. Points from these cross sections were digitized to make them available for computer processing. Figure 48 shows the digitized points connected by lines for these fuselage cross sections. The A488 system could not model the complex fuselage-nacelle shape with its sharp corners and double-valued cross sections, so approximations were made to the actual geometry for the transonic flow calculations. The major simplifications made to the geometry were filling in between the nacelles and blending the inlets into the nose of the aircraft. Figure 49 shows the fuselage cross sections used for the transonic flow solutions. The fuselage took on a pointed wedge shape, although the canopy, inner wing, and details under the inner wing were retained. This proved to be adequate, since accurate pressures were important only on the outer (pivoting) wing panels. Flight test wing pressure data (ref. 10) were used to judge the accuracy of the A488 simulation.

The outer (pivoting) wing definition was supplied by Grumman and was used by both NASA and Boeing as the basic F-14 wing. These coordinates are given in Reference 11. Although the definition at three wing sweeps was supplied, only the 20-deg leading edge definition was used by Boeing. Appendix 2 gives the coordinates of defining sections for this wing. Streamwise section coordinates at 8 wing spanwise stations made up this definition on a trapezoidal planform, along with fuselage station and waterline referencing points. The wing was mated with the fuselage and

minor blending and smoothing was done in the area where the inner (fixed) and outer (pivoting) wing panels met. This included the addition of a fictitious fillet at the wing leading edge break, which was done so the potential flow and boundary layer solutions would not diverge during A488 analyses. Figure 50 shows several views of the grid on the surface of the wing-body combination used to verify the capability of A488 to simulate the transonic characteristics of the F-14 wing.

5.2 CALCULATED AND FLIGHT-TEST WING PRESSURE DISTRIBUTIONS

Flight-test pressure data measured on the basic F-14 wing (ref. 10) were used to judge the accuracy of the calculated pressure distributions from the A488 system. The VSTFE flights are intended to be flown primarily between Mach 0.7 and 0.8 and at high Reynolds number, so the two flight conditions where flight test and computer calculated pressures were compared were:

$M_\infty = 0.75$ Altitude = 7620m (25,000 ft)

$M_\infty = 0.8$ Altitude = 9144m (30,000 ft)

The simulations were intended to match the flight test total aircraft lift coefficients, and six cycles between potential flow and boundary layer analysis were carried out. Since both laminar and turbulent boundary layers can be calculated by the A488 system, it was necessary to give the program as an input the trip location on the wing as a function of span. For these two cases the boundary layer was tripped at 3% chord on both surfaces of the outboard (pivoting) wing and at the leading edge on the inboard wing. The following table compares analysis and test results of several overall parameters at the two flight conditions.

	ANALYSIS	DATA	ANALYSIS	DATA
M_∞	0.75	0.75	0.8	0.8
α, deg	1.50	1.65	1.10	1.37
C_L	0.348	0.33	0.330	0.32
$Re/_m$	0.76×10^6	0.74×10^6	0.70×10^6	0.68×10^6
(Re/ft)	2.5×10^6	2.42×10^6	2.29×10^6	2.24×10^6

Spanwise lift distribution comparisons are shown in Figure 51. Section pressure distribution comparisons are shown in Figures 52 and 53. Overall, the comparisons show the analysis system to be quite good, even though the details of the lift distributions and chordwise pressure distributions do not agree well on the inboard area. Some of this could be explained by noticeable differences be-

tween the smooth theoretical wing definition and the actual wing of the test airplane. There were breaks in the tested wing where the leading edge slat and trailing edge flap mated with the main wing, and leakage may have occurred from lower to upper surface. For trim purposes the flaps on the side of the aircraft where pressures were measured was uprigged (slightly deflected to a negative angle when in the cruise position). This was determined after the flight tests by comparing casts of wing sections 201 and 311 to the theoretical loft sections. The uprig would cause the aircraft to fly at a slightly higher angle of attack to maintain level flight, causing wing upper surface pressures to be higher than indicated by analyses using the theoretical loft. The comparison of analytical and flight test pressure shows that characteristic, particularly inboard, where the uprig was greatest. The influence of the inner fixed wing on the outboard area of the wing is also open to speculation. The details of the geometry of this area were too complicated to be modeled well in the analysis system. Still, the major features of the wing, such as shock location and average pressure gradient ahead of the shock, were represented well on the upper surface in the midspan region. Figures 54 and 55 show isobars (constant pressure lines) on the wing upper surface from the two analyses. It is clear that a broad area exists on this surface that behaves nearly like an infinite swept wing. This would be the intended laminar flow test area for the VSTFE program. From these comparisons it was concluded that the modeling of the F-14 geometry and analysis using A488 was adequate for the test area of the wing, and glove designs were initiated.

5.3 GLOVE LAYOUT AND CONSTRAINTS

Because of the experience with a limited-span glove on the F-111, the decision was made by NASA to utilize as much of the span as possible for the gloves on the F-14. As shown in Figure 56, thge gloves will extend from WBL130 to WBL350. The actual test area of the gloves is shown as the dotted are in Figure 56 (WBL135 to WQBL325), where stringent smoothness tolerances will be maintained while the diagonally hatched areas represent regions where the tolerances will be relaxed. The gloves will extend from about 5 % chord on the lower surface to the spoiler hinge-line on the upper surface (59% chord). In order to restrain the leading-edge slat and prevent a discontinuity at the slat joint, it was determined from simulated 1-g loading tests conducted by NASA on the test airplane) that a glove approximately 1.5 cm (0.6 in) thick would be required near the slat joint. Therefore, a minimum glove thickness of 1.5 cm over the slat joint was a requirement placed on the glove designs. Several other dimensional constraints were also stipulated: a minimum thickness of 0.65 cm (0.25 in) for installing flush static pressure orifices, a maximum overhang (distance ahead of basic wing leading edge) of not more than 2% of local chord, and a thickness at the spoiler hinge line of not more than 2.5 cm (1.0 in). It was also required that the modified wing (basic wing plus glove) generate about the same lift as the basic wing for a given angle of attack.

The minimum sweep angle for the F-14 is 20 deg, and this angle was selected as the nominal design sweep angle for all the gloves. However, it is possible to hold a sideslip angle of 5 deg at Mach 0.8, which will allow a simulated minim sweep angle of 15 deg. The wing can be swept aft to 45 deg at subsonic Mach numbers if needed. The primary altitude ange for the program will be from 6 100m (20,000 ft) to 10 670m (35,000 ft). For 20 deg of sweep, the airplanehas a maximum

dynamic pressure placard of 21,540 Pa (450lbf/ft²) which limits the minimum altitude to about 6 100m at a Mach number of 0.8 Altitudes up to 10 670m can be flown t 20 deg of sweep and Mach 0.8 before ny significant buffet is encountered. With the gloves installed, a limit of 1.5 g will be placed on the aircraft.

5.4 MACH 0.8 GLOVE DESIGN

For a Mach number of 0.8 and 20 deg of sweep, an altitude of 6 100m (20,000 ft) was selected for the design condition to obtain the highest possible Reynolds number. As discussed in the previous section, this is the airplane minimum altitude limit for this Mach number and sweep. For these conditions, a chord Reynolds number of about 26×10^6 can be obtained on the inboard part of the glove near WBL202. It is desirable, however, that the glove produce useful pressure distributions (i.e., no leading-edge peaks) up to altitudes of 10 670m (35,000 ft) and over as broad a Mach number range and sweep range as feasible. In addition, the glove should have a balance between the growth of TS and CF disturbances near the design condition, and transition should occur before the pressure recovery or shock.

As a starting point, calculated pressure distributions for the basic wing at the selected design condition are presented in Figure 57. The transition was assumed for this analysis to be at 3% chord on both wing surfaces. To establish the required pressure distribution for the new glove, the disturbance growth charts (figs. 43-47) were consulted. For a chord Reynolds number of 26×10^6 and sweep of 20 deg, a pressure coefficient gradient, $d\,c_p/d(s/c)$, near -0.6 could apparently have considereable laminar flow but still transition before the shock. For correlating the transition point with calculated N-factors, this would be necessary. At the same flight condition, lower chord Reynolds numbers would prevail for outboard sections, so very similar pressure distributions would be expected to ave longer laminar runs (measured in percent chord).

Since much of the design work for the glove could be accomplished two-dimensionally, it was necessary to estimate sectional lift coefficients for various flight conditions. The highest chord Reynolds number would be obtained on the inboard part of the glove, so much of the 2D design effort was conducted on the normal section at WBL202. The following table shows several possible flight conditions, including the design point, which can be obtained with the F-14 and the corresponding section lift coefficients at WBL202. An airplane weight of 21 770 kg (48,000 lb) was assumed and the section was taken normal to the wing quarter-chord line (fig. 56). For 20 deg of leading-edge sweep, the quarter-chord sweep is 16 deg, and the section lift coefficient is related to total aircraft lift coefficient by $c_l \sim 1.2\, C_L/\cos^2 16$. The 1.2 accounts for the difference between total and section lift coefficient at WBL202, and the cosine term arises from simple sweep theory that relates two-dimensional and three-dimensional lift.

Altitude 100m (1000 ft)	M_∞	q_∞ Pascals(lb/ft^2)	C_L	c_l	Re/m(1/ft) x 10^{-6}	M_N
45.7(15)	0.735	21540(450)	0.19	0.25	1.03(3.37)	0.71
61.0(20)	0.80	20820(435)	0.20	0.26	0.96(3.16)	0.77
76.2(25)	0.80	16750(350)	0.25	0.33	0.82(2.68)	0.77
91.4(30)	0.80	13400(280)	0.32	0.42	0.69(2.27)	0.77
106.7(35)	0.80	11010(230)	0.385	0.50	0.58(1.91)	0.77
61.0(20)	0.70	16040(335)	0.254	0.33	0.84(2.77)	0.67
106.7(35)	0.70	8140(170)	0.50	0.65	0.51(1.67)	0.67

Aircraft Weight = 21 770 kg (48,000 lb)
Wing Reference Area = 52.5 m^2(565 ft^2)

A two-dimensional design code was applied using the desired pressure distribution. Figure 58 shows the desired distribution and the one obtained from the design code. The airfoil shape that produced the desired pressure distribution had, as expected, a much blunter nose than the base airfoil as well as greater maximum thickness. The new airfoil and base airfoil were combined as follows:

- Large-scale plots of the two airfoils were overlaid and shifted so the two shapes were tangent to each other on the undersurface near the nose, and there was about 0.76 cm (0.3 in) physical thickness of the new shape over the base section at x/c = 0.58. This is illustrated in Figure 59.

- The distance between the base and new airfoil shapes measured perpendicular to the base airfoil, was calculated. This glove thickness distribution from the lower surface near the leading edge to the upper surface at x/c = 0.58 was then added to the base airfoil. In this way the appropriate parts of both base and glove airfoils were retained unchanged. The glove thickness distribution, denoted "A", is shown in Figure 60. The combined (or gloved) airfoil was analyzed to confirm that the desired pressure distribution was retained through the combining process. A fictitious fairing was retained on the gloved airfoil aft of x/c = 0.58 for theoretical analyses. The actual glove has been constrained to end at the spoiler hingeline, x/c = 0.59, and it will probably be terminated by a ramp fairing starting at x/c = 0.57 or 0.58. the smoother fairing is important for the theoretical analyses to minimize the large incorrect excursions in pressure that abrupt surface breaks can cause. The actual fairing should not extend more than a couple percent chord upstream of the spoiler hingeline because of shock location. Figure 61 shows pressures from analyses at three closely spaced Mach numbers for the gloved airfoil. The major features of the desired pressure distribution were obtained on the gloved airfoil, although it might have a slightly higher than anticipated design Mach number to push the shock a few percent chord further back.

The boundary layer stability of the glove section was analyzed for normal Mach numbers of 0.76 and 0.78 and a normal chord Reynolds number of 26×10^6. The pressure distributions used were those shown in Figure 61, and the wing sweep was assumed to be 18 deg because disturbance

growth near the front of the wing (especially for the crossflow mode) was considered to be most important. It was necessary to assume a constant sweep since the boundary layer equations used for the stability analyses assume an infinite swept wing. The disturbance growth for TS and CF disturbances is shown in Figures 62 and 63, and the traces of N_{TS} - N_{CF} are shown in Figure 64. The traces show that the design objective of balancing TS and CF disturbance growth and having transition ahead of the pressure recovery/shock was achieved by this glove design, at least as predicted by section analyses.

The added thickness distribution (fig. 60), which forms the glove section from the base section, can be added to sections other than WBL202 since it is presented as t/c versus s/c. However, the resulting glove section at those stations would probably produce the desired pressure distribution only if (1) the base section was nearly the same shape as the one at WBL202, and (2) the base pressure distribution was nearly the same at the design flight condition as that at WBL202. When the glove thickness distribution was added to the base section at WBL256, the design pressure was closely matched (fig. 65) but this was not the case at WBL311 (fig. 66). At WBL311 both the base section shape and design pressure distribution have departed too far from WBL202 for glove thickness distribution "A" to be adequate. A glove design procedure like that used for the WBL202 section was carried out for WBL311. The resulting glove thickness distribution for WBL311, denoted "B", is shown in Figure 67, and its pressure distribution at the glove design condition is compared to the base pressure in Figure 66.

Section glove designs were considered complete when glove designs for sections WBL202, 256, and 311 obtained the desired pressure distributions and the boundary layer stability at section 202 gave desired disturbance growth. These section designs were incorporated onto the basic F-14 wing by adding thickness distribution "A" to the Grumman-supplied sections at WBL164, 202, and 256 and thickness distribution "B" to sections WBL311 and 348. Other sections of the basic wing were not changed. This wing was lofted with linear elements between the defining sections and analyzed by the A488 system. The fuselage and wing modeling used for the clean wing analyses (sec. 5.1) was duplicated for the gloved wing analyses. A design condition of Mach 0.81, angle of attack of -0.15 deg, and Reynolds number of 0.98×10^6 per meter (3.2×10^6 per foot) were used. This resulted in a lift coefficient of about 0.2, which corresponds to an aircraft weight of about 21 770 kg (48,000 lb) and altitude of about 6100m (20,000 ft). The first wing glove design gave a poor isobar pattern as well as a chordwise pressure distribution at WBL202 that had too low a midchord slope. Several iterations were required to arrive at an acceptable wing glove design. The major change during those iterations was the use of a different glove thickness distribution on sections WBL164, 202, and 256. This distribution, called distribution "C", gave an increased midchord pressure gradient, and is shown in Figure 68. The other change involved decreasing the glove thickness on section WBL164 aft of x/c = 0.35 in order to improve the inboard isobar pattern. Figure 69 shows isobars and chordwise pressures for the final wing glove design based on a six-cycle A488 analysis. Appendix 2 gives the coordinates of the defining sections for the F-14 wing with the Mach 0.8 glove included.

For transonic analysis the boundary layer was tripped where it was assumed it might transition naturally. These locations were derived for all the A488 analyses based on a combination of the

wing inviscid pressure distributions, Reynolds number, and results of the parametric study (sec. 4.0) and glove section (2D) boundary layer stability analyses compared to the F-111 transition data. Figure 70 shows these assumed transition locations. These results indicate that the Mach 0.81 speed is probably slightly high since the shock occurred near where the glove would be faired into the basic wing, x/c = 0.59. However, the glove does have a good isobar pattern in the test area, 190 < WBL < 320, as well as chordwise pressure distributions close to those specified in the section designs (when the sweep correction is considered).

The boundary layer stability at the design condition and section (WBL202) was calculated to verify that the earlier section glove stability analyses had carried through to the gloved wing. The pressure distribution used was that from an inviscid A488 analysis at WBL202 at the design flight condition (M_∞ = 0.81, α = -0.15 deg). This inviscid result was used because it is probably closer to a matched viscous-inviscid result at a slightly lower Mach number, which in hindsight would have been a better choice of design condition than M_∞ = 0.81, but was not analyzed. The pressure distribution is transferred from streamwise (3D) to normal (2D) for stability analyses by dividing by the cosine squared of the wing sweep chosen for the stability analyses (18 deg for 20 deg of leading edge sweep). For a normal Mach of 0.77 and chord Reynolds number of 26 x 10^6, the N_{TS} - N_{CF} disturbance growth trace of the gloved wing is compared to the glove section in Figure 71. The two are close, with the wing having somewhat higher cross disturbance growth, arising mostly in the 10 to 20% chord region. This is due to slightly greater crossflow velocities in the boundary layer in this region for the wing boundary layer.

The stability calculations using the wing pressures showed that the section analyses were valid, and the glove design should have the desired and useful range of TS and CF disturbance growth. The physical thickness of this final Boeing glove design is shown as a function of span at various chordwise positions in Figure 72.

Another problem to be considered in maintaining laminar flow over the glove concerned attachment line momentum thickness Reynolds number, $Re_{\theta_{a.l.}}$. Reference 12 outlines the relationship of this parameter to the boundary layer state along the attachment line. If the attachment line boundary layer is turbulent, laminar flow further back on the wing is highly unlikely. The usual criterion for the attachment line boundary layer to remain laminar is for $Re_{\theta_{a.l.}}$ to be less than 100. The boundary layer code in the A488 wing analysis system calculates the boundary layer along the attachment line, making $Re_{\theta_{a.l.}}$ available to the designer. The gloved wing has a high Reynolds number design point and rather blunt leading edge, so the state of the boundary layer along its attachment line is a valid concern. Figure 73 presents $Re_{\theta_{a.l.}}$ versus span for the gloved wing at its design point. The peak value of 93 indicates that attachment line transition at the design point will probably not be a problem. However, the turbulent boundary layer which will surely develop on the attachment line of the highly swept inboard wing should be diverted. This will eliminate the possibility of contaminating the attachment line of the gloved portion of the wing, particularly at wing sweep angles greater than 20 deg.

As outlined in this section, the use of two-dimensional design procedures to arrive at the desired wing glove design was mostly successful. A wing glove design was achieved that had the required

boundary-layer stability characteristics at its flight design condition and which also can provide useful transition data at off-design conditions. All physical constraints placed on the glove were also met. The analysis of this glove at several off-design conditions and its compatibility with the NASA-designed glove is explained in the following section.

5.5 GLOVE ANALYSES
5.5.1 Cleanup Glove

At Mach numbers greater than 0.7, the basic F-14 wing has a very favorable pressure gradient on the upper surface over much of the span. At 0.80 Mach number and 6100m (20,000 ft.) altitude, the pressure gradient slope is similar to that for P12. Therefore, it should be possible to achieve a significant run of laminar flow on a smoothed F-14 wing at low sweep angles. This possibility led to the concept of a "cleanup", or minimum modification glove, which would just be a smoothing of the basic F-14 wing. In addition, since the basic wing pressure distributions would essentially be unchanged, a preflight wind-tunnel test to check flight safety issues would not be needed. The "cleanup" glove will cover the same area of the wing as shown in Figure 56 and will be approximately 1.65 cm (0.65 in) thick. The "cleanup" glove and the other gloves will be constructed of foam and several layers of fiberglass and then smoothed with body filler and paint.

In order to verify that a 1.65-cm constant thickness glove on the wing upper surface extending to the spoiler hinge line would not appreciably change the basic F-14 wing pressures, pressure distributions were calculated for the section normal to the quarter chord at WBL256 with this additional thickness included. Analyses were conducted for section conditions that correspond to Mach numbers of 0.7 and 0.8 and altitudes of 6100m (20,000 ft) and 10 670m (35,000 ft.) (fig. 74). These conditions form the four corner points that bracket the primary flight envelope for the VSTFE. As shown in Figure 74, the clean-up glove does not significantly change the pressure distribution of the basic section.

The fairing of the glove back to the base wing occurs quickly on the lower surface from the leading edge to about 5% chord. The shape of this fairing should not be critical as long as a shock and/or serious boundary layer separation can be avoided for flight conditions of interest. The most critical conditions are at low angles of attack, which occur at high speeds and low altitudes (fig. 74a). The thickness distribution shown in Figure 75 also shows a fairing from the end of the glove at 58% chord to 76% chord. This is a fictitious fairing used only for the glove theoretical analyses, and its purpose was explained in the previous section. As shown in Figure 74a, the shock was near the spoiler hingeline for Mach numbers near 0.8. If the shock occurred on a fairing with high convex curvature, its strength could be substantially increased. A series of theoretical analyses that indicate this are shown in Figure 76. In the flight condition used for these analyses, the shock was at about 52% chord on the basic wing. The glove for these cases had only 0.64 cm (0.25 in) constant thickness. Clearly, the shock strength was increased by the ramp fairings, whereas the sharp edge termination (within 1% chord) gave the weakest shock. Although the geometry of these ramp fairings was not very accurately defined for the theoretical analyses, the results agree with the expected trend of increasing shock strength with increasing surface curvature at the shock. The flight condition will determine the shock location, so there may be conditions for which the termi-

nation of the glove will cause excessive shock strength and/or substantial separation. Terminating the glove more quickly narrows the range of conditions where the shock will occur at the fairing but increases the chance of at least local boundary layer separation. It is uncertain how this area could best be faired, but wind tunnel testing on the Mach 0.8 and Mach 0.7 glove designs should help answer this question.

The boundary layer disturbance growth for the cleanup glove was analyzed at two conditions using the CIS Method as described in Section 4.1. Since the cleanup glove and base wing were shown to have very similar pressures earlier in this section (fig. 74) base wing section analyses were used to calculate the boundary layer for the stability analyses. In order to maximize chord Reynolds number, a wing section toward the inboard of the test area was used, WBL202. The flight conditions assumed were:

	CASE 1	CASE 2
Altitude, m (ft)	7620 (25,000)	4570 (15,000)
M_∞	0.80	0.73
M_N	0.77	0.70
Aircraft weight, kg (lb)	24 950 (55,000)	24 950 (55,000)
Section c_l	0.4	0.3
Chord Reynolds No.	22×10^6	29×10^6

NOTE: Aircraft weight of 24 950 kg (55,000 lb) was revised downward to 21 770 kg (48,000 lb) after these calculations.

A wing leading edge sweep of 20 deg was assumed, and for the stability analyses a sweep of 18 deg was used as explained in Section 5.4. Figures 77 and 78 show the disturbance growth for these two cases for different frequencies, ω, in TS waves and spanwise wave numbers, $\alpha^*_{r_s}$, in CF waves. Figure 79 shows the N_{TS} - N_{CF} traces and compares them to the transition criterion from the F-111 data. At higher Mach numbers, > 0.75, the cleanup glove will be dominated by crossflow instabilities. This can provide useful data in an area not well covered by the F-111 data. At lower Mach numbers and altitudes, the early pressure recovery will promote rapid TS disturbance growth in addition to the CF disturbance. These cases may be of marginal usefulness because high accuracy in the measurement of transition location and pressure distribution will be needed to get a good correlation of transition point with calculated N-factors at transition.

5.5.2 Mach 0.8 Glove

Since NASA currently plans to fly both the Mach 0.8 and Mach 0.7 gloves simultaneously (one on each wing panel), and since it is planned to generate transition data over as broad a Mach, altitude, and sweep range as practical, pressure distributions and boundary-layer disturbance amplification factors were calculated at several flight conditions for both gloves. In particular, it was important to analyze each glove at the other glove's design condition. The two design Mach numbers along with the altitudes of 6100m (20,000 ft) and 10,670m (35,000 ft) form the corner point flight conditions of the testing envelope for 20 deg of sweep, and these are summarized below:

M_∞	h, 100m (1000 ft)	C_L	Re/m (1/ft)
0.8	61 (20)	0.20	0.98×10^6 (3.2×10^6)
0.8	107 (35)	0.385	0.59 (1.94)
0.7	61 (20)	0.255	0.84 (2.76)
0.7	107 (35)	0.50	0.50 (1.65)
Aircraft weight = 21 800 kg (48,000 lb)			

The transition locations assumed in the analyses are shown in Figure 80. Figure 81 presents analysis results at the high Mach, high altitude condition. This case was done at $M_\infty = 0.81$ in order to compare with the earlier design point analysis at $M_\infty = 0.81$, see the previous section. The relatively high lift at this high altitude condition results in a strong shock, one that may cause separation at the shock. This reinforces the conclusion reached from the design point analysis that $M_\infty = 0.81$ may be too high for testing this glove. However, the isobars and chordwise pressure gradients (figs. 69 and 81) indicate that substantial laminar flow may be obtained on this glove at Mach numbers near 0.8 and altitudes from 6100 to 10 670m (20,000 to 35,000 ft). Mach 0.7 analysis results are shown in Figures 82 and 83. The pressure peak near 5% chord would probably cause boundary layer transition, but no shocks of any consequence are seen, and the turbulent boundary layer analyses for these cases show no sign of separation. Therefore these results indicate that the Mach 0.8 glove should have no aerodynamic problems at the design Mach number of the Mach 0.7 glove. The possibility of asymmetry between the two gloves is discussed in the next section.

Boundary-layer stability characteristics and pressure distributions were also calculated at wing sweep angles of 15 and 25 deg for the Mach 0.8 glove. The stability analyses for the design condition were carried out with a pressure distribution assumed to be close to a $M_\infty = 0.8$, viscous solution (it was actually a $M_\infty = 0.81$, inviscid solution). This results in a normal Mach number of 0.77. The two off-design sweep cases analyzed were $\Lambda_{LE} = 15$ deg and 25 deg, and M_∞ was chosen to keep the normal Mach at 0.77 for each case. This was done to isolate the effect of wing sweep on

stability, eliminating pressure distribution effects as much as possible. The wing lofts of the off-design analyses were determined as follows:

(1) The planform was found by rotating the variable sweep portion of the wing about the F-14 wing pivot point.

(2) Defining sections for the new lofts were found by cutting the 20-deg (basic) loft at the appropriate angle and at the defining sections of the 20-deg loft. The new defining sections were at slightly different WBL locations than those of the basic loft due to the rotation.

(3) Slight alterations were made to the planform near the wing-strake juncture to assure a smooth transition region.

This procedure assumes that the F-14 wing can pivot to a leading edge sweep of 15 deg, which it cannot. If this sweep is to be reached in flight, the aircraft must be sideslipped, but simulating sideslip is beyond the capability of the A488 system. The conditions analyzed are given in the following table and the transition locations assumed for the analyses are shown in Figure 84.

Λ_{LE}, deg	M_∞	Re/m (1/ft)	α, deg
15	0.785	$0.98 \times 10^6 (3.2 \times 10^6)$	-0.05
25	0.82	$0.98 \times 10^6 (3.2 \times 10^6)$	-0.25

The isobar and chordwise pressure distributions for these cases are shown in Figures 85 and 86. The isobar patterns show that the large area of nearly "2D" flow (constant chord isobars) is maintained for these cases, but the chordwise pressure distributions did change somewhat, with more concavity in the midchord c_p distribution and a more rearward shock location for the higher sweep.

The boundary layer disturbance growth was analyzed using the pressure distributions from the nominal WBL202 section, after translating them to "normal" (2D) values. Figure 87 compares the normalized pressure distributions for the design sweep of 20 deg and the off-design sweep cases. Instability growth traces for these three cases are shown in Figure 88. As expected, the higher sweep case is dominated by crossflow instabilities and may have very little laminar flow. The lower sweep case may have laminar flow until the adverse gradient is reached. This illustrates the great range of N-factors that can be generated by varying the sweep of an appropriately designed wing.

With regard to attachment-line contamination, $Re_{\theta_{a.l.}}$ is presented for the three wing sweep angles in Figure 89. The higher sweep does cause $Re_{\theta_{a.l.}}$ to exceed 100 at this high unit Reynolds number. This does not necessarily mean an attachment line transition problem exists, but it does reinforce the need to ensure that there is no contamination from the inboard region onto the test panel.

5.5.3 Mach 0.7 Glove

The NASA-designed glove for the VSTFE program was designed to operate primarily at $M_\infty = 0.7$. The geometry necessary to meet the design requirements and physical constraints made it questionable whether this glove could be flown at the Mach 0.8 glove design condition. The Mach 0.7 glove wing definition was analyzed by the same procedure used for the Mach 0.8 glove, and the coordinates of its defining sections are given in Appendix 2. Figure 90 compares the section shapes of the two gloves and the base wing at WBL200. Analyses of the Mach 0.7 glove were carried out in the A488 system with the inboard wing and fuselage modeling identical to that used for the Mach 0.8 glove. The low altitude, 6100m (20,000 ft), high speed ($M_\infty = 0.8$) analysis of the Mach 0.7 glove yielded pressures that are shown in Figure 91. Transition locations assumed for the analyses are shown in Figure 92. The isobar pattern typical of the clean wing is repeated, but a strong shock is generated at or near the termination of the glove. The A488 results indicate minor separation at the shock for this case, even with a smooth fictitious fairing from the end of the glove back to near 90% chord. Since the Mach 0.7 glove is about an inch thick just ahead of the spoilers, the condition of the boundary layer through this region where the glove is abruptly fared back into the wing will be precarious, even without a shock in this area. The Mach 0.7 glove was not analyzed at the higher lift case for $M_\infty = 0.8$ (simulating h = 10 700m (35,000 ft) because excessive shock strengths would have seriously affected the accuracy of the results. Both $M_\infty = 0.7$ flight condition corner points were analyzed for the Mach 0.7 glove. Pressure results are shown in Figures 93 and 94. The Mach 0.7 glove design condition of a nearly flat c_p distribution in the midchord region was met at the higher altitude condition from WBL225 through 290, although the isobars for that condition do not follow constant chord lines as well as for the lower lift case. At the lower altitude (fig. 93), the glove has moderate favorable pressure gradients ($\cong$ -0.6) over much of the span.

Attachment line $Re_{\theta_{a.l.}}$ was examined for the two Mach 0.7 glove analyses at the higher unit Reynolds number conditions (the lower altitude cases). The $Re_{\theta_{a.l.}}$ variation along the span plotted in Figure 95 shows that attachment line transition is less of a concern for the Mach 0.7 glove than for the Mach 0.8 glove.

Boundary layer disturbance growth was examined for the Mach 0.7 glove at three conditions to assess its operating range and usefulness in obtaining transition data. The conditions were:

M_∞	M_N	h, m (ft)	WBL	Re_{c_N}	Sweep, deg
0.8	0.77	6100 (20,000)	202	26×10^6	18
0.7	0.67	6100 (20,000)	202	22×10^6	18
0.7	0.67	10 700 (35,000)	256	11.2×10^6	18

The disturbance growth traces for these three cases are shown in Figure 96. At Mach numbers near 0.8 the Mach 0.7 glove shows disturbance growth similar to the clean wing at that Mach number and is dominated by crossflow instability. Near its design point the Mach 0.7 glove shows the predominance of TS disturbances, which are to be expected for a nearly flat midchord pressure distribution. At conditions that produce pressure distributions with a moderate negative gradient, the Mach 0.7 and Mach 0.8 gloves can produce moderate growth in both instability modes. The

difference between the two gloves is the flight-sweep conditions at which a particular growth characteristic occurs.

In applying the Mach 0.7 and Mach 0.8 gloves to the basic F-14 wing, there was considerable freedom left to the designer after considering the geometric constraints and meeting the design objectives. This made it probable that asymmetries present when flying both glove panels together would require control deflections to trim the aircraft. The most likely asymmetry would be an effective wing incidence change, leading to a lift difference between the two gloves when flying at the same angle of attack, creating a rolling moment. The characteristics of the F-14 dictated that a 0.01 rolling moment could be tolerated before control deflections might compromise the pressure distributions in the laminar flow test areas. This constraint on asymmetry was checked by analyzing both gloves at the same angle of attack and comparing the rolling moment of one side of the configuration. The three cases analyzed for the Mach 0.7 glove were done at the same angle of attack as for the Mach 0.8 glove. The results were:

M_∞	h, m (ft)	α, deg	Difference in rolling moment
0.8	6100 (20,000)	-0.15	0.0001
0.7	6100 (20,000)	0.70	0.0005
0.7	10 700 (35,000)	2.95	0.0007

Considering the accuracy of the analysis system, these results indicate no significant rolling moment asymmetry for these two gloves. This conclusion would change if the aircraft were flown at a condition that caused one glove to have much more separation than the other. This situation might arise if the Mach 0.7 glove is flown at conditions where its shock is very strong.

The off-design analyses described in this section show that both Mach 0.7 and Mach 0.8 glove designs for the VSTFE meet their respective design objectives and perform well at most off-design conditions. Both gloves are capable of generating boundary layer disturbance growth which covers a wide range of interest for laminar flow research. There is very little asymmetry anticipated in flying both gloves simultaneously on the F-14, although the Mach 0.7 glove may be Mach limited due to a strong shock development at Mach numbers approaching 0.8.

This Page Intentionally Left Blank

6.0 CONCLUSIONS

NASA has initiated the Variable Sweep Transition Flight Experiment (VSTFE) to establish a boundary layer transition data base for laminar-flow wing design. The Boeing Company is under contract to NASA to provide design and analyses support for the program. This report documents the results of two initial tasks: a parametric pressure distribution/boundary-layer stability study and the design of an upper surface glove for Mach 0.8. Analyses were also conducted on the "clean-up" glove (smoothed basic wing) and a glove designed by the NASA Langley Research Center for Mach 0.7. Based on the results of the analyses contained herein, the following conclusions were reached:

1. The parametric pressure distribution/boundary-layer stability study provides a matrix of pressure distributions, sweep angles, and Reynolds numbers that generates a broad spectrum of Tollmien-Schlichting (TS) and crossflow (CF) disturbance growth combinations. Several general conclusions can be derived from the results of the study:

   - Of the two stability analysis methods used, the compressible irrotational stationary (CIS) method was considered superior and was used in the glove design task.

   - Decreasing the pressure gradient in the midchord region of a swept wing tends to suppress TS disturbances but promote CF disturbances. Therefore, a good wing design will probably require compromises to have good overall laminar flow, Mach, and lift capability.

   - Increasing Mach number tends to suppress TS disturbances and to promote CF disturbance growth if pressure distributions, Reynolds number, and sweep are held constant.

2. The Boeing A488 transonic flow analysis system can accurately predict the pressures on the pivoting part of the F-14 wing.

3. The "clean-up" glove will provide useful transition data in which cross-flow instabilities will predominate.

4. At the design point of 20 deg of sweep and 6 100m (20,000 ft) altitude, the design pressure distribution of the Mach 0.8 glove has a midchord gradient of about -0.6, and this was achieved over much of the F-14 variable sweep outer wing panel.

5. Analyses at off-design conditions indicate the midchord pressure gradient will be reduced to about -0.45 at 10 700m (35,000 ft) and Mach 0.8, and, as expected, the glove will tend to generate pressure distributions with leading-edge peaks at Mach 0.7. In addition, a +5 deg increment in sweep should not significantly change the pressure distributions if the Mach number is also changed.

6. Analysis of the Mach 0.7 glove indicates that the midchord pressure gradient will vary from about -0.6 at 6 100m altitude to essentially 0.0 at an altitude of 10 700m for Mach 0.7. At Mach 0.8, the pressure distributions will have much steeper favorable pressure gradients (similar to the basic wing) over this altitude range.

7. Both the Mach 0.7 and Mach 0.8 gloves will provide good coverage of TS and CF disturbance growth combinations, and transition on both gloves should occur ahead of the adverse gradient for many conditions.

8. Based on calculation of the attachment line momentum thickness Reynolds number ($Re_{\theta_{a.l.}}$) attachment line contamination should not be a problem for either glove at 20 deg of sweep, however, the calculations indicate that the ($Re_{\theta_{a.l.}}$'s) will exceed the critical value of 100 at 25 deg of sweep for both gloves. Therefore, some form of protection against attachment-line contamination (i.e., Gaster bump) should be considered.

9. The asymmetry that will result from flying the Mach 0.7 and Mach 0.8 gloves concurrently (one on each wing panel) is well within the rolling-moment control authority of the differentially actuated horizontal tail.

10. The possibility of strong shocks causing excessive flow separation on the Mach 0.7 glove at Mach 0.8 is a concern that could not be addressed adequately with existing transonic analysis codes.

11. The fairing of the gloves back to the basic wing, both on the lower surface and just ahead of the spoilers on the upper surface, must be done carefully to prevent excessively strong shocks and minimize boundary layer separation. These areas need to be carefully monitored during the wind-tunnel testing of the gloves.

7.0 REFERENCES

1. Runyan, L. James, Navran, Brent H., and Rozendaal, Roger A., "F-111 Natural Laminar Flow Glove Flight Test Data Analysis and Boundary Layer Stability Analysis," NASA CR-166051, January 1984.

2. Boeing Commercial Airplane Company, "Hybrid Laminar Flow Control Study, Final Technical Report," NASA CR-165930, October 1982.

3. Waggoner, E. G., Campbell, R. L. and Phillips, P. S., "Computational Wing Design in Support of an NLF Variable Sweep Transition Flight Experiment," AIAA Paper 85-4074, 1985.

4. Mack, L. M., "Computation of the Stability of the Laminar Compressible Boundary Layer," Methods in Computational Physics, edited by B. Adler, Academic Press, N.Y., 1965, pp. 247-299.

5. Caughey, D. A. and Jameson, A., "Recent Progress in Finite Volume Calculations for Wing Fuselage Combinations," AIAA Paper 79-1513, July 1979.

6. McLean, J. D. and Randall, J. L., "Computer Program To Calculate Three-Dimensional Boundary Layer Flows Over Wings With Wall Mass Transfer," NASA CR-3123, February 1979.

7. Derbyshire, T. and Sidwell, K. W., "PAN AIR Summary Document, (Version 1.0)", NASA CR-3250, 1982.

8. Mack, L. M., "On the Stability of Boundary Layer on a Transonic Swept Wing," AIAA 17th Aerospace Sciences Meeting Paper 79-0264, New Orleans, La., January 15-17, 1979.

9. Yu, N. J., "Transonic Flow Simulations for Complex Configurations With Surface-Fitted Grids," AIAA Paper 81-1258, 1981.

10. Moes, T. R. and Myer, R. R., "In-Flight Wing Pressure Distributions for the F-14A," NASA TM-85921, June 1985.

11. Boppe, C. W. and Rosen, B. S., "F-14A Aircraft High-Speed Flow Simulations," NASA CR-172559, April 1985.

12. Pfenninger, W., "Flow Problems of Swept Low-Drag Suction Wings of Practical Construction at High Reynolds Numbers, Annals of the N.Y. Academy of Sciences, Vol. 154, Art.2, November 1968, pp. 672-703.
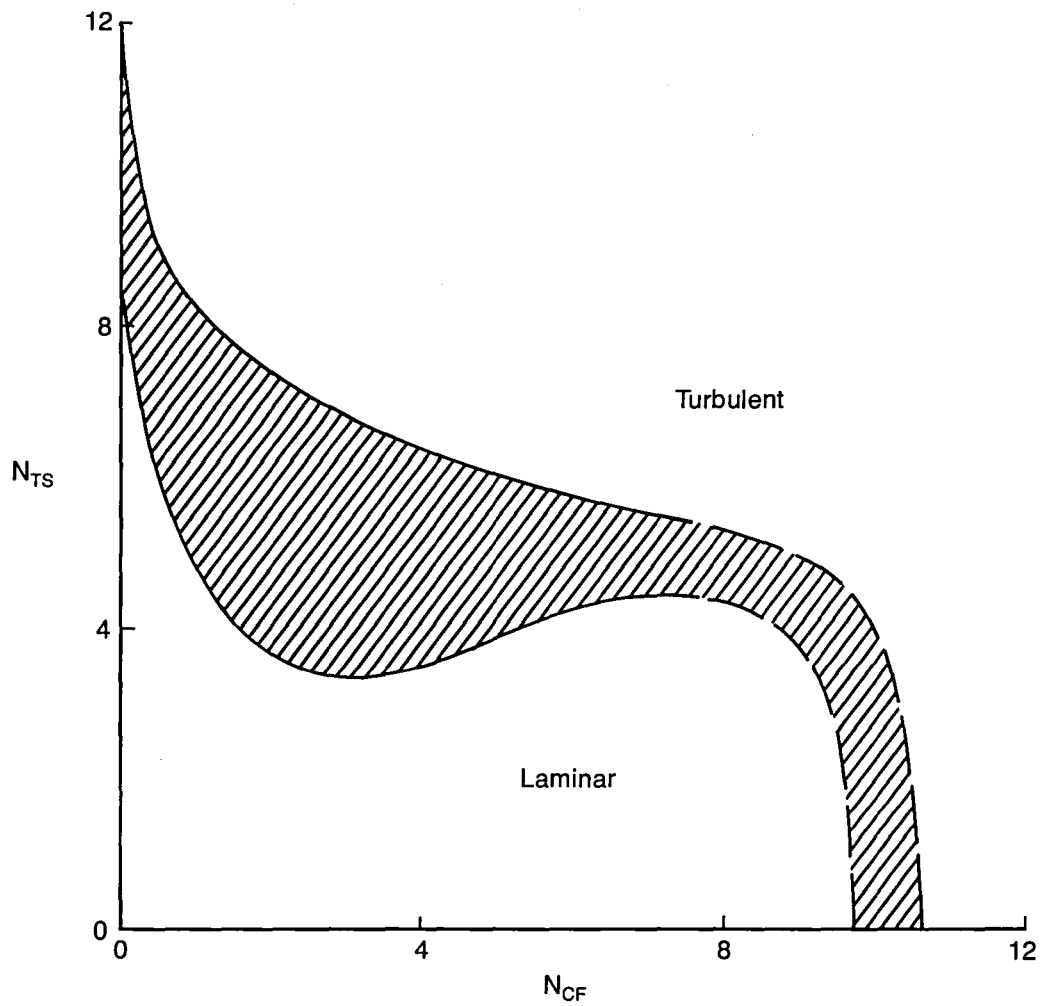
Figure 1. Boundary Layer Transition Criterion Based on F-111 Data

Figure 2. Pressure Distributions Used in the Parametric Study
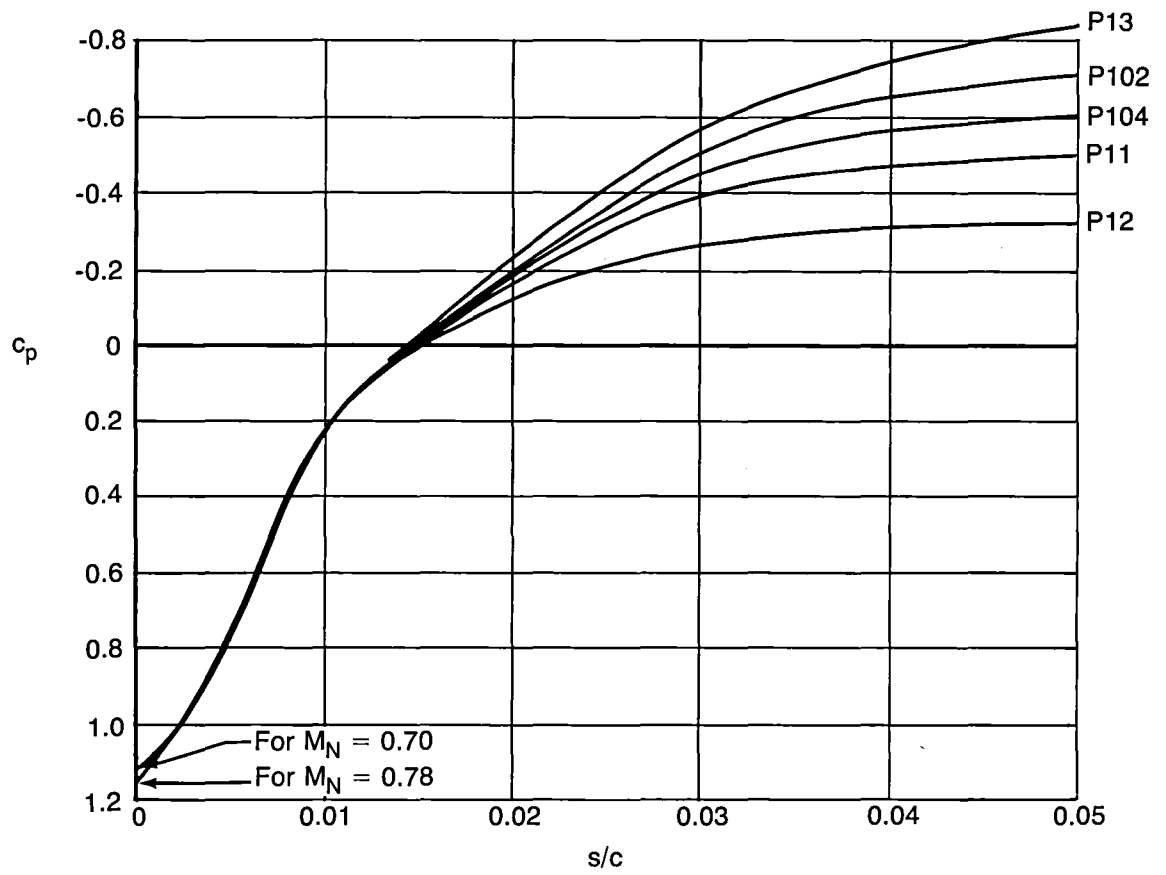
Figure 3. Leading Edge Detail of Pressure Distributions

- P104
- $Re_{c_N} = 15 \times 10^6$
- $\Lambda = 15$ deg
- $M_N = 0.78$

——— Incompressible
— — — Compressible (factored)

Tollmien-Schlichting

$\Psi = 0$ deg
ω^*, Hz
3525
4420
5314
7077
9989

(graph labels: 7077 Hz, 4420 Hz)

N_{TS} axis: 0, 2, 4, 6, 8, 10
s/c axis: 0, 0.2, 0.4, 0.6

Crossflow

$\Psi = 85.6$ deg
ω^*, Hz
791
1108
1488
2089
3482
5001

(graph labels: 3482 Hz, 1488 Hz)

N_{CF} axis: 0, 2, 4
s/c axis: 0, 0.2, 0.4, 0.6

Figure 4. Stability Analyses for Pressure P104, FICA Method, $Re_{c_N} = 15 \times 10^6$, $\Lambda = 15$ deg

- P104
- $Re_{c_N} = 15 \times 10^6$
- $\Lambda = 20$ deg
- $M_N = 0.78$
———— Incompressible
— — — Compressible (factored)

Tollmien-Schlichting

$\Psi = 0$ deg
ω^*, Hz
2 994
4 010
5 025
6 197
10 051

6197 Hz   5025 Hz

Crossflow

$\Psi = 85.6$ deg
ω^*, Hz
737
1261
2113
2948
3685

3685 Hz   2113 Hz

Figure 5. Stability Analyses for Pressure P104, FICA Method, $Re_{c_N} = 15 \times 10^6$, $\Lambda = 20$ deg

- P104
- $Re_{c_N} = 15 \times 10^6$
- $\Lambda = 25$ deg
- $M_N = 0.78$

———— Incompressible

— — — Compressible (factored)

Tollmien-Schlichting

N_{TS}

4140 Hz

6704 Hz

$\Psi = 0$ deg

ω^*, Hz
3 098
4 140
5 369
6 704
10 337

Crossflow

N_{CF}

805 Hz

2397 Hz

$\Psi = 85.6$ deg

ω^*, Hz
805
1096
1370
2397
2996
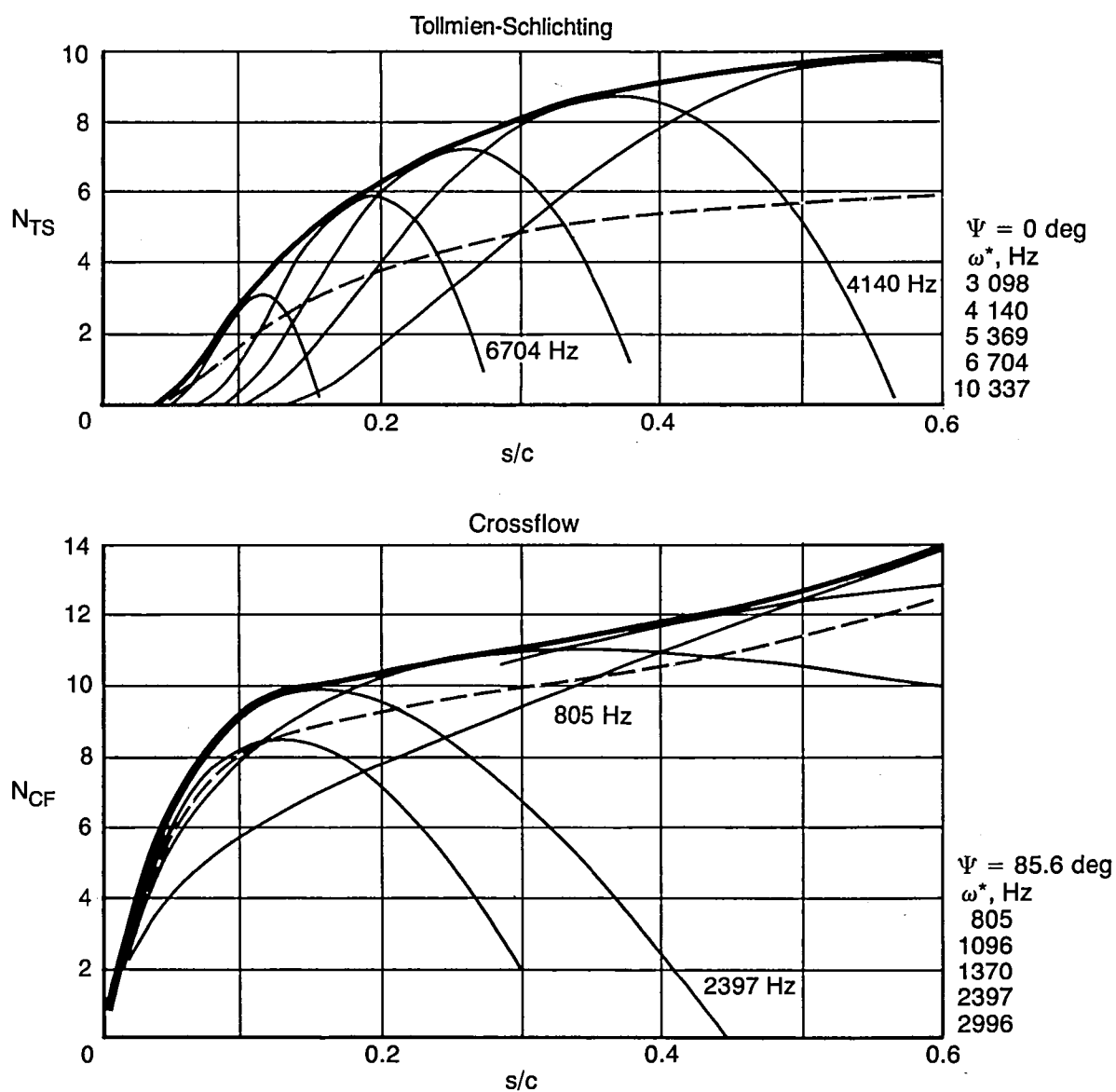
Figure 6. Stability Analyses for Pressure P104, FICA Method, $Re_{c_N} = 15 \times 10^6$, $\Lambda = 25$ deg

- P104
- $Re_{c_N} = 30 \times 10^6$
- $\Lambda = 15$ deg
- $M_N = 0.78$

——— Incompressible
— — — Compressible (factored)

Tollmien-Schlichting

N_{TS}

2631 Hz

3960 Hz

$\Psi = 0$ deg
ω^*, Hz
1584
2095
2631
3960
5288
7051

Crossflow

N_{CF}

886 Hz

1189 Hz

$\Psi = 85.6$ deg
ω^*, Hz
491
696
886
1189
1582
1978
2706

s/c
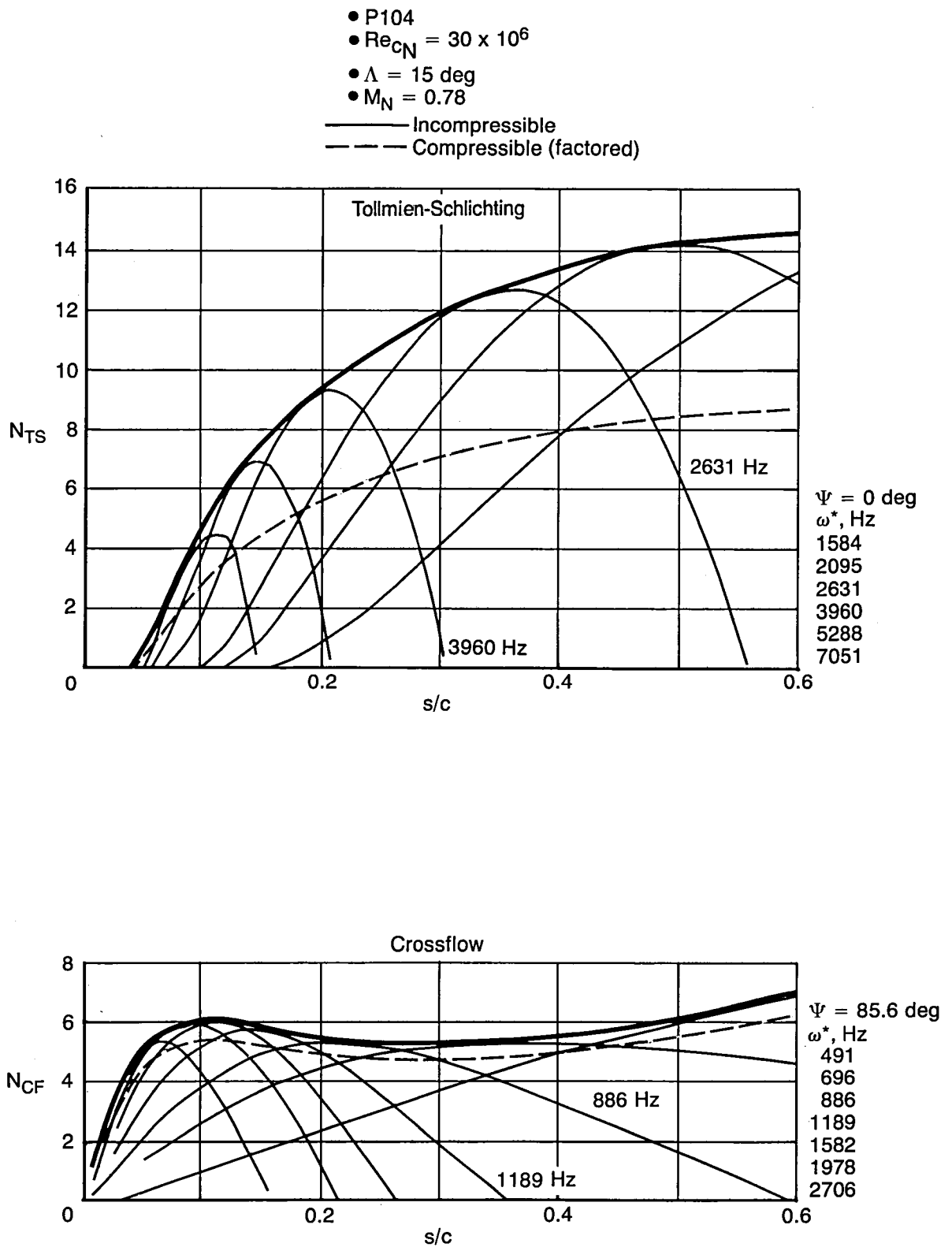
Figure 7. Stability Analyses for Pressure P104, FICA Method, $Re_{c_N} = 30 \times 10^6$, $\Lambda = 15$ deg

Figure 8. Stability Analyses for Pressure P104, FICA Method, $Re_{c_N} = 30 \times 10^6$, $\Lambda = 20$ deg

Figure 9. Stability Analyses for Pressure P102, FICA Method, $Re_{c_N} = 15 \times 10^6$, $\Lambda = 15$ deg

- P102
- $Re_{c_N} = 15 \times 10^6$
- $\Lambda = 20$ deg
- $M_N = 0.78$
——— Incompressible
— — — Compressible (factored)

Tollmien-Schlichting

N_{TS}

4118 Hz

6364 Hz

$\Psi = 0$ deg
ω^*, Hz
3 075
4 118
5 160
6 364
7 754
9 118
10 321

s/c

Crossflow

N_{CF}

1261 Hz

2113 Hz

$\Psi = 85.6$ deg
ω^*, Hz
737
999
1261
2113
2948
3685

s/c

Figure 10. Stability Analyses for Pressure P102, FICA Method, $Re_{c_N} = 15 \times 10^6$, $\Lambda = 20$ deg

43

Figure 11. Stability Analyses for Pressure P102, FICA Method, $Re_{c_N} = 15 \times 10^6$, $\Lambda = 25$ deg
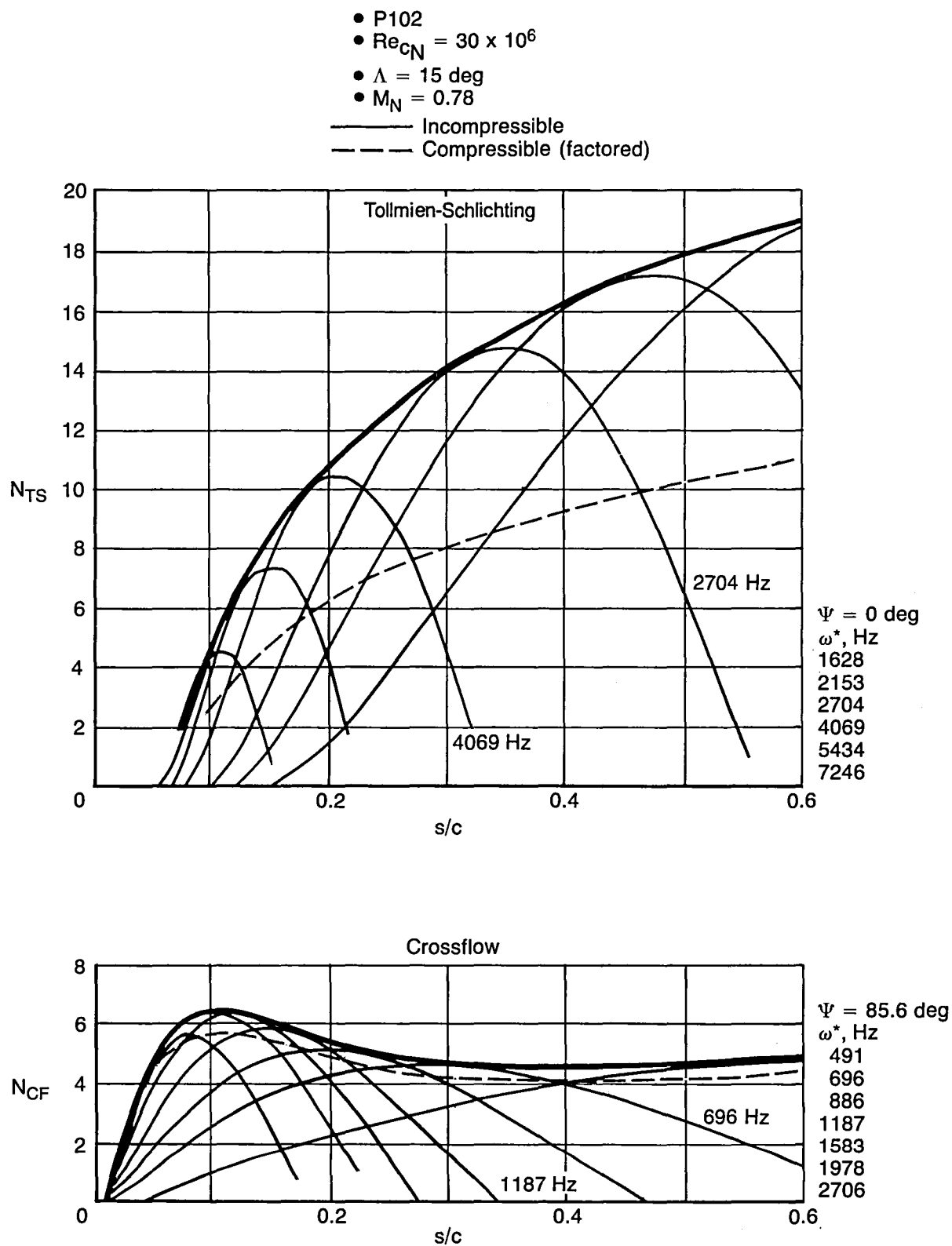
Figure 12. Stability Analyses for Pressure P102, FICA Method, $Re_{c_N} = 30 \times 10^6$, $\Lambda = 15$ deg
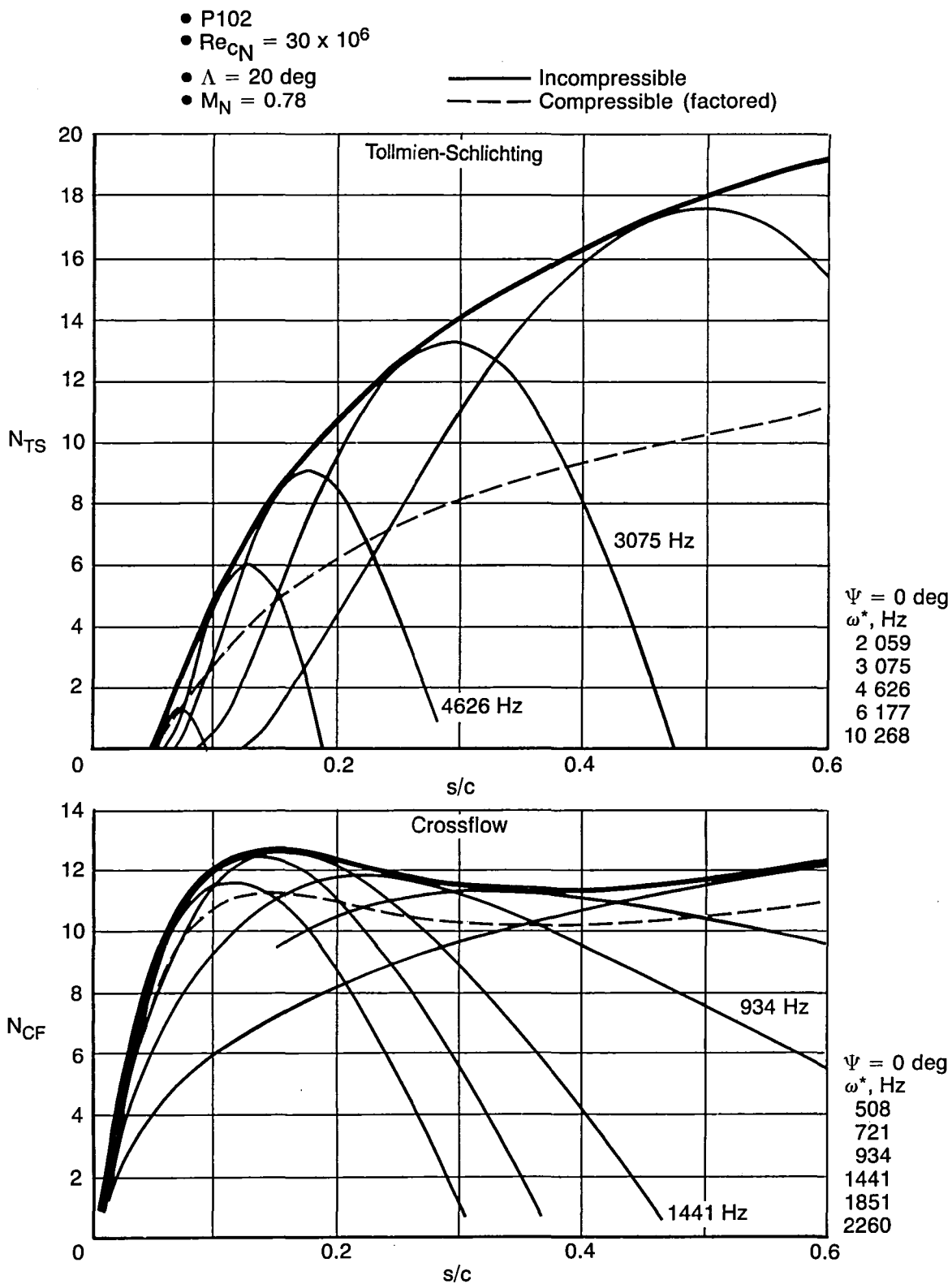
Figure 13. Stability Analyses for Pressure P102, FICA Method, $Re_{c_N} = 30 \times 10^6$, $\Lambda = 20$ deg

- P102
- $Re_{c_N} = 15 \times 10^6$
- $\Lambda = 15$ deg.
- $M_N = 0.78$
- Compressible
- No dissipation

Tollmien-Schlichting

N_{TS}

4042 Hz

6248 Hz

$\Psi = 40$ deg
ω^*, Hz
3 000
4 042
6 248
7 586
8 952
10 000

s/c

Crossflow – Extrapolation Technique Used

N_{CF}

400

250

$\omega^* = 0$ Hz

α_{rs}^* values
from 250 to 1600

s/c

Figure 14. Stability Analyses for Pressure P102, CIS Method, $Re_{c_N} = 15 \times 10^6$, $\Lambda = 15$ deg

- P102
- $Re_{c_N} = 15 \times 10^6$
- $\Lambda = 20$ deg
- $M_N = 0.78$
- Compressible
- No dissipation

Tollmien-Schlichting

N_{TS}

8
6
4
2
0

6230 Hz

4037 Hz

0.2   0.4   0.6
s/c

$\Psi = 40$ deg
ω^*, Hz
3 000
3 676
4 037
5 067
6 230
7 593
8 930
10 000

Crossflow – Extrapolation Technique Used

N_{CF}

4

3

2

1

0

400

300

0.2   0.4   0.6
s/c

$\omega^* = 0$ Hz

α^*_{rs} values
from 300 to 1400

Figure 15. Stability Analyses for Pressure P102, CIS Method, $Re_{c_N} = 15 \times 10^6$, $\Lambda = 20$ deg

- P102
- $Re_{c_N} = 15 \times 10^6$
- $\Lambda = 25$ deg
- $M_N = 0.78$
- Compressible
- No dissipation

Tollmien-Schlichting

$\Psi = 40$ deg
ω^*, Hz
3 074
4 138
5 289
6 385
7 783
10 025

5289 Hz

4138 Hz

Crossflow

300

200

$\omega^* = 0$ Hz

$\alpha^*_{r_s}$ values
from 150 to 1600

Figure 16. Stability Analyses for Pressure P102, CIS Method, $Re_{c_N} = 15 \times 10^6$, $\Lambda = 25$ deg
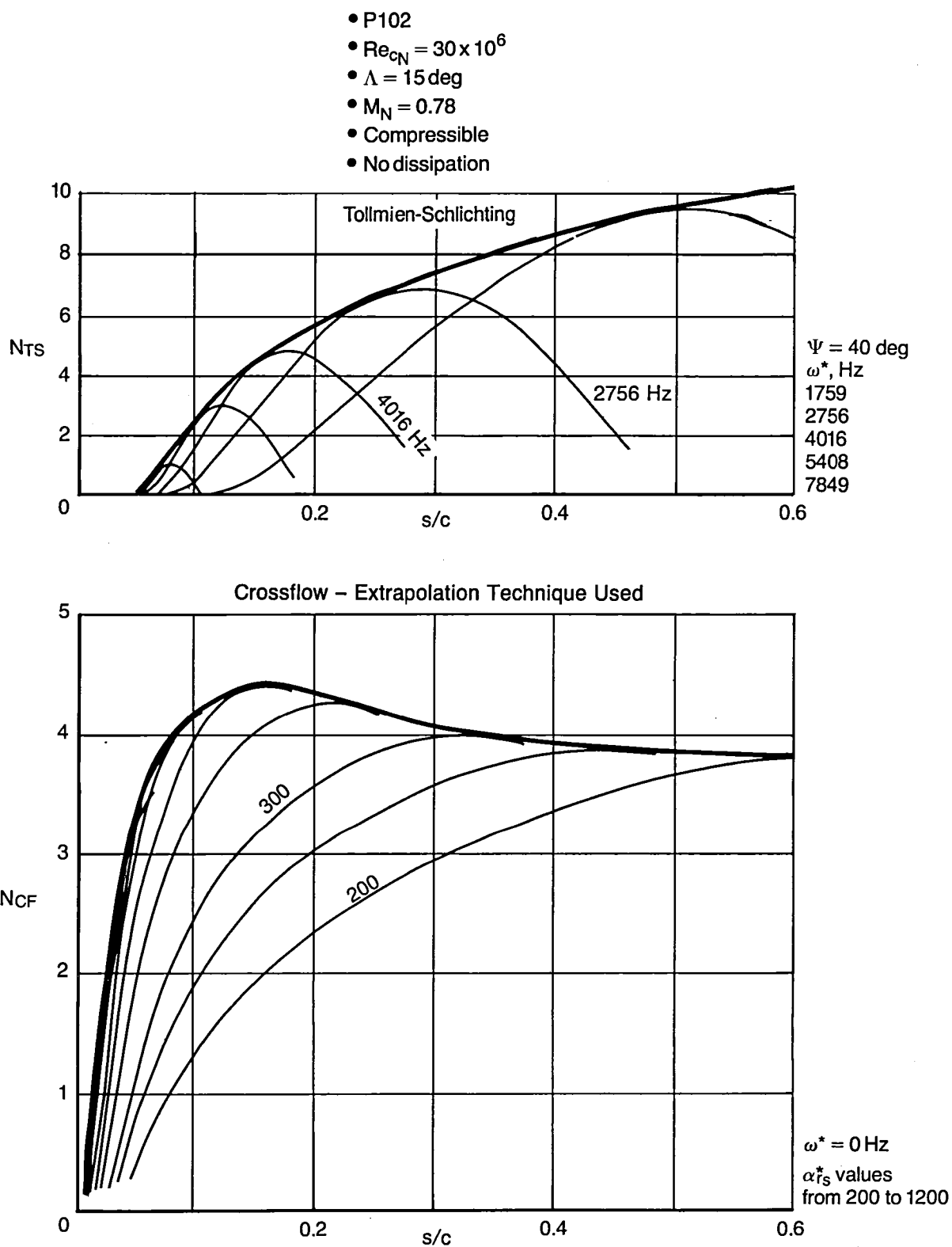
Figure 17. Stability Analyses for Pressure P102, CIS Method, $Re_{c_N} = 30 \times 10^6$, $\Lambda = 15$ deg

- P102
- $Re_{c_N} = 30 \times 10^6$
- $\Lambda = 20$ deg
- $M_N = 0.78$
- Compressible
- No dissipation

Tollmien-Schlichting

N_{TS}

2807 Hz

4091 Hz

$\Psi = 40$ deg
ω^*, Hz
1791
2807
4091
5508

Crossflow

N_{CF}

250

150

$\omega^* = 0$ Hz

α^*_{rs} values
from 150 to 1600
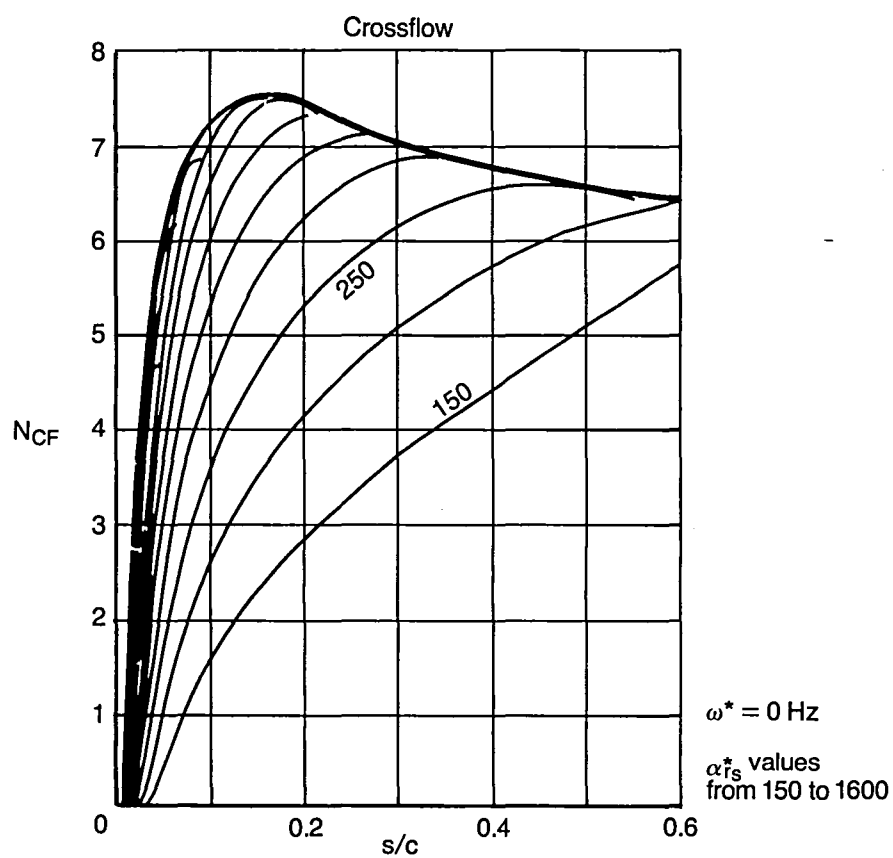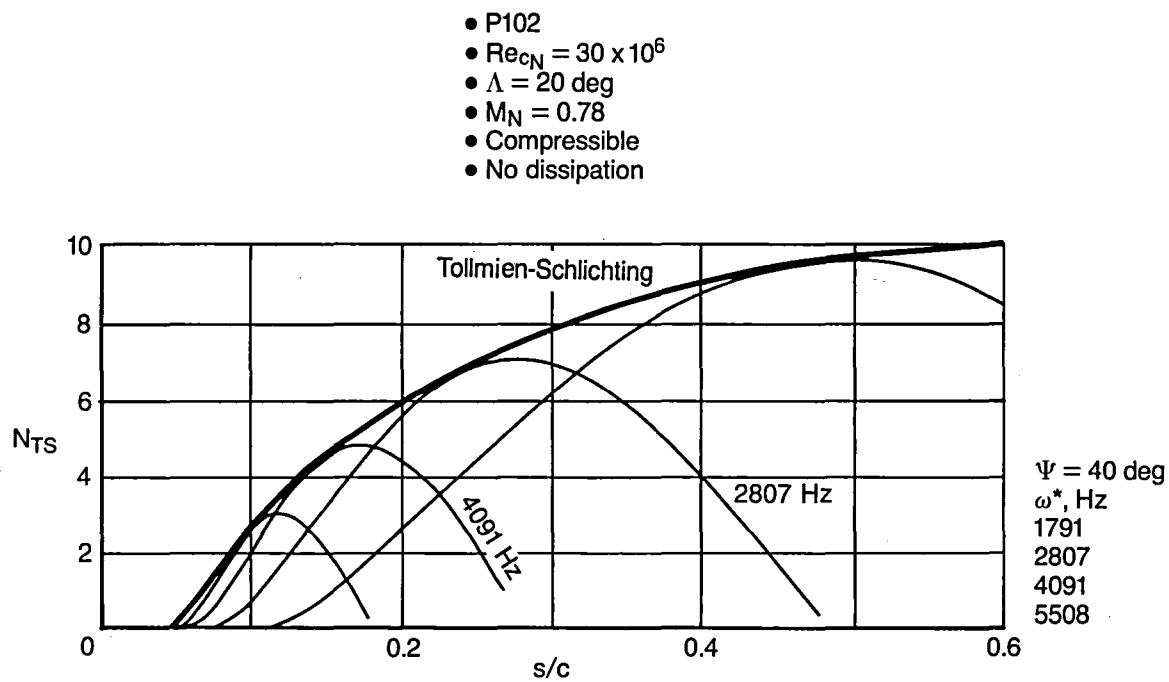
Figure 18. Stability Analyses for Pressure P102, CIS Method, $Re_{c_N} = 30 \times 10^6$, $\Lambda = 20$ deg

- P11
- $Re_{c_N} = 15 \times 10^6$
- $\Lambda = 15$ deg
- $M_N = 0.78$
- Compressible
- No dissipation

Figure 19. Stability Analyses for Pressure P11, CIS Method, $Re_{c_N} = 15 \times 10^6$, $\Lambda = 15$ deg
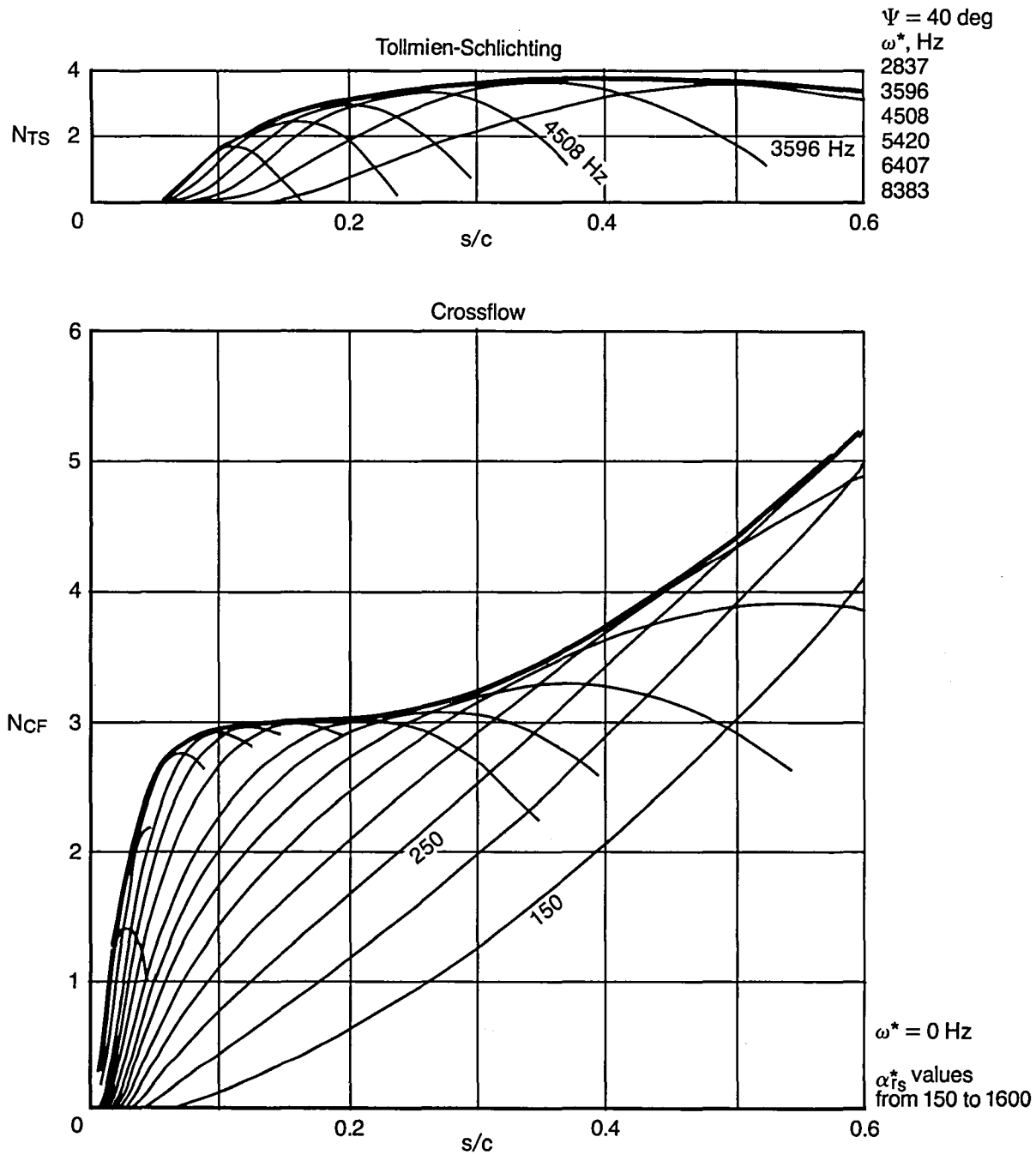
Figure 20. Stability Analyses for Pressure P11, CIS Method, $Re_{c_N} = 15 \times 10^6$, $\Lambda = 20$ deg

- P11
- $Re_{c_N} = 15 \times 10^6$
- $\Lambda = 25$ deg
- $M_N = 0.78$
- Compressible
- No dissipation

Tollmien-Schlichting

$\Psi = 40$ deg
ω^*, Hz
2913
3693
4629
5565
6580

Crossflow – Extrapolation Technique Used

$\omega^* = 0$ Hz

α^*_{rs} values
from 200 to 1400
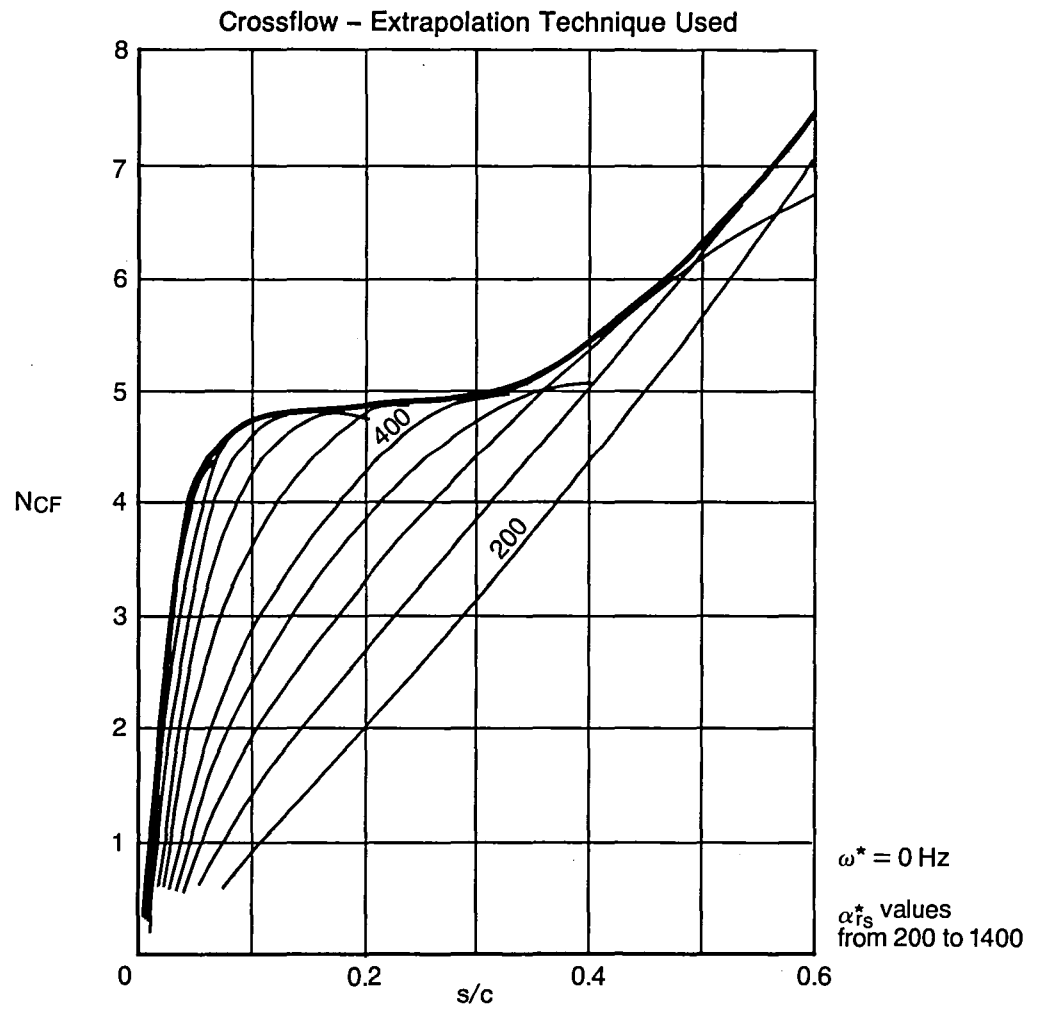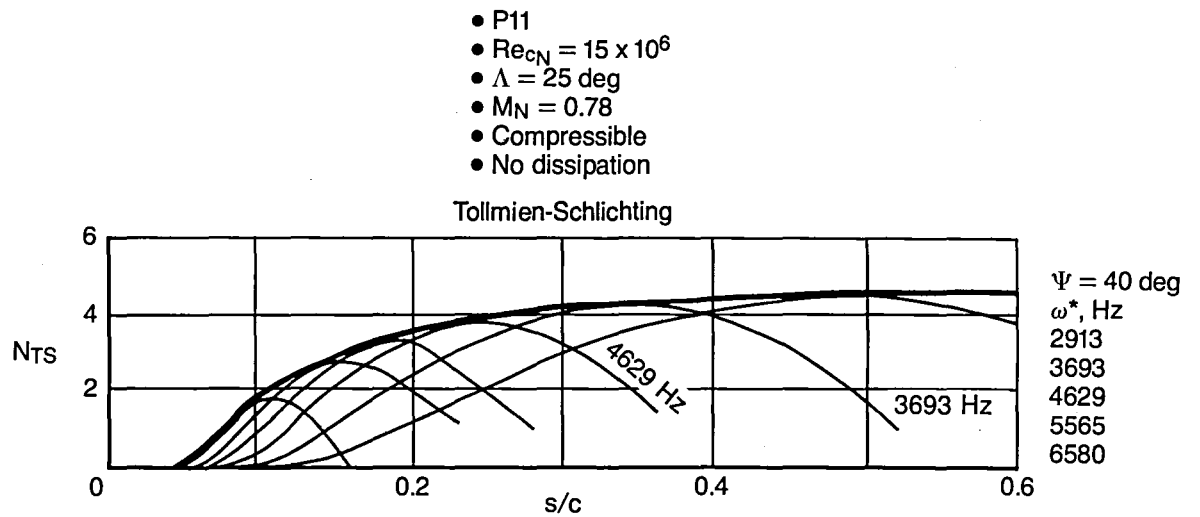
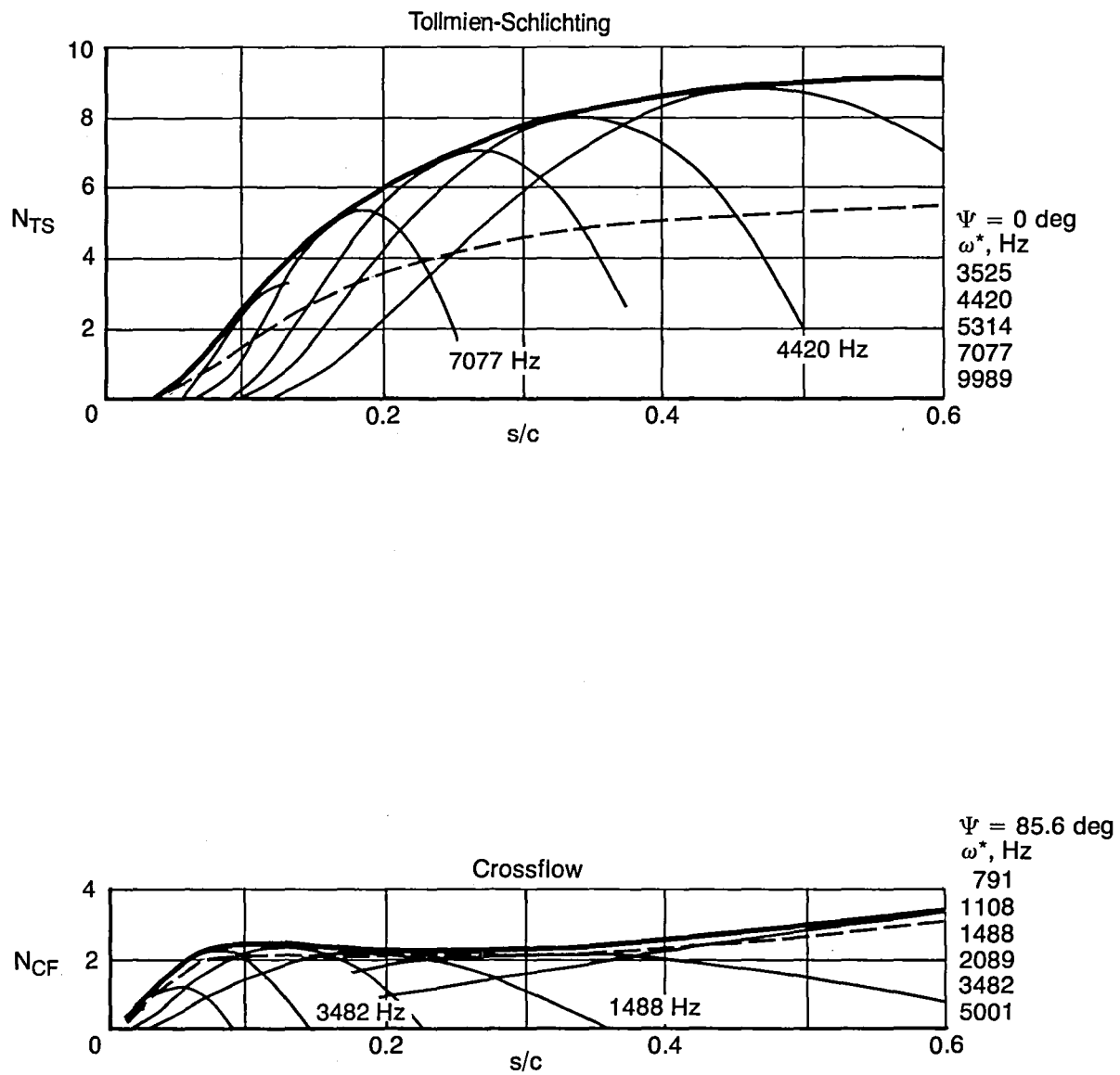*Figure 21. Stability Analyses for Pressure P11, CIS Method, $Re_{c_N} = 15 \times 10^6$, $\Lambda = 25$ deg*

- P11
- $Re_{c_N} = 30 \times 10^6$
- $\Lambda = 15$ deg
- $M_N = 0.78$
- Compressible
- No dissipation

Tollmien-Schlichting

$\Psi = 40$ deg
ω^*, Hz
1500
1912
2880
4047
5115
7000

Crossflow

$\omega^* = 0$ Hz

$\alpha_{r_s}^*$ values
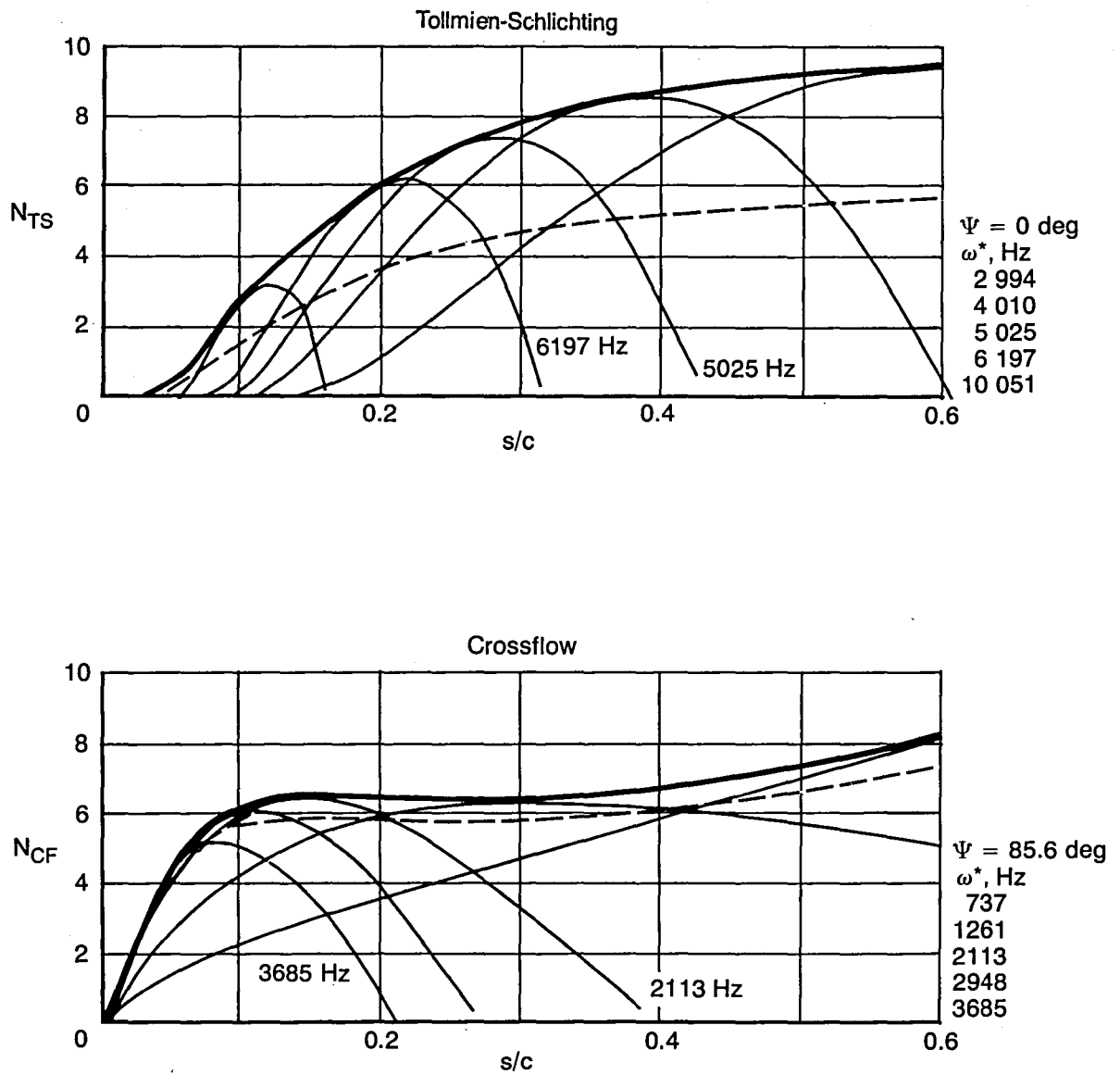from 150 to 1600
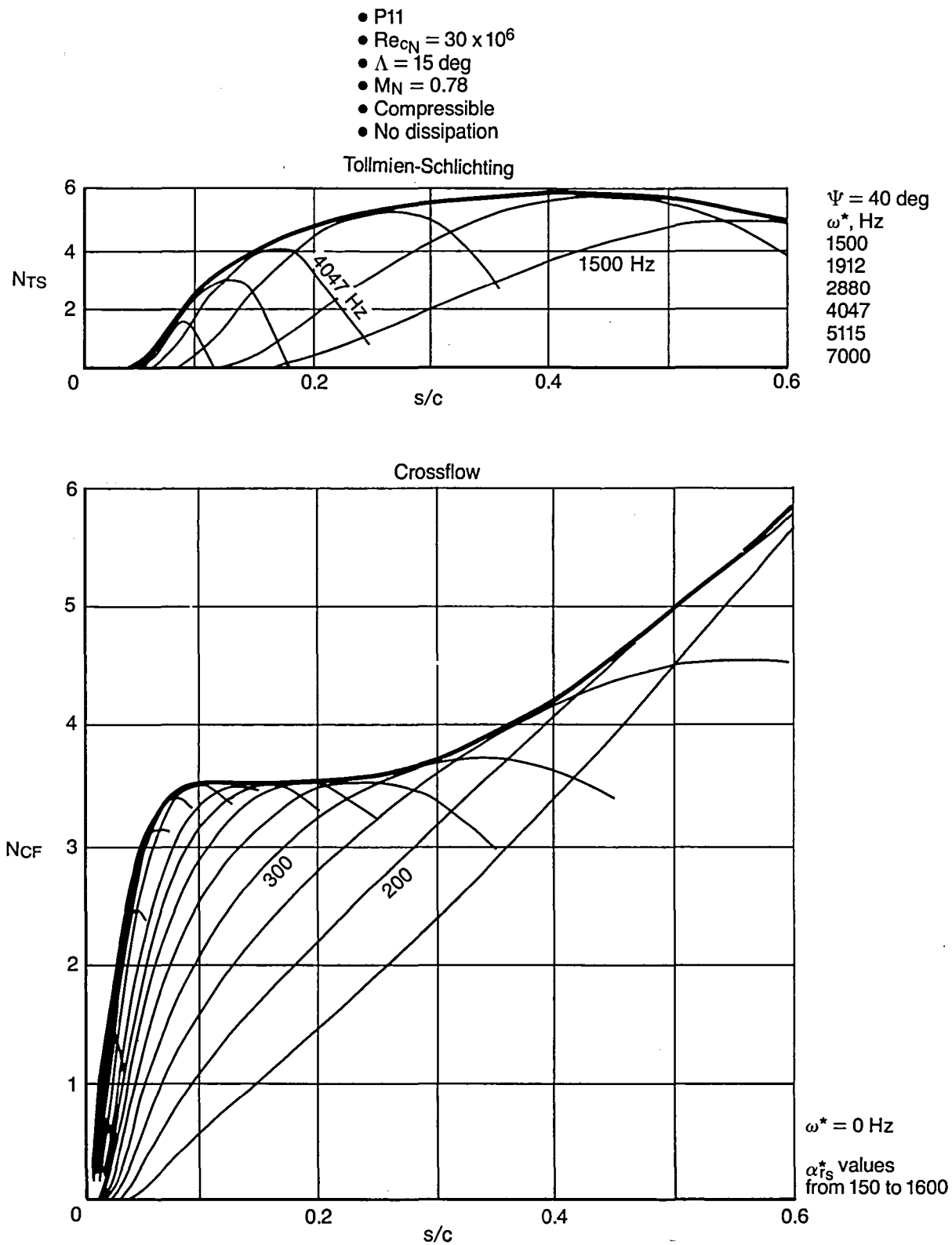
Figure 22. Stability Analyses for Pressure P11, CIS Method, $Re_{c_N} = 30 \times 10^6$, $\Lambda = 15$ deg

- P11
- $Re_{c_N} = 30 \times 10^6$
- $\Lambda = 20$ deg
- $M_N = 0.78$
- Compressible
- No dissipation

Tollmien-Schlichting

$\Psi = 40$ deg
ω^*, Hz
1530
1950
2938
4128
5217
6990

Crossflow – Extrapolation Technique Used

$\omega^* = 0$ Hz

α_{rs}^* values
from 150 to 1600
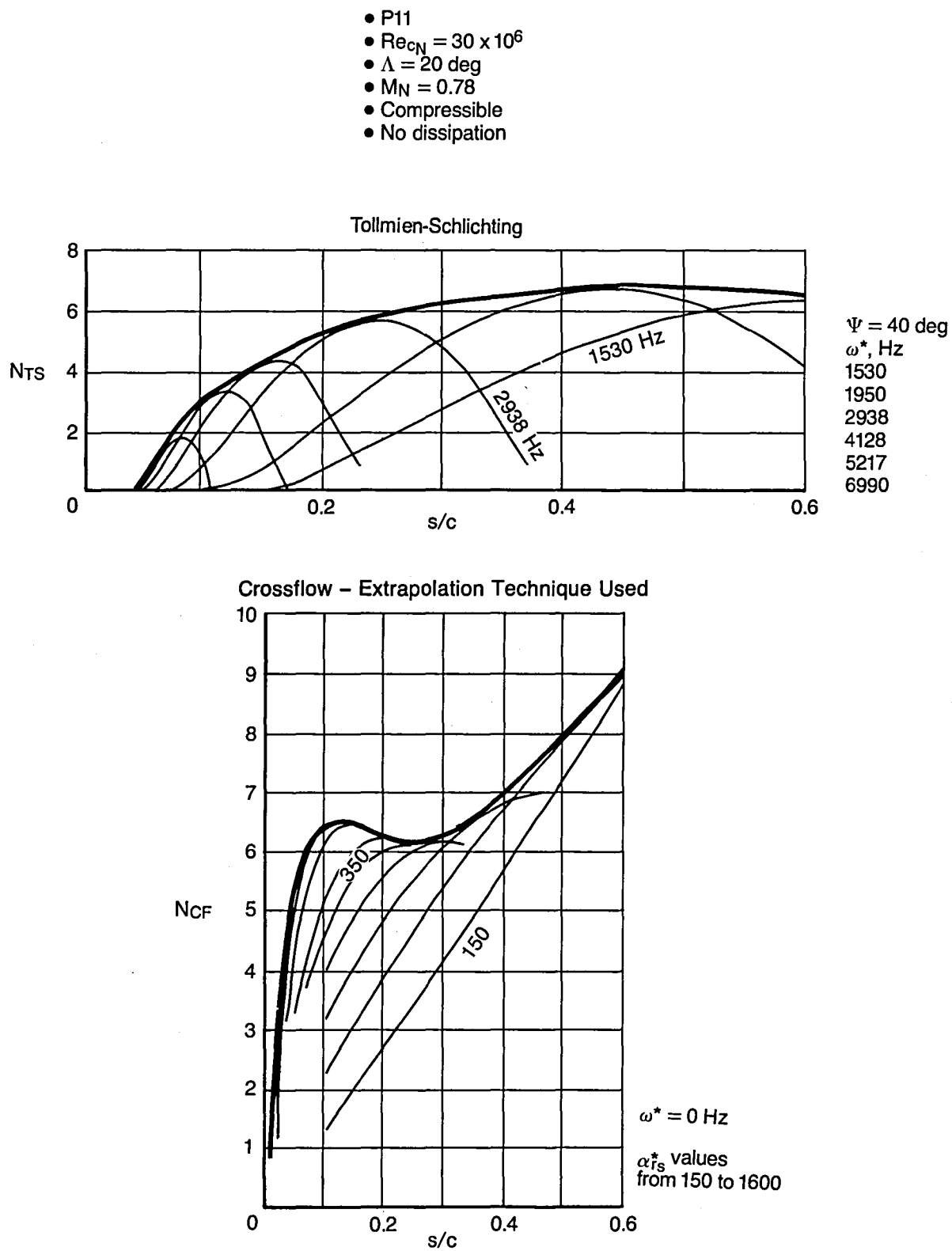
Figure 23. Stability Analyses for Pressure P11, CIS Method, $Re_{c_N} = 30 \times 10^6$, $\Lambda = 20$ deg

56

- P12
- $Re_{c_N} = 15 \times 10^6$
- $\Lambda = 15$ deg
- $M_N = 0.78$
- Compressible
- No dissipation

$\Psi = 40$ deg

ω^*, Hz

3001
3694
5494
6603
8496

Tollmien-Schlichting

6603 Hz

3001 Hz

Crossflow – Extrapolation Technique Used

$\omega^* = 0$ Hz

$\alpha \bar{r}_s$ values
from 175 to 1400

350

175

Figure 24. Stability Analyses for Pressure P12, CIS Method, $Re_{c_N} = 15 \times 10^6$, $\Lambda = 15$ deg

- P12
- $Re_{c_N} = 15 \times 10^6$
- $\Lambda = 20$ deg
- $M_N = 0.78$
- Compressible
- No dissipation

Tollmien-Schlichting

$\Psi = 40$ deg
ω^*, Hz
3068
3776
4719
5616
6749
8684

N_{TS}

5616 Hz

3776 Hz

s/c

Crossflow – Extrapolation Technique Used

N_{CF}

250

150

s/c

$\omega^* = 0$ Hz

α_{rs}^* values
from 150 to 1600
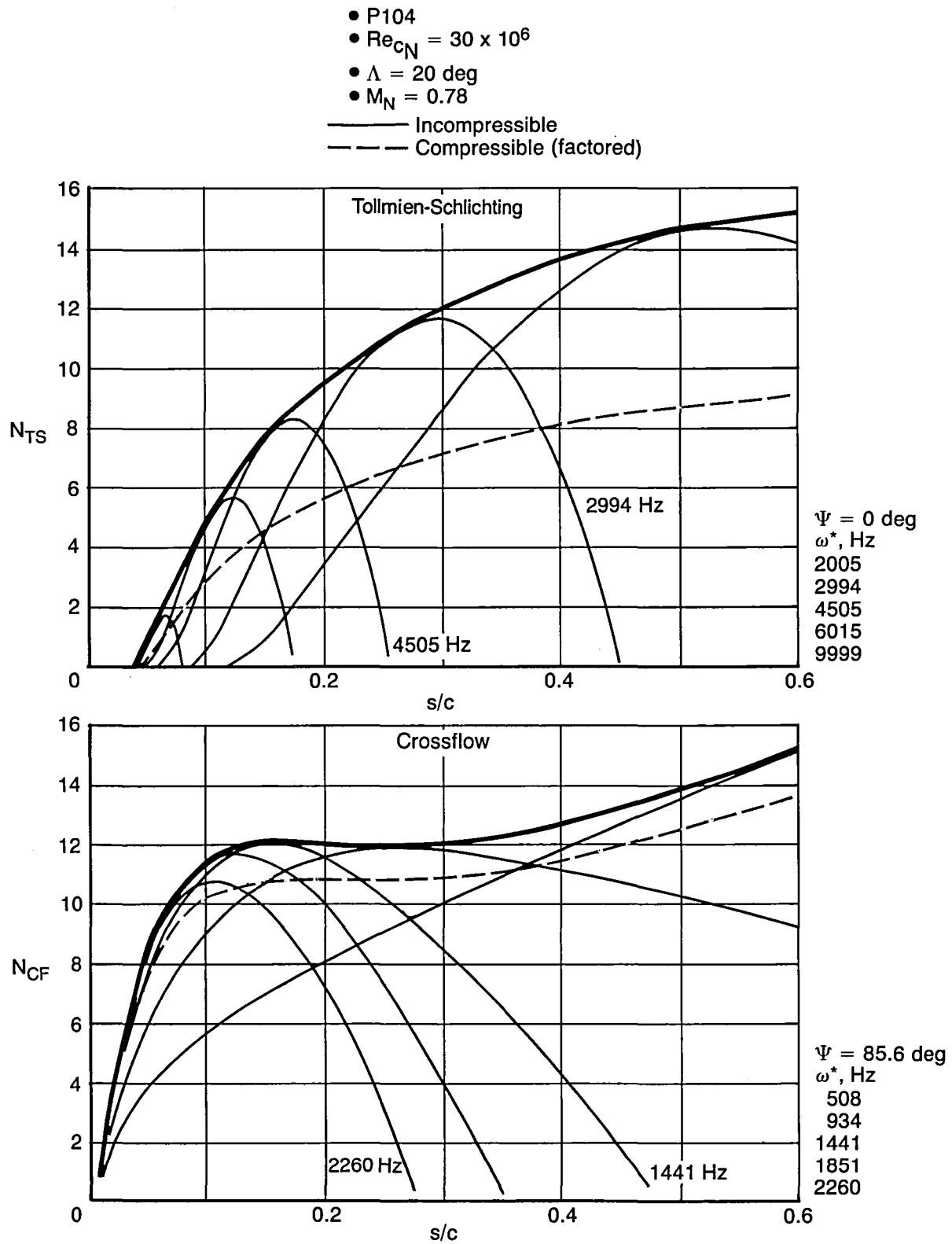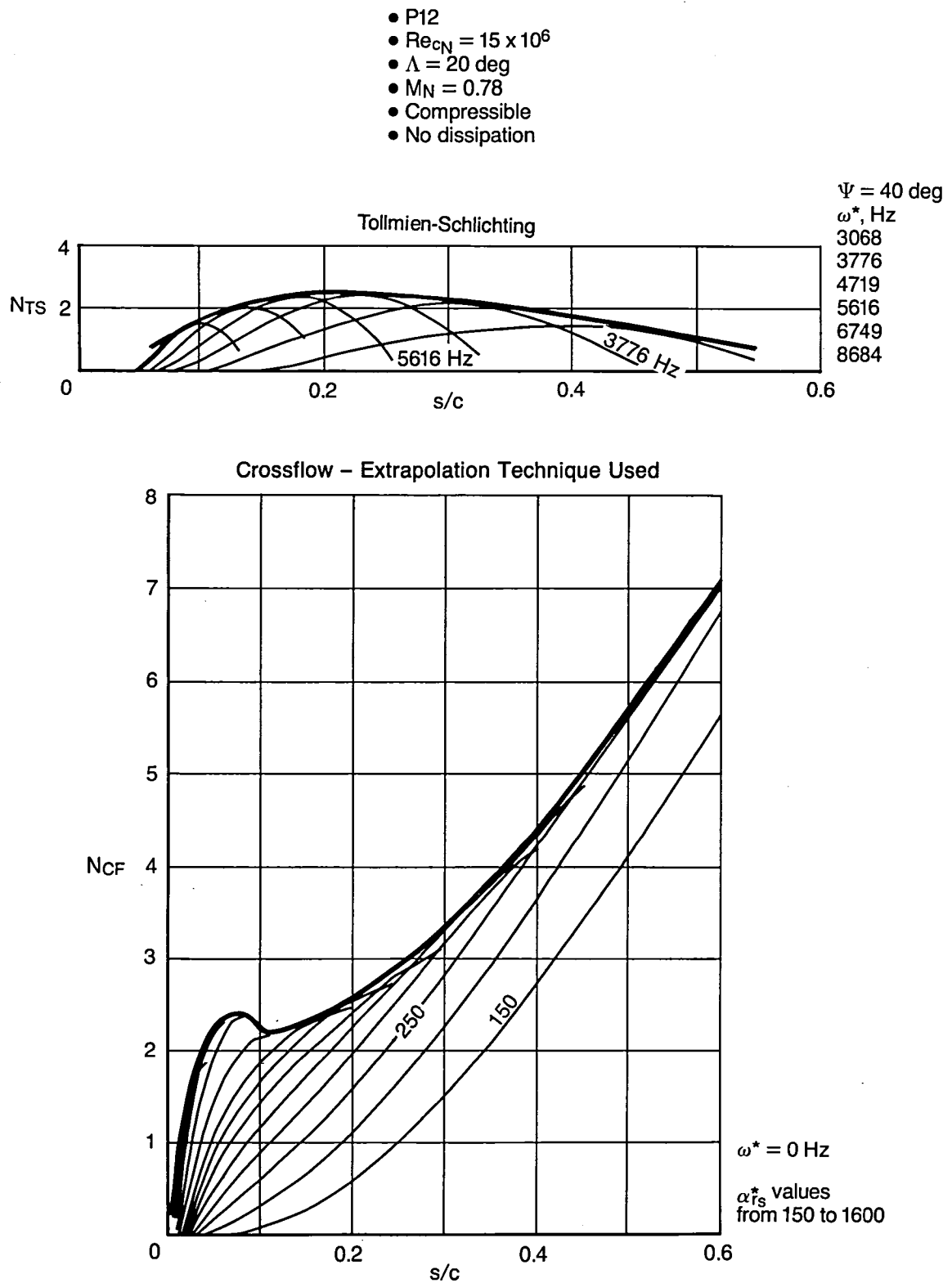
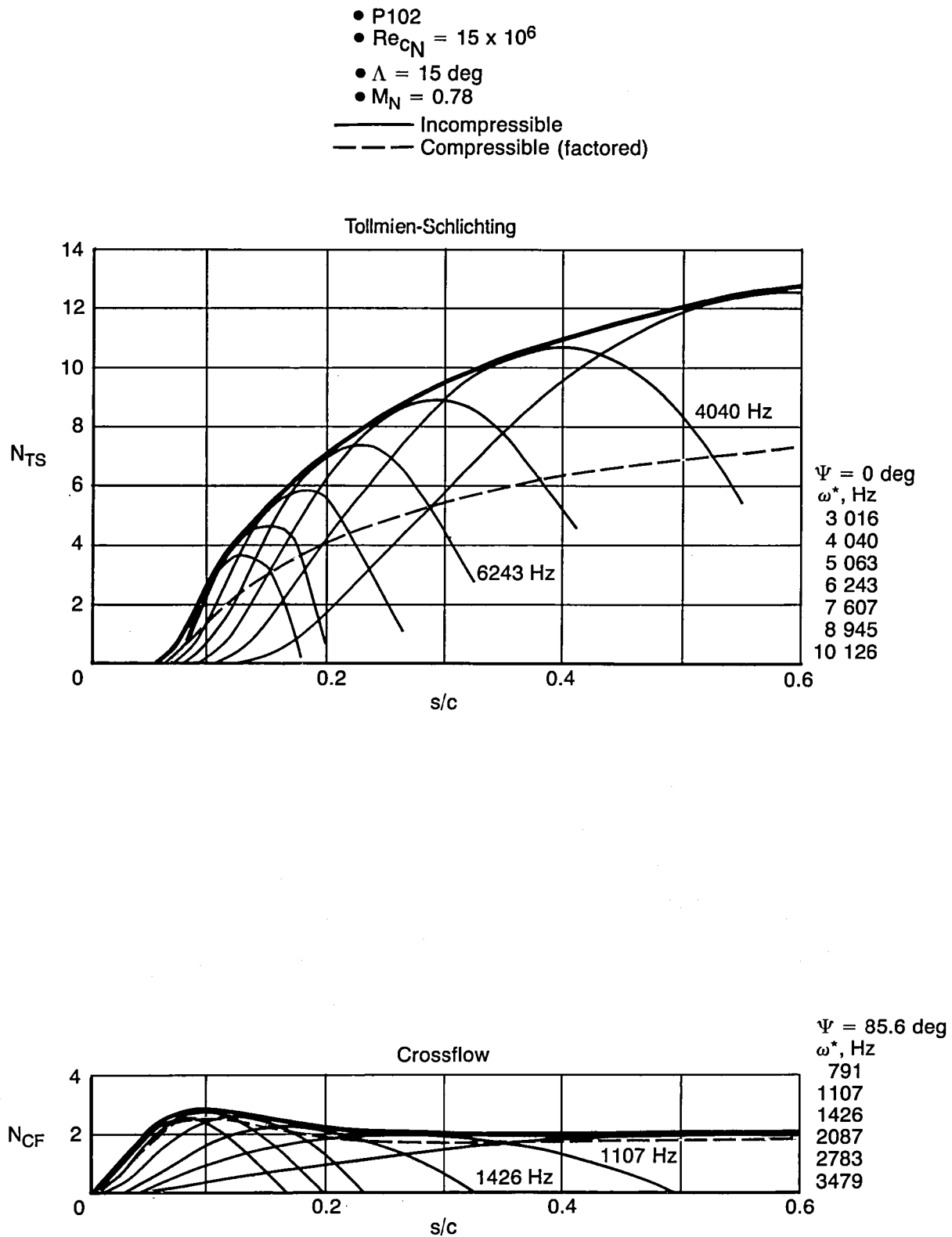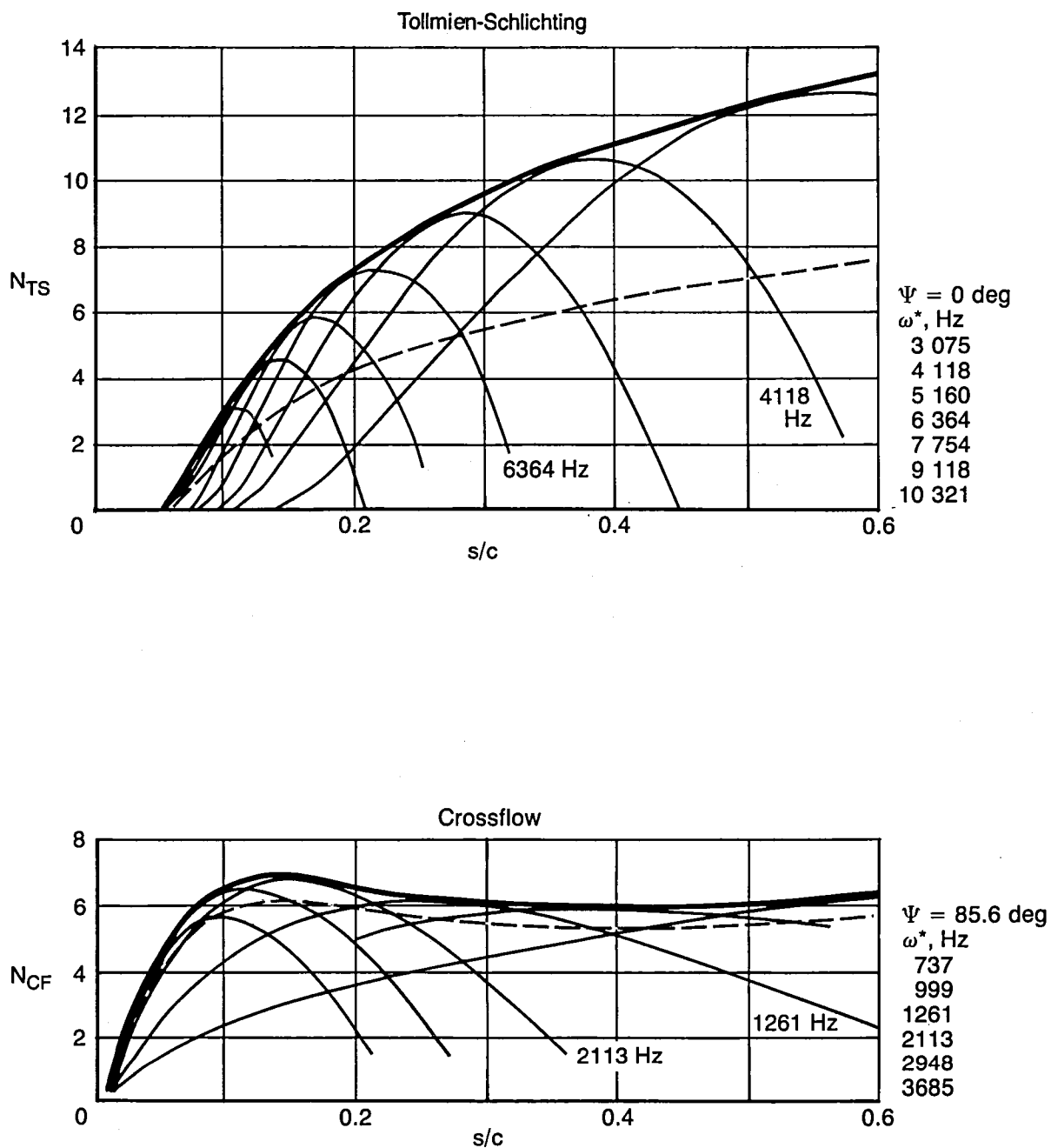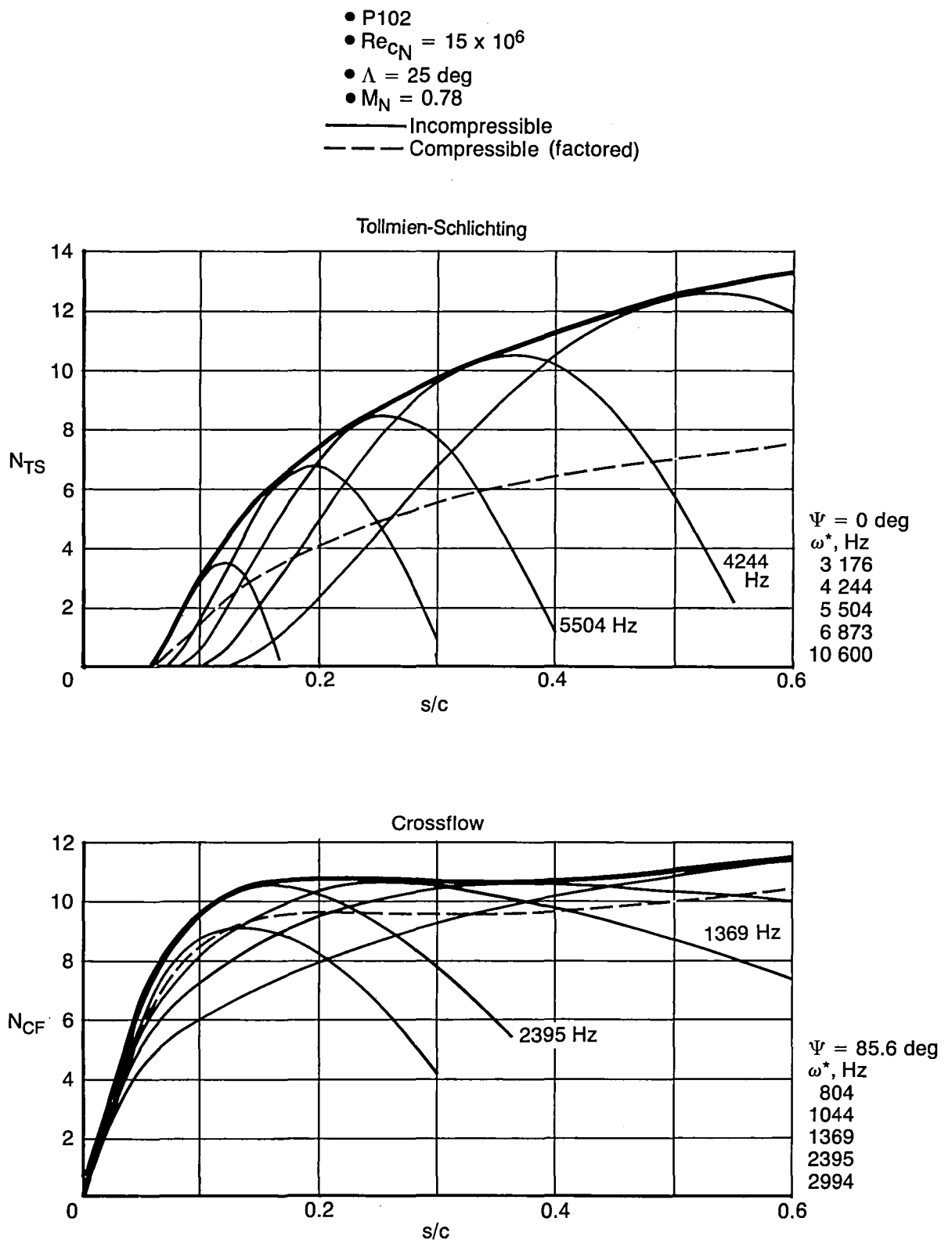Figure 25. Stability Analyses for Pressure P12, CIS Method, $Re_{c_N} = 15 \times 10^6$, $\Lambda = 20$ deg
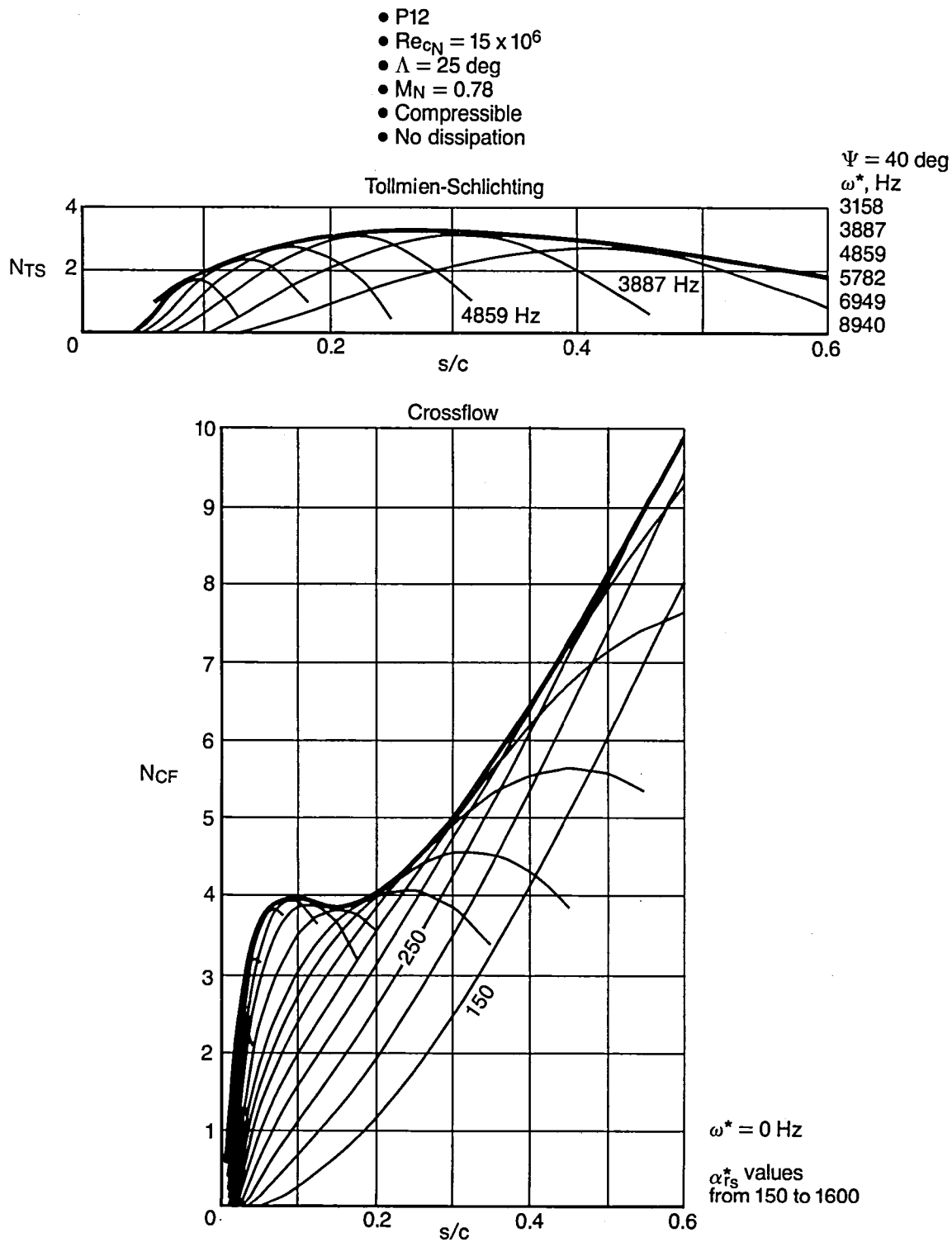
Figure 26. Stability Analyses for Pressure P12, CIS Method, $Re_{c_N} = 15 \times 10^6$, $\Lambda = 25$ deg

- P12
- $Re_{c_N} = 30 \times 10^6$
- $\Lambda = 15\,\text{deg}$
- $M_N = 0.78$
- Compressible
- No dissipation

Tollmien-Schlichting

$\Psi = 40\,\text{deg}$

ω^*, Hz

1847
2770
3694
4848
6464

3694 Hz

2770 Hz

N_{TS}

s/c

Crossflow – Extrapolation Technique Used

N_{CF}

300

150

$\omega^* = 0\,\text{Hz}$

α^*_{rs} values
from 150 to 1600

s/c
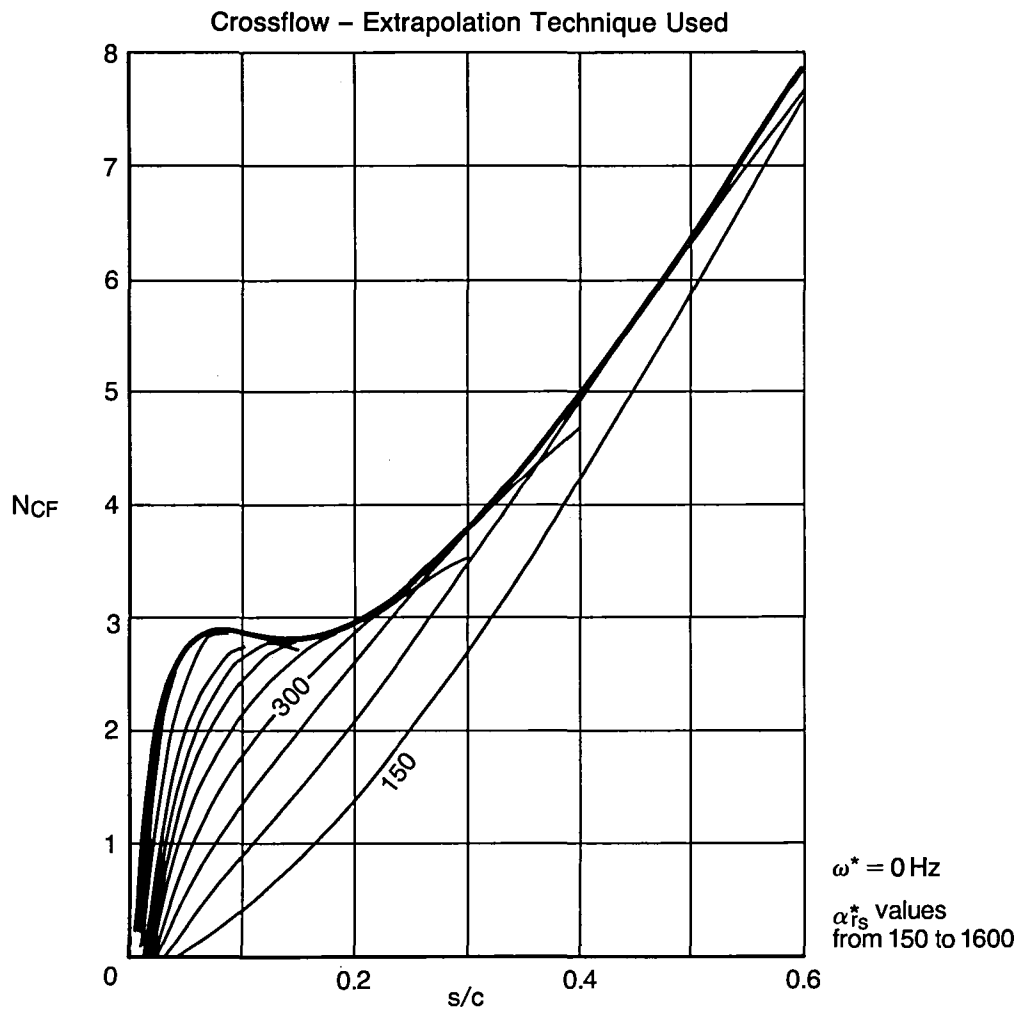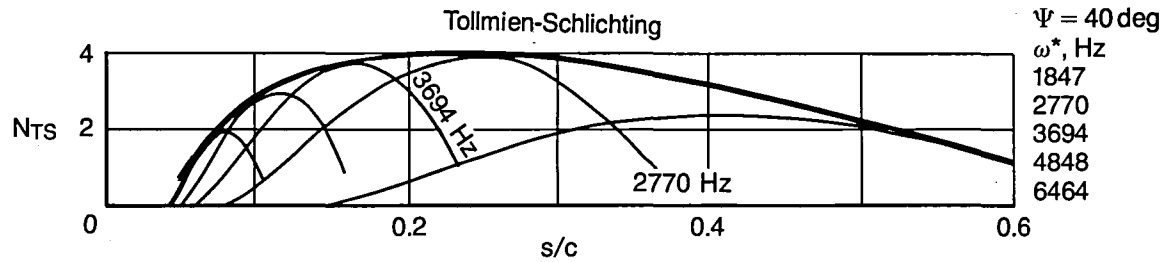
Figure 27. Stability Analyses for Pressure P12, CIS Method, $Re_{c_N} = 30 \times 10^6$, $\Lambda = 15\,\text{deg}$

60

- P12
- $Re_{c_N} = 30 \times 10^6$
- $\Lambda = 20$ deg
- $M_N = 0.78$
- Compressible
- No dissipation

Tollmien-Schlichting

$\Psi = 40$ deg
ω^*, Hz
1888
2832
3776
6607

Crossflow

$\omega^* = 0$ Hz

$\alpha^*_{r_s}$ values
from 150 to 1600
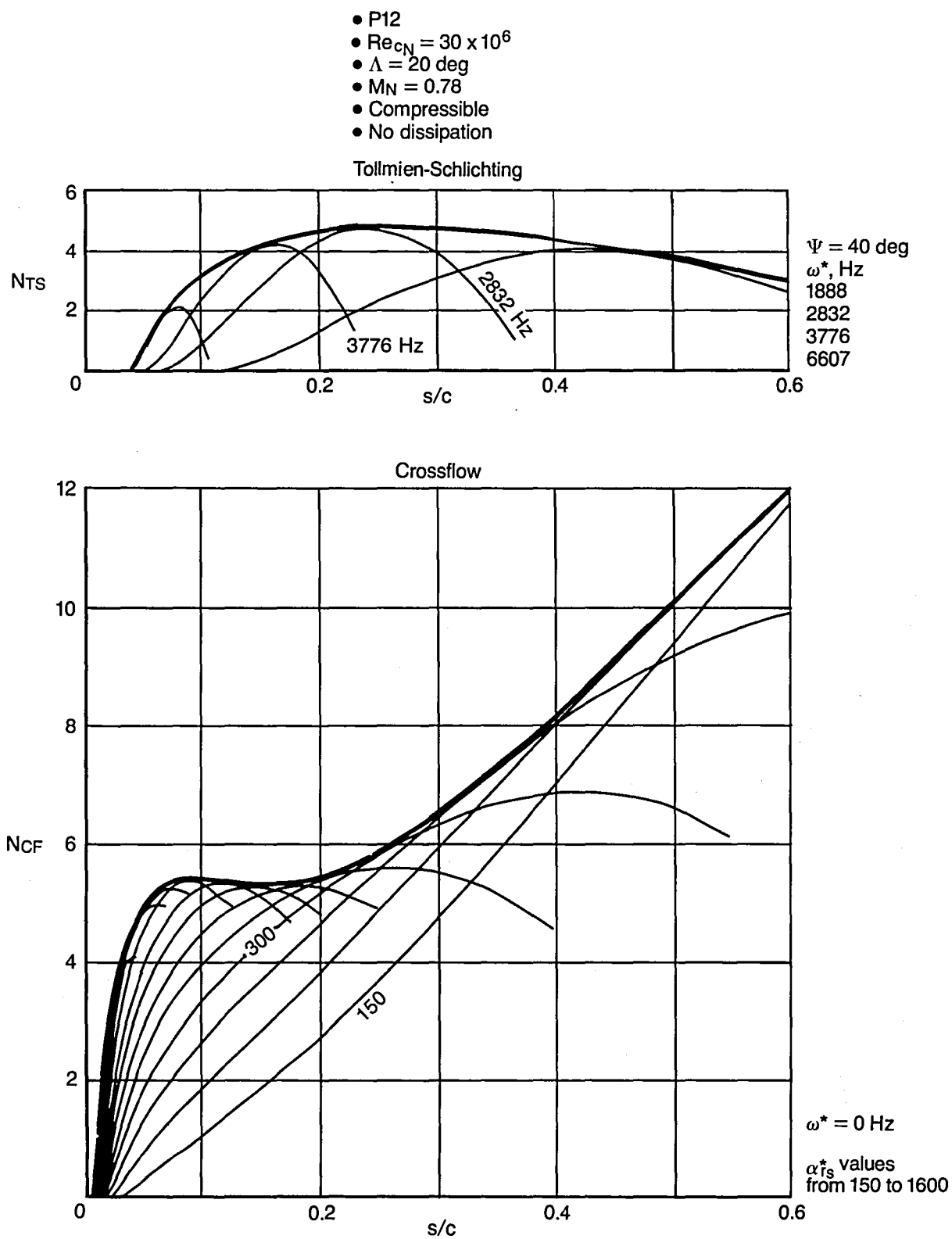
Figure 28. Stability Analyses for Pressure P12, CIS Method, $Re_{c_N} = 30 \times 10^6$, $\Lambda = 20$ deg

- P102
- $Re_{c_N} = 15 \times 10^6$
- $\Lambda = 25$ deg
- $M_N = 0.70$
- Compressible
- No dissipation

Tollmien-Schlichting

$\Psi = 40$ deg
ω^*, Hz
2785
3292
4051
5064
6077
7343
9368

Crossflow

350

200
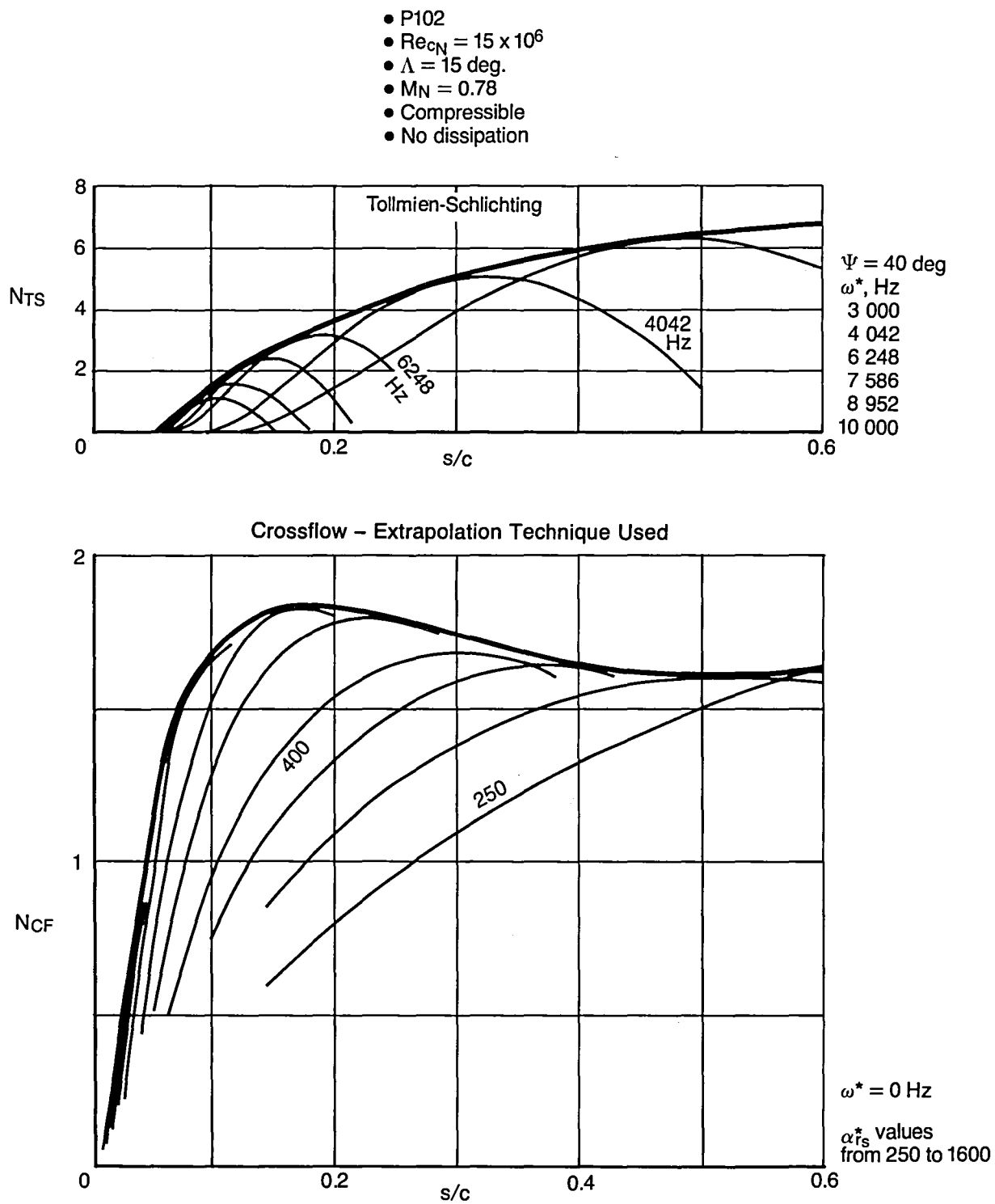
$\omega^* = 0$ Hz

α_{rs}^* values
from 150 to 1600
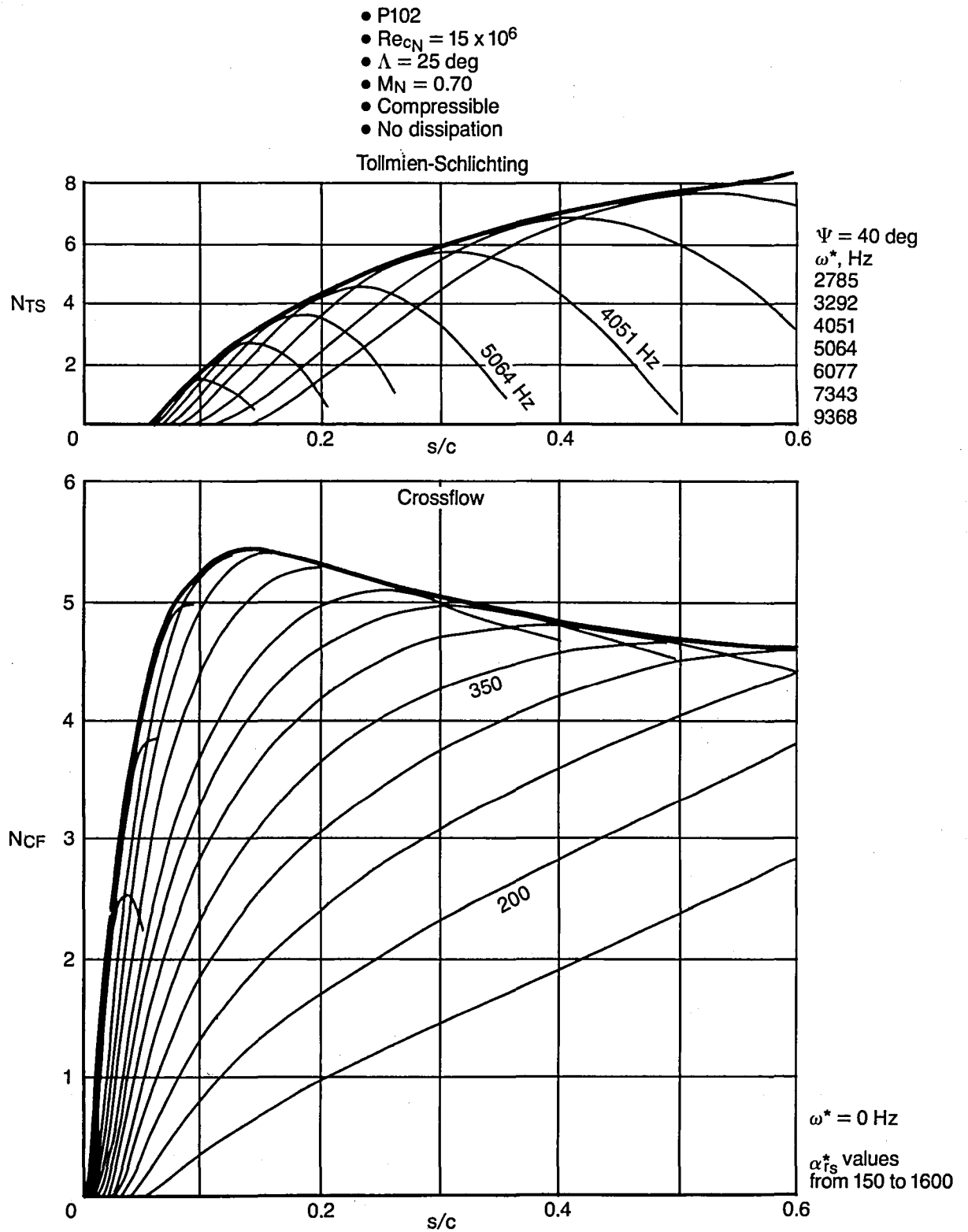
Figure 29. Stability Analyses for Pressure P102, $M_N = 0.7$, $Re_{c_N} = 15 \times 10^6$, $\Lambda = 25$ deg
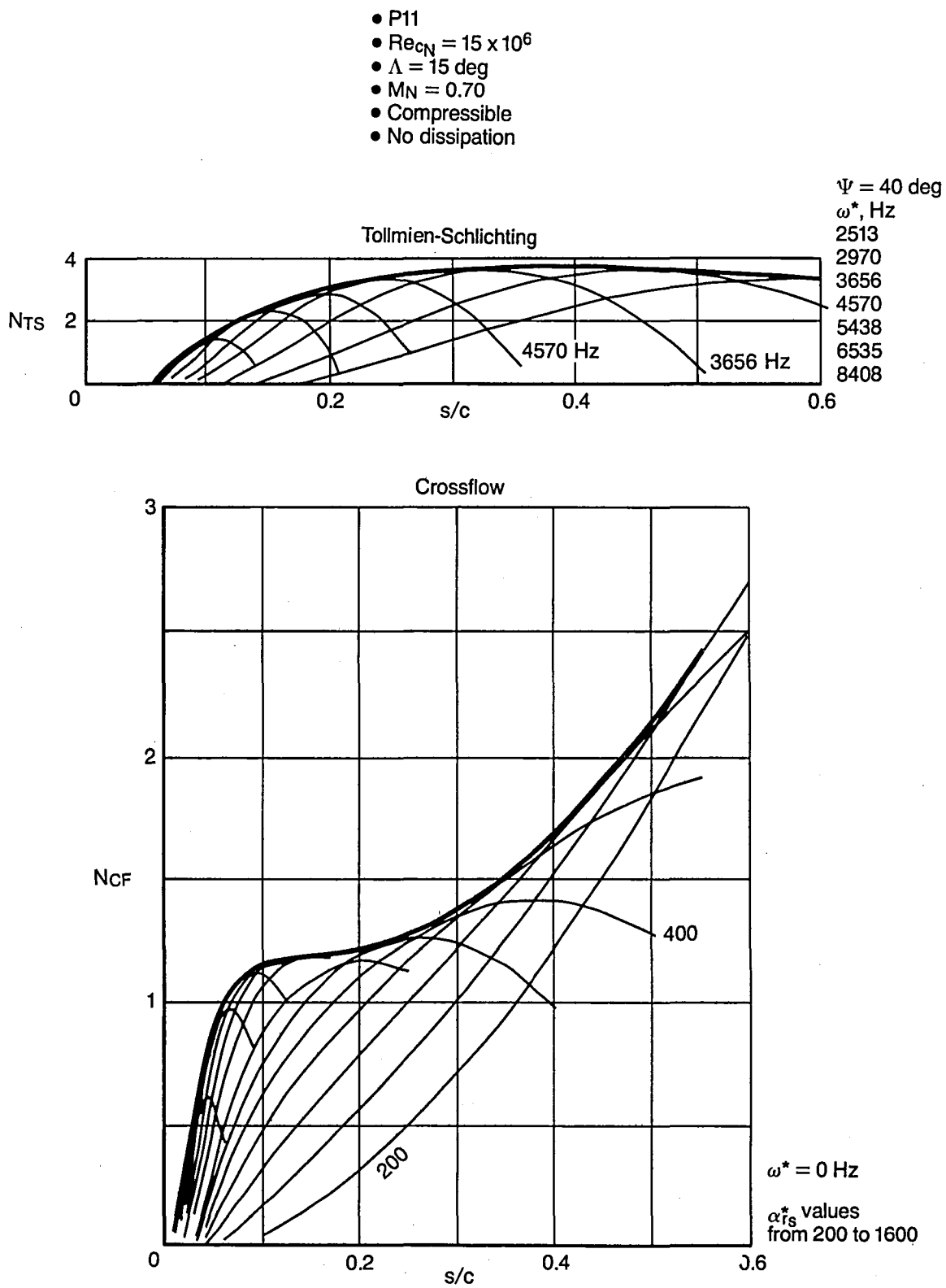
Figure 30. *Stability Analyses for Pressure P11, $M_N = 0.7$, $Re_{c_N} = 15 \times 10^6$, $\Lambda = 15$ deg*

- P11
- $Re_{c_N} = 15 \times 10^6$
- $\Lambda = 25$ deg
- $M_N = 0.70$
- Compressible
- No dissipation

Tollmien-Schlichting

NTS

$\Psi = 40$ deg
ω^*, Hz
3112
3830
4787
5697
6846
8809

3830 Hz

4787 Hz

s/c

Crossflow

N_{CF}

350

150

$\omega^* = 0$ Hz

α^*_{rs} values
from 150 to 1600

s/c
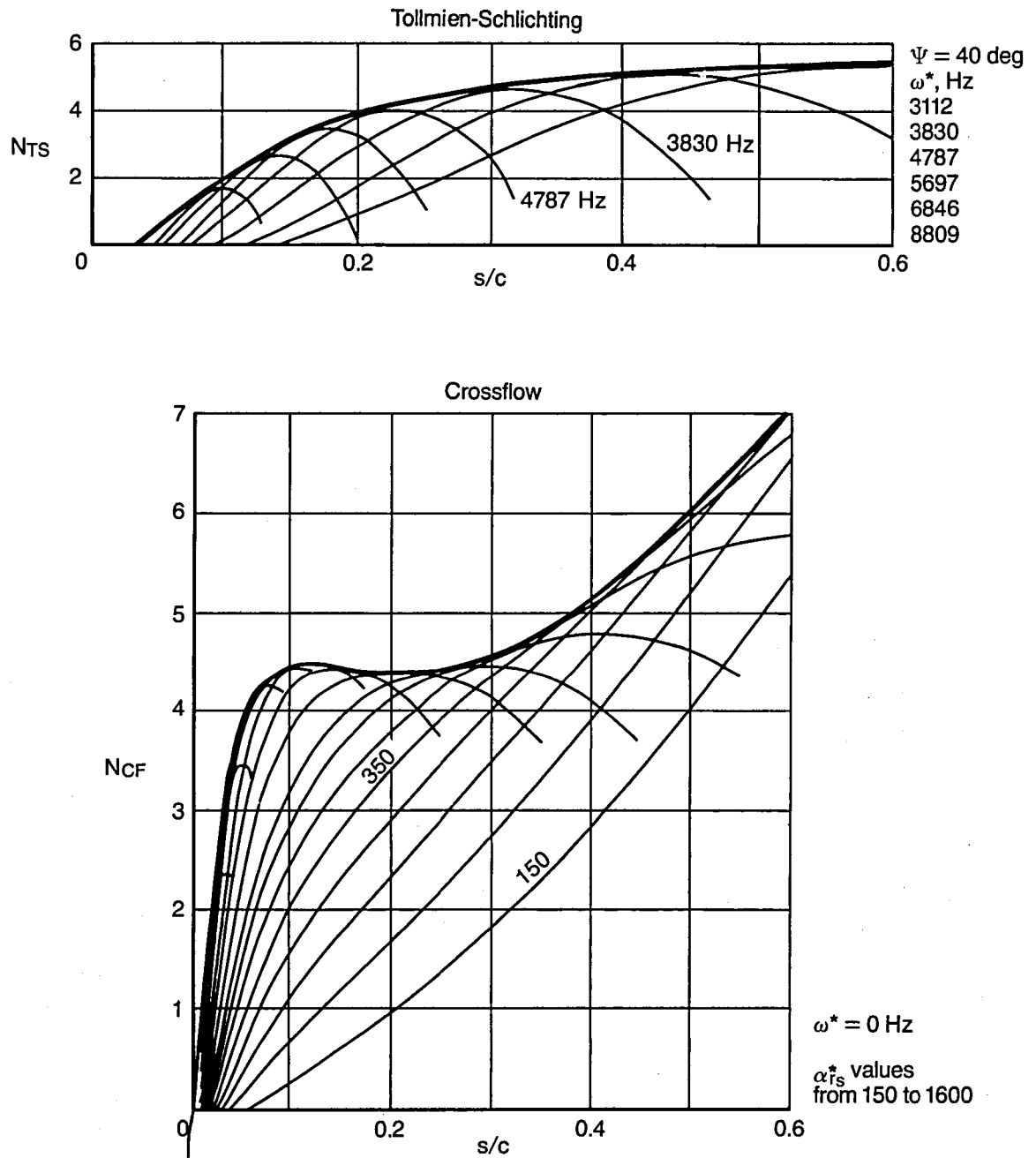
Figure 31. Stability Analyses for Pressure P11, $M_N = 0.7$, $Re_{c_N} = 15 \times 10^6$, $\Lambda = 25$ deg
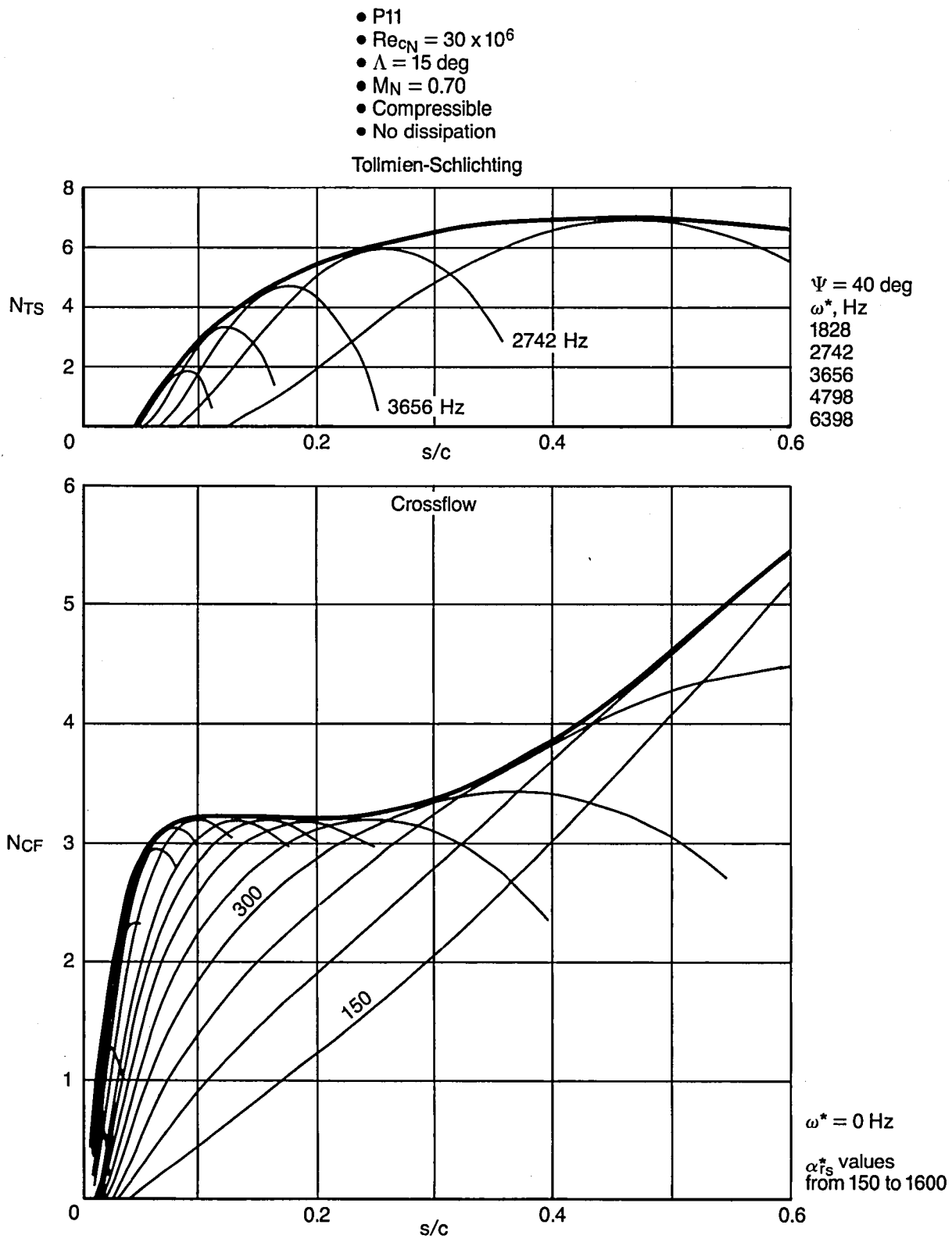
Figure 32. Stability Analyses for Pressure P11, $M_N = 0.7$, $Re_{c_N} = 30 \times 10^6$, $\Lambda = 15$ deg

- P12
- $Re_{c_N} = 15 \times 10^6$
- $\Lambda = 25$ deg
- $M_N = 0.70$
- Compressible
- No dissipation

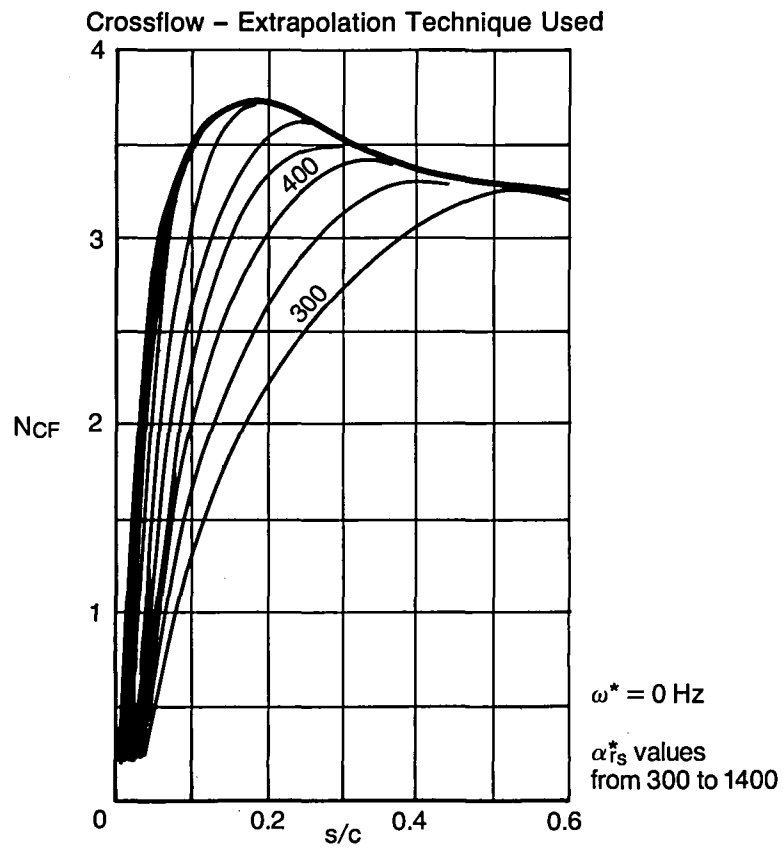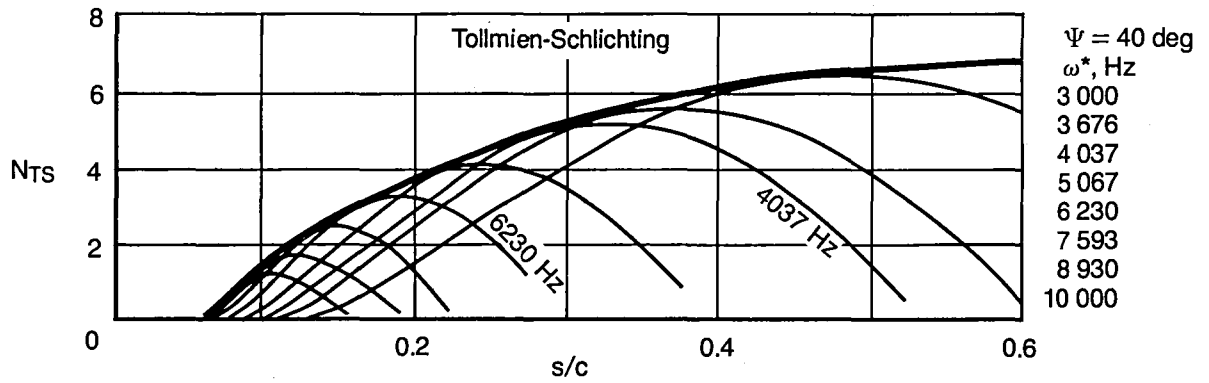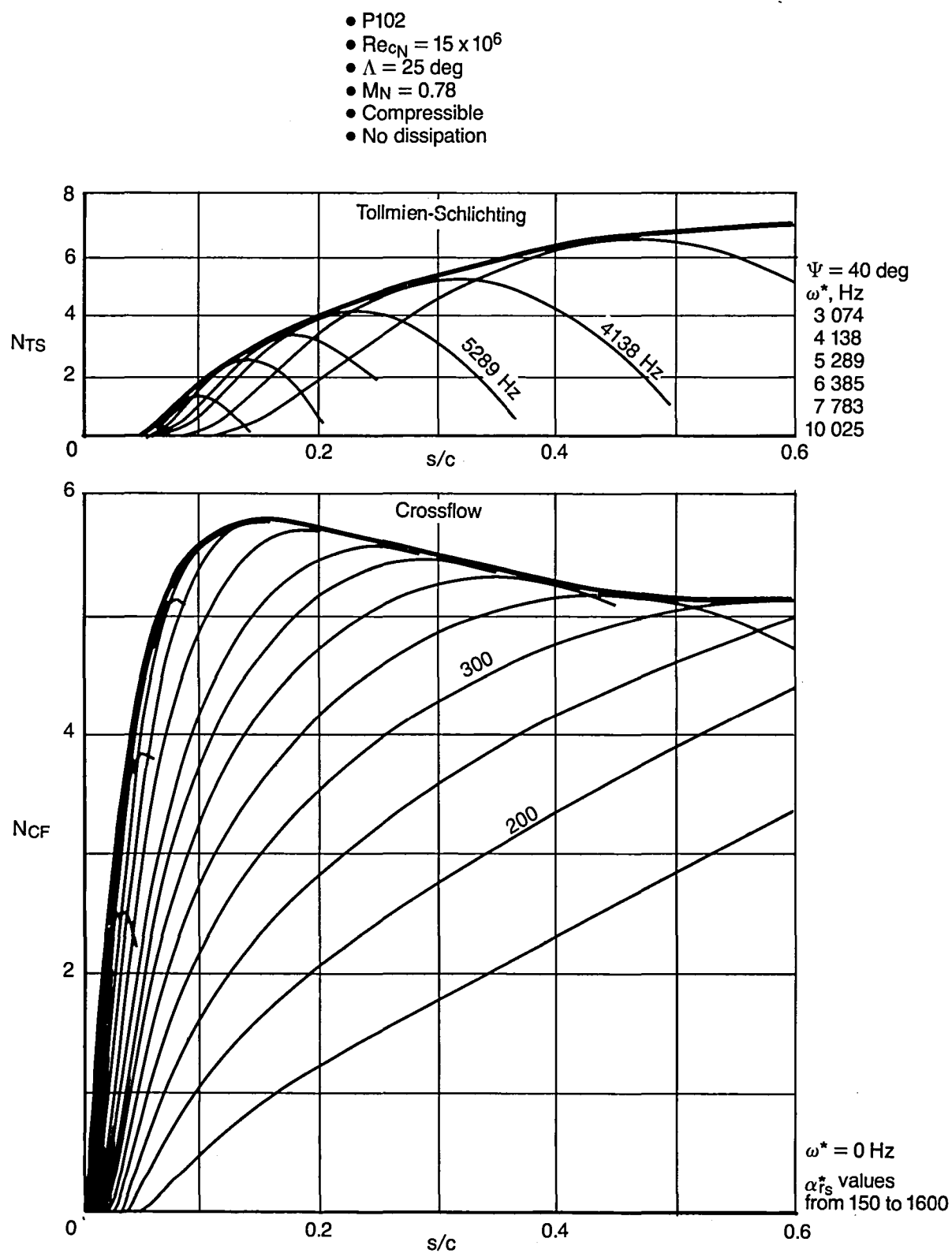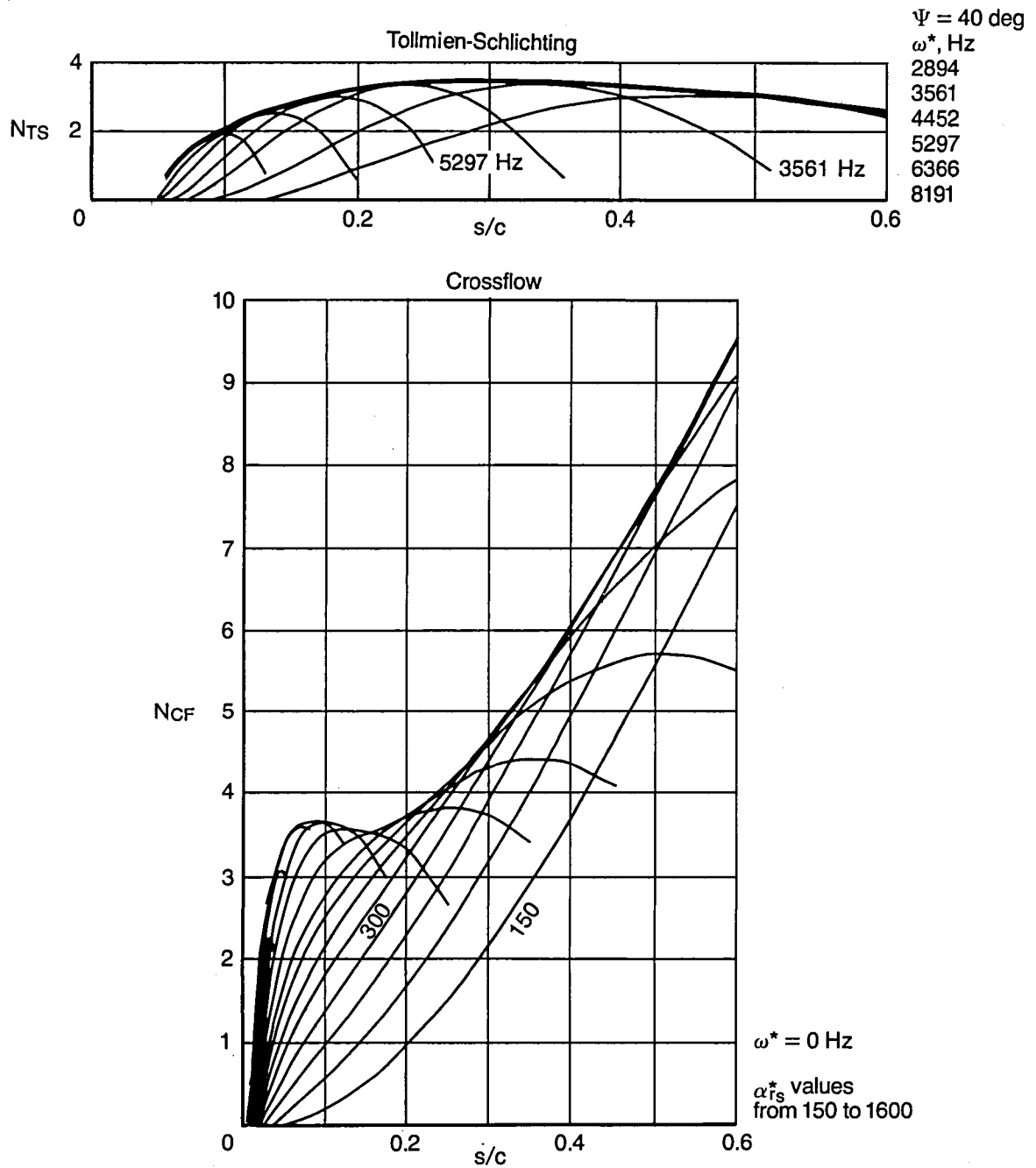Figure 33. Stability Analyses for Pressure P12, $M_N = 0.7$, $Re_{c_N} = 15 \times 10^6$, $\Lambda = 25$ deg
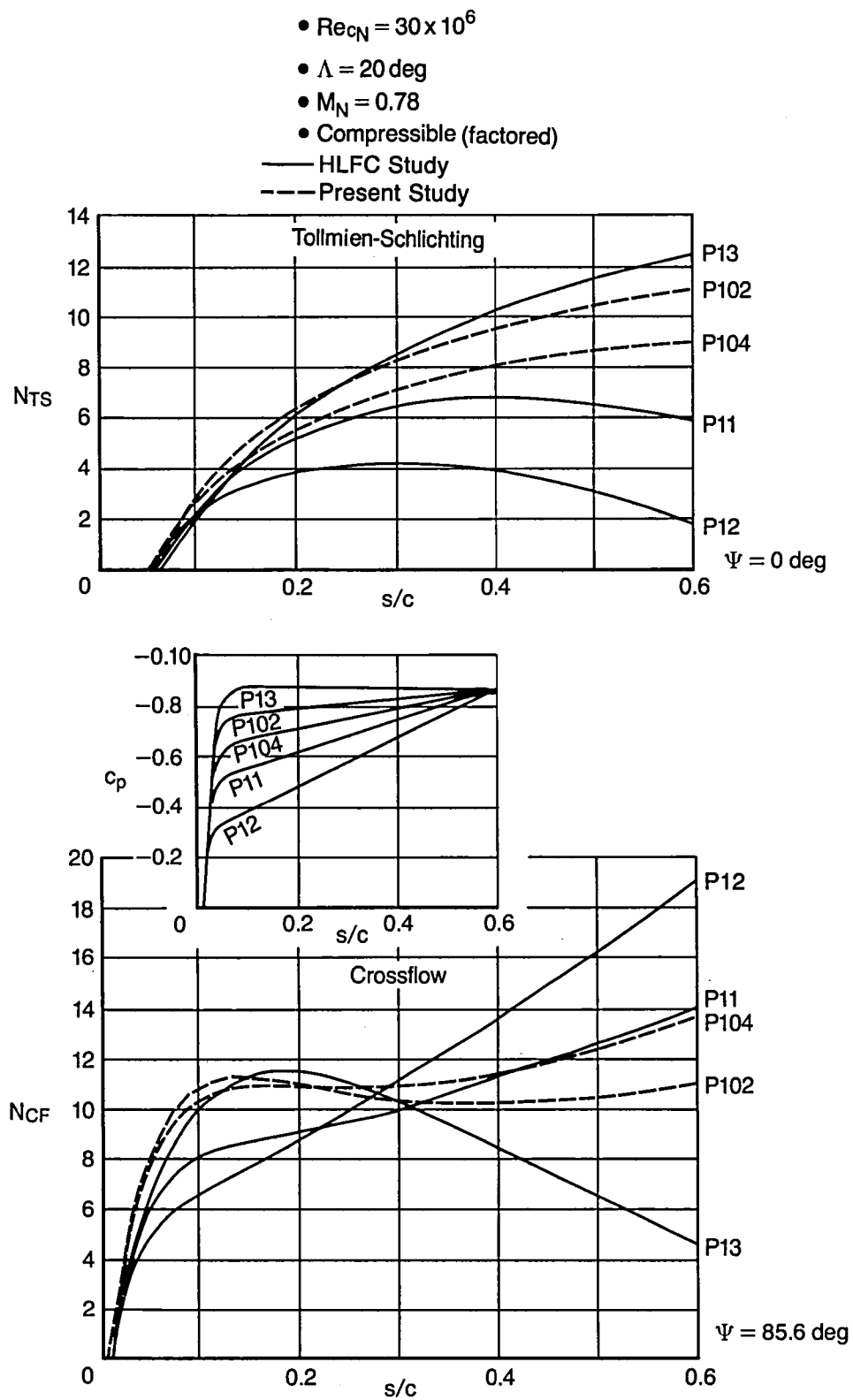
Figure 34. Comparison of Envelopes of Pressure Distribution Range, FICA Method

- $Re_{c_N} = 30 \times 10^6$
- $\Lambda = 20$ deg
- $M_N = 0.78$
- Compressible

Tollmien-Schlichting

P102

P11

P12

$\psi = 40$ deg

Crossflow

P12

P11

P102

Irrotational
$\omega = 0$

s/c
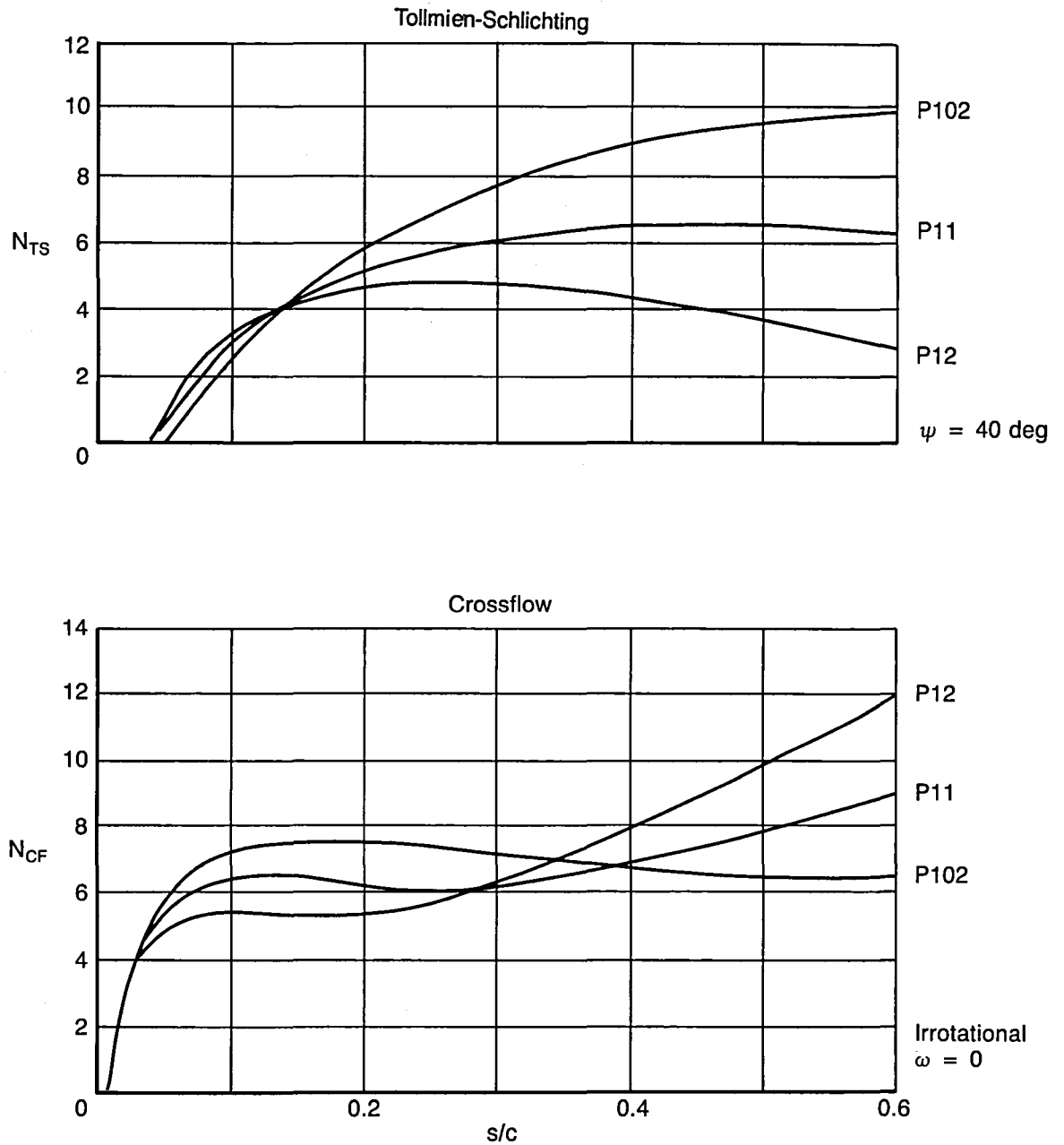
Figure 35. Comparison of Envelopes of Pressure Distribution Range, CIS Method

68

- FICA Method
- $M_N = 0.78$
- $s/c = 0.4$
- Shaded symbols calculated in present study
- Open symbols calculated in HLFC study
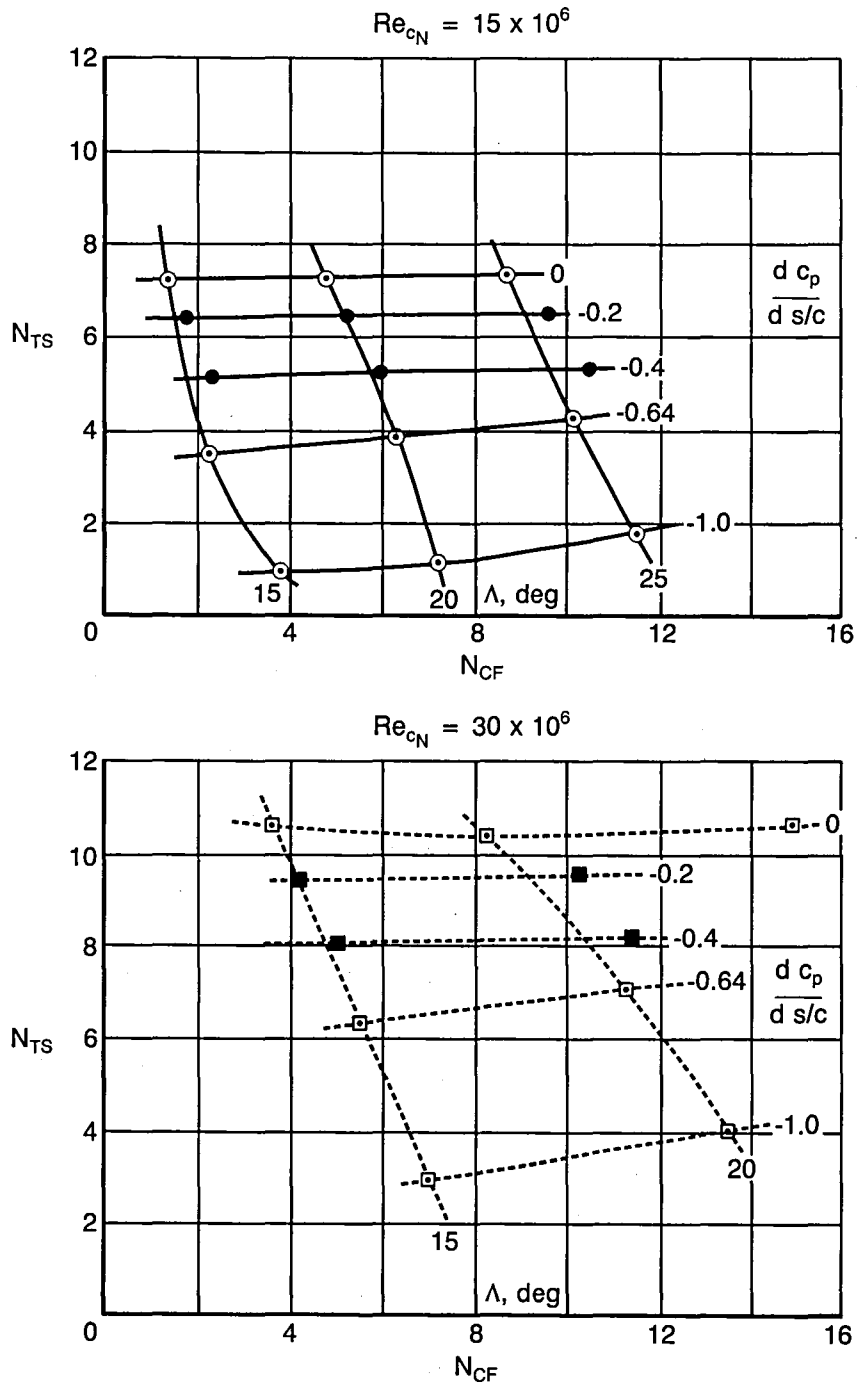
Figure 36. Additional Points for HLFC Study Parametric Results

- P102
- $Re_{c_N} = 30 \times 10^6$
- $M_N = 0.78$

——— CIS Method
– – – FICA Method

Tollmien-Schlichting

$\Lambda = 20$ deg

$\Lambda = 15$ deg

N_{TS}

s/c

Crossflow

$\Lambda = 20$ deg

$\Lambda = 15$ deg

N_{CF}

s/c
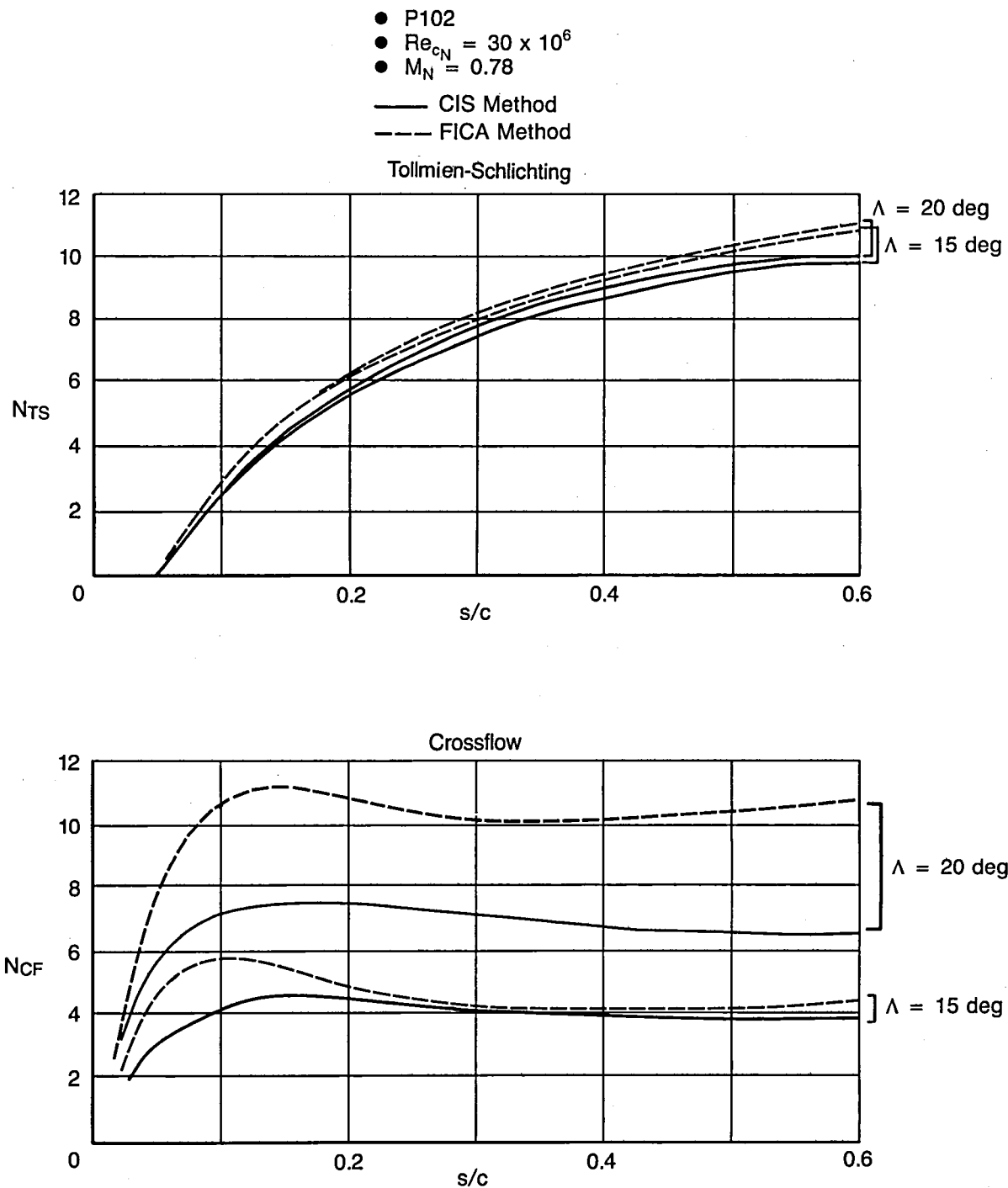
Figure 37. Comparison of FICA and CIS Analysis Methods, Pressure P102

70

- P11
- $Re_{c_N} = 30 \times 10^6$
- $\Lambda = 15$ deg
- $M_N = 0.78$
—— CIS Method
——— FICA Method

Tollmien-Schlichting

NTS vs s/c

Crossflow

NCF vs s/c
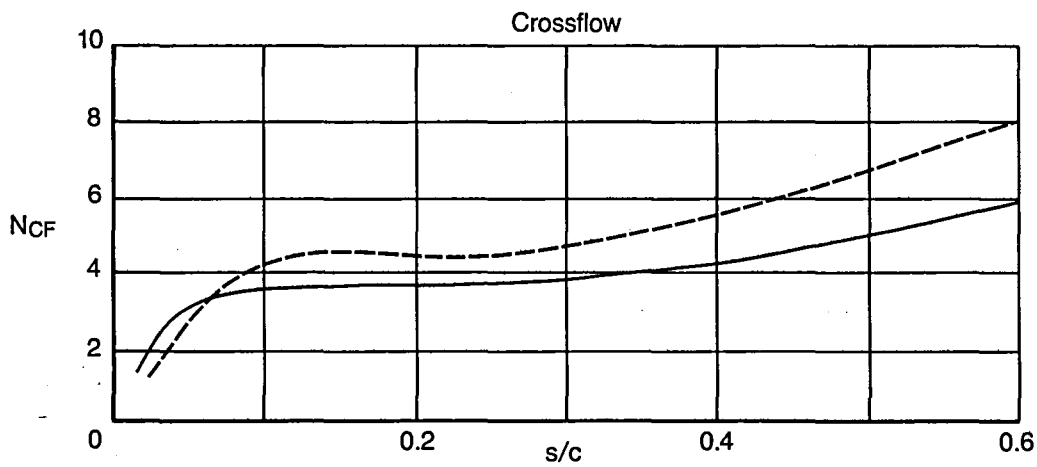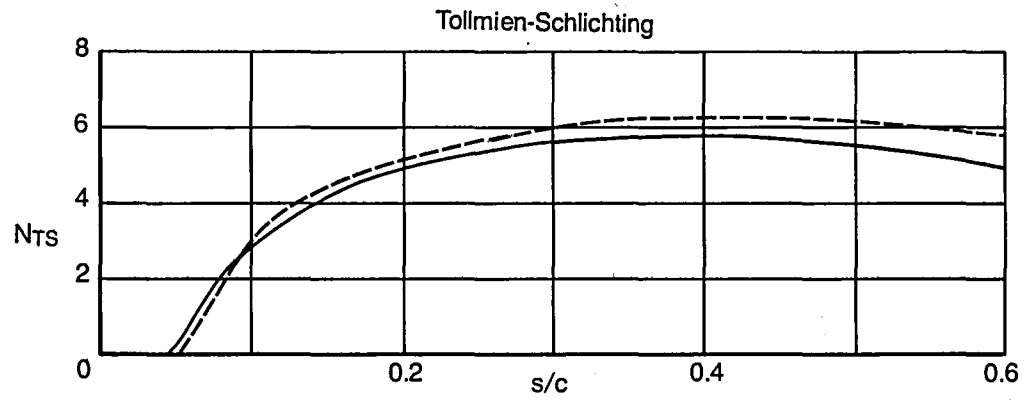
Figure 38. Comparison of FICA and CIS Analysis Methods, Pressure P11
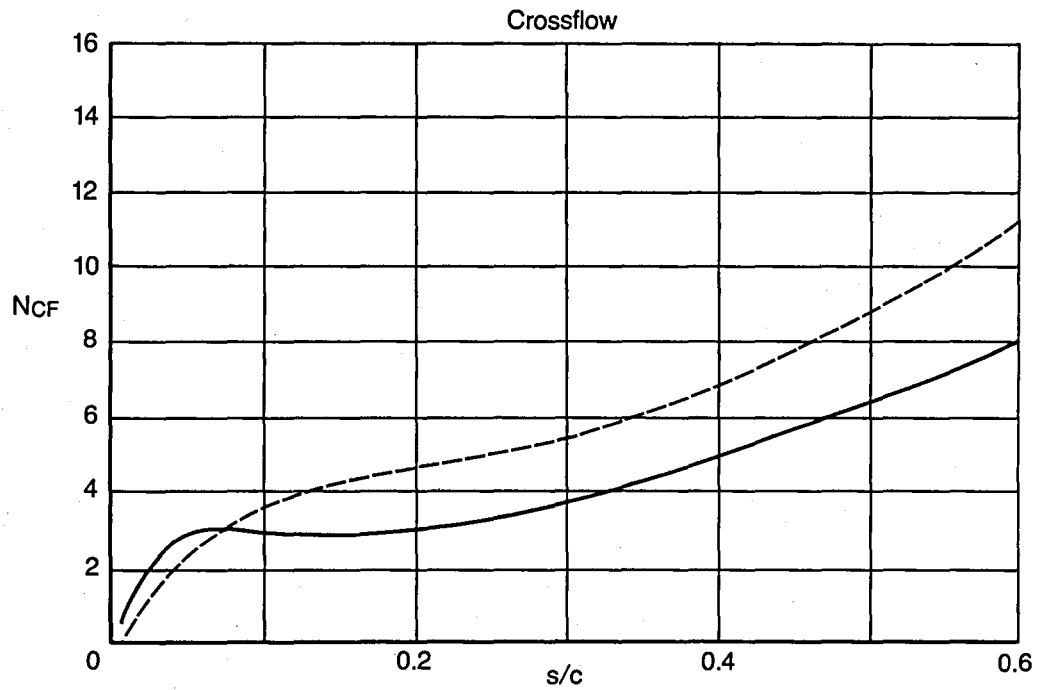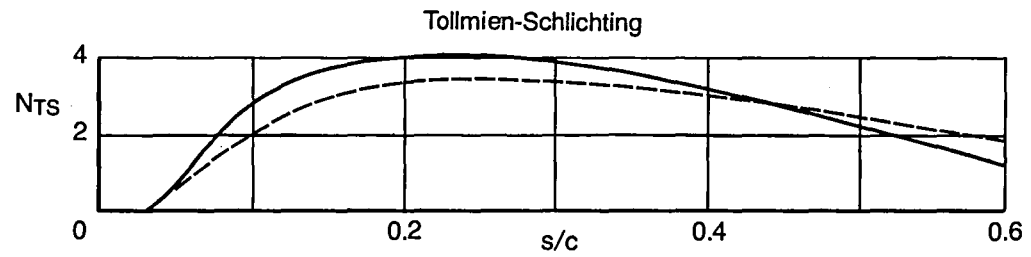
Figure 39. Comparison of FICA and CIS Analysis Methods, Pressure P12

- $M_N = 0.78$
- $s/c = 0.4$
- Open symbols, FICA Method
- Shaded symbols, CIS Method

$Re_{c_N} = 15 \times 10^6$
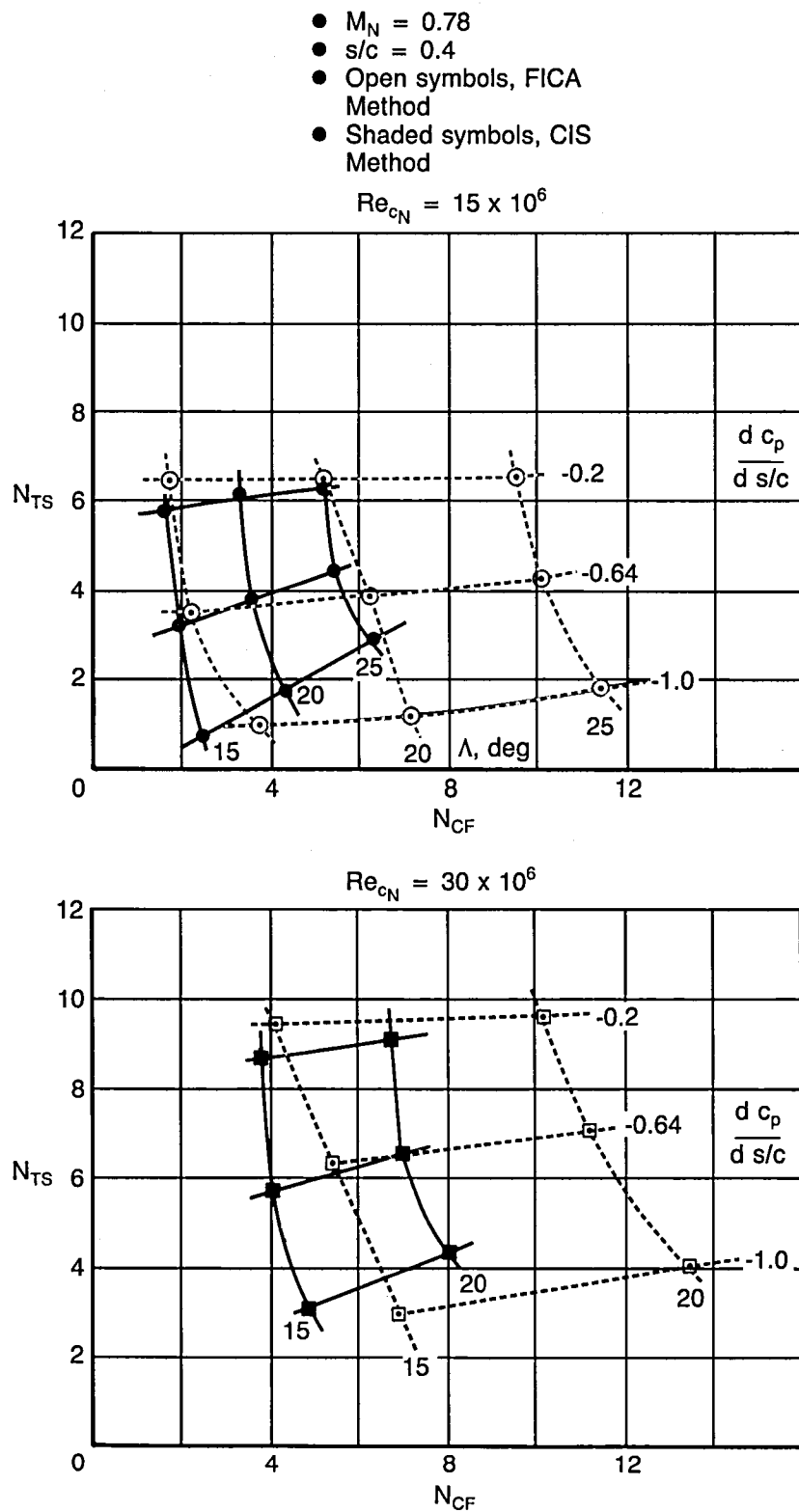
$Re_{c_N} = 30 \times 10^6$

Figure 40. Comparison of FICA and CIS Analysis Methods at $s/c = 0.4$

Tollmien-Schlichting

Crossflow
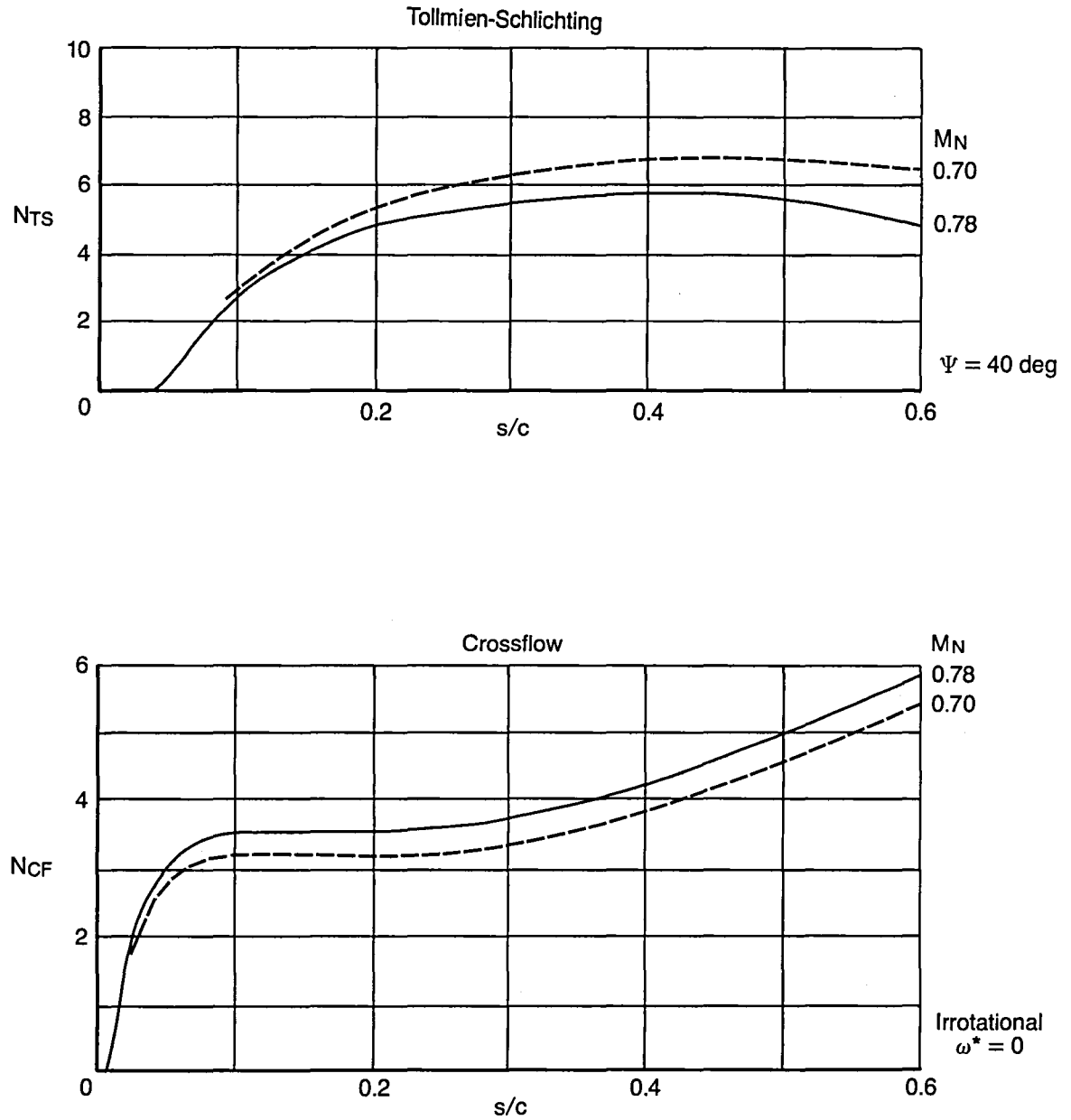
Figure 41. Effect of Mach Number on a Disturbance Amplification Envelope, CIS Method
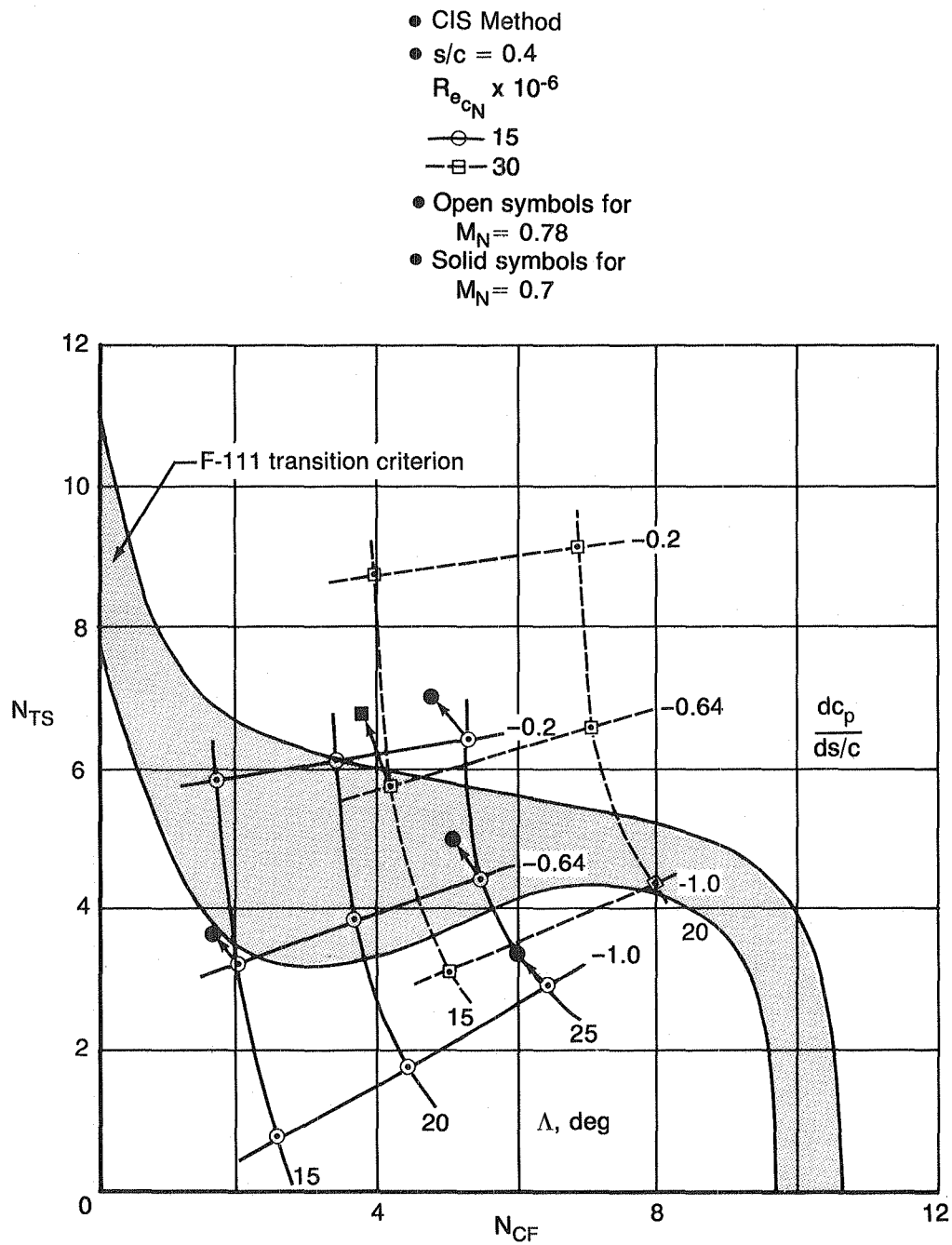
Figure 42. Effect of Mach Number on Disturbance Amplification at s/c = 0.4
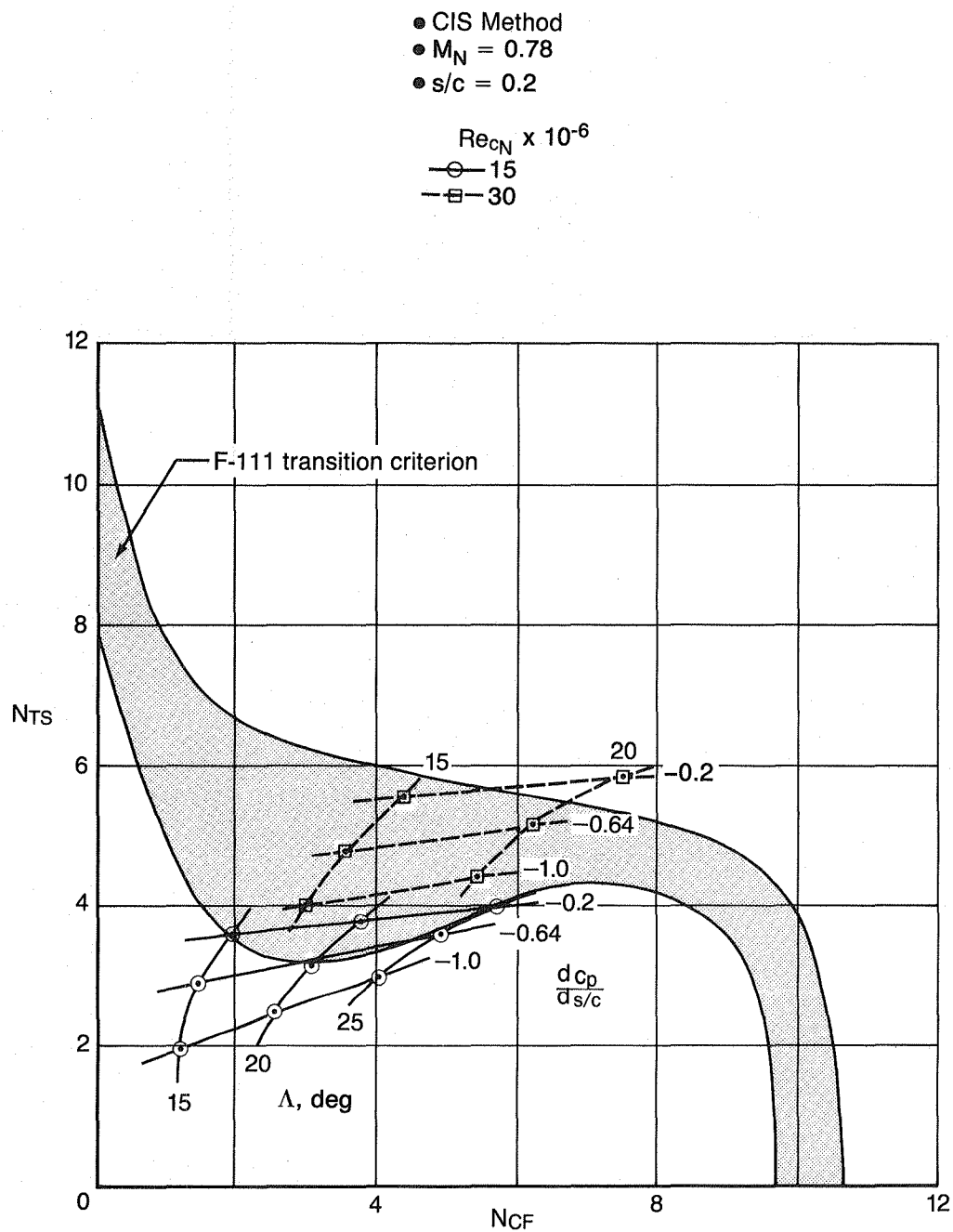
Figure 43. Disturbance Amplification at s/c = 0.2
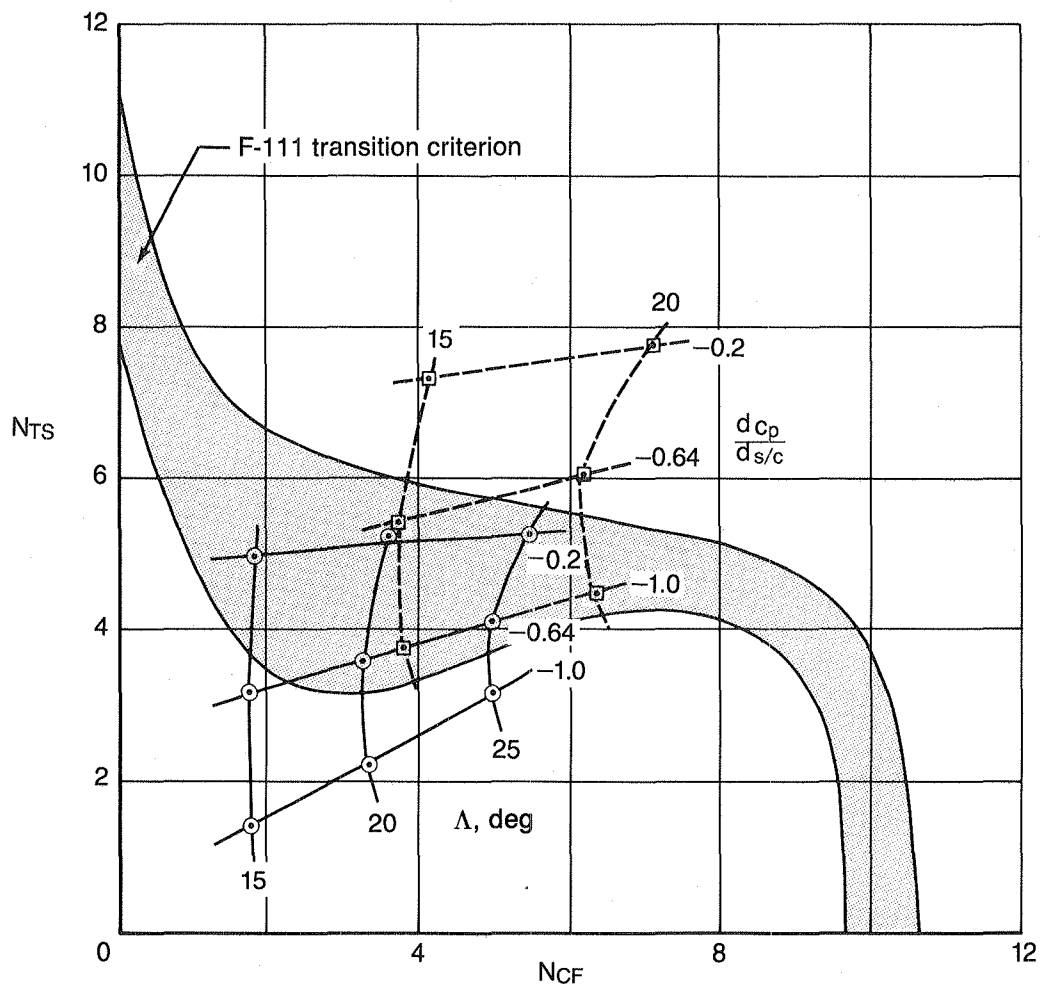
Figure 44. Disturbance Amplification at s/c = 0.3
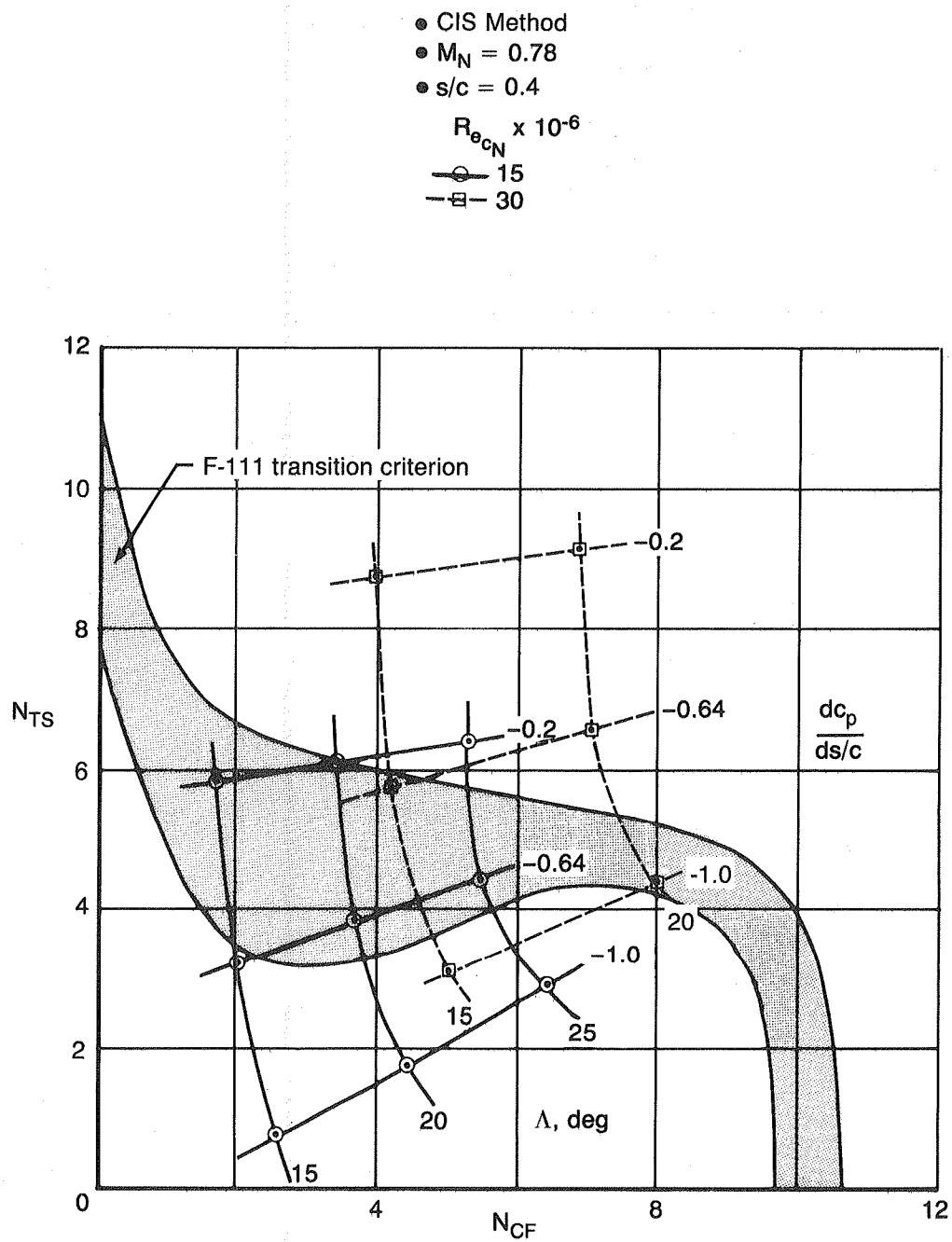
Figure 45. Disturbance Amplification at s/c = 0.4
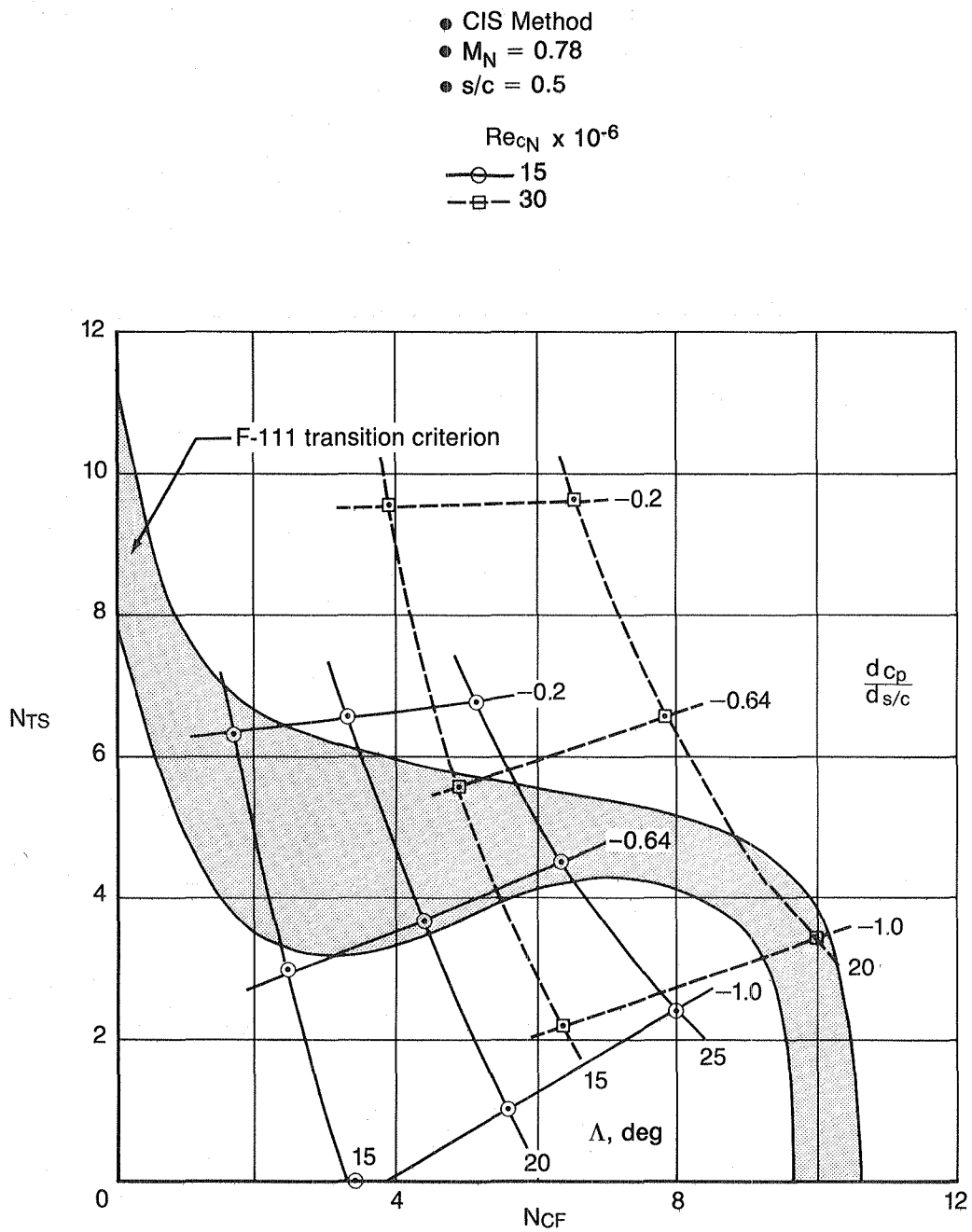
Figure 46. Disturbance Amplification at s/c = 0.5

- CIS Method
- $M_N = 0.78$
- $s/c = 0.6$

$Re_{c_N} \times 10^{-6}$
- ⊝— 15
- ⊟— 30
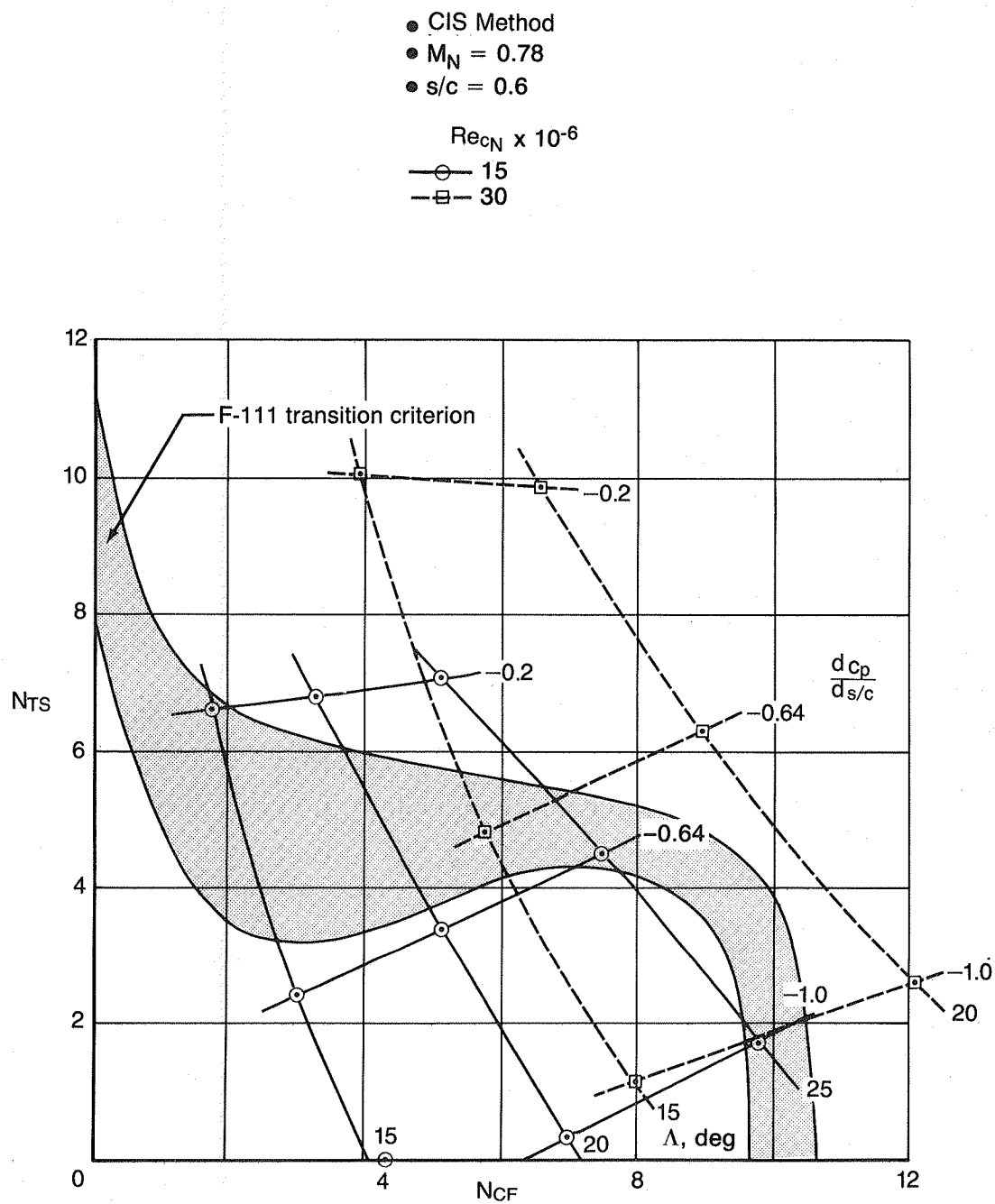
Figure 47. Disturbance Amplification at s/c = 0.6
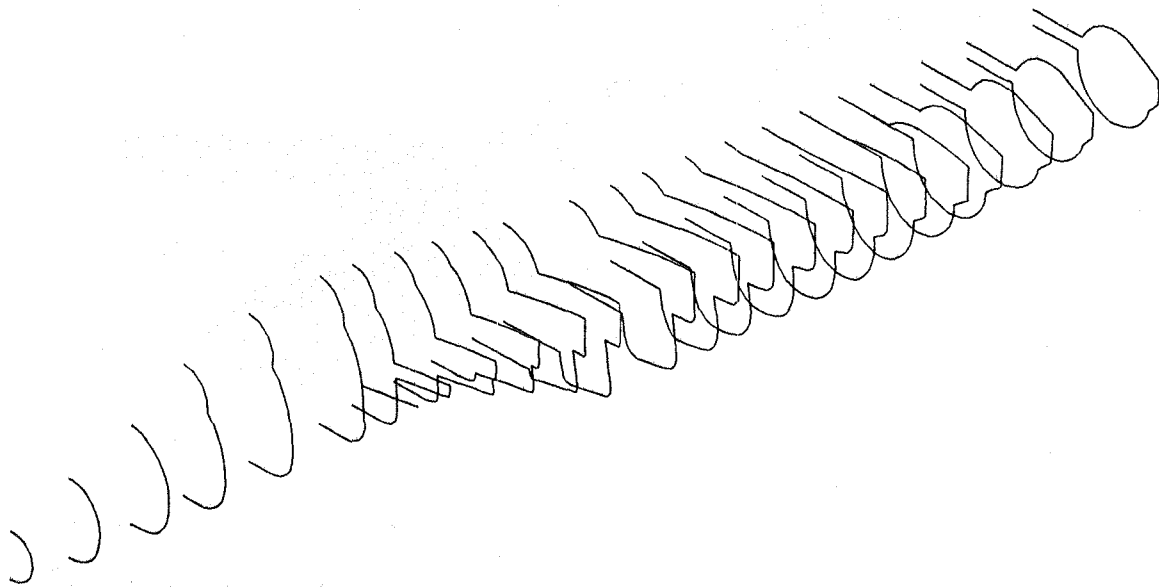
Figure 48. F-14 Body Cross Sections
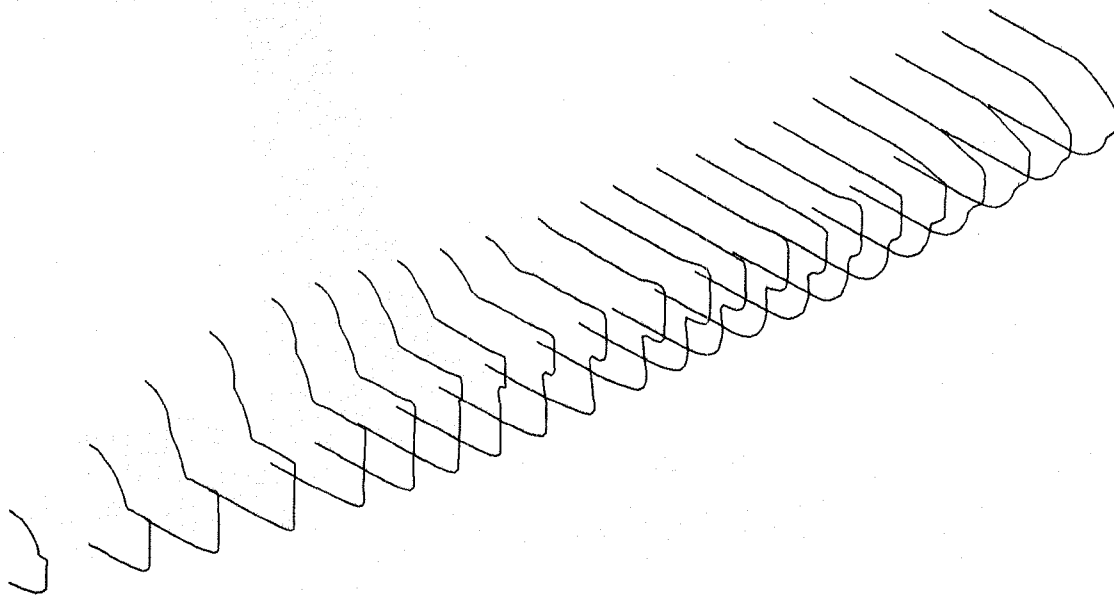
Figure 49. F-14 Body Cross Sections Modified for A488 Code
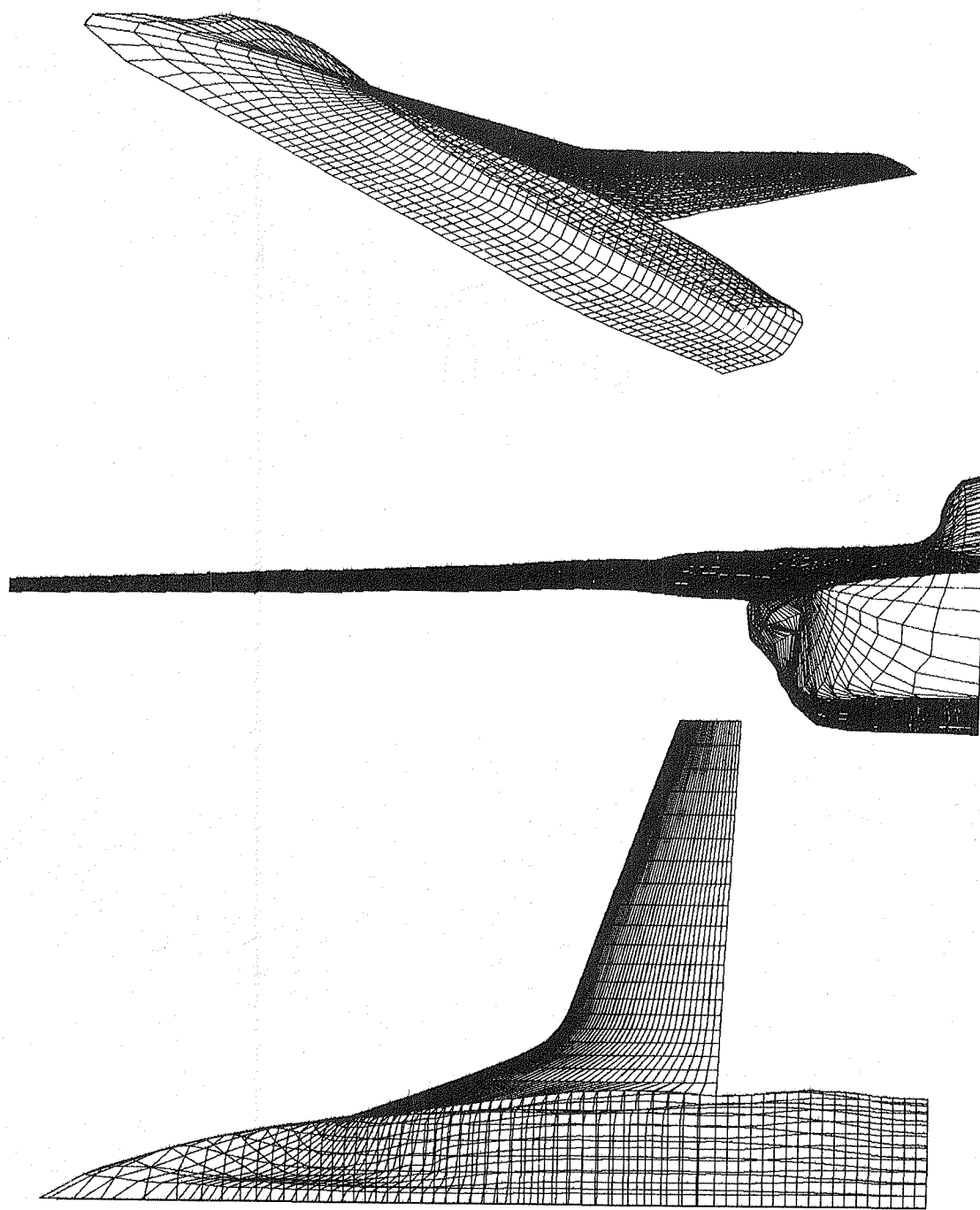
Figure 50. Surface Grid of F-14 in A488 Code
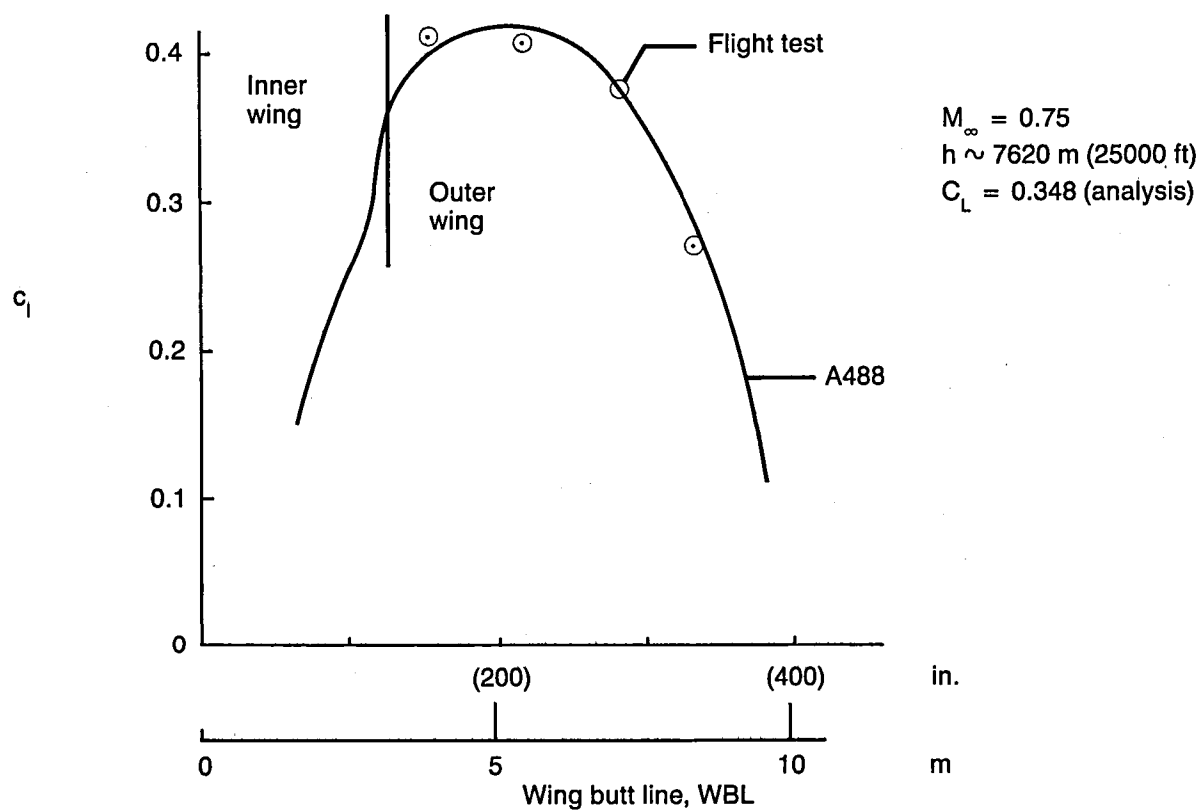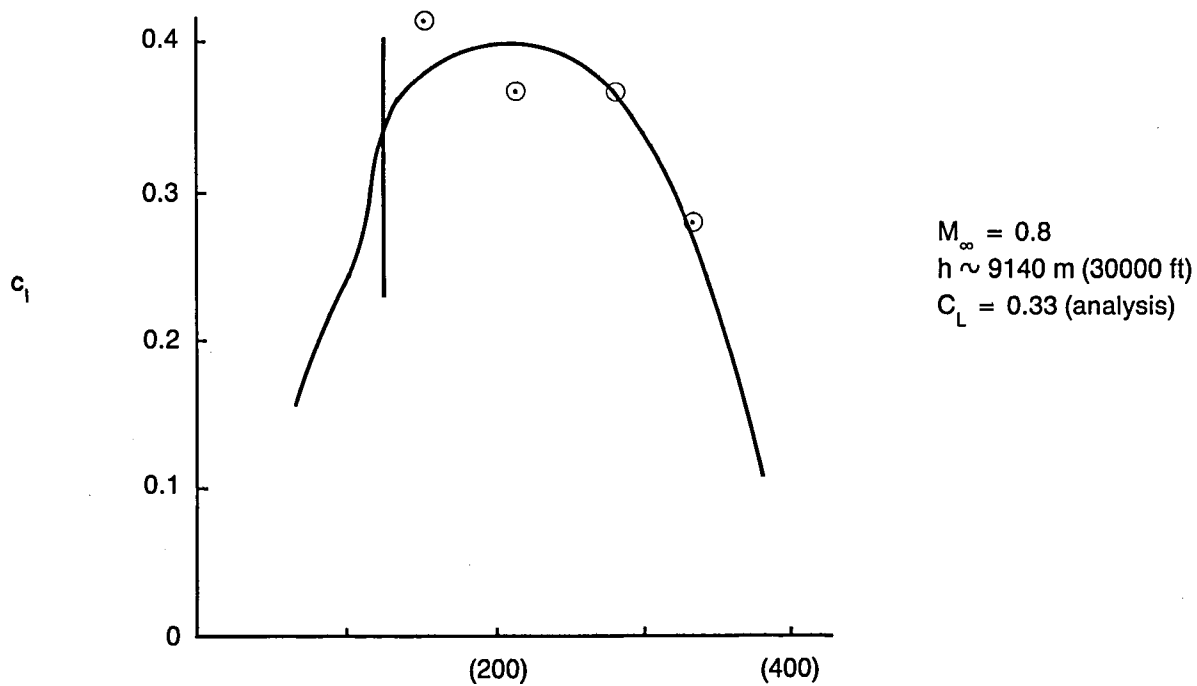
Figure 51. Flight Data/Analyses Comparisons of Spanwise Lift Distribution
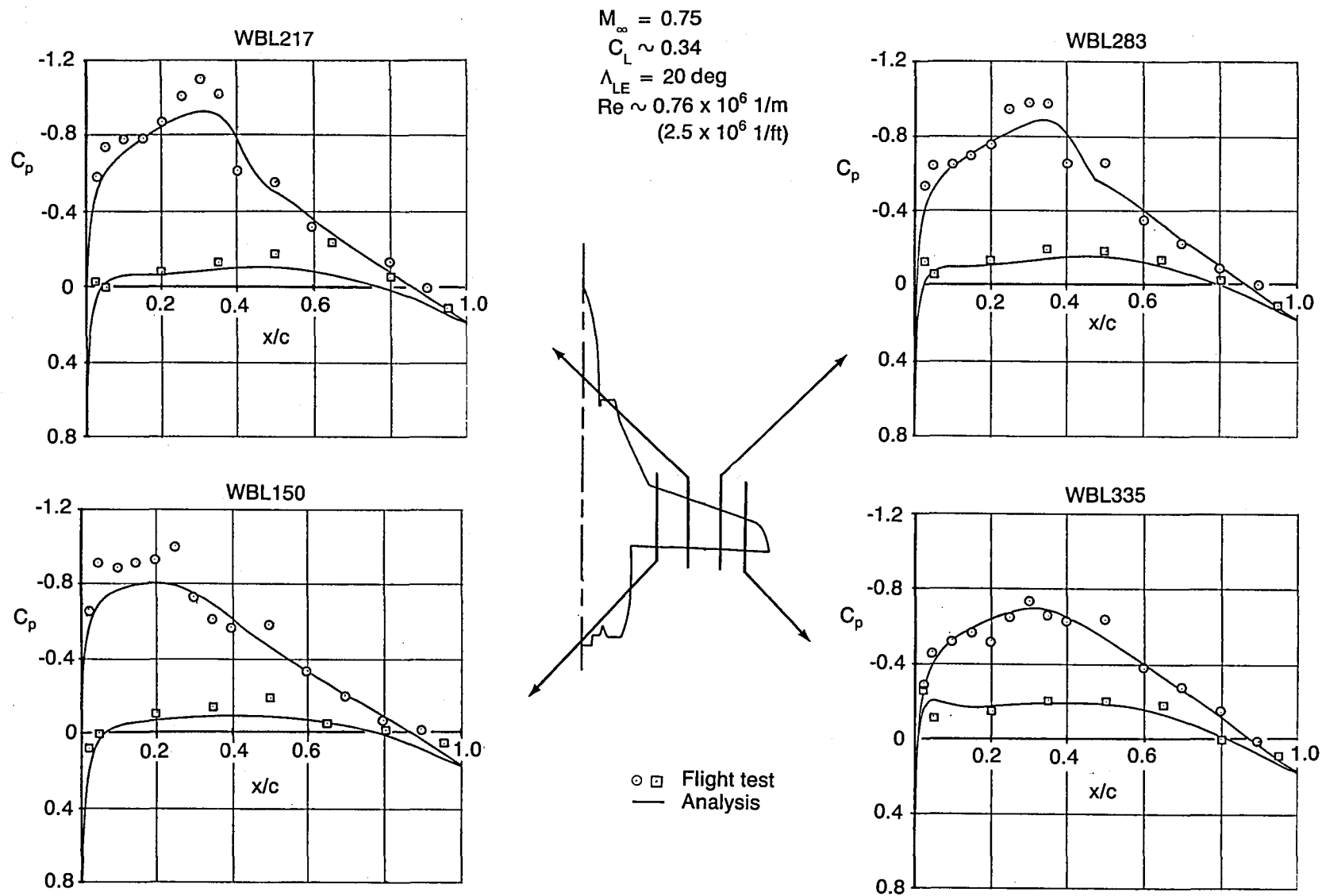
Figure 52. Comparison of F-14 Wing Pressures From Flight and Analysis, $M_\infty = 0.75$

$M_\infty = 0.8$
$C_L \sim 0.33$
$\Lambda_{LE} = 20$ deg
$Re \sim 0.69 \times 10^6$ 1/m
$(2.25 \times 10^6 1/ft)$

⊙ ⊡ Flight test
—— Analysis
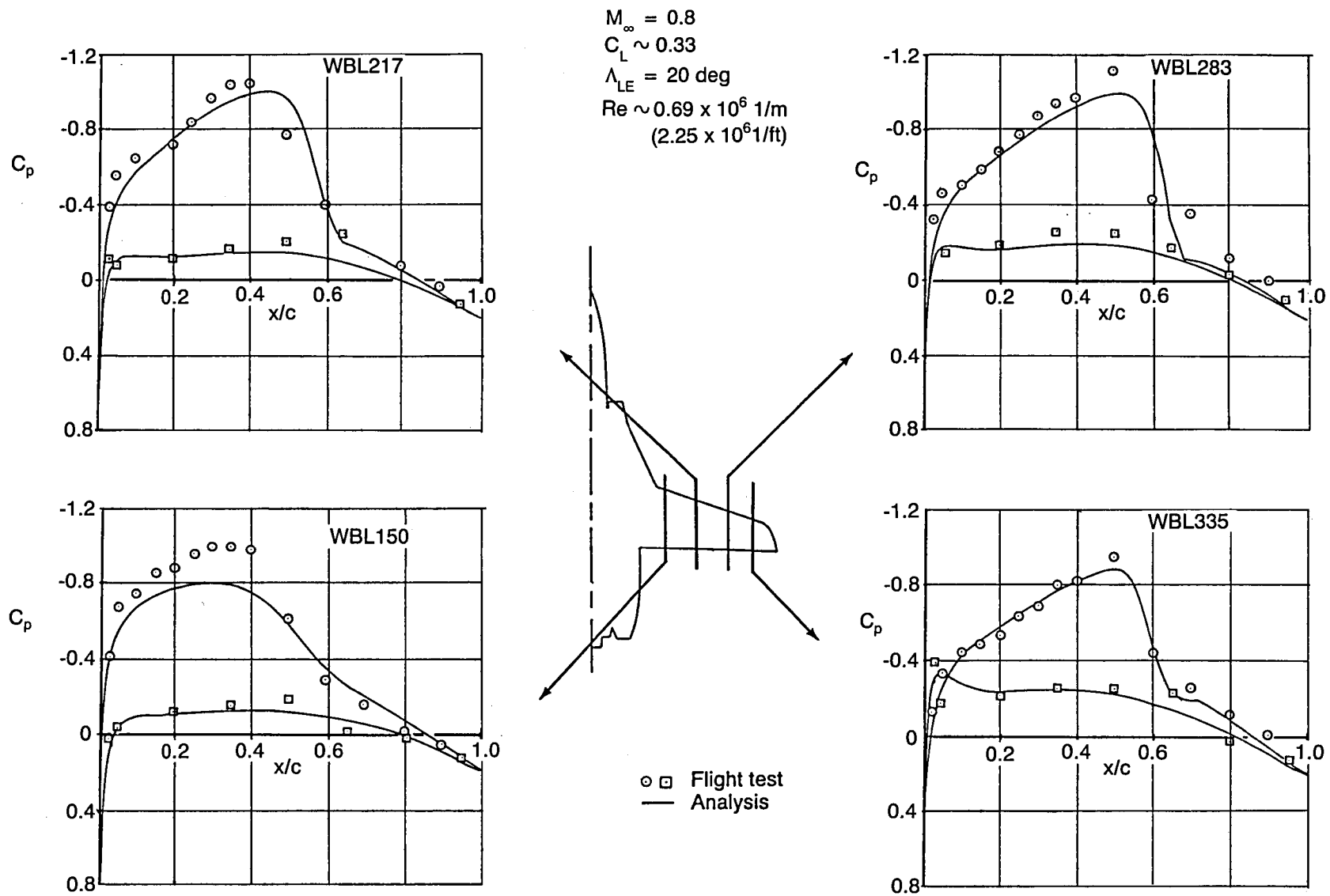
Figure 53. Comparison of F-14 Wing Pressures From Flight and Analysis, $M_\infty = 0.8$

$M_\infty = 0.75$
$\alpha = 1.5$ deg
$C_L = 0.35$
$R_e \sim 0.76 \times 10^6$ 1/m (2.5×10^6 1/ft)
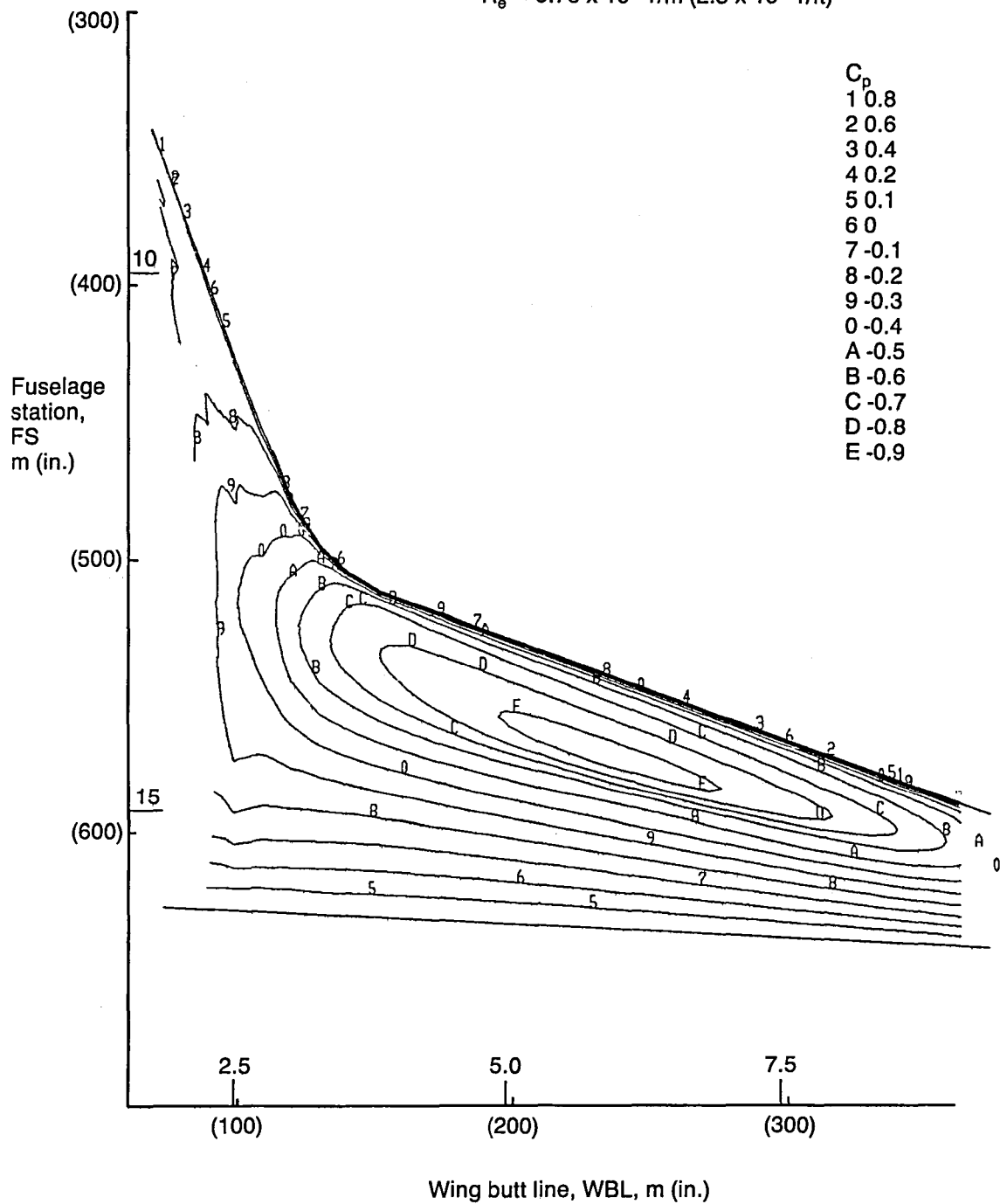
Figure 54. Isobars for F-14 Wing Analysis, $M_\infty = 0.75$

$M_\infty = 0.8$
$\alpha = 1.1$ deg
$C_L = 0.33$
$Re \sim 0.70 \times 10^6$ 1/m (2.29×10^6 1/ft)
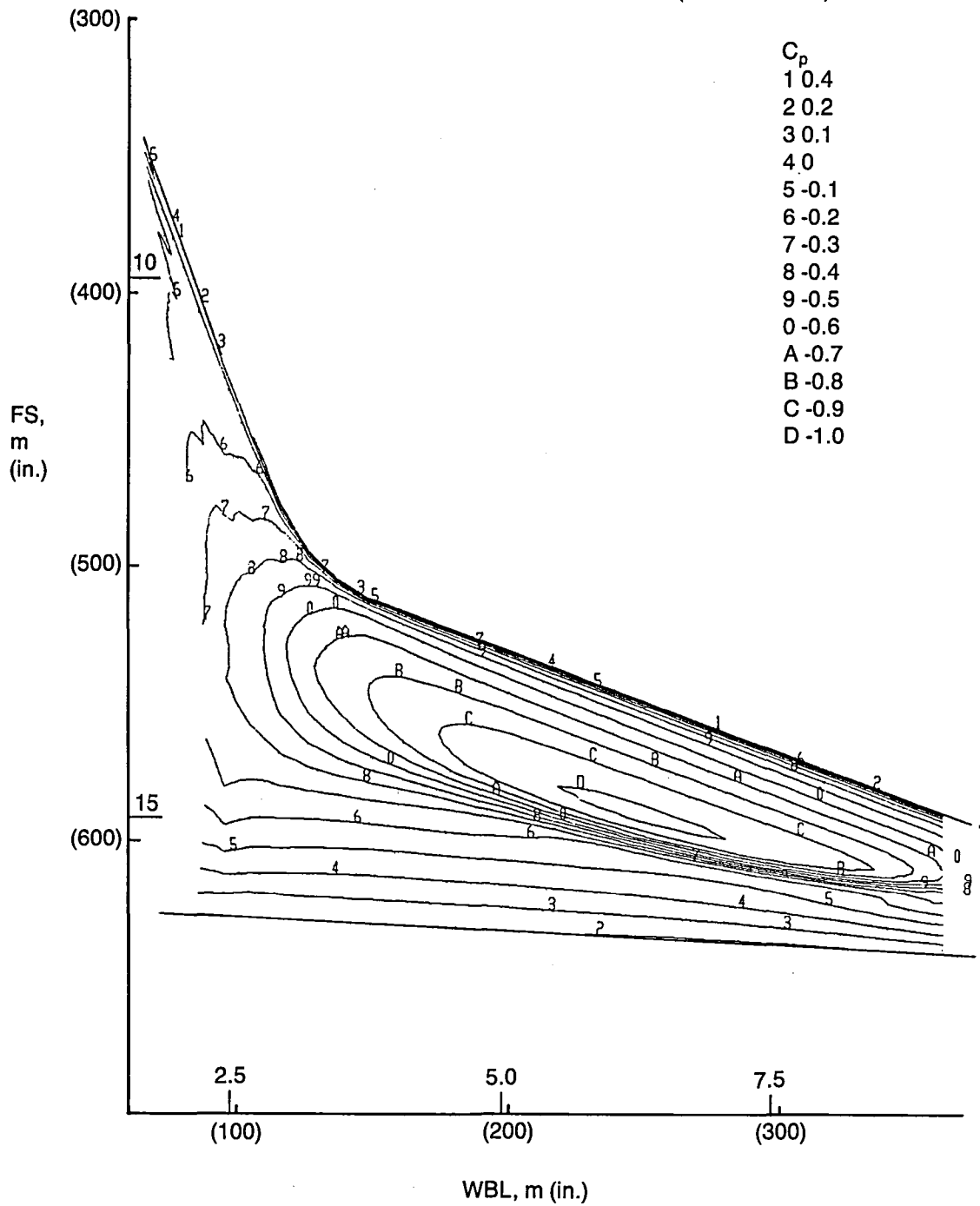
Figure 55. Isobars for F-14 Wing Analysis, $M_\infty = 0.8$

0   (100)   (200)   (300)   (400)
                  5
10 ─┤   10
(400)┤

Wing butt line, WBL, m (in.)

Fuselage
station,
FS, m
(in.)

(500)

20 deg

Pressure
orifices

Quarter chord line

Leading-edge
Slat joint

59% C

15
(600)

2.59   2.16   1.70
(102)   (85)   (67)

Normal chord length, m (in.)
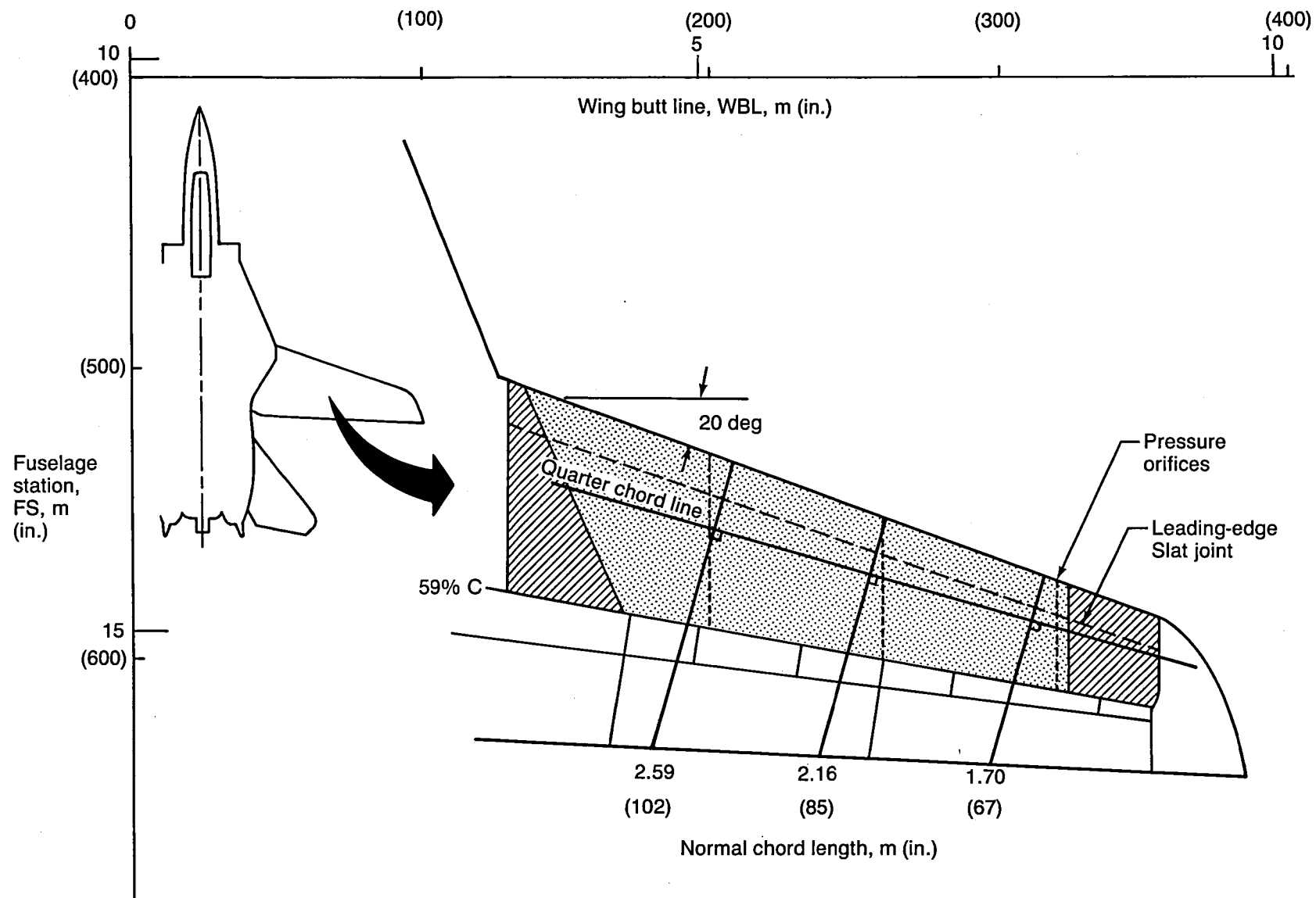
Figure 56. F-14 Outer Wing Planform at 20-deg Leading Edge Sweep With Glove Layout

$M_\infty = 0.8$ $\Lambda_{LE} = 20$ deg $h \sim 6100$ m (20,000 ft.)
$C_L \sim 0.21$ $Re \sim 0.96 \times 10^6$ 1/m $(3.15 \times 10^6$ 1/ft)
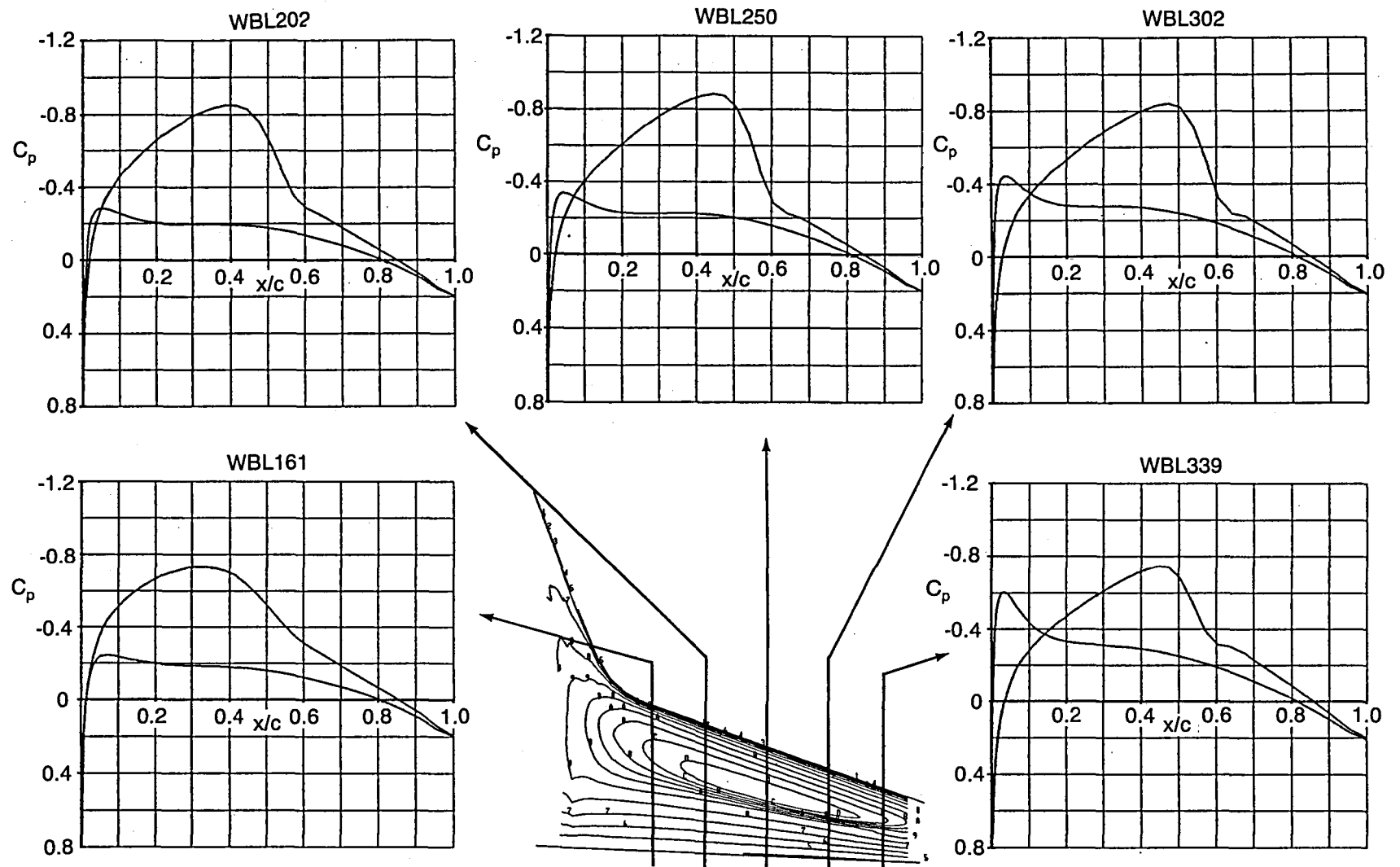
Figure 57. Analytical Wing Pressures for F-14 Base Wing at Mach 0.8 Glove Design Condition

WBL202
$M_N = 0.77$
$c_i \sim 0.26$

Base section

Desired c_p distribution

Design code result
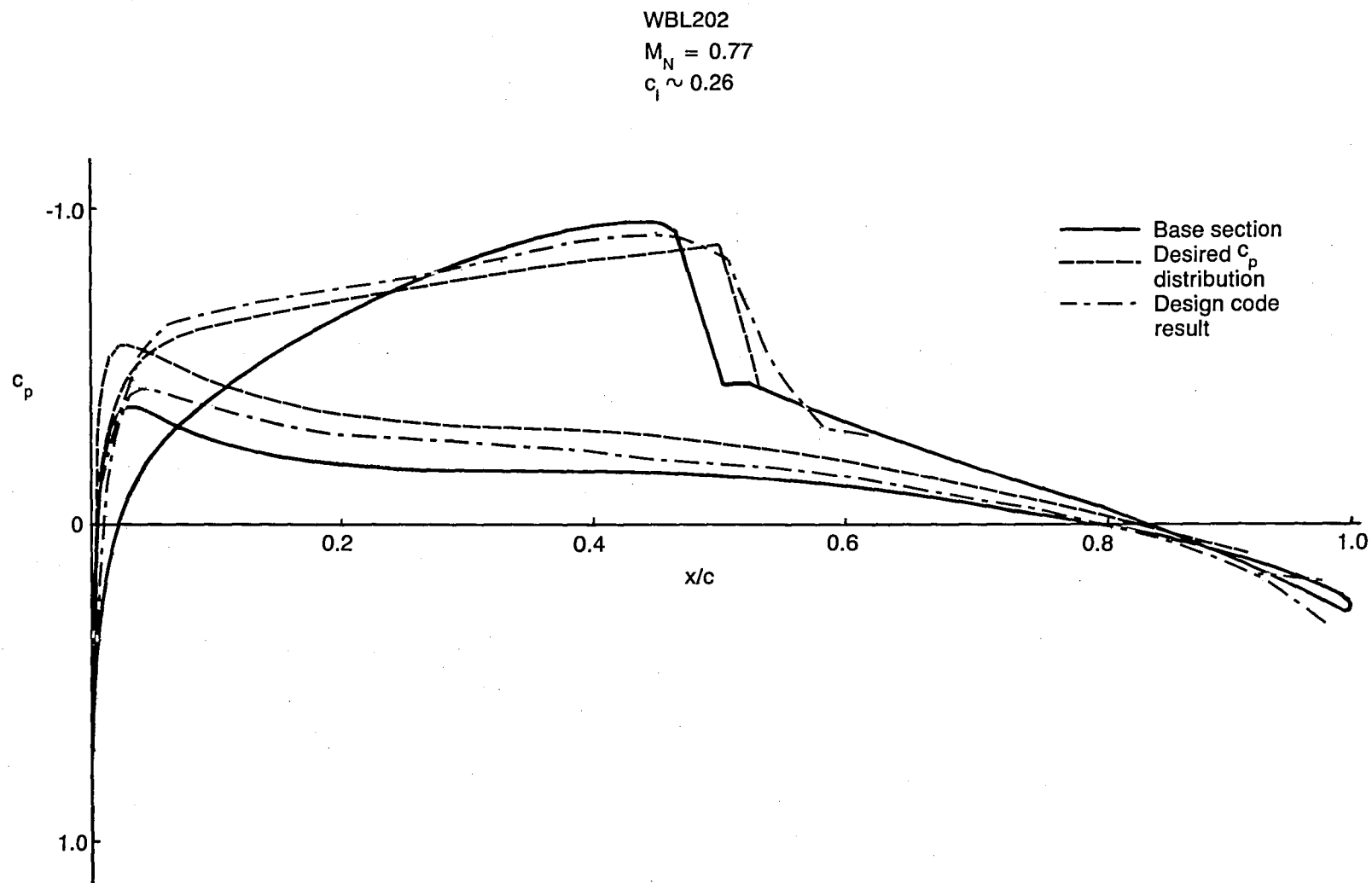
Figure 58. Design Section Pressure Distribution for the Mach 0.8 Glove
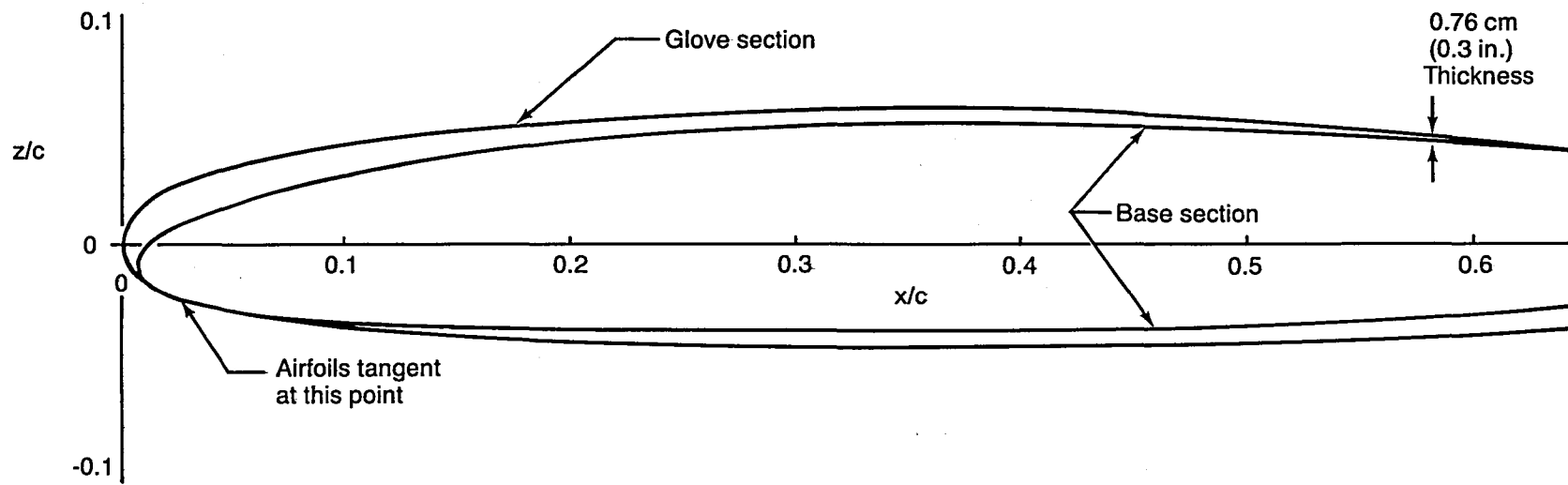
Figure 59. Mach 0.8 Glove Placement on Base Section

- Section at WBL202
- Chord ~ 2.59 m
  (102) in)
- Thickness distribution A

Glove thickness
measured perpendicular
to base airfoil

Glove
thickness / Chord
t/c

0.02

0.01

0

2.54 cm
(1.0 in.)

Fictitious
fairing

Actual glove fairing

Leading edge
of base airfoil

S

0.2   0.4   0.6   0.8   1.0   1.2

Surface distance/chord, s/c
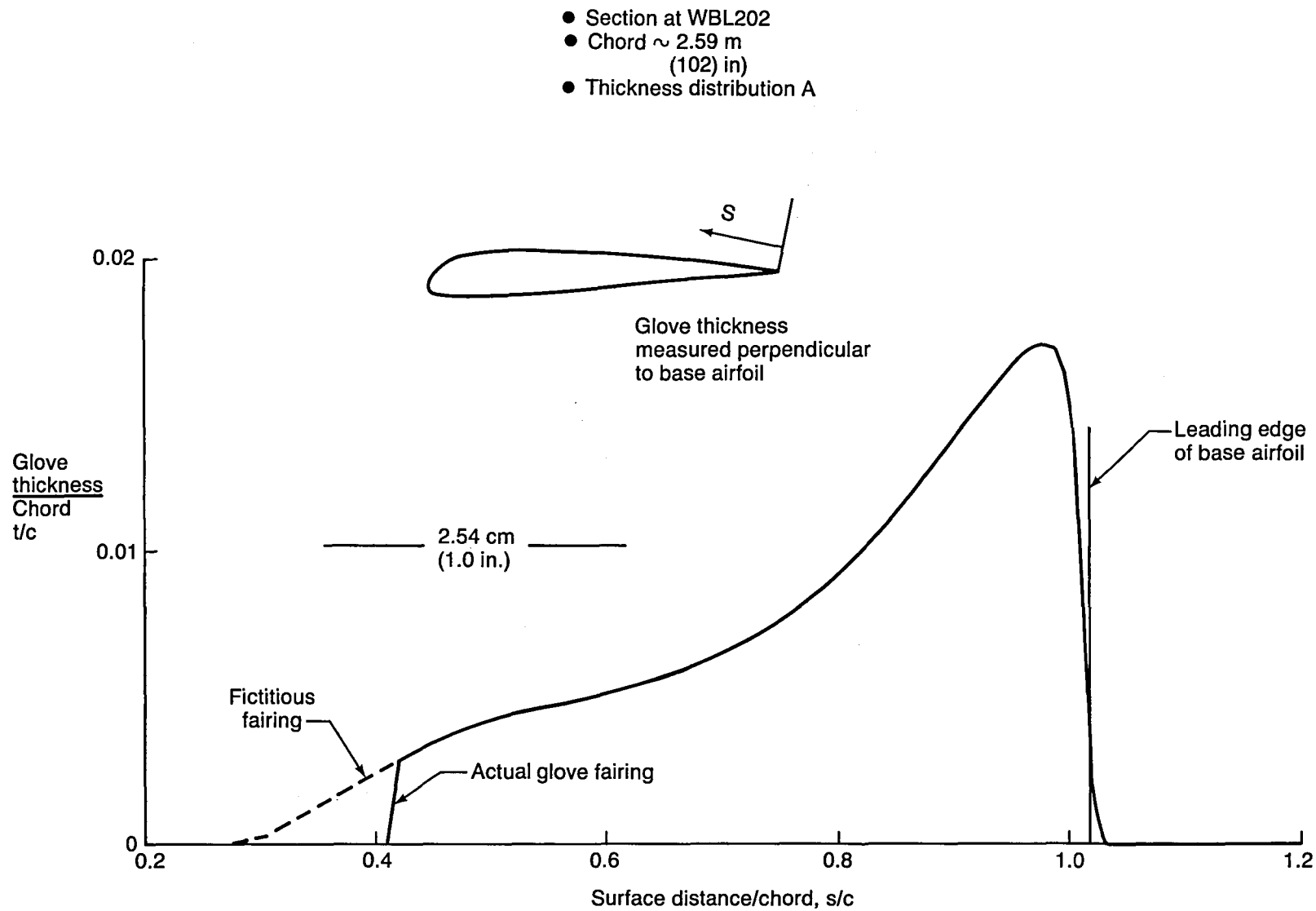
Figure 60. Mach 0.8 Glove Thickness Distribution A
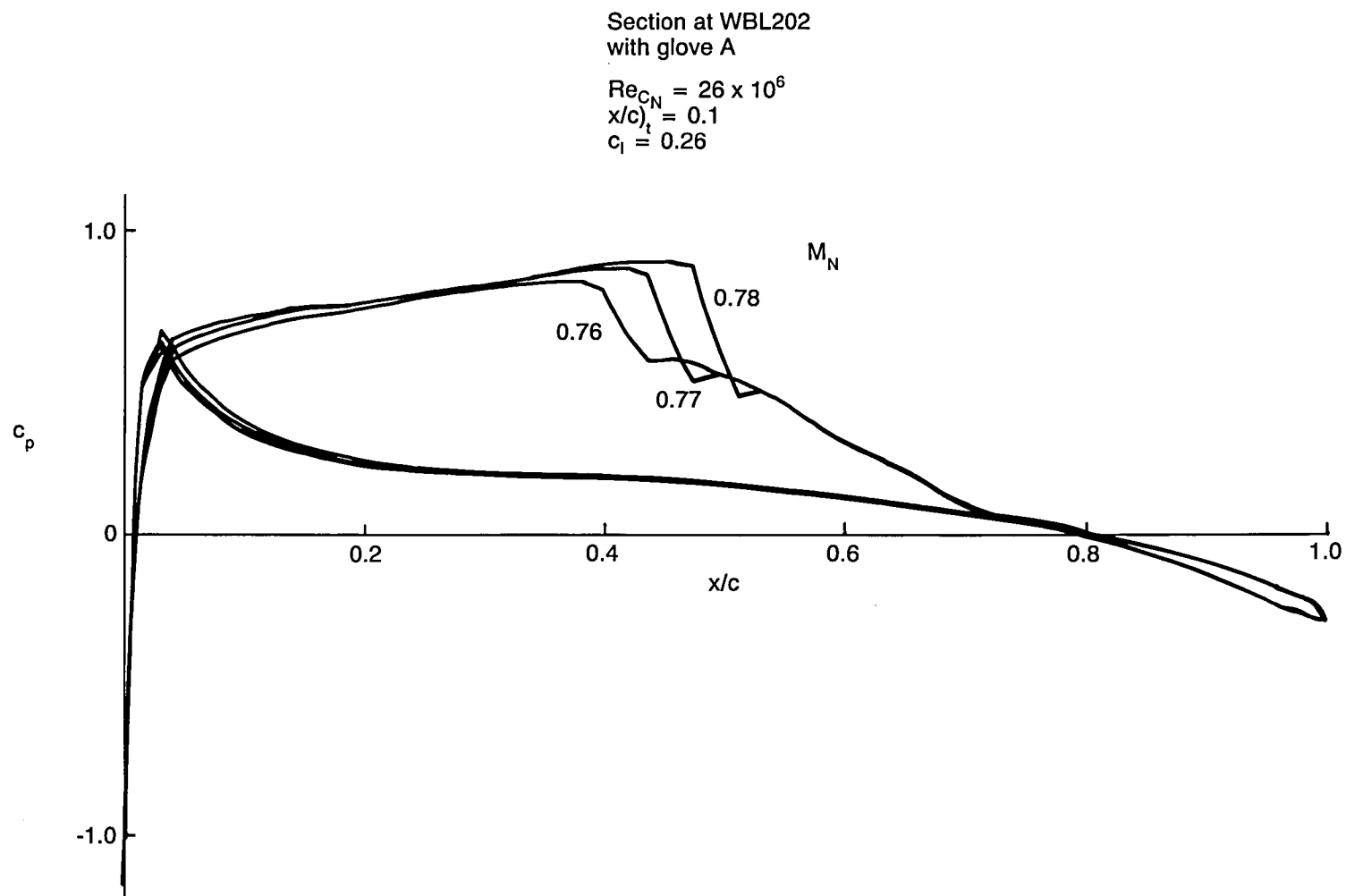
Figure 61. Mach 0.8 Glove Section Pressure Distributions Near the Design Point

Tollmien-Schlichting

$\Psi = 40$ deg

ω, Hz

4277
5018
5817
6843
9010
11976

Crossflow

$\omega = 0$

α^*r_s

1900
1600
1300
1000
800
700
600
500
400
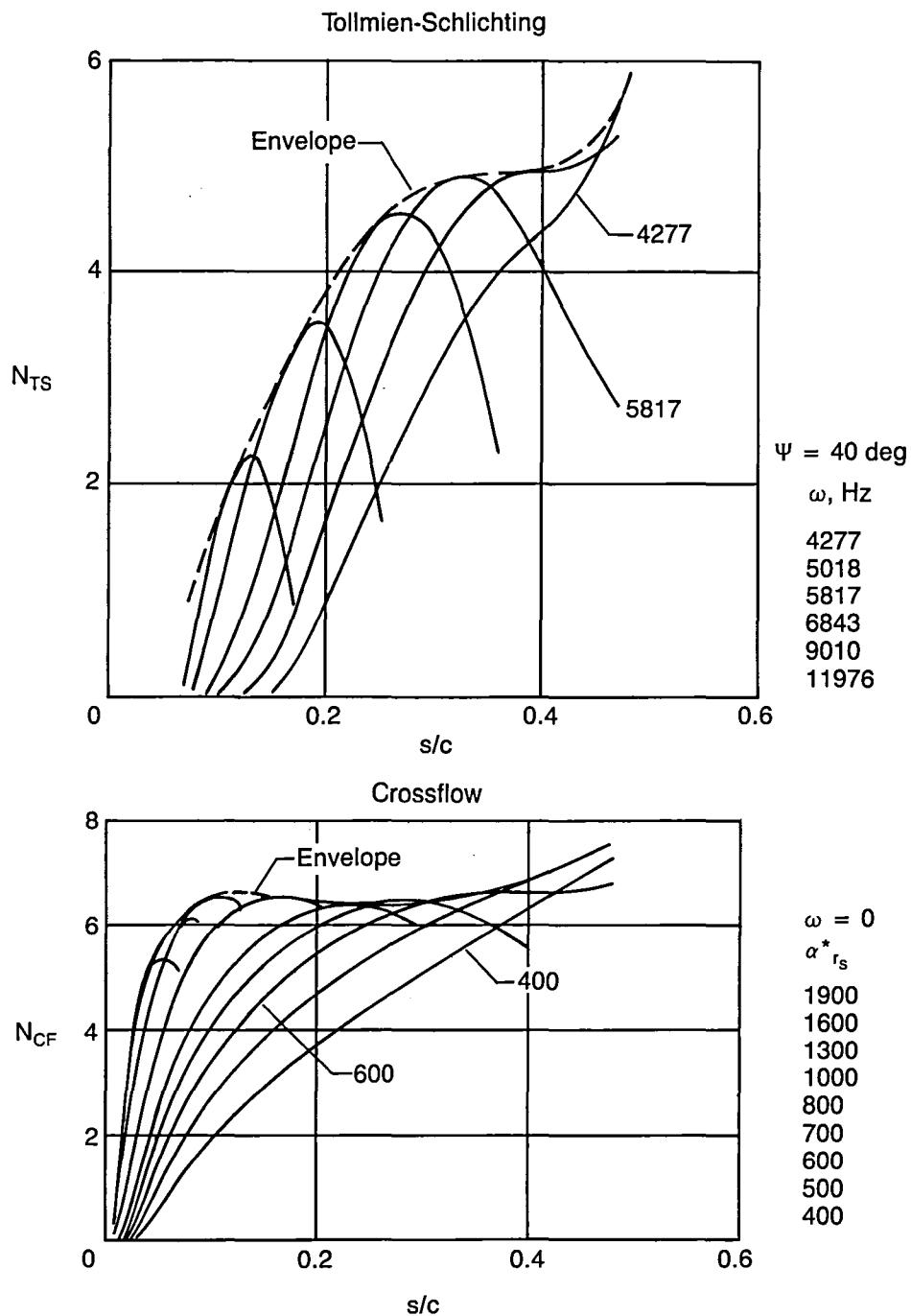
Figure 62. Disturbance Growth on the Mach 0.8 Glove From Section Analyses, $M_N = 0.78$
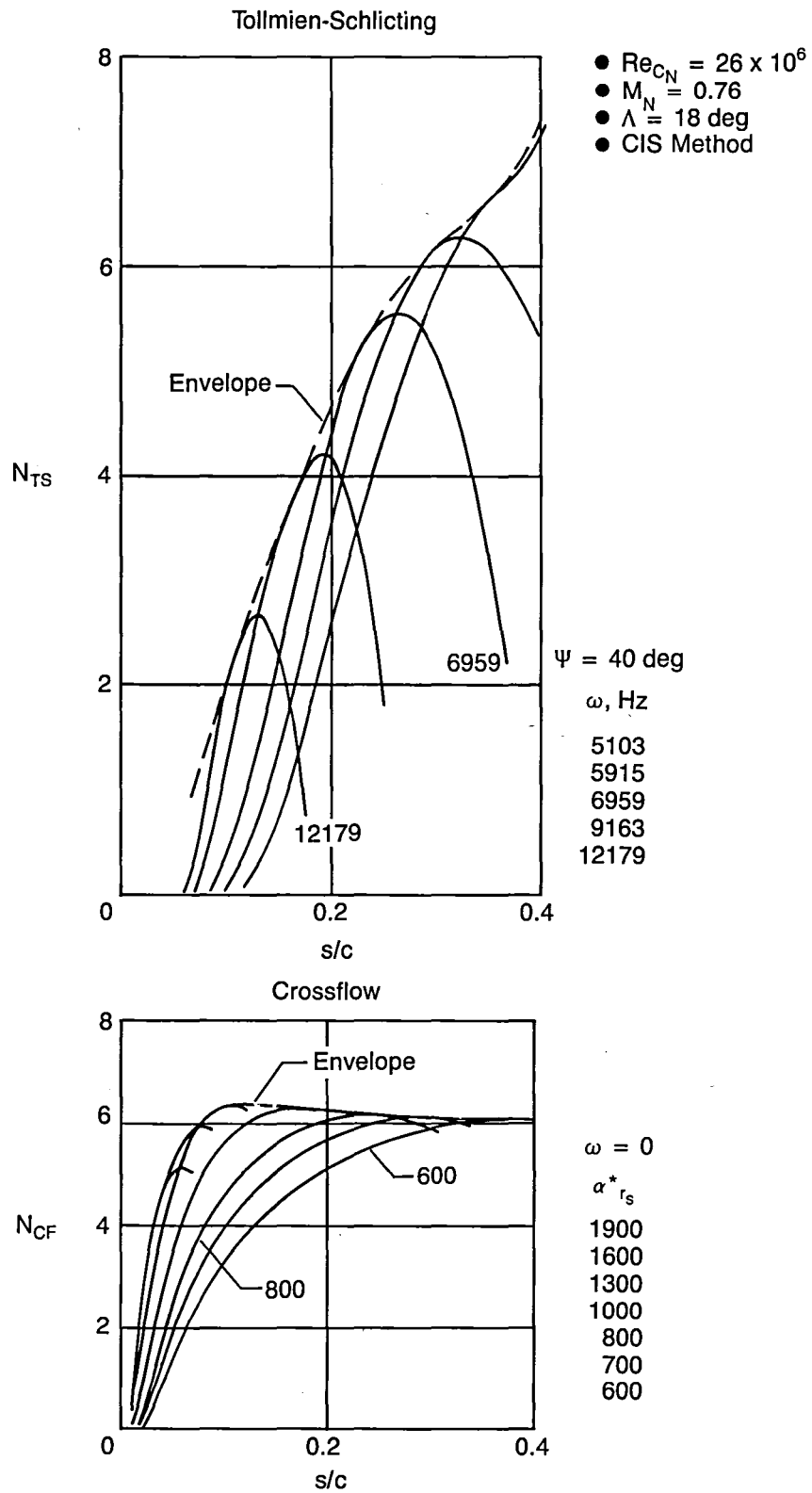
Figure 63. Disturbance Growth on the Mach 0.8 Glove From Section Analyses, $M_N = 0.76$

WBL202 with
glove A
$Re_{C_N} = 26 \times 10^6$
$\Lambda = 18$ deg
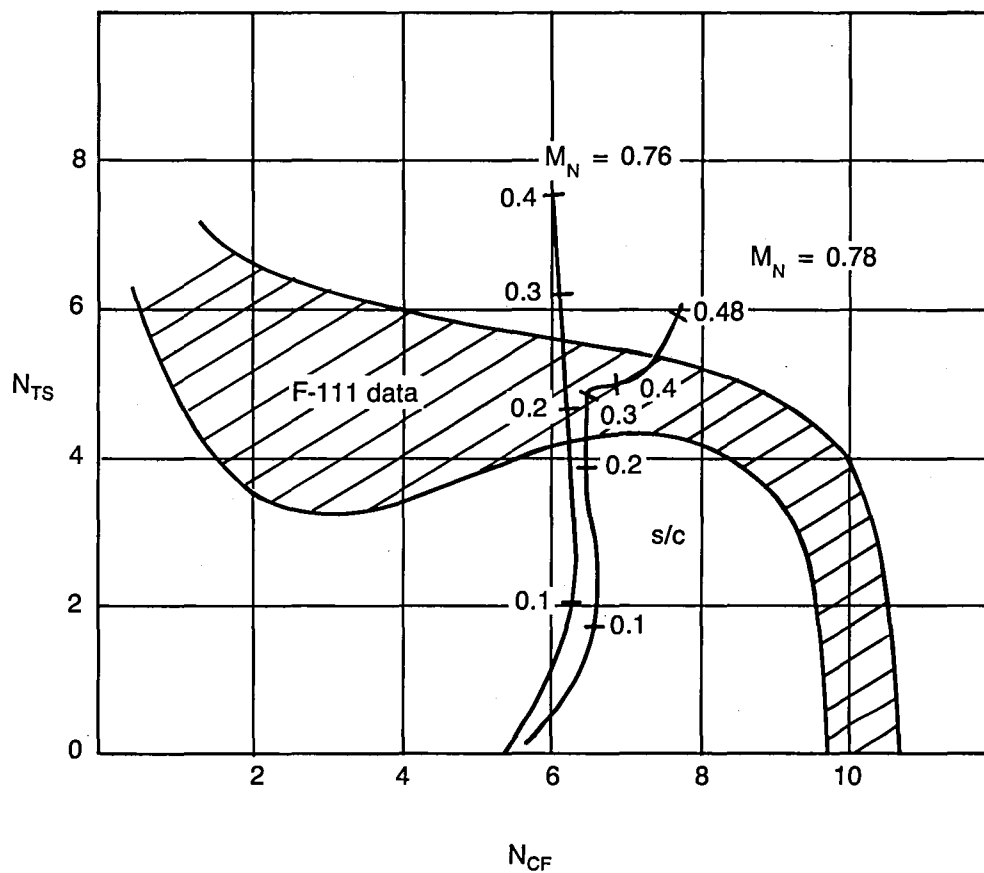
Figure 64. Disturbance Growth Traces for the Mach 0.8 Glove From Section Analyses
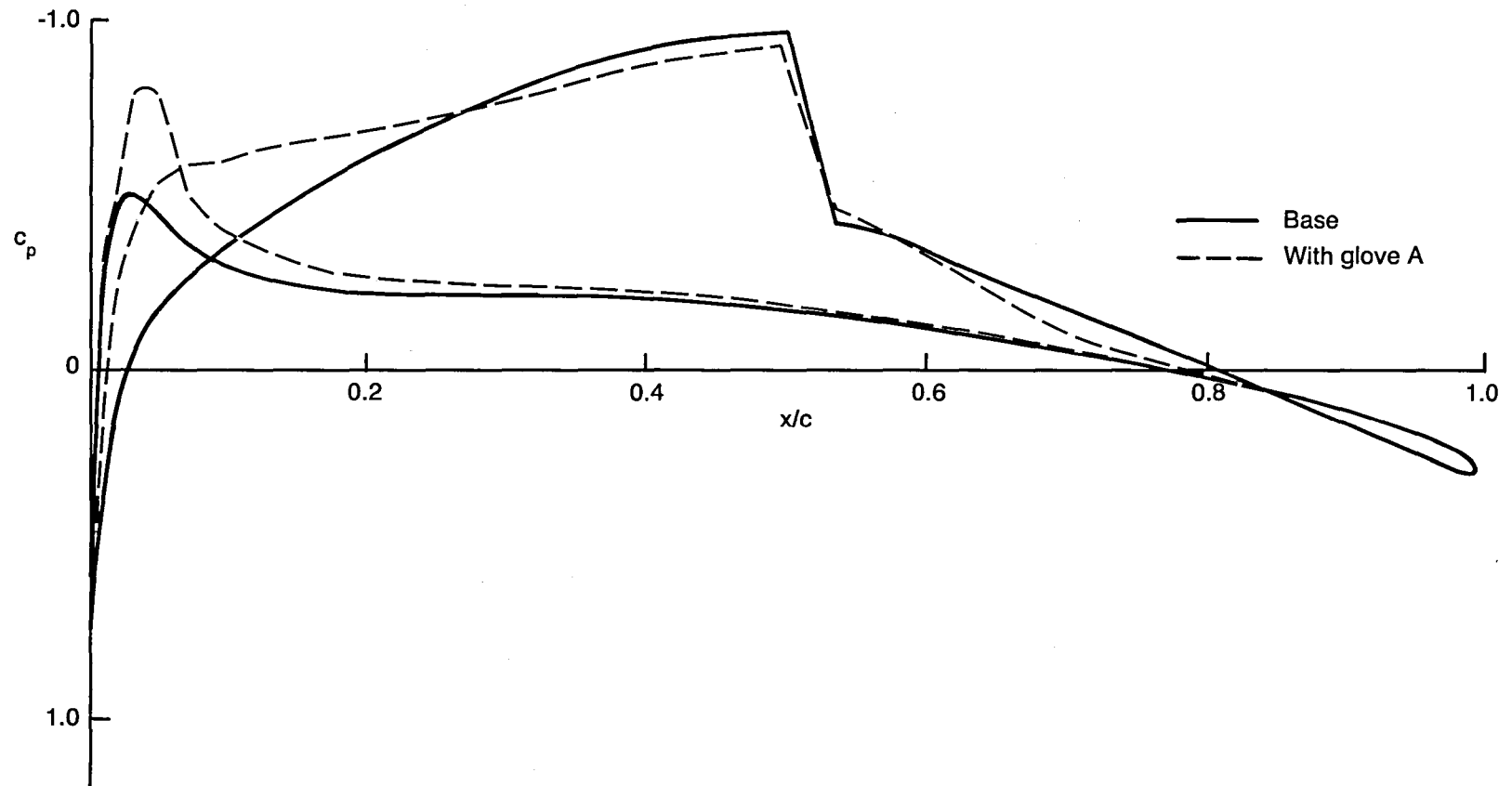
Figure 65. Pressure Distribution of Wing Section WBL256 With Thickness Distribution A

Section at
WBL311
$M_N = 0.78$
$c_l = 0.185$

$Re_{c_N} = 17 \times 10^6$
$x/c)_t = 0.1$

Base
With glove A
With glove B
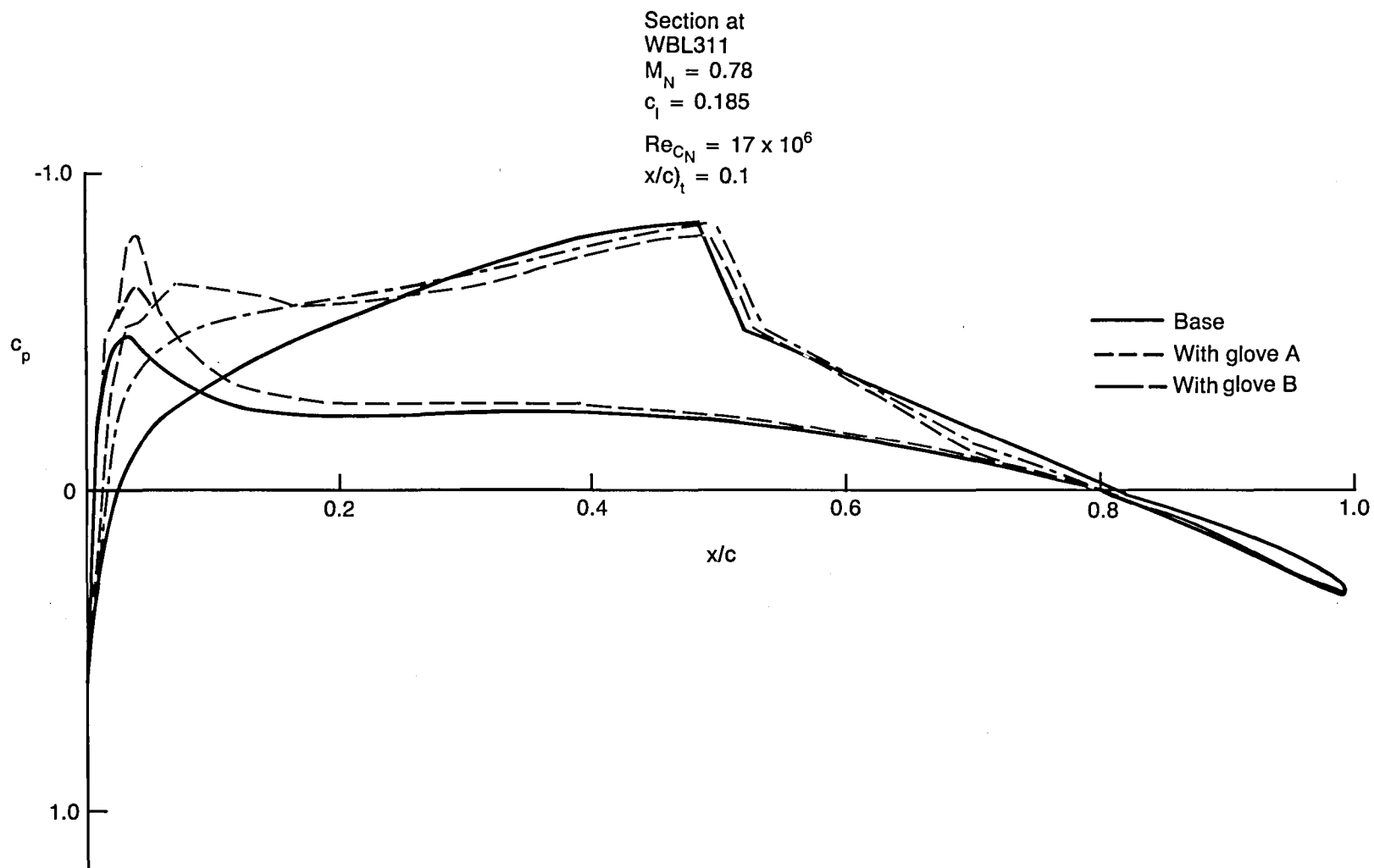
Figure 66. Pressure Distributions of Wing Section WBL311 With Thickness Distributions A and B
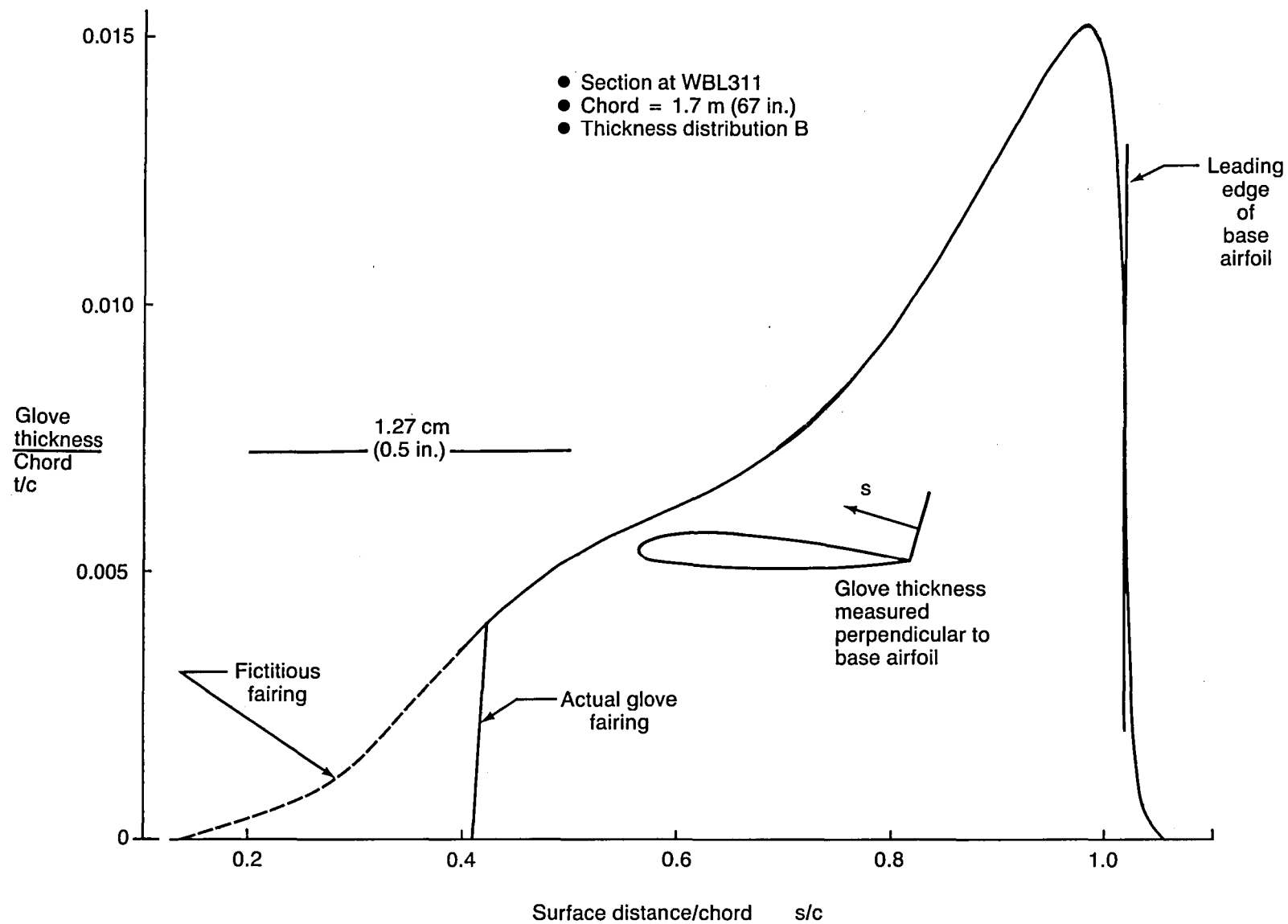
Figure 67. Mach 0.8 Glove Thickness Distribution B
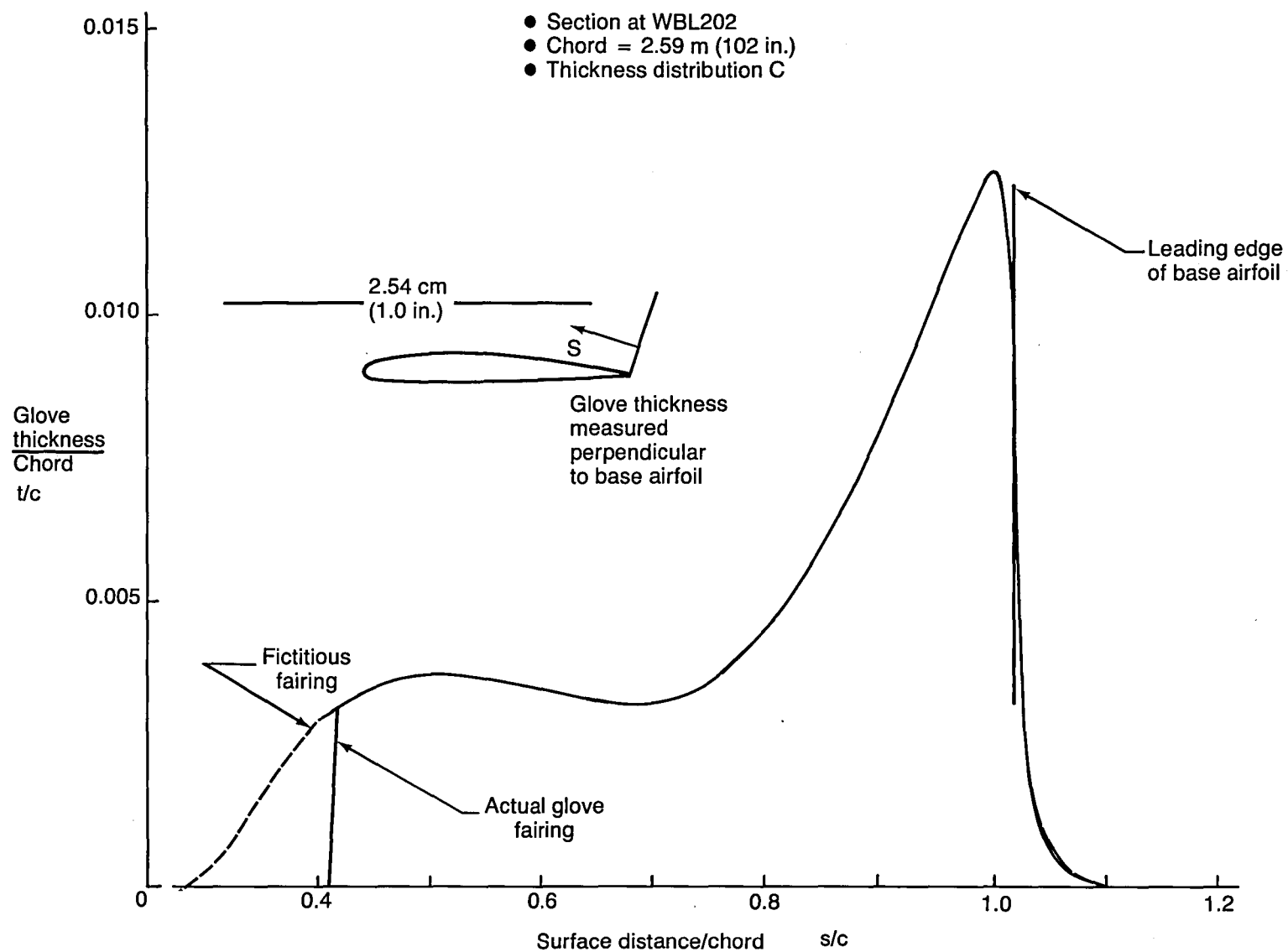
Figure 68. Mach 0.8 Glove Thickness Distribution C

$M_{\infty} = 0.81$ $C_L \sim 0.20$ $h \sim 6100m$ (20,000 ft)
$\Lambda_{LE} = 20$ deg $Re \sim 0.98 \times 10^6 1/m$ (3.2×10^6 1/ft)
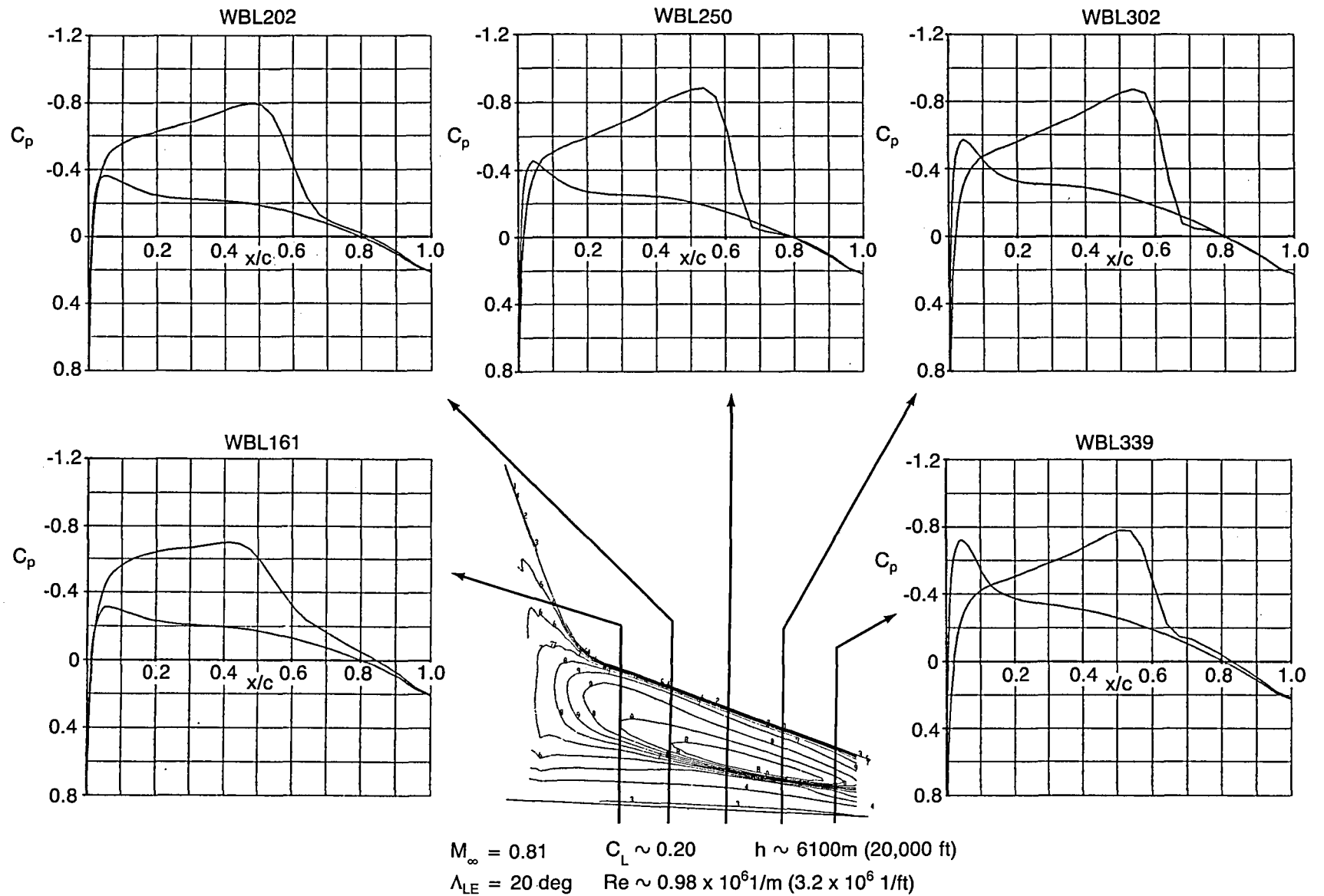
Figure 69. Analytical Wing Pressures of Mach 0.8 Glove at Design Condition
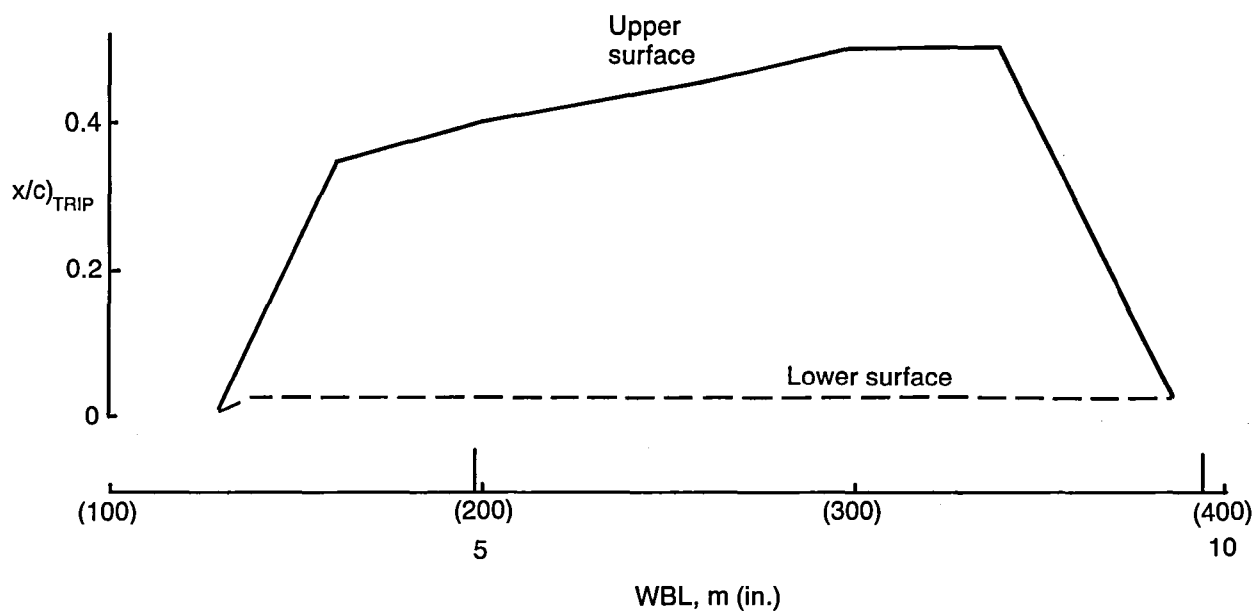
Figure 70. Assumed Transition Locations for Mach 0.8 Glove at Design Condition
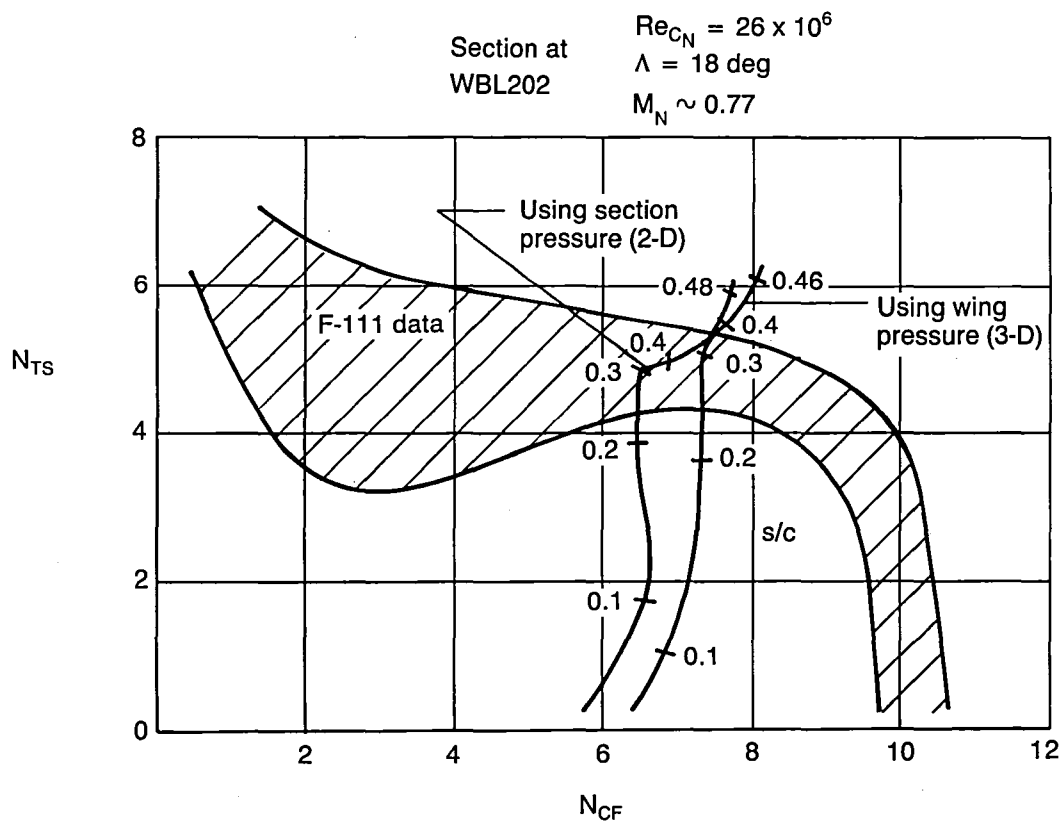
Figure 71. Comparison of Disturbance Growth Traces for Mach 0.8 Glove From Section and Wing Pressures
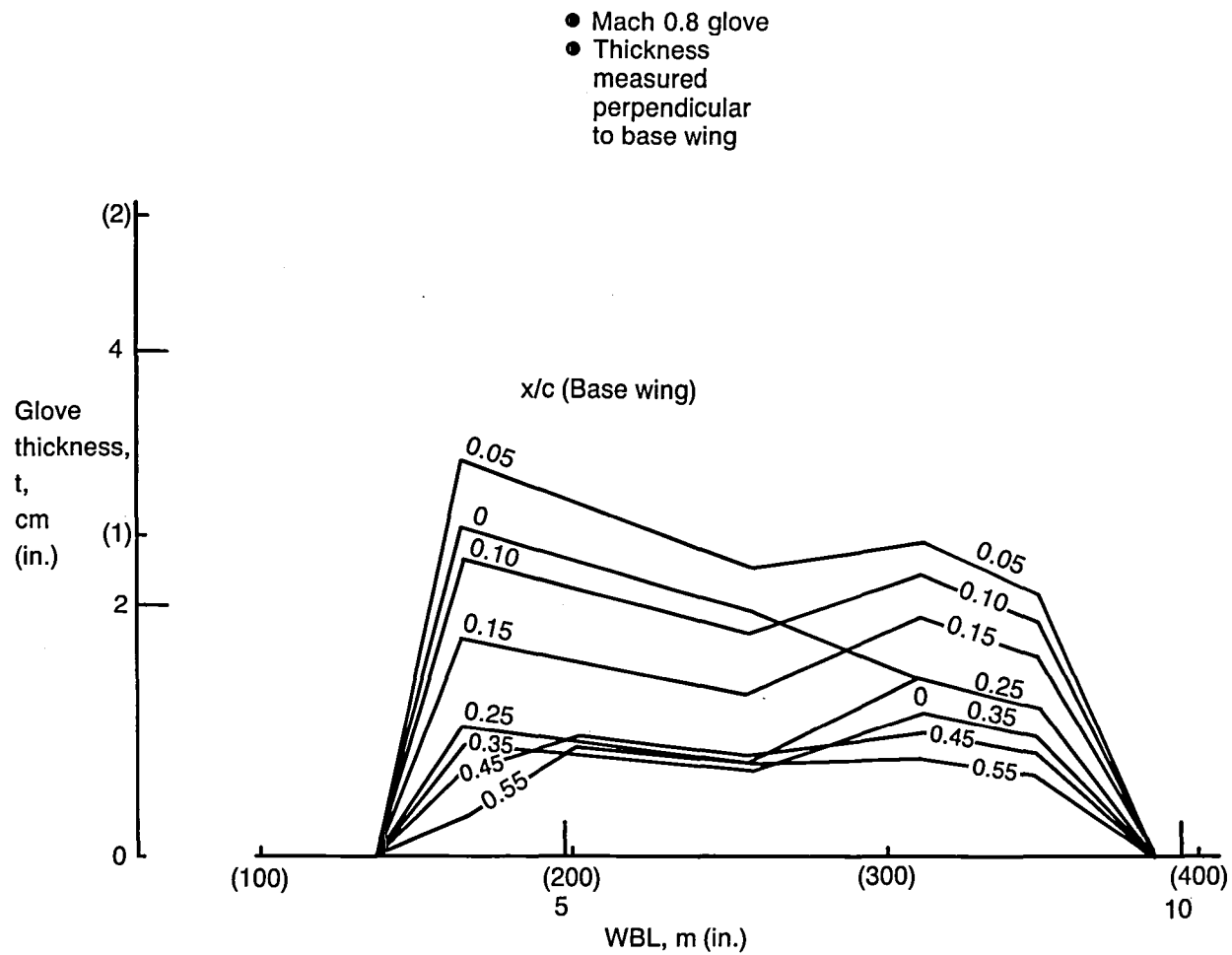
Figure 72. Physical Thickness of Mach 0.8 Glove Across the Wing

$M_\infty = 0.81$
$Re = 0.98 \times 10^6/m \ (3.2 \times 10^6/ft)$
$C_L = 0.2$
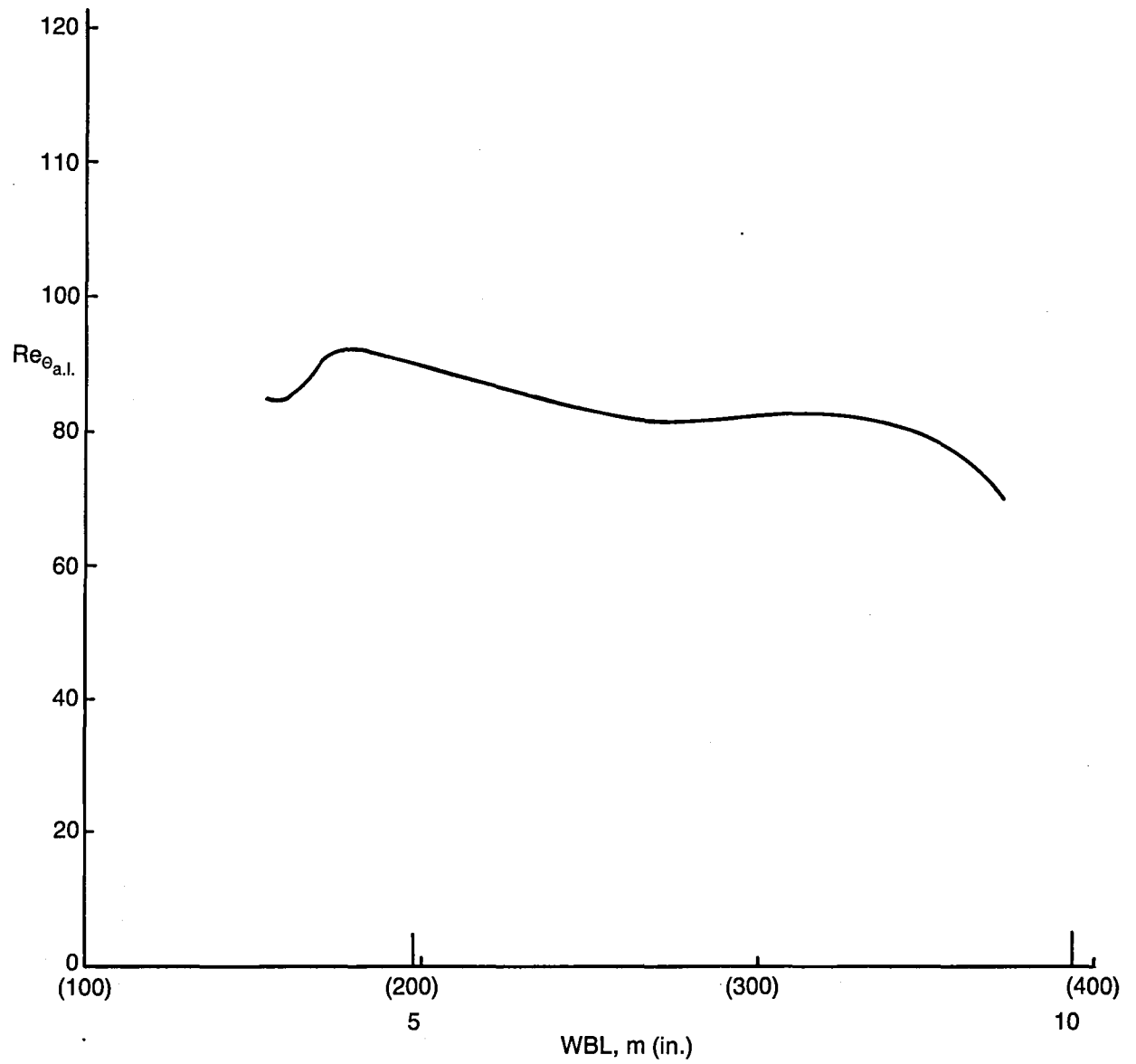
Figure 73. Attachment Line Reynolds No. for Mach 0.8 Glove at the Design Condition
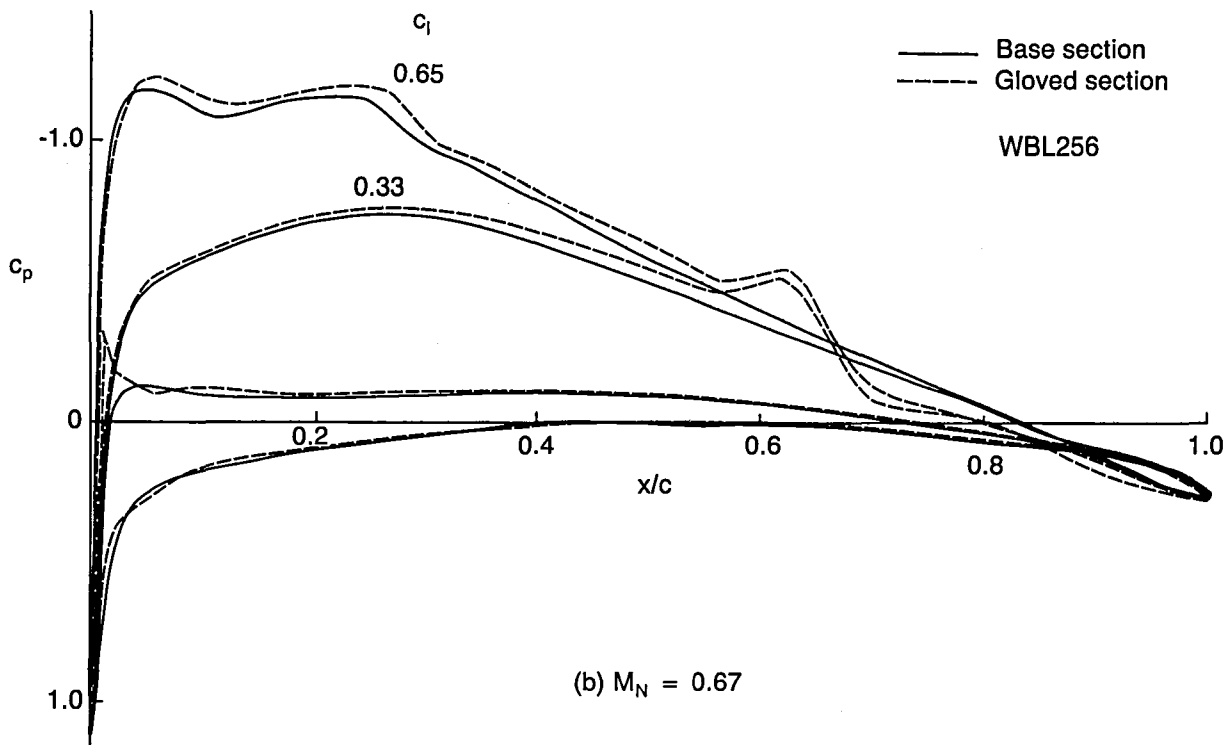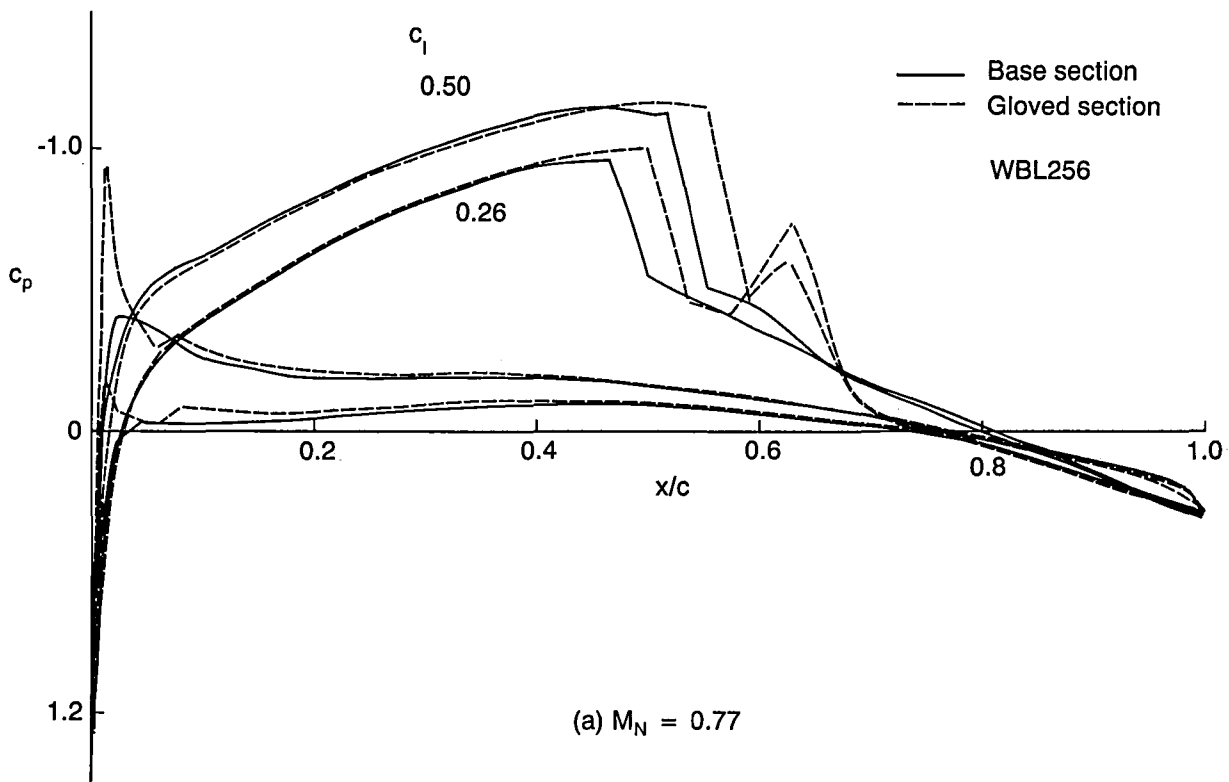
Figure 74. Comparison of Pressures of Base Section and Cleanup Glove
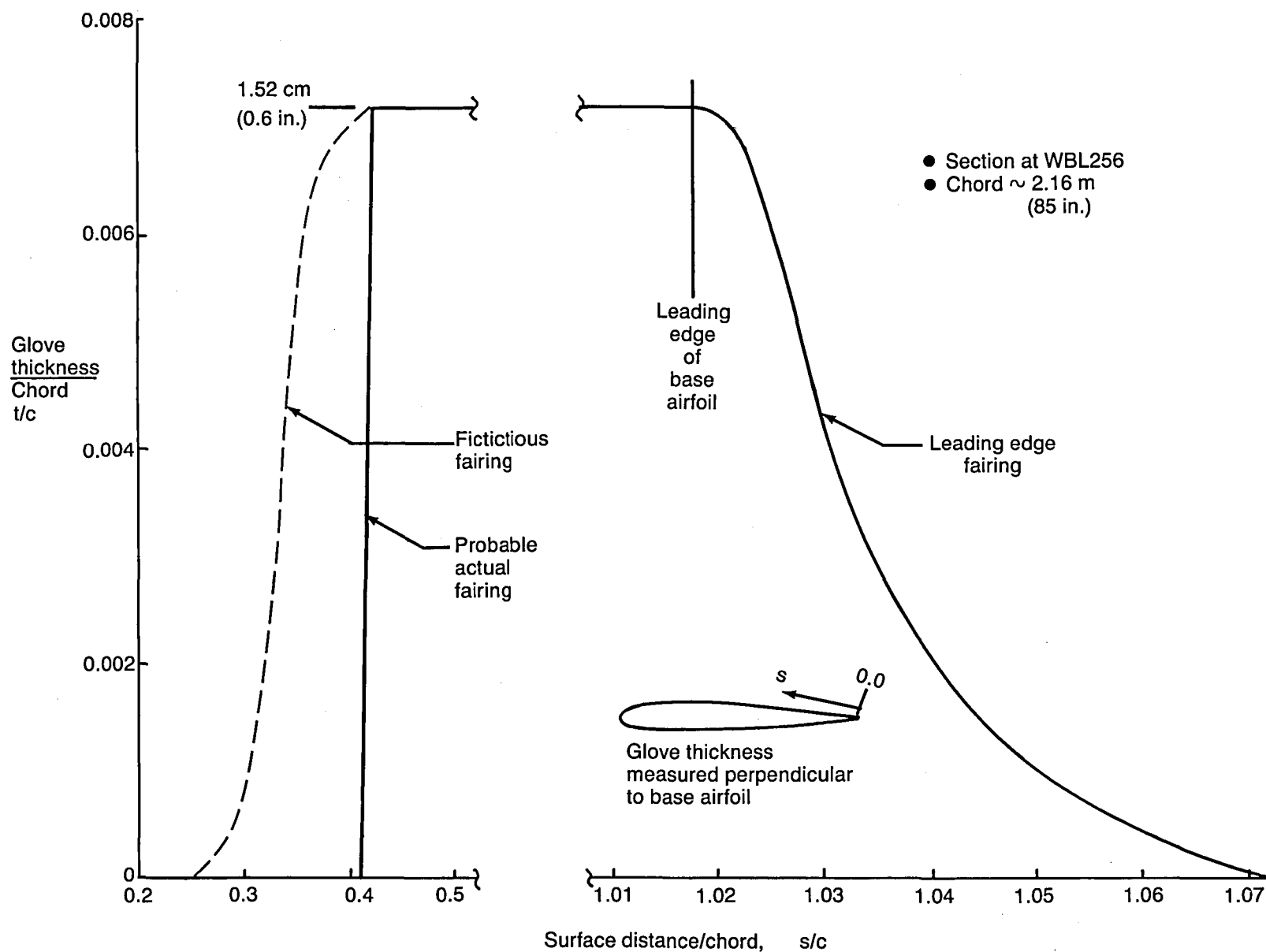
Figure 75. Cleanup Glove Thickness Distribution

Surface distance/chord,   s/c

0.008

1.52 cm
(0.6 in.)

0.006

Glove
thickness
Chord
t/c

0.004

0.002

0

0.2   0.3   0.4   0.5

Fictictious
fairing

Probable
actual
fairing

Leading
edge
of
base
airfoil

● Section at WBL256
● Chord ~ 2.16 m
        (85 in.)

Leading edge
fairing

s   0.0

Glove thickness
measured perpendicular
to base airfoil

1.01   1.02   1.03   1.04   1.05   1.06   1.07
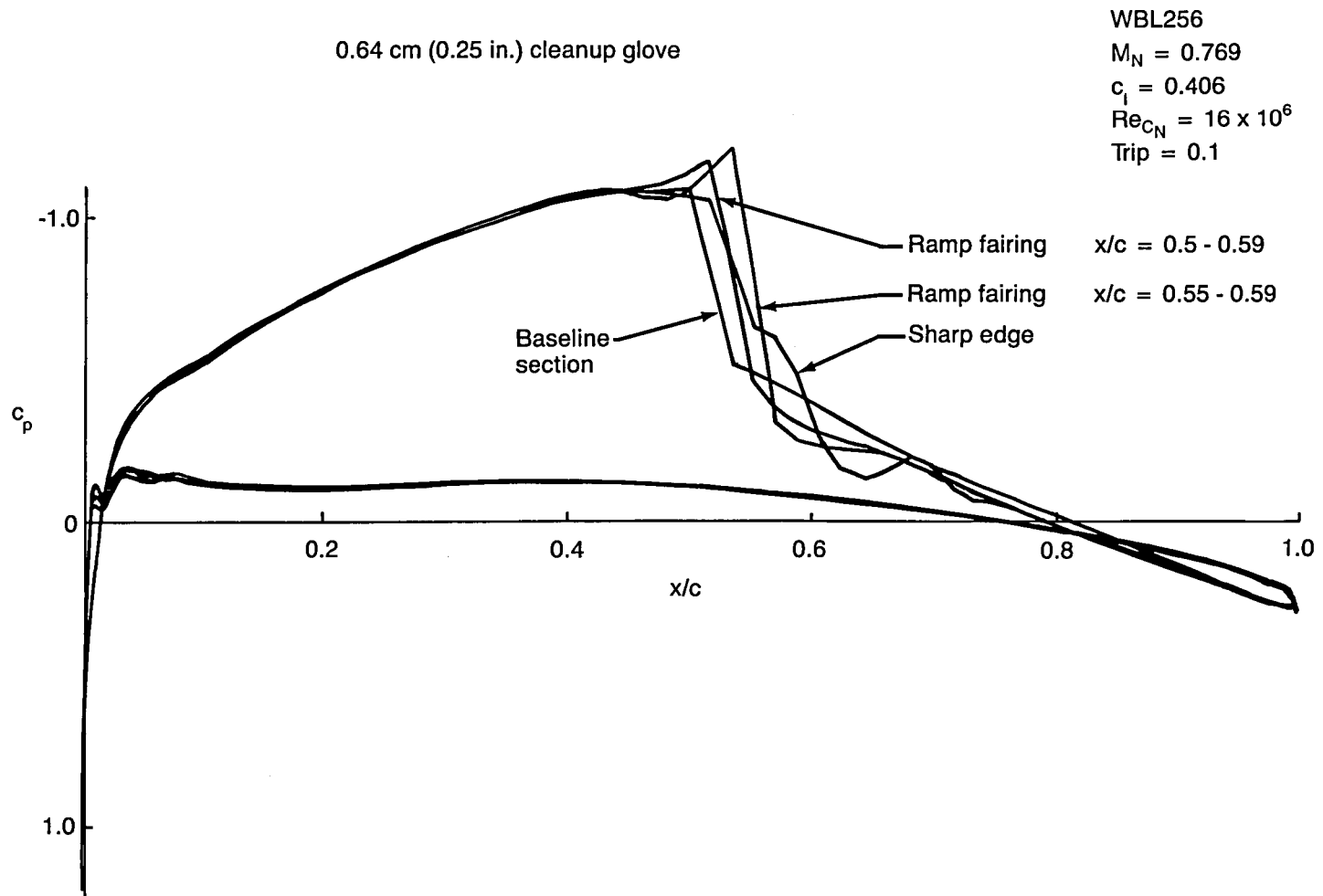
Figure 76. Effect on Pressures of Different Glove Termination Fairings

- $Re_{C_N} = 22 \times 10^6$
- $M_N = 0.77$
- $\Lambda = 18$ deg
- CIS Method

Tollmien-Schlichting

N_{TS}

Envelope

4987

9002

$\Psi = 40$ deg

ω, Hz

4057
4501
4987
6002
7523
6720
9002
10482

s/c

Crossflow

N_{CF}

Envelope

400

1000

$\omega = 0$

$\alpha^*{}_{r_s}$

1900
1600
1300
1000
800
700
600
500
450
400

s/c
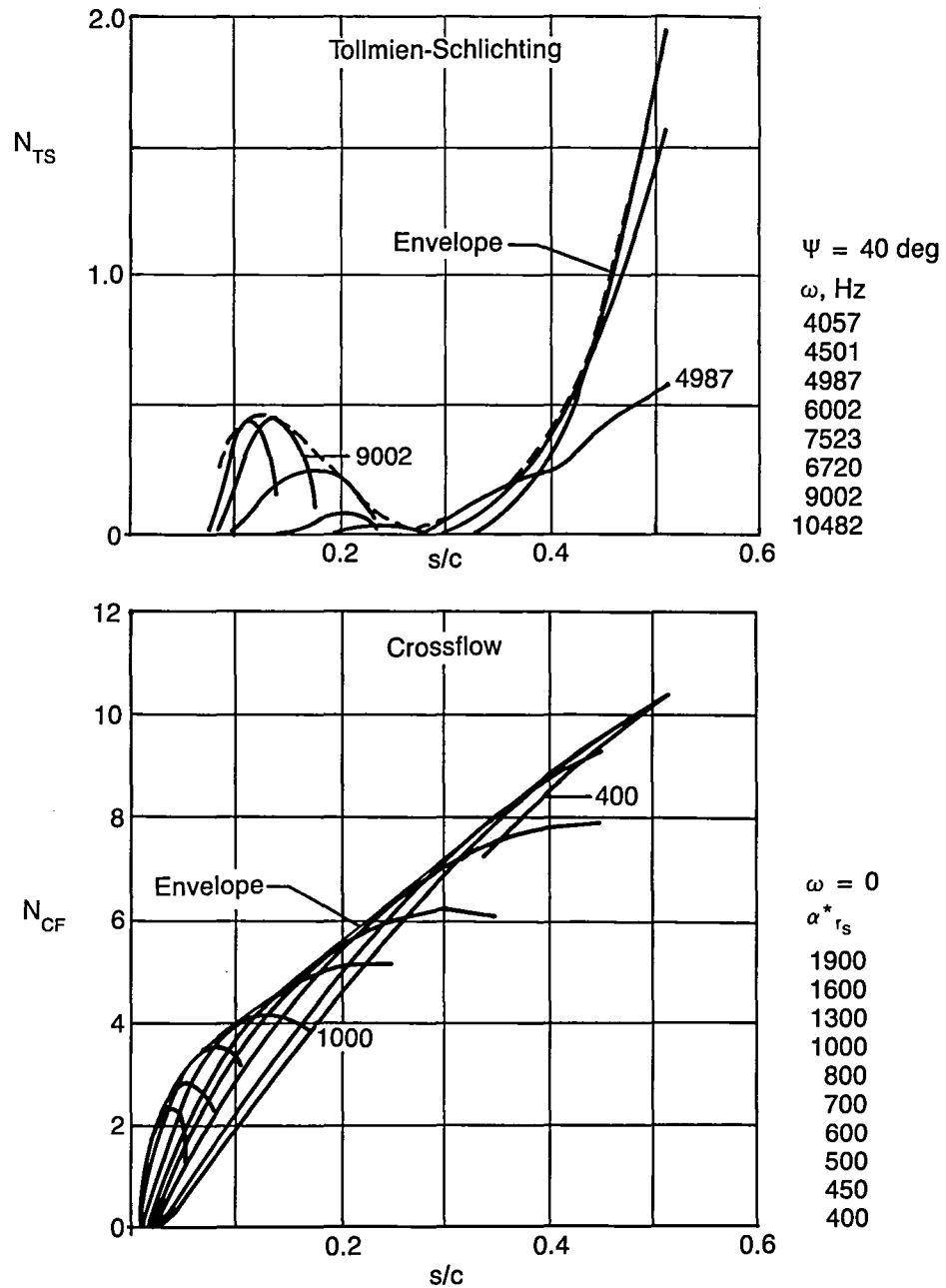
Figure 77. Disturbance Growth on the Cleanup Glove, $M_N = 0.77$

- $Re_{C_N} = 29 \times 10^6$
- $M_N = 0.70$
- $\Lambda = 18$ deg
- CIS Method

Tollmien-Schlichting

N_{TS}

Envelope

6499

8523

$\Psi = 40$ deg

ω, Hz
5002
5487
6499
8523
11986

0.2 0.4
s/c

Crossflow

N_{CF}

Envelope

600

1600

$\omega = 0$

$\alpha^* r_s$
1900
1600
1300
1000
800
700
600
500

0.2 0.4
s/c
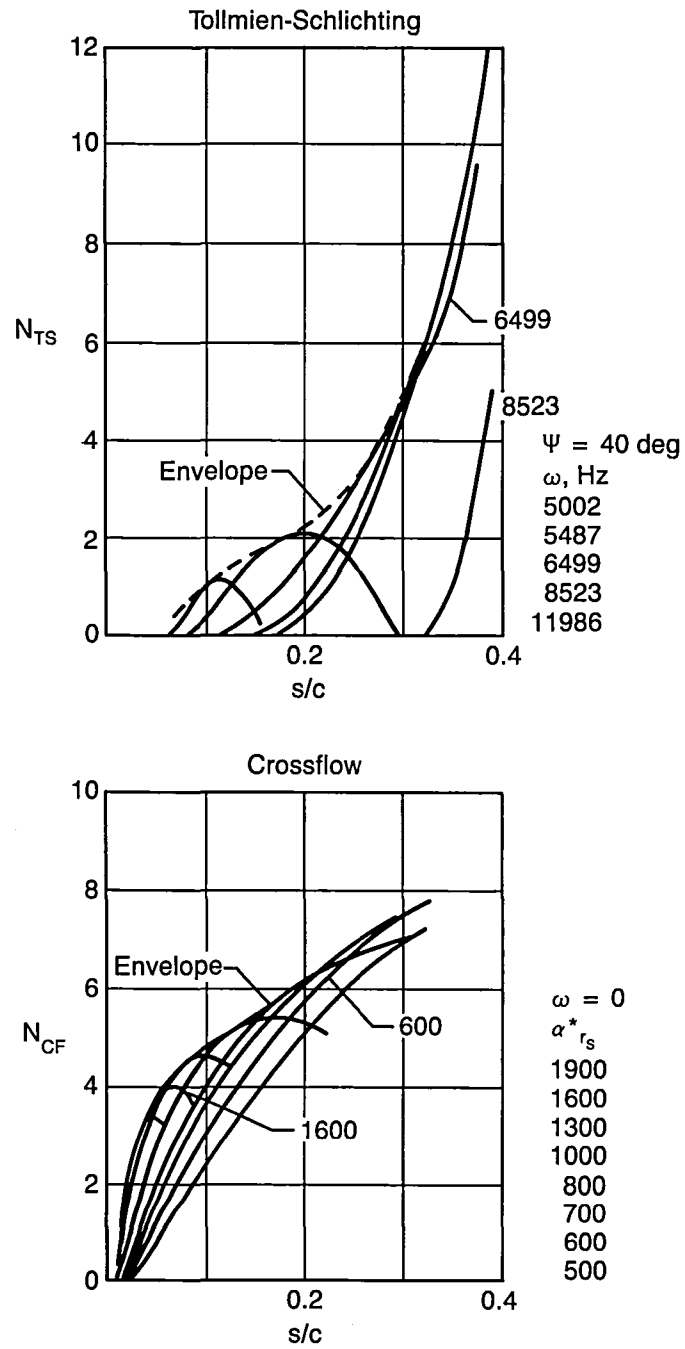
Figure 78. Disturbance Growth on the Cleanup Glove, $M_N = 0.70$

Figure 79. Disturbance Growth Traces for the Cleanup Glove
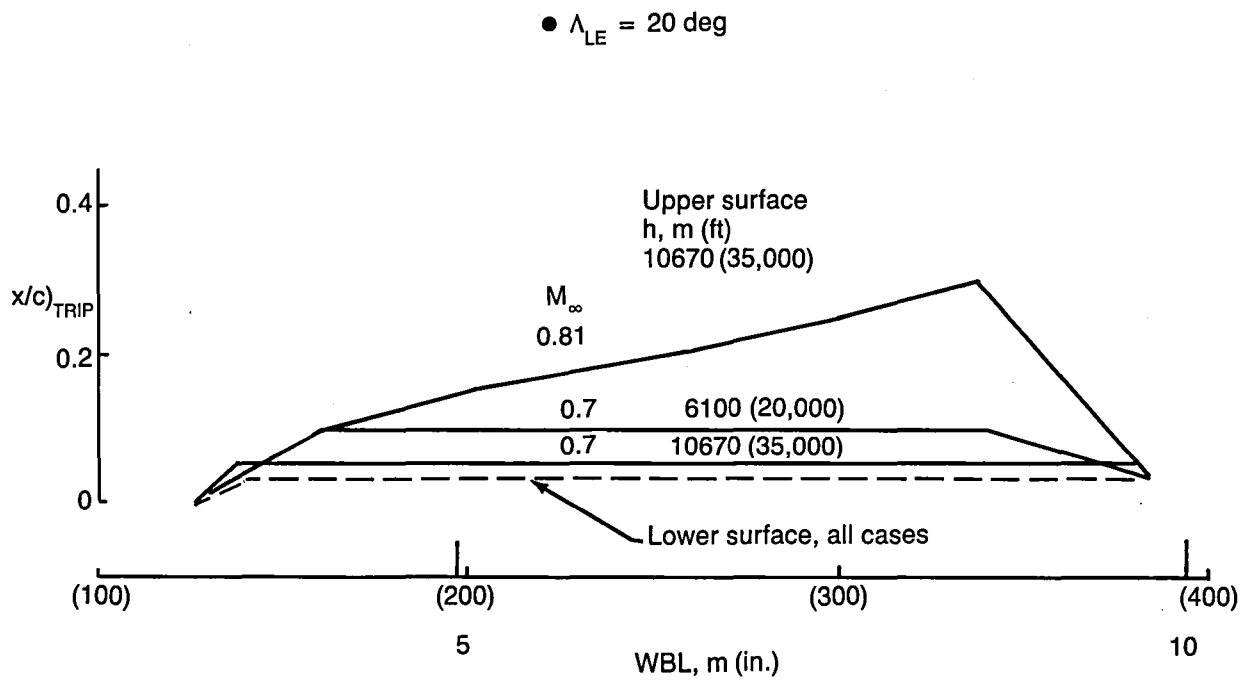
Figure 80. Assumed Transition Locations for Mach 0.8 Glove at Off-Design Conditions

$M_\infty = 0.81$ $C_L \sim 0.38$ $h \sim 10\ 670m\ (35,000\ ft)$

$\Lambda_{LE} = 20\ deg$ $Re \sim 0.59 \times 10^6\ 1/m$
$(1.96 \times 10^6 1/ft)$
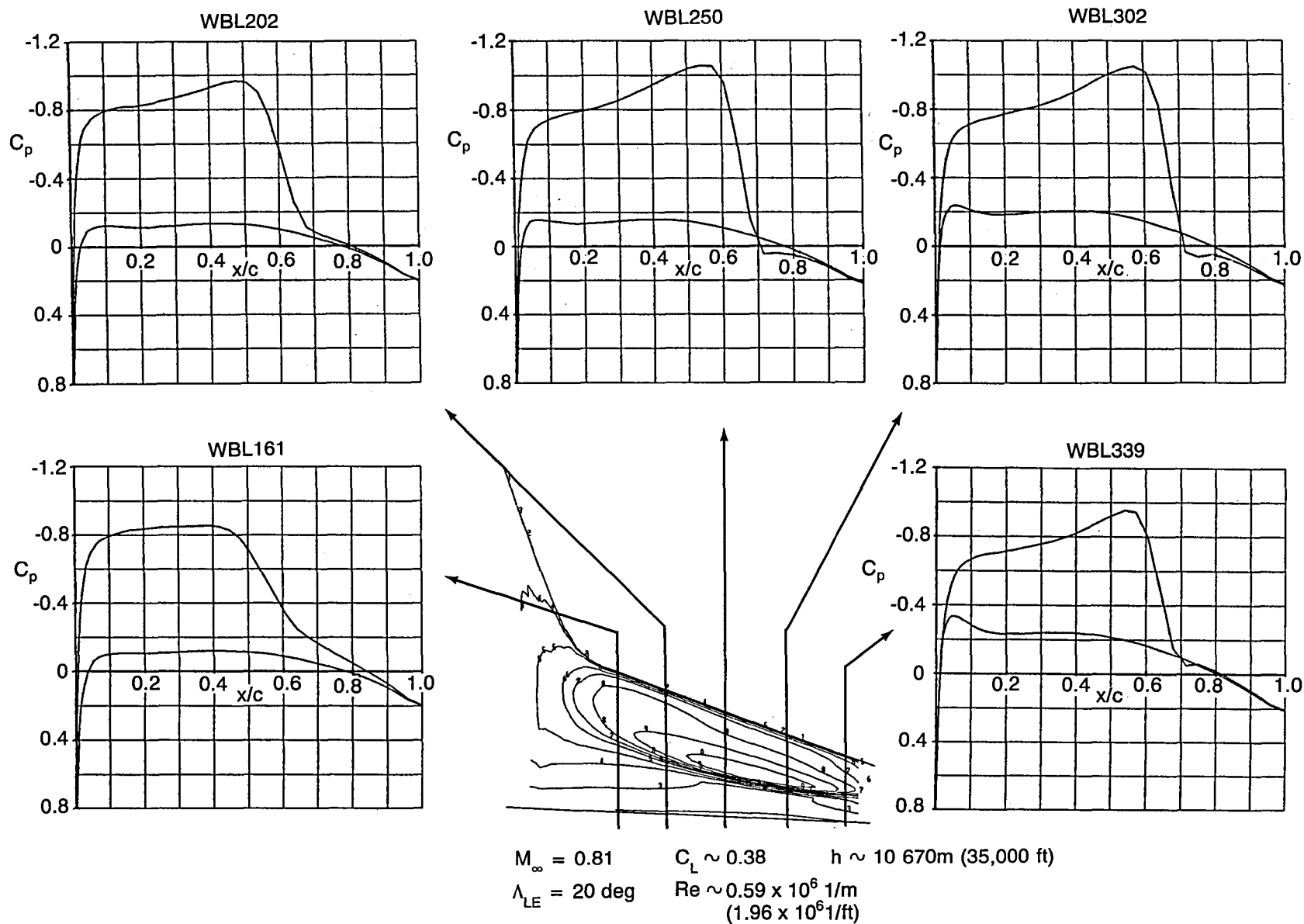
Figure 81. Analytical Wing Pressures of Mach 0.8 Glove at High Altitude and Speed
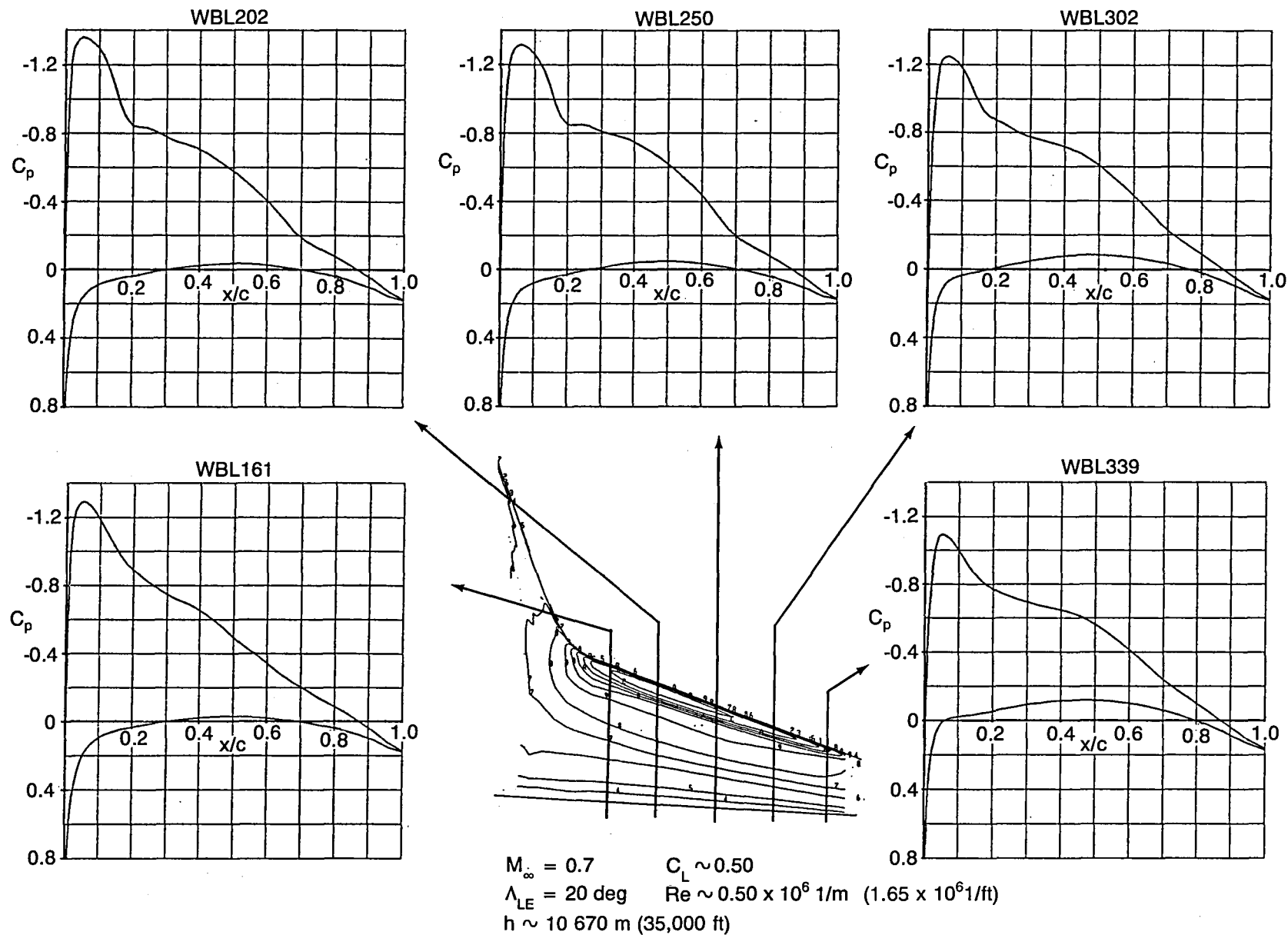
Figure 82. *Analytical Wing Pressures of Mach 0.8 Glove at High Altitude, Low Speed*
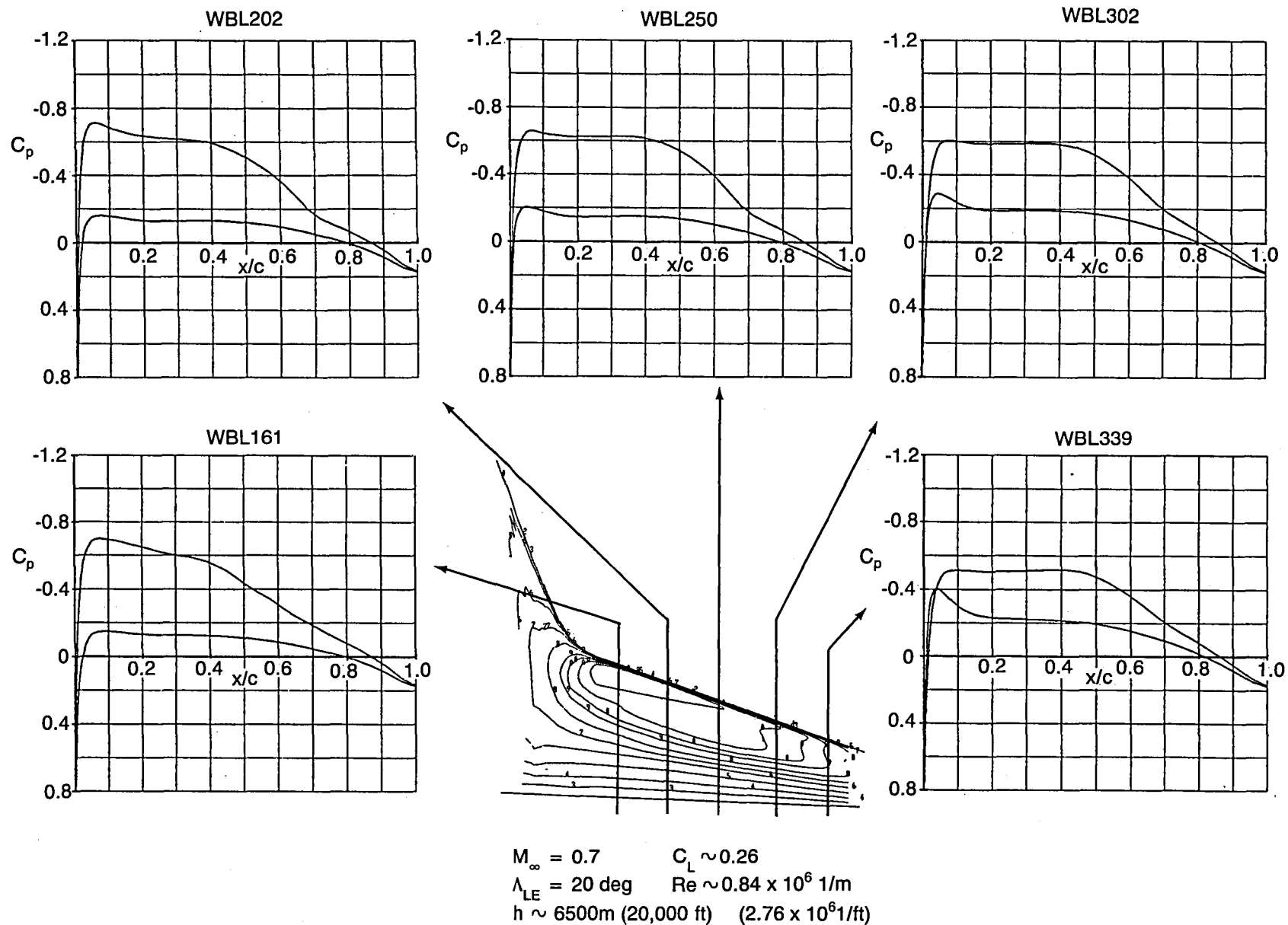
Figure 83. *Analytical Wing Pressures of Mach 0.8 Glove at Low Altitude and Speed*
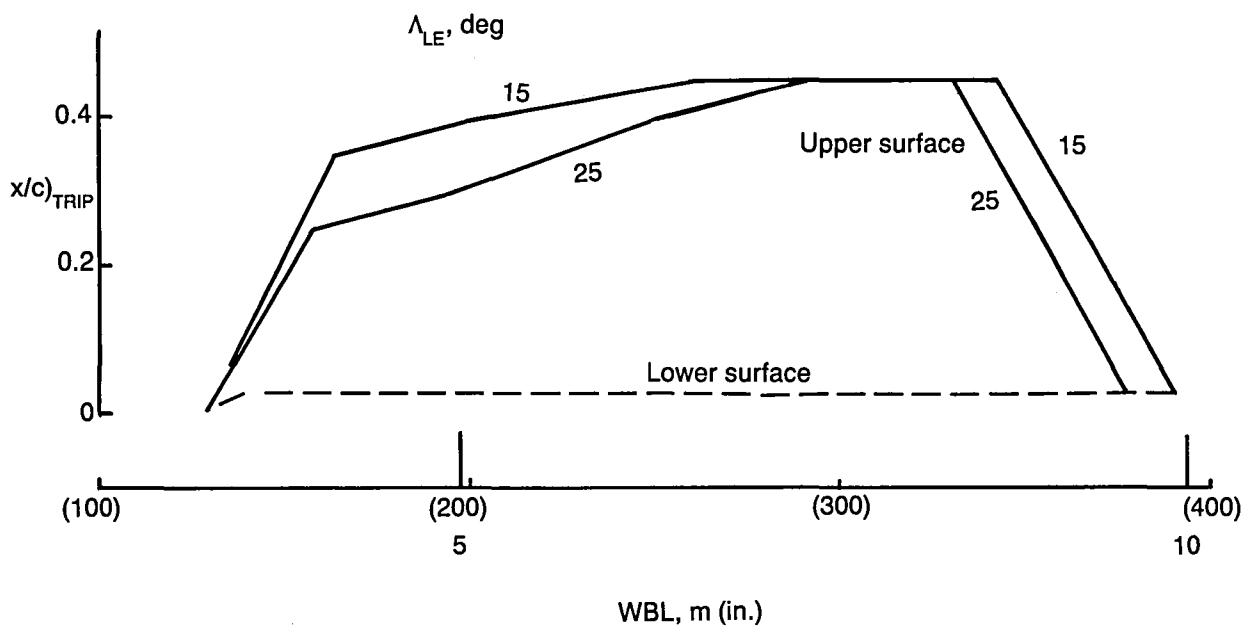
Figure 84. Assumed Transition Locations for Mach 0.8 Glove at Off-Design Sweep

WBL201

WBL247

WBL298

WBL161

WBL333

$M_\infty = 0.82$ $\Lambda_{LE} = 25$ deg $h \sim 6500m$ (20,000 ft)

$C_L \sim 0.19$ $Re \sim 0.98 \times 10^6 1/m$ (3.2×10^6 1/ft)
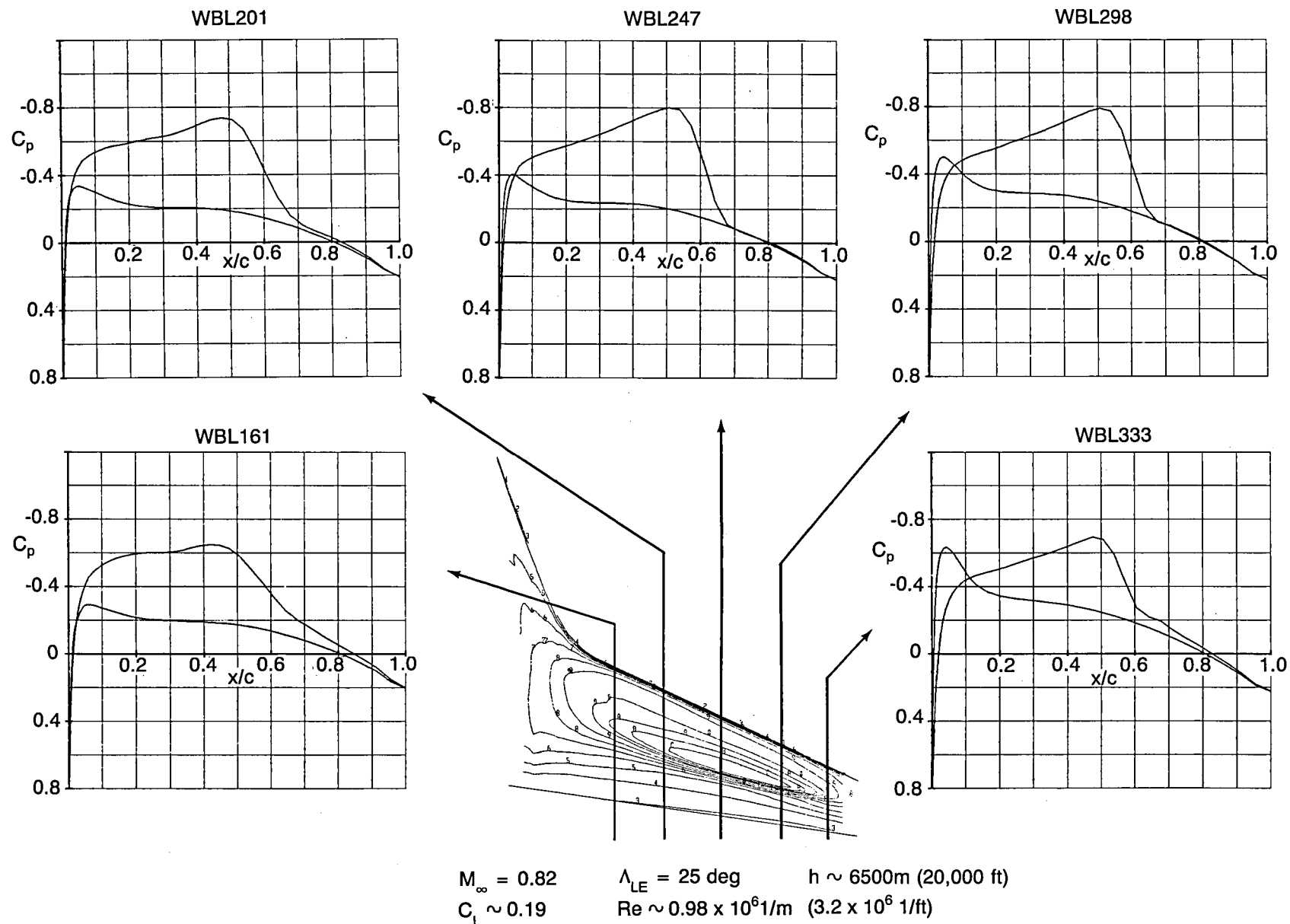
Figure 85. Analytical Wing Pressures of Mach 0.8 Glove at High Wing Sweep

Figure 86. Analytical Wing Pressures of Mach 0.8 Glove at Low Wing Sweep
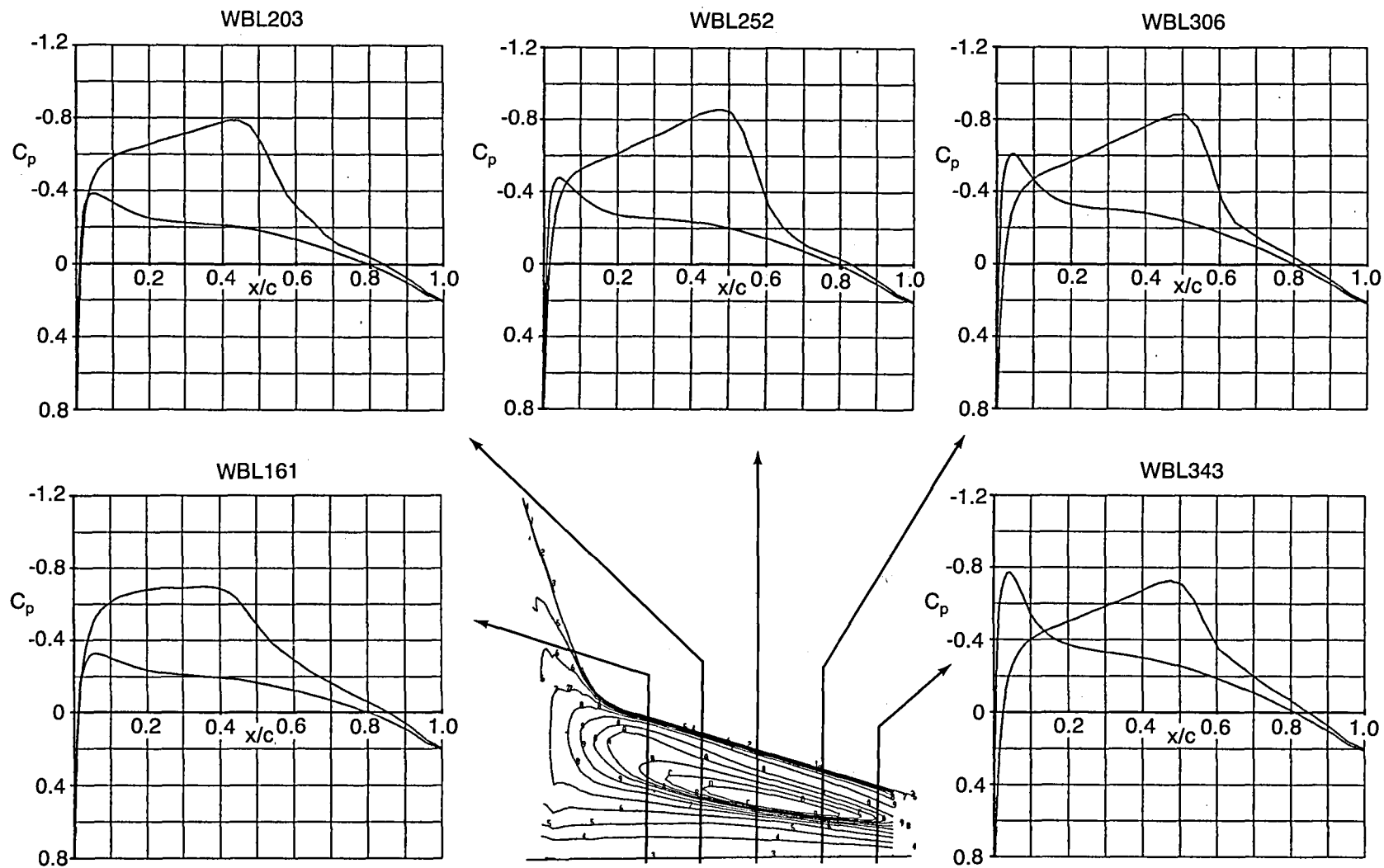
M_∞ = 0.785 $C_L \sim$ 0.20   h $\sim$ 6500m (20,000 ft)

Λ_{LE} = 15 deg   Re $\sim$ 0.98 x $10^6$1/m   (3.2 x 10^6 1/ft)

"Normalized" c_p
from wing
analyses
Section WBL202
$M_N \sim 0.77$
$C_L \sim 0.20$
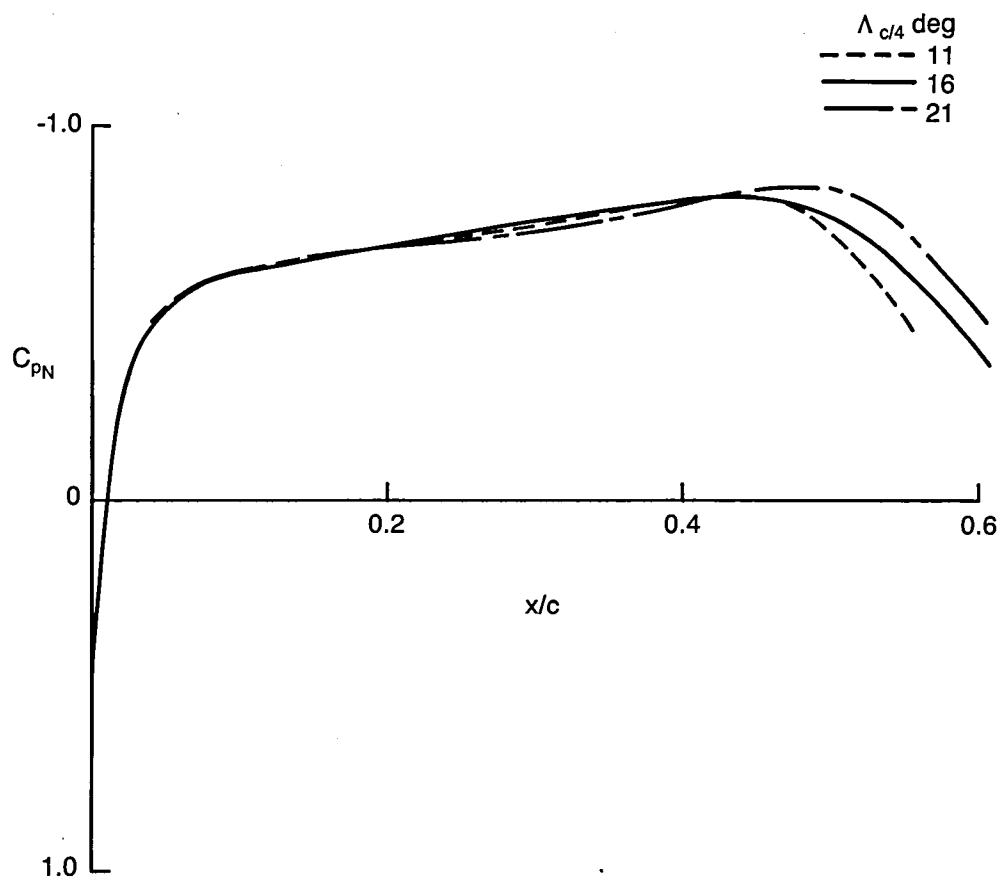
Figure 87. "Normalized" Pressure at Section WBL202 for Mach 0.8 Glove for Λ_{LE} = 15, 20, 25 deg

Mach 0.8 glove
section at WBL202

$Re_{C_N} = 26 \times 10^6$

$M_N = 0.77$
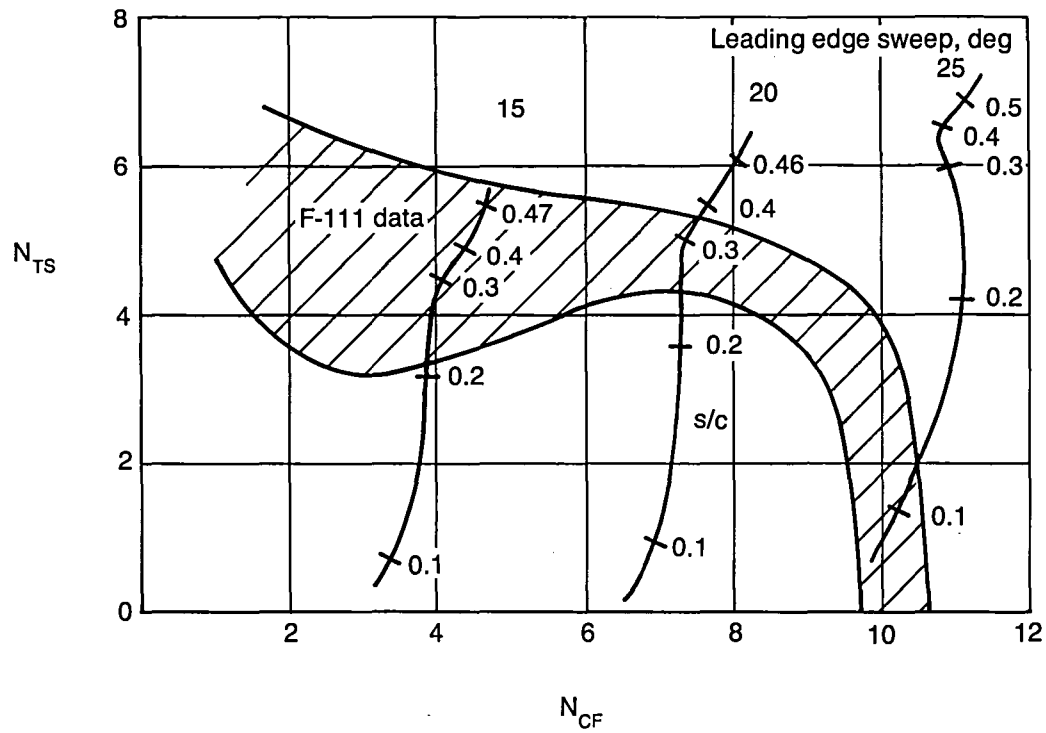
Figure 88. Sweep Effect on Disturbance Growth Trace for the Mach 0.8 Glove
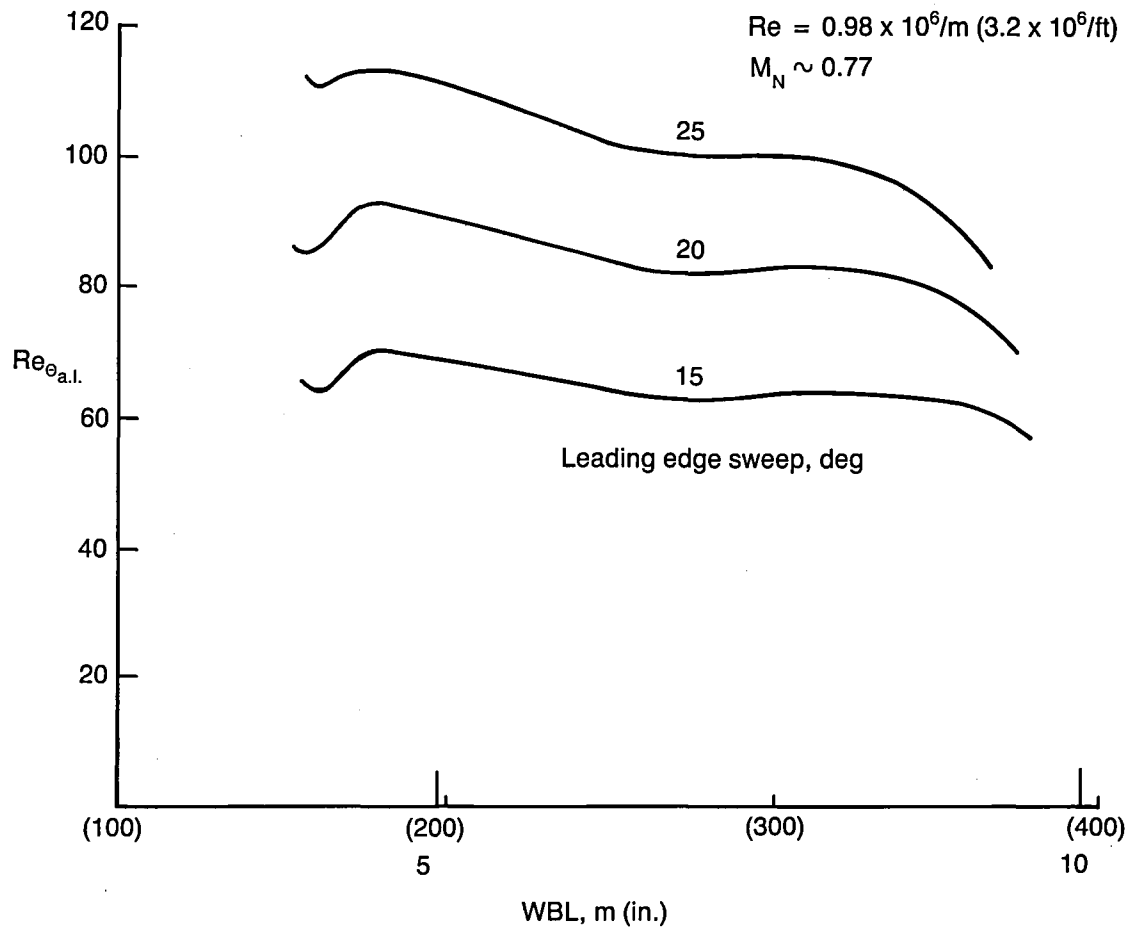
Figure 89. Sweep Effect on Attachment Line Reynolds No. for the Mach 0.8 Glove
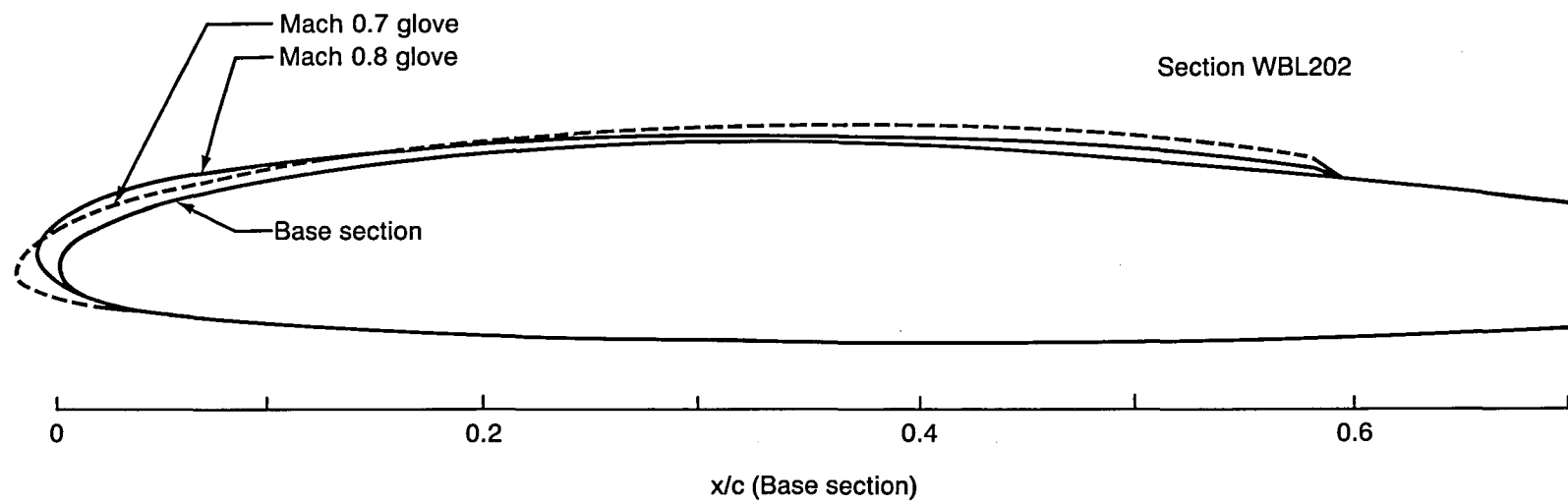
Figure 90. Comparison of Glove Section Shapes for Mach 0.8 and Mach 0.7 Gloves
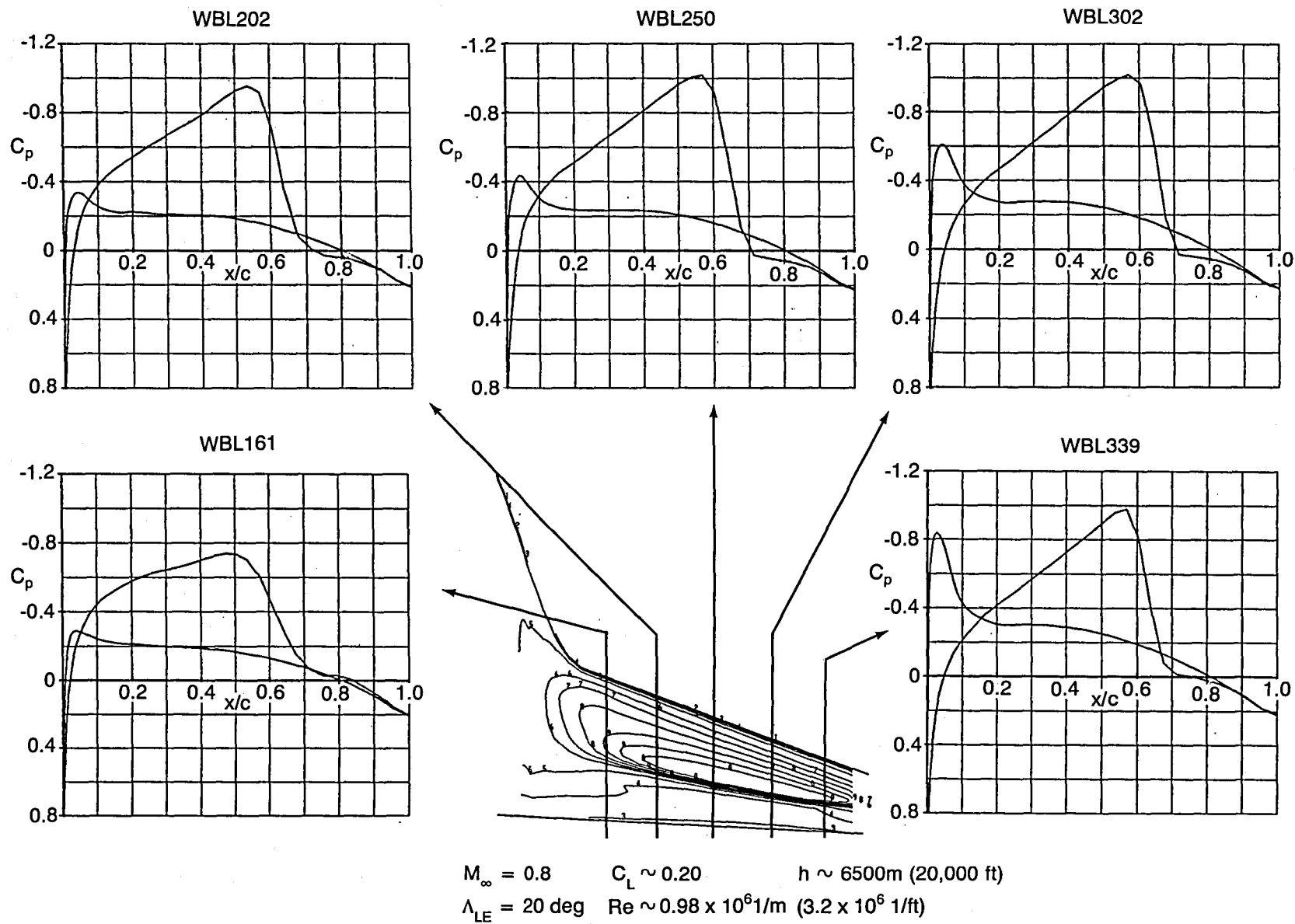
Figure 91. Analytical Wing Pressures of Mach 0.7 Glove at Low Altitude, High Speed
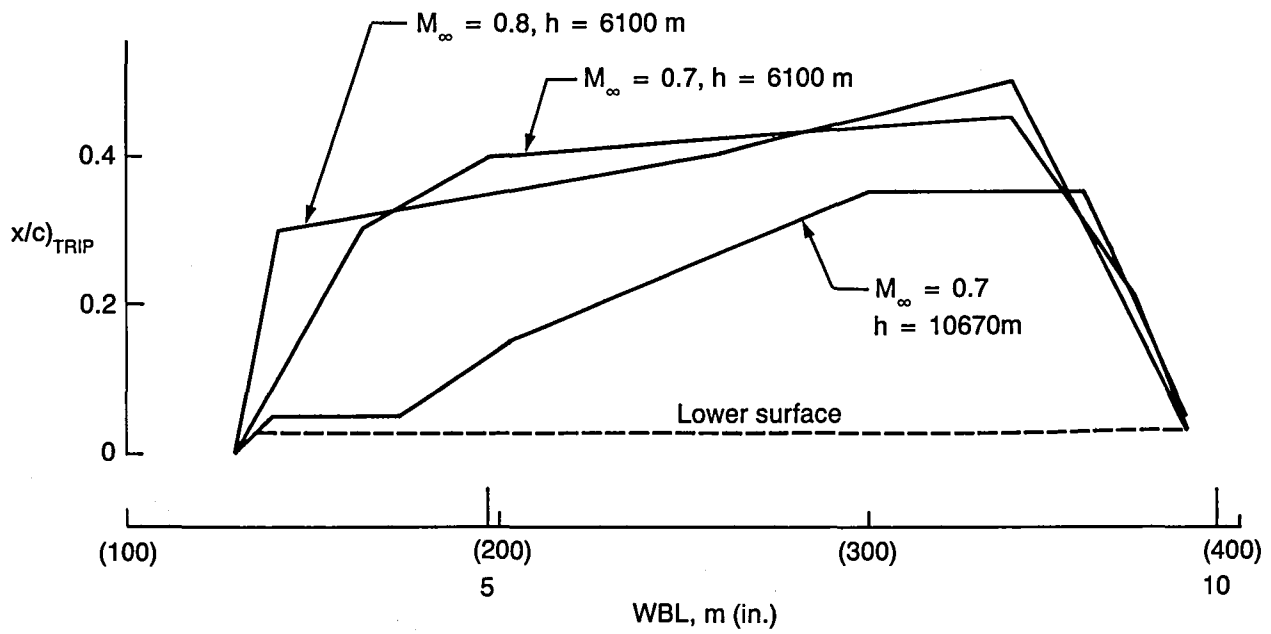
Figure 92. Assumed Transition Locations for Mach 0.7 Glove
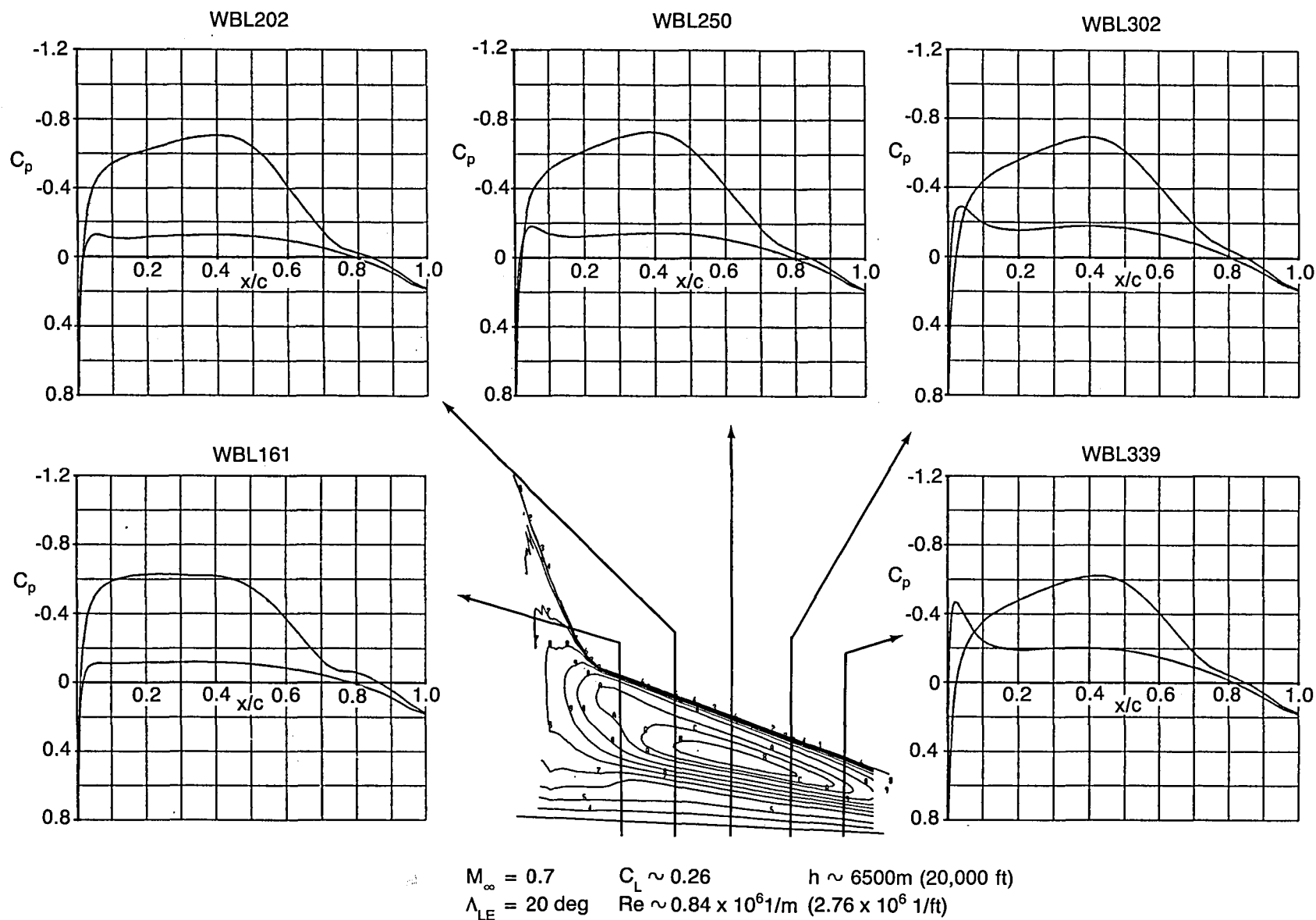
Figure 93. *Analytical Wing Pressures of Mach 0.7 Glove at Low Altitude and Speed*
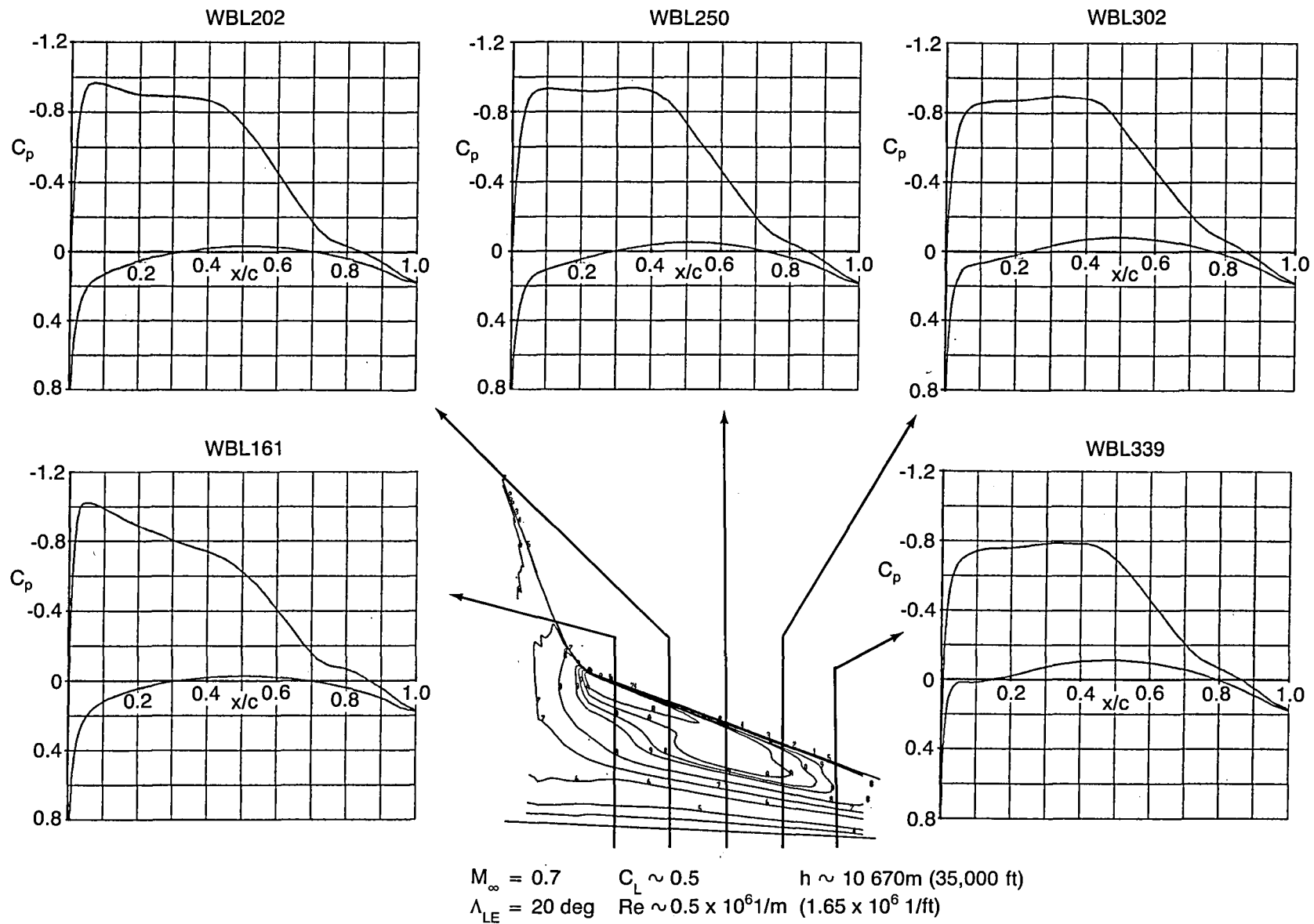
Figure 94. Analytical Wing Pressures of Mach 0.7 Glove at High Altitude, Low Speed

$M_\infty = 0.7$ $C_L \sim 0.5$ $h \sim 10\ 670m\ (35{,}000\ ft)$
$\Lambda_{LE} = 20\ deg$ $Re \sim 0.5 \times 10^6 1/m\ (1.65 \times 10^6\ 1/ft)$
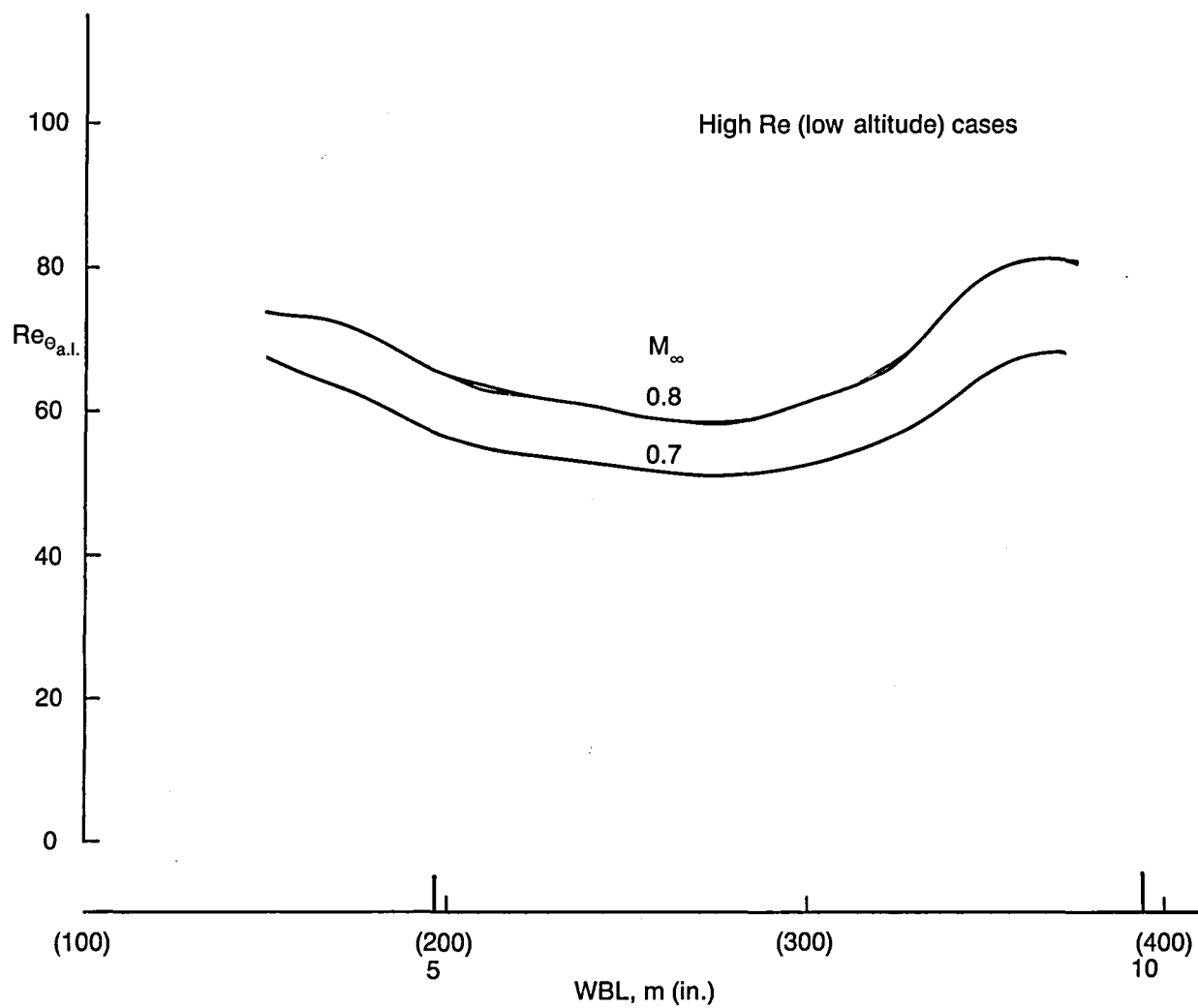
Figure 95. Attachment Line Reynolds No. for the Mach 0.7 Glove
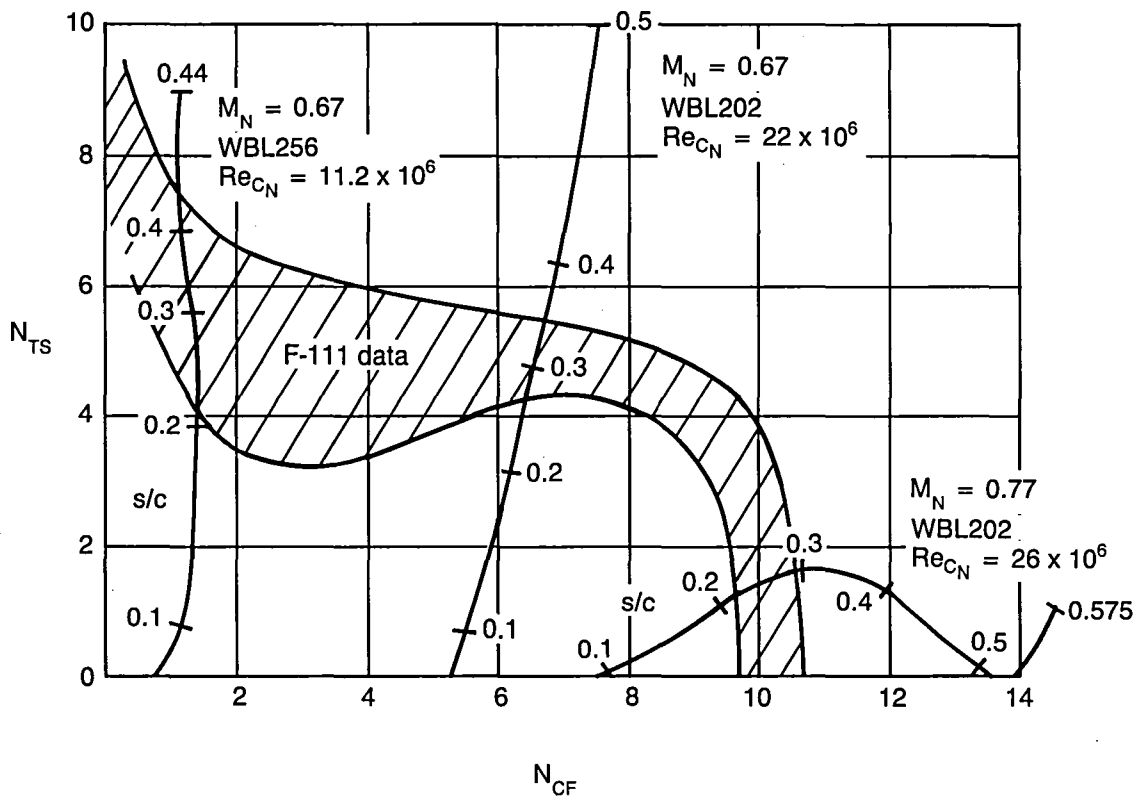
Figure 96. Disturbance Growth Traces for the Mach 0.7 Glove

APPENDIX 1

COMPARISON OF EXTRAPOLATION AND "EXACT" CALCULATIONS
FOR DISTURBANCE AMPLIFICATION ENVELOPES

To address the problem encountered early in this study when the Mack code did not converge for crossflow instabilities with high wave angles, α_r, an extrapolation technique was first used. To illustrate the problem, note that the disturbance amplification envelope for the "irrotational" condition is the envelope defined by curves of:

$$N_{CF} = \int_{s/c}^{s/c} -(\alpha_i^* \cdot c)|_{\alpha_{r_s}^* = \text{constant}} \, d(s/c)$$

NEUTRAL
STABILITY

Because $-(\alpha_i^* \cdot c)$ is the slope of the curve of N_{CF}, if a portion of the envelope of N_{CF} has zero or negative slope, it is necessary to have $-(\alpha_i^* \cdot c)$ values equal to or less than zero. The low α_i values on this branch of the instability curve correspond to relatively high α_r values, and this was exactly where the Mack code would not converge.

Figure A-1 helps explain this. As the code calculates points on the line labeled A in the direction of the arrow, it is continually increasing α_r, the wave number. A α_r approached 2, a solution to the eigenvalue problem became more and more difficult, and eventually the estimate for the next point on curve A became inadequate for the solution to converge. The last point on the curve usually had a value of $-(\alpha_i^* \cdot c)$ considerably higher than zero, so if additional points were needed to define more of the $N_{CF}|_{\alpha_{r_s}^*} = \text{constant}$ curves, extrapolation was required. When necessary, this extrapolation was carried out assuming the curves were symmetric about their peaks. This assumption seemed reasonable after examining many curves that were defined far past their peaks.

After the stability code had been successfully modified under IR&D to calculate the high wave number cases, the extrapolation technique was checked. Figure A-2 compares spatial amplification rate curves, $-(\alpha_i^* \cdot c)$, from converged solutions and the extrapolation assumption. Because disturbance amplification envelopes, N, are one goal of this study, five envelopes that had been constructed with extrapolated amplification rate curves were recalculated with the modified Mack code. Figure A-3 compares envelopes from extrapolation and converged calculations for the case where the two disagreed most. Even for this case, the s/c point of greatest disagreement near 0.20 shows N_{CF} values differing by only 2.5%. Therefore, the extrapolation technique was judged to have acceptable accuracy.

130
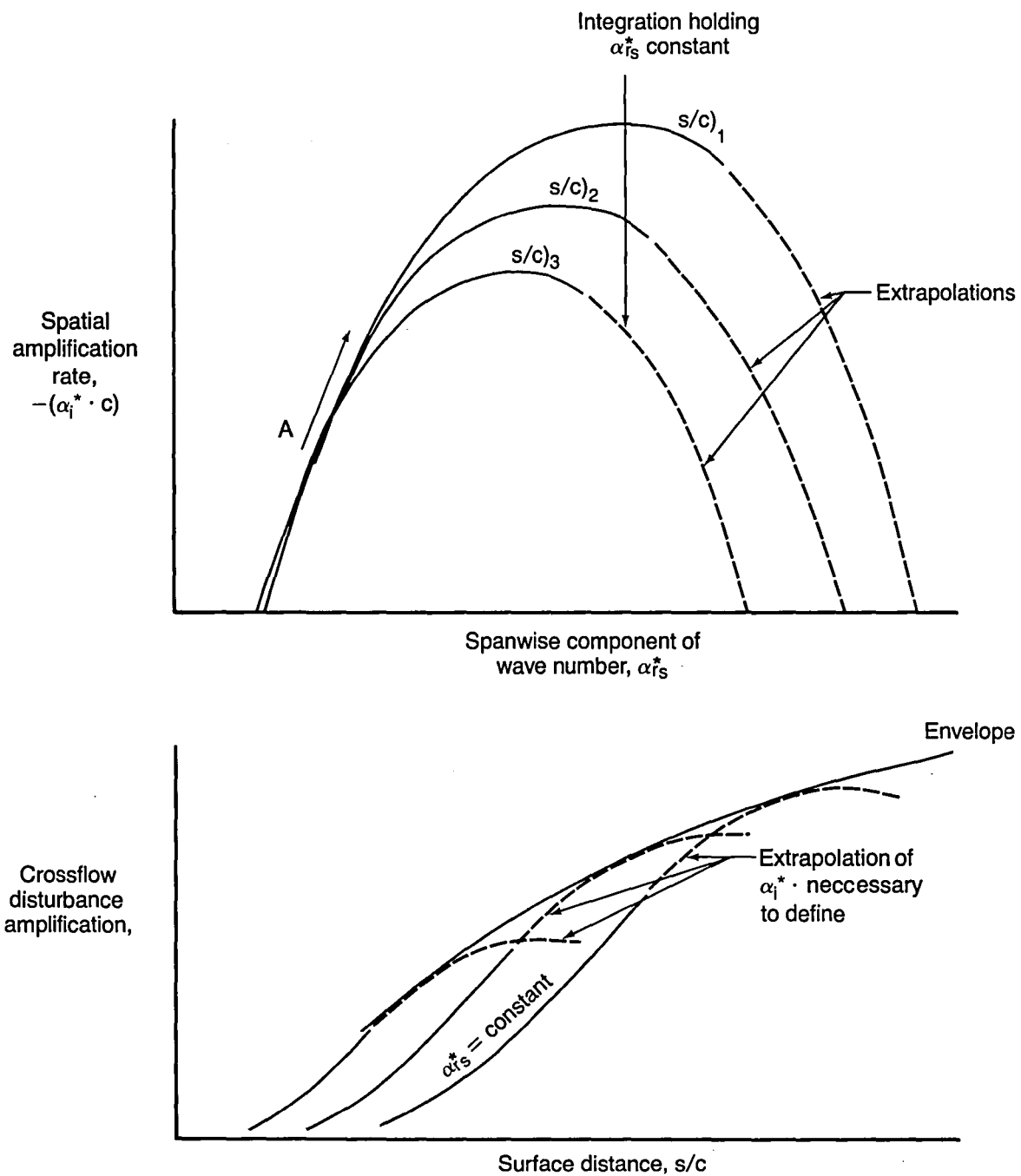
Figure A-1. Explanation of Extrapolation Technique

- P102
- $Re_{c_N} = 15 \times 10^6$
- $\Lambda = 25$ deg
- $M_N = 0.78$
- $\omega^* = 0$ Hz
- Compressible
- No dissipation
- ——— "Exact" calculations
- ——— Extrapolations

s/c

0.035

Extrapolation
beyond this
point

0.05

$-(\alpha_i^* \cdot c)$ 50

0.07

100

0

500

1000

1500

αr_s^*
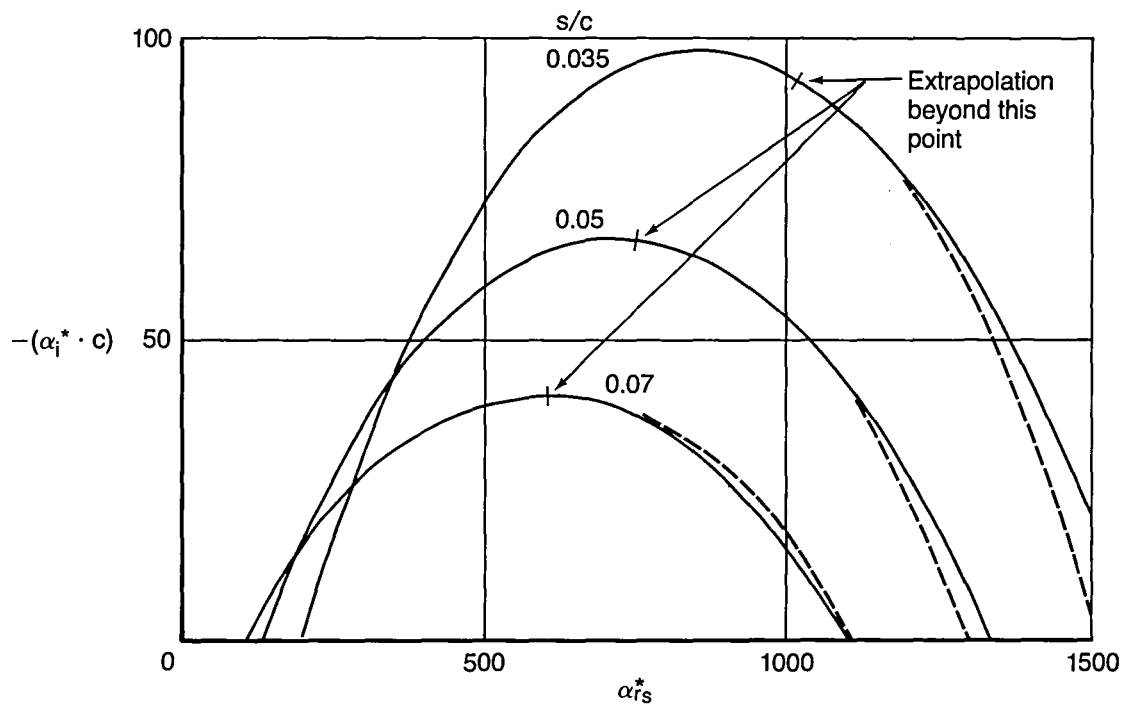
Figure A-2. Comparison of Extrapolation and Calculated Growth Rates

- P102
- $Re_{c_N} = 15 \times 10^6$
- $\Lambda = 25$ deg
- $\omega^* = 0$ Hz
- Irrotational
- $M_N = 0.78$
- Compressible
- No dissipation
- ——— "Exact" calculations
- – – – Extrapolation technique
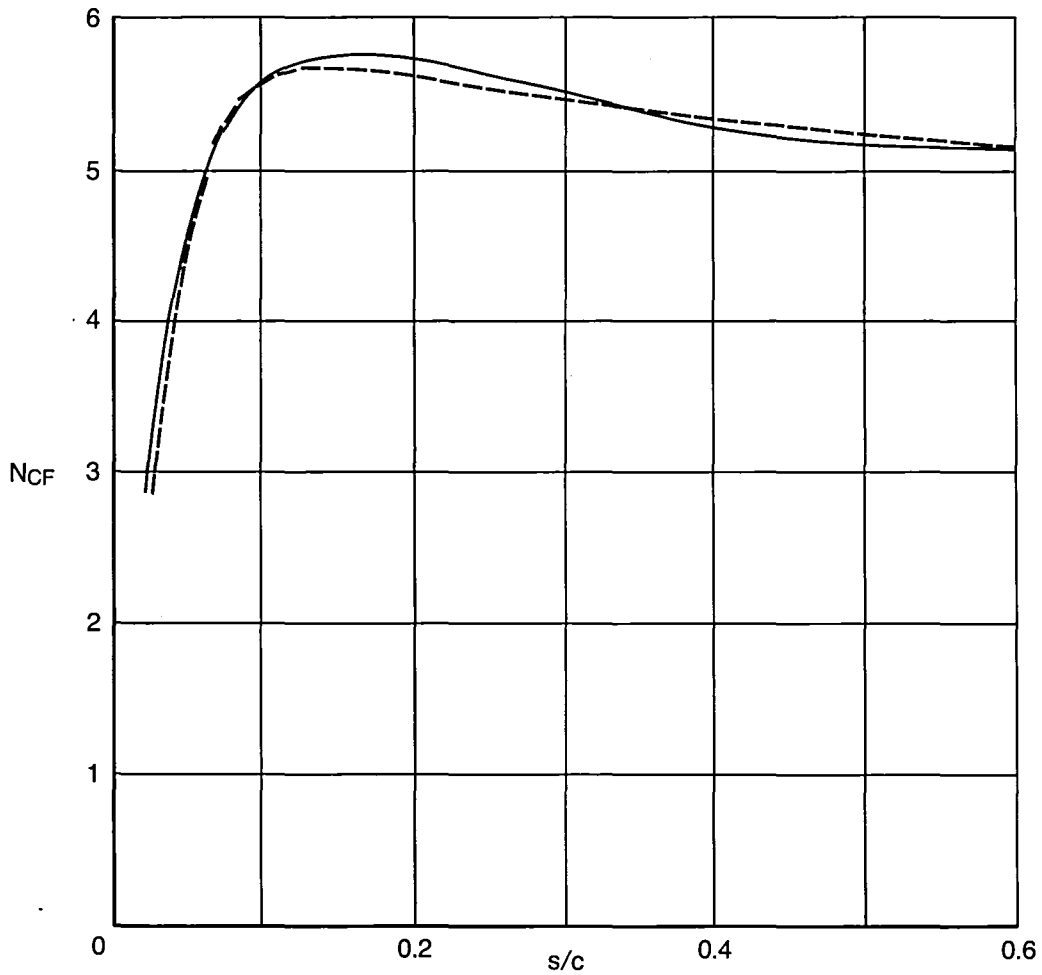
Figure A-3. Comparison of Extrapolated and Calculated Envelopes

APPENDIX 2

DEFINING SECTIONS—BASIC AND GLOVED WINGS

This appendix contains the coordinates of the defining sections for the F-14 basic outboard wing panel and the panel with both Mach 0.8 and Mach 0.7 gloves added to it. The defining sections are all in the streamwise direction with the wing at a leading-edge sweep of 20 degrees. Wing incidence is built into these coordinates. Specific locations in inches on the wings in the airplane coordinate system can be found from the following equations.

x = (x AT THE LEADING EDGE) + (x/c) (c)
where c in this case equals
(x AT THE TRAILING EDGE) - (x AT THE LEADING EDGE)

y = (y/c) (c) + REFERENCE VERTICAL LOC.

The lofts used for the analyses of the Mach 0.7 and Mach 0.8 glove wings presented in this report and those used to manufacture the wind tunnel wing panels were slightly different.

- Lofts used for analyses

  Both wings were lofted with straight line elements between constant percent chord points of adjacent defining sections. The gloves were terminated in the inboard area of the wing, by linearly fairing down to the base wing at:

  - WBL 137 for the Mach 0.8 glove

  - WBL 131 for the Mach 0.7 glove

- Lofts used for wind tunnel model

  Both wings were lofted for computer controlled machining with curve fitting along constant percent chord lines using the wing defining stations. The gloves for each wing were extended inboard to WBL 130 and terminated abruptly at this inboard station as well as at the outboard most defining station, WBL348.

GRUMMAN DEFINITION OF THE BASIC F-14 WING (20-DEG SWEEP)

```
WBL                            = 127.23000
X AT THE LEADING EDGE          = 502.90542
X AT THE TRAILING EDGE         = 629.37012
REFERENCE VERTICAL LOC.        = 159.93018
```

X/C	Y/C(UPPER)	X/C	Y/C(LOWER)
.000000	.007560	.000000	.007560
.001910	.013570	.001910	.001820
.004910	.017100	.004910	-.001760
.009950	.021010	.009950	-.005480
.020000	.026720	.020000	-.010130
.039930	.034850	.039930	-.015670
.060000	.040950	.060000	-.019220
.080000	.045820	.080000	-.021780
.100000	.049830	.100000	-.023750
.120000	.053170	.120000	-.025320
.140000	.055960	.140000	-.026610
.160000	.058270	.160000	-.027680
.180000	.060170	.180000	-.028570
.200000	.061700	.200000	-.029320
.220000	.062910	.220000	-.029940
.240000	.063810	.240000	-.030460
.260000	.064440	.260000	-.030870
.280000	.064820	.280000	-.031200
.300000	.064960	.300000	-.031440
.320000	.064890	.320000	-.031600
.340000	.064620	.340000	-.031680
.360000	.064160	.360000	-.031690
.380000	.063520	.380000	-.031630
.400000	.062710	.400000	-.031500
.420000	.061750	.420000	-.031300
.440000	.060640	.440000	-.031050
.460000	.059380	.460000	-.030730
.480000	.058000	.480000	-.030360
.500000	.056480	.500000	-.029930
.520000	.054850	.520000	-.029450
.560000	.051240	.560000	-.028340
.600000	.047220	.600000	-.027060
.640000	.042840	.640000	-.025620
.680000	.038120	.680000	-.024050
.700000	.035660	.700000	-.023220
.720000	.033130	.720000	-.022360
.740000	.030540	.740000	-.021480
.760000	.027900	.760000	-.020580
.780000	.025210	.780000	-.019660
.800000	.022470	.800000	-.018720
.820000	.019700	.820000	-.017770

.840000	.016890	.840000	-.016800
.860000	.014050	.860000	-.015820
.880000	.011190	.880000	-.014840
.900000	.008300	.900000	-.013850
.920000	.005400	.920000	-.012850
.940000	.002490	.940000	-.011850
.960000	-.000430	.960000	-.010850
.980000	-.003350	.980000	-.009840
1.000000	-.006280	1.000000	-.008840

```
WBL                       = 164.01460
X AT THE LEADING EDGE     = 516.19336
X AT THE TRAILING EDGE    = 631.00684
REFERENCE VERTICAL LOC.   = 159.12769
```

X/C	Y/C(UPPER)	X/C	Y/C(LOWER)
.000000	.008780	.000000	.008780
.001910	.014880	.001910	.003240
.004910	.018310	.004910	-.000230
.009950	.022050	.009950	-.003620
.020000	.027420	.020000	-.007780
.039930	.034980	.039930	-.012730
.060000	.040630	.060000	-.015890
.080000	.045190	.080000	-.018190
.100000	.049010	.100000	-.019970
.120000	.052260	.120000	-.021420
.140000	.055020	.140000	-.022630
.160000	.057370	.160000	-.023660
.180000	.059340	.180000	-.024550
.200000	.060970	.200000	-.025340
.220000	.062290	.220000	-.026040
.240000	.063310	.240000	-.026650
.260000	.064060	.260000	-.027200
.280000	.064560	.280000	-.027670
.300000	.064810	.300000	-.028080
.320000	.064830	.320000	-.028430
.340000	.064640	.340000	-.028710
.360000	.064240	.360000	-.028930
.380000	.063650	.380000	-.029090
.400000	.062880	.400000	-.029180
.420000	.061930	.420000	-.029200
.440000	.060810	.440000	-.029170
.460000	.059530	.460000	-.029070
.480000	.058110	.480000	-.028900
.500000	.056540	.500000	-.028680
.520000	.054840	.520000	-.028390
.560000	.051070	.560000	-.027650
.600000	.046850	.600000	-.026680
.640000	.042240	.640000	-.025520
.680000	.037300	.680000	-.024170
.700000	.034730	.700000	-.023430
.720000	.032090	.720000	-.022660

.740000	.029390	.740000	-.021850
.760000	.026650	.760000	-.021000
.780000	.023860	.780000	-.020130
.800000	.021030	.800000	-.019230
.820000	.018180	.820000	-.018310
.840000	.015290	.840000	-.017360
.860000	.012390	.860000	-.016390
.880000	.009470	.880000	-.015410
.900000	.006530	.900000	-.014420
.920000	.003590	.920000	-.013420
.940000	.000640	.940000	-.012410
.960000	-.002310	.960000	-.011390
.980000	-.005260	.980000	-.010370
1.000000	-.008210	1.000000	-.009350

```
WBL                        = 200.79919
X AT THE LEADING EDGE      = 529.58618
X AT THE TRAILING EDGE     = 632.64380
REFERENCE VERTICAL LOC.    = 158.07434
```

X/C	Y/C(UPPER)	X/C	Y/C(LOWER)
.000000	.007220	.000000	.007220
.001910	.013270	.001910	.001650
.004910	.016570	.004910	-.001730
.009950	.020330	.009950	-.005030
.020000	.025640	.020000	-.008970
.039930	.033000	.039930	-.013570
.060000	.038520	.060000	-.016500
.080000	.043010	.080000	-.018630
.100000	.046820	.100000	-.020290
.120000	.050100	.120000	-.021640
.140000	.052940	.140000	-.022770
.160000	.055400	.160000	-.023750
.180000	.057510	.180000	-.024610
.200000	.059300	.200000	-.025370
.220000	.060780	.220000	-.026060
.240000	.061980	.240000	-.026680
.260000	.062910	.260000	-.027230
.280000	.063590	.280000	-.027720
.300000	.064020	.300000	-.028160
.320000	.064210	.320000	-.028530
.340000	.064190	.340000	-.028840
.360000	.063950	.360000	-.029090
.380000	.063510	.380000	-.029280
.400000	.062870	.400000	-.029400
.420000	.062050	.420000	-.029450
.440000	.061050	.440000	-.029440
.460000	.059890	.460000	-.029360
.480000	.058560	.480000	-.029210
.500000	.057080	.500000	-.029000
.520000	.055460	.520000	-.028710
.560000	.051820	.560000	-.027950

.600000	.047700	.600000	-.026940
.640000	.043170	.640000	-.025700
.680000	.038280	.680000	-.024240
.700000	.035720	.700000	-.023430
.720000	.033100	.720000	-.022580
.740000	.030420	.740000	-.021680
.760000	.027700	.760000	-.020740
.780000	.024920	.780000	-.019770
.800000	.022110	.800000	-.018760
.820000	.019270	.820000	-.017720
.840000	.016400	.840000	-.016650
.860000	.013510	.860000	-.015560
.880000	.010610	.880000	-.014450
.900000	.007700	.900000	-.013320
.920000	.004780	.920000	-.012170
.940000	.001850	.940000	-.011020
.960000	-.001070	.960000	-.009860
.980000	-.004000	.980000	-.008690
1.000000	-.006920	1.000000	-.007530

```
WBL                        = 237.58369
X AT THE LEADING EDGE      = 542.98340
X AT THE TRAILING EDGE     = 634.28076
REFERENCE VERTICAL LOC.    = 156.86511
```

X/C	Y/C(UPPER)	X/C	Y/C(LOWER)
.000000	.003160	.000000	.003160
.001910	.009280	.001910	-.002590
.004910	.012600	.004910	-.005810
.009950	.016420	.009950	-.009040
.020000	.021800	.020000	-.012920
.039930	.029280	.039930	-.017390
.060000	.034900	.060000	-.020190
.080000	.039490	.080000	-.022200
.100000	.043410	.100000	-.023750
.120000	.046820	.120000	-.025010
.140000	.049810	.140000	-.026060
.160000	.052430	.160000	-.026960
.180000	.054720	.180000	-.027750
.200000	.056710	.200000	-.028440
.220000	.058400	.220000	-.029060
.240000	.059820	.240000	-.029620
.260000	.060980	.260000	-.030100
.280000	.061890	.280000	-.030520
.300000	.062560	.300000	-.030880
.320000	.063010	.320000	-.031170
.340000	.063230	.340000	-.031390
.360000	.063240	.360000	-.031550
.380000	.063040	.380000	-.031630
.400000	.062650	.400000	-.031640
.420000	.062070	.420000	-.031580
.440000	.061310	.440000	-.031440

.460000	.060380	.460000	-.031230
.480000	.059280	.480000	-.030940
.500000	.058020	.500000	-.030570
.520000	.056620	.520000	-.030140
.560000	.053380	.560000	-.029050
.600000	.049640	.600000	-.027680
.640000	.045450	.640000	-.026050
.680000	.040870	.680000	-.024180
.700000	.038460	.700000	-.023160
.720000	.035980	.720000	-.022090
.740000	.033420	.740000	-.020970
.760000	.030810	.760000	-.019800
.780000	.028150	.780000	-.018590
.800000	.025440	.800000	-.017340
.820000	.022700	.820000	-.016060
.840000	.019920	.840000	-.014740
.860000	.017120	.860000	-.013400
.880000	.014300	.880000	-.012030
.900000	.011460	.900000	-.010640
.920000	.008610	.920000	-.009230
.940000	.005750	.940000	-.007810
.960000	.002900	.960000	-.006380
.980000	.000040	.980000	-.004940
1.000000	-.002820	1.000000	-.003500

```
WBL                        = 274.36816
X AT THE LEADING EDGE      = 556.38062
X AT THE TRAILING EDGE     = 635.91772
REFERENCE VERTICAL LOC.    = 155.65588
```

X/C	Y/C(UPPER)	X/C	Y/C(LOWER)
.000000	-.002100	.000000	-.002100
.001910	.004120	.001910	-.007870
.004910	.007540	.004910	-.011230
.009950	.011340	.009950	-.014270
.020000	.016800	.020000	-.017990
.039930	.024410	.039930	-.022260
.060000	.030160	.060000	-.024900
.080000	.034880	.080000	-.026740
.100000	.038930	.100000	-.028140
.120000	.042490	.120000	-.029260
.140000	.045650	.140000	-.030190
.160000	.048450	.160000	-.030980
.180000	.050940	.180000	-.031670
.200000	.053140	.200000	-.032270
.220000	.055070	.220000	-.032800
.240000	.056750	.240000	-.033250
.260000	.058170	.260000	-.033630
.280000	.059360	.280000	-.033950
.300000	.060320	.300000	-.034190
.320000	.061060	.320000	-.034360
.340000	.061580	.340000	-.034460

.360000	.061890	.360000	-.034470
.380000	.062000	.380000	-.034410
.400000	.061910	.400000	-.034260
.420000	.061640	.420000	-.034040
.440000	.061180	.440000	-.033730
.460000	.060540	.460000	-.033340
.480000	.059740	.480000	-.032860
.500000	.058770	.500000	-.032300
.520000	.057650	.520000	-.031670
.560000	.054960	.560000	-.030150
.600000	.051730	.600000	-.028330
.640000	.048020	.640000	-.026220
.680000	.043880	.680000	-.023840
.700000	.041680	.700000	-.022560
.720000	.039390	.720000	-.021220
.740000	.037020	.740000	-.019820
.760000	.034580	.760000	-.018370
.780000	.032090	.780000	-.016870
.800000	.029540	.800000	-.015320
.820000	.026940	.820000	-.013740
.840000	.024310	.840000	-.012110
.860000	.021640	.860000	-.010460
.880000	.018940	.880000	-.008770
.900000	.016230	.900000	-.007060
.920000	.013490	.920000	-.005330
.940000	.010750	.940000	-.003580
.960000	.008000	.960000	-.001830
.980000	.005250	.980000	-.000060
1.000000	.002490	1.000000	.001710

```
WBL                        = 311.15283
X AT THE LEADING EDGE      = 569.77783
X AT THE TRAILING EDGE     = 637.55469
REFERENCE VERTICAL LOC.    = 154.44666
```

X/C	Y/C(UPPER)	X/C	Y/C(LOWER)
.000000	-.009190	.000000	-.009190
.001910	-.003000	.001910	-.014990
.004910	.000610	.004910	-.018310
.009950	.004520	.009950	-.021310
.020000	.010080	.020000	-.024870
.039930	.017870	.039930	-.028830
.060000	.023780	.060000	-.031180
.080000	.028650	.080000	-.032780
.100000	.032870	.100000	-.033960
.120000	.036590	.120000	-.034880
.140000	.039930	.140000	-.035630
.160000	.042940	.160000	-.036260
.180000	.045660	.180000	-.036790
.200000	.048100	.200000	-.037220
.220000	.050300	.220000	-.037580
.240000	.052260	.240000	-.037860

.260000	.053990	.260000	-.038060
.280000	.055500	.280000	-.038180
.300000	.056790	.300000	-.038220
.320000	.057880	.320000	-.038180
.340000	.058760	.340000	-.038050
.360000	.059440	.360000	-.037840
.380000	.059920	.380000	-.037530
.400000	.060220	.400000	-.037150
.420000	.060330	.420000	-.036670
.440000	.060260	.440000	-.036100
.460000	.060010	.460000	-.035450
.480000	.059600	.480000	-.034700
.500000	.059020	.500000	-.033870
.520000	.058280	.520000	-.032960
.560000	.056340	.560000	-.030870
.600000	.053840	.600000	-.028460
.640000	.050830	.640000	-.025730
.680000	.047350	.680000	-.022720
.700000	.045450	.700000	-.021110
.720000	.043470	.720000	-.019430
.740000	.041390	.740000	-.017690
.760000	.039230	.760000	-.015900
.780000	.037000	.780000	-.014040
.800000	.034710	.800000	-.012140
.820000	.032350	.820000	-.010190
.840000	.029940	.840000	-.008200
.860000	.027490	.860000	-.006170
.880000	.025000	.880000	-.004100
.900000	.022490	.900000	-.002010
.920000	.019940	.920000	.000110
.940000	.017380	.940000	.002250
.960000	.014810	.960000	.004400
.980000	.012230	.980000	.006560
1.000000	.009650	1.000000	.008730

```
WBL                        = 347.93726
X AT THE LEADING EDGE      = 583.17480
X AT THE TRAILING EDGE     = 639.19165
REFERENCE VERTICAL LOC.    = 153.24487
```

X/C	Y/C(UPPER)	X/C	Y/C(LOWER)
.000000	-.019120	.000000	-.019120
.001910	-.012950	.001910	-.025250
.004910	-.009370	.004910	-.028510
.009950	-.005400	.009950	-.031390
.020000	.000370	.020000	-.034700
.039930	.008440	.039930	-.038160
.060000	.014560	.060000	-.040020
.080000	.019630	.080000	-.041170
.100000	.024040	.100000	-.041950
.120000	.027960	.120000	-.042510
.140000	.031510	.140000	-.042930

.160000	.034740	.160000	-.043220
.180000	.037710	.180000	-.043420
.200000	.040430	.200000	-.043530
.220000	.042930	.220000	-.043540
.240000	.045210	.240000	-.043470
.260000	.047290	.260000	-.043320
.280000	.049170	.280000	-.043080
.300000	.050850	.300000	-.042750
.320000	.052350	.320000	-.042340
.340000	.053660	.340000	-.041840
.360000	.054790	.360000	-.041250
.380000	.055740	.380000	-.040580
.400000	.056520	.400000	-.039820
.420000	.057120	.420000	-.038970
.440000	.057550	.440000	-.038030
.460000	.057810	.460000	-.037000
.480000	.057910	.480000	-.035880
.500000	.057850	.500000	-.034680
.520000	.057640	.520000	-.033380
.560000	.056760	.560000	-.030540
.600000	.055310	.600000	-.027350
.640000	.053330	.640000	-.023850
.680000	.050870	.680000	-.020030
.700000	.049470	.700000	-.018010
.720000	.047960	.720000	-.015920
.740000	.046350	.740000	-.013760
.760000	.044660	.760000	-.011540
.780000	.042870	.780000	-.009260
.800000	.041010	.800000	-.006920
.820000	.039080	.820000	-.004520
.840000	.037080	.840000	-.002080
.860000	.035030	.860000	.000400
.880000	.032920	.880000	.002920
.900000	.030780	.900000	.005480
.920000	.028600	.920000	.008060
.940000	.026390	.940000	.010670
.960000	.024160	.960000	.013290
.980000	.021920	.980000	.015920
1.000000	.019680	1.000000	.018560

```
WBL                        = 384.69995
X AT THE LEADING EDGE      = 596.56421
X AT THE TRAILING EDGE     = 640.82764
REFERENCE VERTICAL LOC.    = 152.03552
```

X/C	Y/C(UPPER)	X/C	Y/C(LOWER)
.000000	-.034510	.000000	-.034510
.001910	-.028160	.001910	-.040970
.004910	-.024430	.004910	-.044000
.009950	-.020280	.009950	-.046630
.020000	-.014350	.020000	-.049350
.039930	-.005910	.039930	-.051350

.060000	.000530	.060000	-.051670
.080000	.005870	.080000	-.051490
.100000	.010530	.100000	-.051150
.120000	.014700	.120000	-.050760
.140000	.018500	.140000	-.050360
.160000	.022000	.160000	-.049950
.180000	.025250	.180000	-.049510
.200000	.028270	.200000	-.049030
.220000	.031090	.220000	-.048510
.240000	.033730	.240000	-.047930
.260000	.036180	.260000	-.047290
.280000	.038470	.280000	-.046580
.300000	.040600	.300000	-.045800
.320000	.042560	.320000	-.044950
.340000	.044370	.340000	-.044010
.360000	.046020	.360000	-.042990
.380000	.047520	.380000	-.041870
.400000	.048870	.400000	-.040670
.420000	.050070	.420000	-.039380
.440000	.051120	.440000	-.037990
.460000	.052020	.460000	-.036500
.480000	.052780	.480000	-.034920
.500000	.053400	.500000	-.033240
.520000	.053880	.520000	-.031470
.560000	.054440	.560000	-.027630
.600000	.054490	.600000	-.023410
.640000	.054050	.640000	-.018840
.680000	.053170	.680000	-.013920
.700000	.052570	.700000	-.011350
.720000	.051870	.720000	-.008690
.740000	.051070	.740000	-.005970
.760000	.050190	.760000	-.003170
.780000	.049230	.780000	-.000310
.800000	.048200	.800000	.002610
.820000	.047090	.820000	.005580
.840000	.045920	.840000	.008590
.860000	.044700	.860000	.011660
.880000	.043430	.880000	.014750
.900000	.042120	.900000	.017880
.920000	.040780	.920000	.021040
.940000	.039410	.940000	.024210
.960000	.038020	.960000	.027400
.980000	.036620	.980000	.030600
1.000000	.035210	1.000000	.033800

MACH 0.8 NLF GLOVE DEFINITION ON THE F-14 WING (BOEING DESIGN)

```
WBL                          = 127.23000
X AT THE LEADING EDGE        = 502.90542
X AT THE TRAILING EDGE       = 629.37012
REFERENCE VERTICAL LOC.      = 159.93018
```

COORDINATES AT THIS STATION ARE THE SAME AS FOR THE BASIC WING

```
WBL                          = 130.00000
X AT THE LEADING EDGE        = 503.81358
X AT THE TRAILING EDGE       = 629.49337
REFERENCE VERTICAL LOC.      = 159.86975
```

X/C	Y/C(UPPER)	X/C	Y/C(LOWER)
-.010000	.012650	-.010000	.012650
-.008280	.019750	-.009070	.007510
-.003770	.025990	-.002540	-.000710
.002810	.031370	.002700	-.003920
.014500	.037610	.009010	-.006840
.036220	.045380	.019700	-.010710
.057350	.050670	.039870	-.015700
.078040	.054630	.059990	-.019030
.098540	.057740	.080000	-.021510
.118910	.060250	.100000	-.023470
.139190	.062260	.120000	-.025030
.159400	.063850	.140000	-.026310
.179560	.065170	.160000	-.027380
.199690	.066190	.180000	-.028270
.219780	.066960	.200000	-.029020
.239850	.067530	.220000	-.029650
.259910	.067910	.240000	-.030170
.279960	.068120	.260000	-.030590
.299990	.068160	.280000	-.030930
.320030	.068050	.300000	-.031190
.340060	.067740	.320000	-.031360
.360080	.067220	.340000	-.031460
.380110	.066490	.360000	-.031480
.400130	.065590	.380000	-.031440
.420140	.064470	.400000	-.031330
.440150	.063200	.420000	-.031140
.460150	.061740	.440000	-.030910
.480150	.060130	.460000	-.030600
.500150	.058370	.480000	-.030250
.520140	.056480	.500000	-.029840
.560100	.052290	.520000	-.029370

.570090	.051130	.560000	-.028290
.580070	.049920	.600000	-.027030
.590000	.048230	.640000	-.025610
.600000	.047190	.680000	-.024060
.610000	.046120	.700000	-.023240
.640000	.042790	.720000	-.022380
.680000	.038060	.740000	-.021510
.700000	.035590	.760000	-.020610
.720000	.033050	.780000	-.019700
.740000	.030450	.800000	-.018760
.760000	.027810	.820000	-.017810
.780000	.025110	.840000	-.016840
.800000	.022360	.860000	-.015860
.820000	.019590	.880000	-.014880
.840000	.016770	.900000	-.013890
.860000	.013920	.920000	-.012890
.880000	.011060	.940000	-.011890
.900000	.008170	.960000	-.010890
.920000	.005260	.980000	-.009880
.940000	.002350	1.000000	-.008880
.960000	-.000570		
.980000	-.003490		
1.000000	-.006430		

```
WBL                        = 164.01460
X AT THE LEADING EDGE      = 516.19336
X AT THE TRAILING EDGE     = 631.00684
REFERENCE VERTICAL LOC.    = 159.12769
```

X/C	Y/C(UPPER)	X/C	Y/C(LOWER)
-.010000	.013780	-.010000	.013780
-.008240	.021050	-.009070	.008520
-.003630	.027250	-.002580	.000510
.003030	.032480	.002710	-.002620
.014750	.038390	.009040	-.005210
.036440	.045590	.019710	-.008590
.057510	.050440	.039880	-.012990
.078140	.054100	.059990	-.015950
.098580	.057020	.080000	-.018190
.118920	.059440	.100000	-.019970
.139180	.061420	.120000	-.021420
.159390	.063040	.140000	-.022630
.179540	.064420	.160000	-.023660
.199660	.065520	.180000	-.024550
.219760	.066400	.200000	-.025340
.239830	.067080	.220000	-.026040
.259890	.067570	.240000	-.026650
.279940	.067880	.260000	-.027200
.299980	.068020	.280000	-.027670
.320010	.067990	.300000	-.028080
.340050	.067760	.320000	-.028430
.360080	.067290	.340000	-.028710

.380100	.066610	.360000	-.028930
.400120	.065750	.380000	-.029090
.420140	.064640	.400000	-.029180
.440150	.063360	.420000	-.029200
.460160	.061880	.440000	-.029170
.480160	.060240	.460000	-.029070
.500150	.058430	.480000	-.028900
.520140	.056480	.500000	-.028680
.560110	.052160	.520000	-.028390
.570100	.050980	.560000	-.027650
.580080	.049780	.600000	-.026680
.590030	.048200	.640000	-.025520
.600000	.046850	.680000	-.024170
.610000	.045730	.700000	-.023430
.640000	.042240	.720000	-.022660
.680000	.037300	.740000	-.021850
.700000	.034730	.760000	-.021000
.720000	.032090	.780000	-.020130
.740000	.029390	.800000	-.019230
.760000	.026650	.820000	-.018310
.780000	.023860	.840000	-.017360
.800000	.021030	.860000	-.016390
.820000	.018180	.880000	-.015410
.840000	.015290	.900000	-.014420
.860000	.012390	.920000	-.013420
.880000	.009470	.940000	-.012410
.900000	.006530	.960000	-.011390
.920000	.003590	.980000	-.010370
.940000	.000640	1.000000	-.009350
.960000	-.002310		
.980000	-.005260		
1.000000	-.008210		

```
WBL                          = 200.79919
X AT THE LEADING EDGE        = 529.58618
X AT THE TRAILING EDGE       = 632.64380
REFERENCE VERTICAL LOC.      = 158.07434
```

X/C	Y/C(UPPER)	X/C	Y/C(LOWER)
-.010000	.012220	-.010000	.012220
-.008150	.019580	-.009070	.007000
-.003540	.025580	-.002540	-.001110
.003030	.030760	.002730	-.004160
.014820	.036650	.009060	-.006640
.036510	.043650	.019720	-.009800
.057550	.048350	.039880	-.013840
.078150	.051930	.059990	-.016570
.098580	.054840	.080000	-.018630
.118900	.057290	.100000	-.020290
.139150	.059340	.120000	-.021640
.159350	.061070	.140000	-.022770
.179500	.062590	.160000	-.023750

.199630	.063850	.180000	-.024610
.219720	.064890	.200000	-.025370
.239800	.065750	.220000	-.026060
.259860	.066420	.240000	-.026680
.279910	.066910	.260000	-.027230
.299950	.067230	.280000	-.027720
.319990	.067390	.300000	-.028160
.340020	.067380	.320000	-.028530
.360060	.067200	.340000	-.028840
.380090	.066840	.360000	-.029090
.400130	.066300	.380000	-.029280
.420160	.065560	.400000	-.029400
.440190	.064610	.420000	-.029450
.460230	.063510	.440000	-.029440
.480260	.062230	.460000	-.029360
.500290	.060780	.480000	-.029210
.520310	.059120	.500000	-.029000
.560330	.055170	.520000	-.028710
.570330	.054070	.560000	-.027950
.580310	.052850	.600000	-.026940
.590000	.048770	.640000	-.025700
.600000	.047700	.680000	-.024240
.610000	.046600	.700000	-.023430
.640000	.043170	.720000	-.022580
.680000	.038280	.740000	-.021680
.700000	.035720	.760000	-.020740
.720000	.033100	.780000	-.019770
.740000	.030420	.800000	-.018760
.760000	.027700	.820000	-.017720
.780000	.024920	.840000	-.016650
.800000	.022110	.860000	-.015560
.820000	.019270	.880000	-.014450
.840000	.016400	.900000	-.013320
.860000	.013510	.920000	-.012170
.880000	.010610	.940000	-.011020
.900000	.007700	.960000	-.009860
.920000	.004780	.980000	-.008690
.940000	.001850	1.000000	-.007530
.960000	-.001070		
.980000	-.004000		
1.000000	-.006920		

```
WBL                       = 237.58369
X AT THE LEADING EDGE     = 542.98340
X AT THE TRAILING EDGE    = 634.28076
REFERENCE VERTICAL LOC.   = 156.86511
```

X/C	Y/C(UPPER)	X/C	Y/C(LOWER)
-.010000	.008160	-.010000	.008160
-.008170	.015570	-.009070	.002990
-.003590	.021570	-.002420	-.005370
.002960	.026800	.002790	-.008260

.014760	.032780	.009070	-.010650
.036460	.039900	.019730	-.013750
.057500	.044710	.039880	-.017660
.078110	.048390	.059990	-.020260
.098530	.051410	.080000	-.022200
.118850	.053990	.100000	-.023750
.139110	.056190	.120000	-.025010
.159310	.058090	.140000	-.026060
.179460	.059790	.160000	-.026960
.199580	.061250	.180000	-.027750
.219680	.062500	.200000	-.028440
.239760	.063580	.220000	-.029060
.259820	.064480	.240000	-.029620
.279870	.065200	.260000	-.030100
.299910	.065770	.280000	-.030520
.319950	.066190	.300000	-.030880
.339980	.066420	.320000	-.031170
.360020	.066490	.340000	-.031390
.380050	.066380	.360000	-.031550
.400080	.066080	.380000	-.031630
.420120	.065580	.400000	-.031640
.440150	.064880	.420000	-.031580
.460180	.064000	.440000	-.031440
.480220	.062950	.460000	-.031230
.500250	.061730	.480000	-.030940
.520270	.060280	.500000	-.030570
.560290	.056730	.520000	-.030140
.570290	.055730	.560000	-.029050
.580280	.054520	.600000	-.027680
.590000	.050620	.640000	-.026050
.600000	.049640	.680000	-.024180
.610000	.048630	.700000	-.023160
.640000	.045450	.720000	-.022090
.680000	.040870	.740000	-.020970
.700000	.038460	.760000	-.019800
.720000	.035980	.780000	-.018590
.740000	.033420	.800000	-.017340
.760000	.030810	.820000	-.016060
.780000	.028150	.840000	-.014740
.800000	.025440	.860000	-.013400
.820000	.022700	.880000	-.012030
.840000	.019920	.900000	-.010640
.860000	.017120	.920000	-.009230
.880000	.014300	.940000	-.007810
.900000	.011460	.960000	-.006380
.920000	.008610	.980000	-.004940
.940000	.005750	1.000000	-.003500
.960000	.002900		
.980000	.000040		
1.000000	-.002820		

```
WBL                        = 274.36816
X AT THE LEADING EDGE      = 556.38062
X AT THE TRAILING EDGE     = 635.91772
REFERENCE VERTICAL LOC.    = 155.65588
```

X/C	Y/C(UPPER)	X/C	Y/C(LOWER)
-.010000	.002900	-.010000	.002900
-.008250	.010310	-.009070	-.002300
-.003660	.016460	-.002460	-.010580
.002950	.021720	.002820	-.013650
.014700	.027740	.009110	-.015900
.036400	.035000	.019740	-.018820
.057450	.039940	.039880	-.022530
.078060	.043760	.059990	-.024970
.098480	.046900	.080000	-.026740
.118800	.049630	.100000	-.028140
.139050	.052010	.120000	-.029260
.159250	.054090	.140000	-.030190
.179410	.055990	.160000	-.030980
.199530	.057660	.180000	-.031670
.219630	.059160	.200000	-.032270
.239710	.060500	.220000	-.032800
.259770	.061660	.240000	-.033250
.279820	.062670	.260000	-.033630
.299860	.063530	.280000	-.033950
.319900	.064240	.300000	-.034190
.339930	.064770	.320000	-.034360
.359970	.065140	.340000	-.034460
.380000	.065340	.360000	-.034470
.400030	.065340	.380000	-.034410
.420060	.065150	.400000	-.034260
.440100	.064750	.420000	-.034040
.460130	.064160	.440000	-.033730
.480160	.063410	.460000	-.033340
.500190	.062480	.480000	-.032860
.520220	.061320	.500000	-.032300
.560250	.058310	.520000	-.031670
.570250	.057440	.560000	-.030150
.580230	.056240	.600000	-.028330
.590000	.052580	.640000	-.026220
.600000	.051730	.680000	-.023840
.610000	.050840	.700000	-.022560
.640000	.048020	.720000	-.021220
.680000	.043880	.740000	-.019820
.700000	.041680	.760000	-.018370
.720000	.039390	.780000	-.016870
.740000	.037020	.800000	-.015320
.760000	.034580	.820000	-.013740
.780000	.032090	.840000	-.012110
.800000	.029540	.860000	-.010460
.820000	.026940	.880000	-.008770
.840000	.024310	.900000	-.007060
.860000	.021640	.920000	-.005330

```
.880000    .018940              .940000    -.003580
.900000    .016230              .960000    -.001830
.920000    .013490              .980000    -.000060
.940000    .010750             1.000000     .001710
.960000    .008000
.980000    .005250
1.000000   .002490
```

```
WBL                          = 311.15283
X AT THE LEADING EDGE        = 569.77783
X AT THE TRAILING EDGE       = 637.55469
REFERENCE VERTICAL LOC.      = 154.44666
```

X/C	Y/C(UPPER)	X/C	Y/C(LOWER)
-.010000	-.002190	-.010000	-.002190
-.008480	.003060	-.008260	-.009350
-.004640	.010160	-.001370	-.017040
.001800	.016320	.003590	-.019850
.013320	.023600	.009530	-.022150
.035080	.032070	.019920	-.025150
.056260	.037710	.039930	-.028830
.076950	.042080	.060000	-.031180
.097460	.045660	.080000	-.032780
.117860	.048720	.100000	-.033960
.138180	.051410	.120000	-.034880
.158450	.053760	.140000	-.035630
.178680	.055860	.160000	-.036260
.198880	.057740	.180000	-.036790
.219050	.059400	.200000	-.037220
.239210	.060870	.220000	-.037580
.259340	.062150	.240000	-.037860
.279460	.063260	.260000	-.038060
.299560	.064200	.280000	-.038180
.319650	.064980	.300000	-.038220
.339730	.065590	.320000	-.038180
.359810	.066050	.340000	-.038050
.379870	.066330	.360000	-.037840
.399940	.066470	.380000	-.037530
.419990	.066410	.400000	-.037150
.440050	.066170	.420000	-.036670
.460090	.065710	.440000	-.036100
.480140	.065090	.460000	-.035450
.500170	.064270	.480000	-.034700
.520200	.063250	.500000	-.033870
.560240	.060680	.520000	-.032960
.570250	.059920	.560000	-.030870
.580240	.058950	.600000	-.028460
.590000	.054510	.640000	-.025730
.600000	.053840	.680000	-.022720
.610000	.053130	.700000	-.021110
.640000	.050830	.720000	-.019430
.680000	.047350	.740000	-.017690

.700000	.045450	.760000	-.015900
.720000	.043470	.780000	-.014040
.740000	.041390	.800000	-.012140
.760000	.039230	.820000	-.010190
.780000	.037000	.840000	-.008200
.800000	.034710	.860000	-.006170
.820000	.032350	.880000	-.004100
.840000	.029940	.900000	-.002010
.860000	.027490	.920000	.000110
.880000	.025000	.940000	.002250
.900000	.022490	.960000	.004400
.920000	.019940	.980000	.006560
.940000	.017380	1.000000	.008730
.960000	.014810		
.980000	.012230		
1.000000	.009650		

```
WBL                         = 347.93726
X AT THE LEADING EDGE       = 583.17480
X AT THE TRAILING EDGE      = 639.19165
REFERENCE VERTICAL LOC.     = 153.24487
```

X/C	Y/C(UPPER)	X/C	Y/C(LOWER)
-.010000	-.012120	-.010000	-.012120
-.008450	-.006860	-.008260	-.019140
-.004640	.000160	-.001240	-.027250
.001670	.006310	.003650	-.030020
.013120	.013790	.009550	-.032220
.034930	.022580	.019920	-.034970
.056130	.028450	.039930	-.038160
.076830	.033020	.060000	-.040020
.097340	.036800	.080000	-.041170
.117740	.040060	.100000	-.041950
.138060	.042950	.120000	-.042510
.158330	.045530	.140000	-.042930
.178550	.047880	.160000	-.043220
.198750	.050040	.180000	-.043420
.218920	.052000	.200000	-.043530
.239060	.053790	.220000	-.043540
.259190	.055420	.240000	-.043470
.279310	.056900	.260000	-.043320
.299410	.058240	.280000	-.043080
.319500	.059430	.300000	-.042750
.339580	.060470	.320000	-.042340
.359660	.061380	.340000	-.041840
.379720	.062140	.360000	-.041250
.399780	.062760	.380000	-.040580
.419840	.063190	.400000	-.039820
.439900	.063450	.420000	-.038970
.459950	.063510	.440000	-.038030
.479990	.063390	.460000	-.037000
.500040	.063090	.480000	-.035880

.520070	.062600	.500000	-.034680
.560100	.061100	.520000	-.033380
.570140	.060690	.560000	-.030540
.580140	.059590	.600000	-.027350
.590000	.055720	.640000	-.023850
.600000	.055310	.680000	-.020030
.610000	.054860	.700000	-.018010
.640000	.053330	.720000	-.015920
.680000	.050870	.740000	-.013760
.700000	.049470	.760000	-.011540
.720000	.047960	.780000	-.009260
.740000	.046350	.800000	-.006920
.760000	.044660	.820000	-.004520
.780000	.042870	.840000	-.002080
.800000	.041010	.860000	.000400
.820000	.039080	.880000	.002920
.840000	.037080	.900000	.005480
.860000	.035030	.920000	.008060
.880000	.032920	.940000	.010670
.900000	.030780	.960000	.013290
.920000	.028600	.980000	.015920
.940000	.026390	1.000000	.018560
.960000	.024160		
.980000	.021920		
1.000000	.019680		

```
WBL                          = 384.69995
X AT THE LEADING EDGE        = 596.56421
X AT THE TRAILING EDGE       = 640.82764
REFERENCE VERTICAL LOC.      = 152.03552
```

COORDINATES AT THIS STATION ARE THE SAME AS FOR THE BASIC WING

MACH 0.7 NLF GLOVE DEFINITION ON THE F-14 WING (NASA DESIGN)

```
WBL                         = 127.23000
X AT THE LEADING EDGE       = 502.90542
X AT THE TRAILING EDGE      = 629.37012
REFERENCE VERTICAL LOC.     = 159.93018
```

COORDINATES AT THIS STATION ARE THE SAME AS FOR THE BASIC WING

```
WBL                         = 130.00000
X AT THE LEADING EDGE       = 501.81358
X AT THE TRAILING EDGE      = 629.49337
REFERENCE VERTICAL LOC.     = 159.86975
```

X/C	Y/C(UPPER)	X/X	Y/C(LOWER)
0.000000	.007560	0.000000	.007560
.001910	.012690	.001910	.002390
.004560	.017250	.004960	-.000890
.009950	.021910	.009950	-.003980
.020000	.028230	.020000	-.008130
.039930	.036420	.039930	-.013340
.060000	.042350	.060000	-.016970
.080000	.047100	.080000	-.019770
.100000	.051090	.100000	-.022010
.120000	.054510	.120000	-.023850
.140000	.057490	.140000	-.025350
.160000	.060080	.160000	-.026570
.180000	.062350	.180000	-.027580
.200000	.064320	.200000	-.028420
.220000	.066030	.220000	-.029110
.240000	.067490	.240000	-.029680
.260000	.068720	.260000	-.030170
.280000	.069710	.280000	-.030540
.300000	.070500	.300000	-.030820
.320000	.071090	.320000	-.031030
.340000	.071450	.340000	-.031150
.360000	.071620	.360000	-.031200
.380000	.071590	.380000	-.031180
.400000	.071330	.400000	-.031090
.420000	.070820	.420000	-.030910
.440000	.070030	.440000	-.030680
.460000	.068980	.460000	-.030400
.480000	.067630	.480000	-.030050
.500000	.066000	.500000	-.029640
.520000	.064090	.520000	-.029180
.560000	.059370	.560000	-.028110
.600000	.053510	.600000	-.026850
.640000	.046800	.640000	-.025430
.680000	.039650	.680000	-.023880

.700000	.036000	.700000	-.023050
.720000	.032280	.720000	-.022200
.740000	.028640	.740000	-.021340
.760000	.026150	.760000	-.020430
.780000	.024580	.780000	-.019500
.800000	.021960	.800000	-.018570
.820000	.019130	.820000	-.017630
.840000	.016260	.840000	-.016660
.860000	.013360	.860000	-.015680
.880000	.010430	.880000	-.014700
.900000	.007490	.900000	-.013710
.920000	.004550	.920000	-.012710
.940000	.001610	.940000	-.011720
.960000	-.001340	.960000	-.010710
.980000	-.004300	.980000	-.009700
1.000000	-.007250	1.000000	-.008700

```
WBL                       = 164.01460
X AT THE LEADING EDGE     = 514.19336
X AT THE TRAILING EDGE    = 631.00684
REFERENCE VERTICAL LOC.   = 159.12769
```

X/C	Y/C(UPPER)	X/C	Y/C(LOWER)
.000000	.006740	.000000	.006740
.001910	.011870	.001910	.001670
.004960	.016430	.004960	-.001530
.009950	.021090	.009950	-.004320
.020000	.027410	.020000	-.008020
.039930	.035600	.039930	-.012150
.060000	.041530	.060000	-.014870
.080000	.046280	.080000	-.016920
.100000	.050270	.100000	-.018600
.120000	.053690	.120000	-.020050
.140000	.056670	.140000	-.021320
.160000	.059260	.160000	-.022460
.180000	.061530	.180000	-.023480
.200000	.063500	.200000	-.024370
.220000	.065210	.220000	-.025140
.240000	.066670	.240000	-.025810
.260000	.067900	.260000	-.026400
.280000	.068890	.280000	-.026920
.300000	.069680	.300000	-.027360
.320000	.070270	.320000	-.027740
.340000	.070630	.340000	-.028070
.360000	.070800	.360000	-.028320
.380000	.070770	.380000	-.028510
.400000	.070510	.400000	-.028640
.420000	.070000	.420000	-.028700
.440000	.069210	.440000	-.028690
.460000	.068160	.460000	-.028630
.480000	.066810	.480000	-.028490

.500000	.065180	.500000	-.028290
.520000	.063270	.520000	-.028030
.560000	.058550	.560000	-.027340
.600000	.052690	.600000	-.026400
.640000	.045980	.640000	-.025270
.680000	.038840	.680000	-.023950
.700000	.035180	.700000	-.023220
.720000	.031460	.720000	-.022460
.740000	.027820	.740000	-.021660
.760000	.025330	.760000	-.020820
.780000	.023760	.780000	-.019950
.800000	.021140	.800000	-.019050
.820000	.018310	.820000	-.018140
.840000	.015440	.840000	-.017200
.860000	.012540	.860000	-.016230
.880000	.009610	.880000	-.015250
.900000	.006670	.900000	-.014260
.920000	.003730	.920000	-.013260
.940000	.000790	.940000	-.012250
.960000	-.002160	.960000	-.011230
.980000	-.005120	.980000	-.010210
1.000000	-.008070	1.000000	-.009190

```
WBL                        = 200.79919
X AT THE LEADING EDGE      = 527.58618
X AT THE TRAILING EDGE     = 632.64380
REFERENCE VERTICAL LOC.    = 158.07434
```

X/C	Y/C(UPPER)	X/C	Y/C(LOWER)
.000000	.005030	.000000	.005030
.001910	.009250	.001910	.000540
.004960	.013260	.004960	-.002430
.009950	.017810	.009950	-.004810
.020000	.024250	.020000	-.008210
.039930	.032820	.039930	-.012480
.060000	.038970	.060000	-.015200
.080000	.043910	.080000	-.017080
.100000	.048090	.100000	-.018650
.120000	.051690	.120000	-.020010
.140000	.054840	.140000	-.021200
.160000	.057630	.160000	-.022270
.180000	.060090	.180000	-.023300
.200000	.062270	.200000	-.024270
.220000	.064190	.220000	-.025070
.240000	.065860	.240000	-.025730
.260000	.067300	.260000	-.026340
.280000	.068520	.280000	-.026870
.300000	.069510	.300000	-.027340
.320000	.070270	.320000	-.027760
.340000	.070810	.340000	-.028100
.360000	.071120	.360000	-.028380

X/C	Y/C(UPPER)	X/C	Y/C(LOWER)
.380000	.071220	.380000	-.028610
.400000	.071080	.400000	-.028780
.420000	.070690	.420000	-.028870
.440000	.070060	.440000	-.028890
.460000	.069170	.460000	-.028840
.480000	.068010	.480000	-.028730
.500000	.066580	.500000	-.028550
.520000	.064870	.520000	-.028300
.560000	.060600	.560000	-.027600
.600000	.055190	.600000	-.026640
.640000	.048860	.640000	-.025440
.680000	.041960	.680000	-.024010
.700000	.038370	.700000	-.023220
.720000	.034740	.720000	-.022380
.740000	.031170	.740000	-.021500
.760000	.027920	.760000	-.020570
.780000	.025040	.780000	-.019600
.800000	.022230	.800000	-.018600
.820000	.019390	.820000	-.017560
.840000	.016530	.840000	-.016500
.860000	.013650	.860000	-.015410
.880000	.010740	.880000	-.014300
.900000	.007830	.900000	-.013170
.920000	.004910	.920000	-.012030
.940000	.001980	.940000	-.010880
.960000	-.000940	.960000	-.009720
.980000	-.003860	.980000	-.008550
1.000000	-.006790	1.000000	-.007390

```
WBL                          = 274.36816
X AT THE LEADING EDGE        = 554.38062
X AT THE TRAILING EDGE       = 635.91772
REFERENCE VERTICAL LOC.      = 155.65588
```

X/C	Y/C(UPPER)	X/C	Y/C(LOWER)
.000000	-.002880	.000000	-.002880
.001910	.001060	.001910	-.007660
.004960	.004290	.004960	-.011100
.009950	.008390	.009950	-.013930
.020000	.014640	.020000	-.017520
.039930	.023760	.039930	-.021910
.060000	.030440	.060000	-.024440
.080000	.035800	.080000	-.025990
.100000	.040360	.100000	-.027140
.120000	.044330	.120000	-.028110
.140000	.047840	.140000	-.028940
.160000	.050980	.160000	-.029690
.180000	.053780	.180000	-.030360
.200000	.056290	.200000	-.030930
.220000	.058550	.220000	-.031480
.240000	.060560	.240000	-.032020

.260000	.062330	.260000	-.032460
.280000	.063860	.280000	-.032840
.300000	.065170	.300000	-.033150
.320000	.066240	.320000	-.033380
.340000	.067100	.340000	-.033530
.360000	.067720	.360000	-.033620
.380000	.068120	.380000	-.033620
.400000	.068290	.400000	-.033530
.420000	.068200	.420000	-.033360
.440000	.067860	.440000	-.033120
.460000	.067260	.460000	-.032790
.480000	.066390	.480000	-.032370
.500000	.065260	.500000	-.031860
.520000	.063890	.520000	-.031270
.560000	.060500	.560000	-.029850
.600000	.056350	.600000	-.028100
.640000	.051530	.640000	-.026070
.680000	.046120	.680000	-.023740
.700000	.043220	.700000	-.022490
.720000	.040250	.720000	-.021170
.740000	.037310	.740000	-.019780
.760000	.034530	.760000	-.018350
.780000	.031970	.780000	-.016870
.800000	.029430	.800000	-.015330
.820000	.026840	.820000	-.013760
.840000	.024220	.840000	-.012140
.860000	.021560	.860000	-.010480
.880000	.018870	.880000	-.008810
.900000	.016160	.900000	-.007100
.920000	.013430	.920000	-.005370
.940000	.010690	.940000	-.003620
.960000	.007940	.960000	-.001870
.980000	.005190	.980000	-.000100
1.000000	.002430	1.000000	.001670

```
WBL                        = 347.93726
X AT THE LEADING EDGE      = 581.17480
X AT THE TRAILING EDGE     = 639.19165
REFERENCE VERTICAL LOC.    = 153.24487
```

X/C	Y/C(UPPER)	X/C	Y/C(LOWER)
.000000	-.021320	.000000	-.021320
.001910	-.014980	.001910	-.028110
.004960	-.010330	.004960	-.031100
.009950	-.005480	.009950	-.033450
.020000	.001170	.020000	-.036240
.039930	.010010	.039930	-.038820
.060000	.016790	.060000	-.040070
.080000	.022510	.080000	-.040600
.100000	.027520	.100000	-.041030
.120000	.032000	.120000	-.041370

.140000	.036030	.140000	-.041630
.160000	.039710	.160000	-.041830
.180000	.043090	.180000	-.041940
.200000	.046230	.200000	-.041960
.220000	.049130	.220000	-.041980
.240000	.051820	.240000	-.042050
.260000	.054290	.260000	-.042000
.280000	.056560	.280000	-.041880
.300000	.058620	.300000	-.041660
.320000	.060480	.320000	-.041350
.340000	.062140	.340000	-.040960
.360000	.063580	.360000	-.040470
.380000	.064820	.380000	-.039890
.400000	.065840	.400000	-.039230
.420000	.066630	.420000	-.038480
.440000	.067180	.440000	-.037620
.460000	.067470	.460000	-.036680
.480000	.067500	.480000	-.035650
.500000	.067250	.500000	-.034520
.520000	.066710	.520000	-.033300
.560000	.064810	.560000	-.030600
.600000	.061890	.600000	-.027540
.640000	.058030	.640000	-.024150
.680000	.053540	.680000	-.020430
.700000	.051110	.700000	-.018440
.720000	.048590	.720000	-.016380
.740000	.046110	.740000	-.014260
.760000	.043930	.760000	-.012070
.780000	.042050	.780000	-.009820
.800000	.040200	.800000	-.007500
.820000	.038310	.820000	-.005120
.840000	.036330	.840000	-.002690
.860000	.034300	.860000	-.000220
.880000	.032210	.880000	.002290
.900000	.030080	.900000	.004850
.920000	.027910	.920000	.007430
.940000	.025710	.940000	.010030
.960000	.023480	.960000	.012650
.980000	.021240	.980000	.015280
1.000000	.019000	1.000000	.017920

```
WBL                      = 384.69995
X AT THE LEADING EDGE    = 596.56421
X AT THE TRAILING EDGE   = 640.82764
REFERENCE VERTICAL LOC.  = 152.03552
```

COORDINATES AT THIS STATION ARE THE SAME AS FOR THE BASIC WING

1. Report No. NASA CR-3992	2. Government Accession No.	3. Recipient's Catalog No.
4. Title and Subtitle VARIABLE SWEEP TRANSITION FLIGHT EXPERIMENT (VSTFE)-PARAMETRIC PRESSURE DISTRIBUTION BOUNDARY LAYER STABILITY STUDY AND WING GLOVE DESIGN TASK		5. Report Date June 1986
		6. Performing Organization Code
7. Author(s) Rodger A. Rozendaal		8. Performing Organization Report No. D6-52511
9. Performing Organization Name and Address Boeing Commercial Airplane Company P.O. Box 3707 Seattle, WA 98124		10. Work Unit No.
		11. Contract or Grant No. NAS1-15325
12. Sponsoring Agency Name and Address National Aeronautics and Space Administration Washington, DC 20546-0001		13. Type of Report and Period Covered Contractor Report Feb. 1983-Nov. 1984
		14. Sponsoring Agency Code 505-60-31-01

15. Supplementary Notes

Technical Monitors: D. B. Middleton/D.W. Bartlett
NASA-Langley Research Center

16. Abstract

NASA has initiated the Variable Sweep Transition Flight Experiment (VSTFE) to establish a boundary-layer transition data base for laminar flow wing design. For this experiment, full-span upper-surface gloves will be fitted to a variable sweep F-14 aircraft. The Boeing Company is under contract to NASA to provide design and analyses support for the program. This report documents the results of two initial tasks: a parametric pressure distribution/boundary-layer stability study and the design of an upper-surface glove for Mach 0.8. The first task was conducted to provide a data base from which wing-glove pressure distributions could be selected for glove designs. Boundary-layer stability analyses were conducted on a set of pressure distributions for various wing sweep angles, Mach numbers, and Reynolds number in the range of those anticipated for the flight-test program. The design procedure for the Mach 0.8 glove is described, and boundary-layer stability calculations and pressure distributions are presented both at design and off-design conditions. Also included is the analysis of the "clean-up" glove (smoothed basic wing) that will be flight-tested initially and the analysis of a Mach 0.7 glove designed at the NASA Langley Research Center.

17. Key Words (Suggested by Author(s)) •Computational fluid dynamics •Wing design •Crossflow disturbances •Transition •Linear stability theory •Boundary layer •Natural laminar flow (NLF) •Wing glove •Tollmein-Schlichting disturbances •F-14	18. Distribution Statement FEDD-Distribution. Subject Category 02		
19. Security Classif. (of this report) Unclassified	20. Security Classif. (of this page) Unclassified	21. No. of Pages 166	22. Price

Available: NASA's Industrial Applications Centers

End of Document